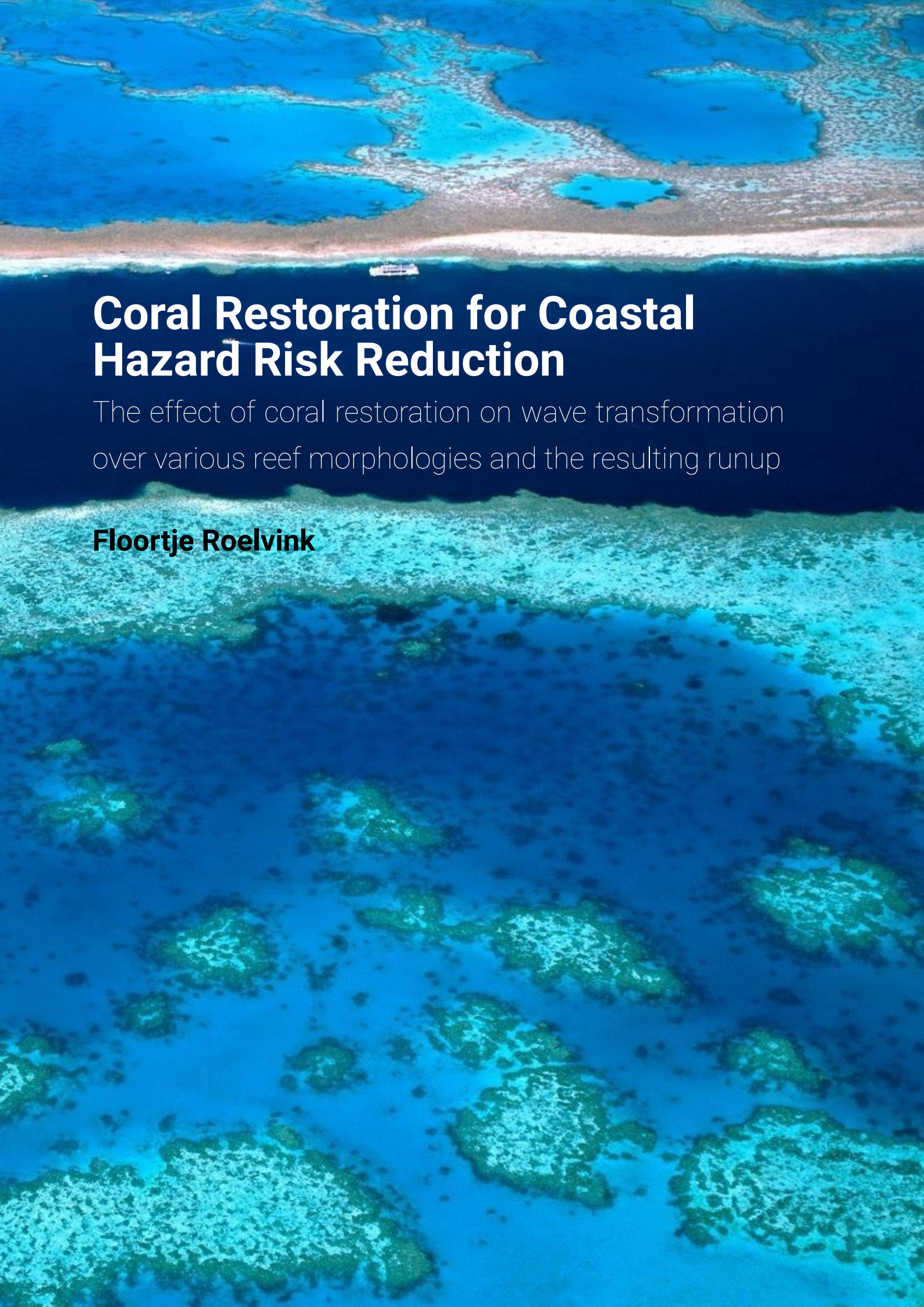

Coral Restoration for Coastal Hazard Risk Reduction

The effect of coral restoration on wave transformation over various reef morphologies and the resulting runup

Floortje Roelvink

Coral Restoration for Coastal Hazard Risk Reduction

The effect of coral restoration on wave transformation over various reef morphologies and the resulting runup

by

F.E. (Floortje) Roelvink

in partial fulfillment of the requirements for the degree of

Master of Science
in Civil Engineering

at the Delft University of Technology (TU Delft),
to be defended publicly on Wednesday July 3, 2019 at 16:00 .

Student number:	4249917	
Thesis committee:	dr. ir. M.F.S. Tissier,	Delft University of Technology
	ir. S.G. Pearson,	Delft University of Technology & Deltares
	ir. C.D. Storlazzi,	USGS-Pacific Coastal and Marine Science Center
	dr. A.R. van Dongeren,	Deltares
	Prof. dr. ir. A.J.H.M. Reniers,	Delft University of Technology

An electronic version of this thesis is available at http://repository.tudelft.nl/.

Cover: Great Barrier Reef as effective wave absorber
©surfertoday.com

In collaboration with:

Deltares
Enabling Delta Life

USGS
science for a changing world

Summary

Coral reefs are degrading at an alarming rate, affecting not only the precarious coral ecosystem but also human habitat. The combination of coral degradation, sea level rise and its exacerbated effect in the tropics, and the possible storm intensification increases the flood vulnerability of low-lying tropical islands. To protect reef fronted coasts against flooding, coral restoration is put forward as measure to increase coastal safety. This study addresses the effects and efficiency of coral restoration in four steps. First, a simple *reef hydrodynamic model* is formulated to identify important drivers of runup at a reef fronted beach, to be used as a quick scan tool before using more intensive process-based models. Next, 30.000 US reef profiles are classified to gain insight into the *prevalence of different reef shapes*. Four dominant reef profiles are then used in the subsequent modeling step, in which the *hydrodynamics and flood vulnerability of different reef shapes* are investigated using the XBeach process-based model. With the knowledge gained, the *hydrodynamic effects and runup reduction potential of different restoration configurations* at various reef morphologies can be assessed.

The runup at a reef fronted coast is highly dependent on local reef morphological conditions and hydrodynamic forcing, showing little correlation to existing formulations for runup at sandy coastlines (e.g. Stockdon et al. [150] and Gomes da Silva et al. [55]). Therefore, a simple reef hydrodynamic model was set up to give a first order indication of wave transformation and runup at reefs. In this model, the short wave transformation and setup are solved by the Janssen and Battjes [73] model. As no simple formulations for the infragravity (IG) wave height exist, the IG wave height at the reef crest is empirically derived based on numerical simulations of a fringing reef. The IG wave height is shown to be highly dependent on the offshore short wave height, wave steepness, water level and forereef slope. The subsequent shoaling and dissipation of the IG waves is modeled according to van Dongeren et al. [159]. The beach toe wave heights and setup, solved by the model, are input for the derived runup formulations. The short wave runup component is well described using beach toe short wave heights, the water level and the beach slope, whereas the IG runup is highly dependent on both the IG and short wave energy at the beach toe.

Cluster analysis of 30.000 US reef profiles with the k-means model shows the prevalence of 10 reef profile shapes. Four of these profiles have a relatively high frequency of occurrence and distinct features: the typical fringing reef profile, the convex profile (in which the transition between the forereef and reef flat is gradual), the straight profile and the three-slope profile (a steep nearshore slope, followed by a shelf and an offshore forereef slope). Together, these reefs represent approximately 70 % of all surveyed reefs.

Wave transformation and flooding of reef fronted coastlines is greatly affected by the reef profile shape and profile dimensions. Short wave dissipation and setup over the four reef morphologies show clear patterns, where a narrow surfzone (steep slope) leads to a large setup. The degree of wave breaking and frictional wave dissipation (determined by the reef flat / shelf width and submergence) determines the beach toe short wave heights and the resulting setup between the beach toe and the shore. The generation of IG and very low frequency (VLF) waves is highly dependent on the forereef slope. The IG and VLF propagation is, however, more complex, showing both progressive growing and progressive dissipative behaviour across the different shapes. Of the four modeled shapes, the straight profile is most vulnerable to coastal flooding, as no reef flat or shelf is present to damp part of the incoming short wave energy.

Mechanisms responsible for runup reduction by coral restoration are similar across the various reef morphologies. At the steep interface of the restoration, waves are reflected, limiting the wave energy reaching the coast. Across the restoration, short and IG waves are further dissipated. The reduction of short wave heights decreases the setup near the shore due to the smaller radiation stress gradients. Moreover, the IG wave runup decreases due to the IG wave height reduction and the diminished transfer of energy from short waves to the infragravity waves.

Restoration potential is distinctly different among varying profile shapes. The typical fringing reef and the convex reef feature a reef flat that acts as a natural wave attenuator, diminishing the flood risk reduction

effect of the coral restoration. The straight and three-slope profile are relatively unprotected from wave action, rendering them vulnerable to coastal flooding, but also responsive to restoration measures. Average runup reductions of around 40 % are observed for the three-slope profile due to the effective reflection at shelf restorations. For the straight profile, runup reductions of up to 20 % are accomplished, while runup reduction across the typical fringing and convex reef are stalled at approximately 5 to 10 %. For the typical fringing and convex profile, the restoration location also significantly affects the runup reduction potential, as restorations near the baseline scenario breakpoint can strongly increase the setup across the reef flat, an effect not observed in other profiles.

This research has focused on the efficient reduction of runup by coral restoration, giving insight into profile shapes and restoration locations with runup reduction potential. It does not only provide valuable insight into reef hydrodynamics, but also serves as a promising example of green infrastructure to enhance coastal safety. By allocating ever limited funds to well-designed coral restorations, vulnerable coastal areas may receive the much needed support in combating the effects of climate change.

Acknowledgments

This thesis completes the Master of Science programme at Delft University of Technology. The research was carried out at Deltares in Delft, in a joint cooperation with the USGS-Pacific Coastal and Marine Science Center in Santa Cruz, California.

The past ten months have been an amazing experience, thanks to the highly interesting topic of the project and, equally important, the people involved in it. Stuart's enthusiasm for reefs is highly contagious, so from the first meeting on I was rather fascinated by the world of coral reefs. Not only because of the very interesting and sometimes inexplicable hydrodynamics across the reef, but also because of the social relevance of coral reefs that brings in the bigger picture of the project. I would like to thank my graduation committee immensely for their enthusiasm, inspirational amount of knowledge and useful feedback during the project. I would like to thank Stuart Pearson for his infinite energy and enthusiasm during our weekly talks, and for his extensive feedback. Thanks to Ap van Dongeren for the inspiring and helpful insights into the reef hydrodynamics and for taking the time for valuable supervision. I would like to thank Marion Tissier for chairing the committee, for the critical questions and many useful suggestions. Thanks to Ad Reniers for uncovering the inaccuracies in results and formulations and extensive theoretical knowledge. Lastly, I would like to thank Curt Storlazzi from the USGS, who funded this study and made indispensable data available, for your incredible enthusiasm for coral reefs and this project, for your insights into reef restorations and for your practical recommendations.

To my friends and family, especially Wouter and Esther, a big thank you for distracting me from work. Enjoy reading!

Floortje Roelvink
Delft, June 2019

Contents

List of Figures

List of Tables

List of Symbols

Symbol	Units	Description
β	-	Slope (subscripts f for forereef and b for beach)
c_f	-	Coefficient of friction
c_g	m/s	Wave group velocity
E	J/m^2	Wave energy density
ϵ	W/m^2	Dissipation rate
η	m	Dynamic sea level or wave setup
η_0	m	Offshore water level
f_p	Hz	Peak wave frequency
f_x	m/s	Spatially averaged canopy resistance
g	m/s^2	Gravity (9.81)
γ_b	-	Breaking wave height relative to depth ratio
h	m	Water depth
h_b	m	Depth at breakpoint
H_b	m	Wave height at breaking point
H_0	m	Offshore wave height
H_{SS}	m	Significant Sea-Swell (SS) wave height
H_{IG}	m	Significant infragravity (IG) wave height
H_{VLF}	m	Significant very low frequency (VLF) wave height
k	1/m	Wave number (2π/L)
K_{sh}	-	Shoaling factor
L	m	Local wave length
L_0	m	Offshore wave length
ω	1/s	Angular frequency (2π/T)
P	kg/m/s^2	Pressure
Q	-	Fraction of breaking waves
qOT	l/s/m	Overtopping discharge
R	-	Reflection
$R_{2\%}$	m	Wave runup at the 2% exceedance level
ρ	kg/m^3	Density
S_{inc}	m	Incident short swash
S_{IG}	m	Infragravity swash
S_{xx}	J/m^2	Cross-shore component of the radiation stress
T	s	Wave period
τ_{xy}	$kg/m/s^2$	Shear stress
u	m/s	Velocity
W_{reef}	m	Reef width
ξ	-	Surf similarity parameter

I

System Analysis

An elaboration of why and how this research is conducted, by analyzing the posed problem and elaborating on the state of the art research, in order to come up with a research strategy that efficiently tackles the research needs

Ch 1. Introduction

Ch 2. Literature review

Ch 3. Thesis outline and objectives

1 Introduction

1.1. Context

Coral reefs provide a wealth of ecosystem services such as fisheries, opportunities for tourism and leisure, and shoreline protection [48]. These services support millions of people with food and income, of which the net value is estimated at US$30 billion each year [36]. Shoreline protection alone is estimated to bring about a damage reduction of more than US$4 billion each year, damages that are projected to double without reefs [19]. The effectiveness of the reef ecosystem as a nature-based coastal defense has been reviewed in numerous studies (e.g. Narayan et al. [108], Beck and Lange [20], Storlazzi et al. [151] and [128]). Both by wave breaking near the reef crest and frictional dissipation at the reef slope and reef flat, wave energy is reduced [93]. Ferrario et al. [50] list wave reduction capacities of reef crests (on average 86 % of the incident wave energy) and flats (65 % of the remaining energy). This generally leads to smaller impacts of waves at the shoreline, although complex feedback mechanisms between incident wave conditions, water levels and reef characteristics exist that make the prediction of the shoreline impact difficult [101].

The threat to the coastal protection service delivered by coral reefs is alarming. On smaller scales, anthropogenic disturbances such as vessel grounding, freshwater discharges and nutrient loading are detrimental to reef ecosystems [177], but of much larger impact are the long-term, large scale effects of climate change. The main pressures of climate change on the ocean environment are ocean acidification due to the absorption of CO_2, an increase in ocean temperature, sea level rise (SLR) and possibly an increase in storm intensity [167]. Ocean acidification negatively impacts coral skeleton formation, which slows or even halts reef growth [169]. Moreover, as corals and especially the microalgae that supply energy to the corals are sensitive to thermal conditions, rising ocean temperatures often lead to coral bleaching [48]. Another impact of climate change is sea level rise and its exacerbated effect in the tropics, where an amplified SLR in combination with the low elevation of coral islands can lead to frequent flooding and inundation [153]. This effect is aggravated by an increase in storm intensity, which can also cause massive coral destruction. Under less stringent conditions, coral reefs regenerate from these disturbances by natural recovery. However, rapid degradation and (partial) destruction of the coral reef can irreversibly damage the ecosystem, a process that has already caused the annual decline in coral cover of 1-2% over the last decades [29]. As a result the shoreline protection function is threatened, which raises the demand for active intervention.

Coral restoration as an instrument for coastal hazard risk reduction is promising [135][134]. Both Narayan et al. [108] and Ferrario et al. [50] stipulate the economic efficiency of coral reefs compared to engineered defences based on a meta-analysis of the wave attenuation capacity of different (engineered and natural) coastal habitats. Here, focus is on the effect of having a reef or not, instead of restoring an existing reef. Knowledge on coral restoration techniques, upscaling of restoration works and reef management has also expanded significantly over the last years [46][115][47]. Both literature reviews on coral restoration efforts [84] and large scale experiments [102][145] have shown the effectiveness of restoration operations for ecological purposes. Montoya-Maya et al. [102] successfully transplanted more than 24.000 coral plants in three years, which aided the natural recovery of the reef. Moreover, coral reproduction techniques are advancing to a point where climate resilient corals can be made using 'assisted evolution' techniques [77]. But although the

effects of coral restorations for coastal protection also seem promising, little research has been concerned with the actual hydrodynamic effects of coral restorations. A quantified assessment of these effects is crucial to invest in coral restoration as a green alternative for coastal hazard risk reduction.

1.2. Problem Statement

Around the world reefs are degrading at an alarming rate, which not only threatens the coral habitat and its occupants but also coastal communities and economic assets. To regain and strengthen the reef's vital function of coastal protection, coral restoration works could prove valuable. The large spatial scales of reefs, operational restraints of recovery actions and often limited funds ask for an efficient approach in restoring the reefs. Information on hydrodynamic regimes and reef morphologies that are worth restoration efforts for hazard risk reduction is however not readily available. Furthermore, it is unknown where along the cross-shore profile reefs should be restored to give the largest reduction in runup, and which hydrodynamic processes are modified as a result of the intervention. Insight into this could significantly increase the impact of coral restoration efforts, assisting a range of stakeholders from governments, private institutes and engineering companies to small entrepreneurs and individuals in their ambition of improving the functioning and health of coral reefs and reducing the risk of coastal hazards, by allowing them to make efficient use of ever limited resources.

1.3. Significance

Need of adaptation measures for future sea level rise
An increasing amount of scientific evidence demonstrates the threat of climate change to the environment and society [168], whereby impacts are traced, measured and extrapolated to expose future scenarios. They display a discomforting future. Hall et al. [61] project a sea level rise of 0.2 to 2 m by 2100. The threat of climate change to our society is also stipulated in the many awareness programs, mitigating policies and sustainability goals, drawn up at levels ranging from education institutes and private organizations to governments and intergovernmental organizations. The urgency to decrease the atmospheric content of carbon dioxide (CO_2) is clear, however mitigation efforts are obstructed by both public actions and reluctant governments. Therefore, apart from mitigating measures, we must focus on climate adaptation measures to prepare for the unknown future. We need to create a resilient, adaptive (coastal) infrastructure that is able to protect our society against SLR and other impacts of climate change. Coral restoration could partly fulfill the need for increased coastal protection, provided that the actual effects of different restoration configurations are known.

Increasing attention to coral degradation and restoration
The relation between climate change and coral degradation is becoming increasingly evident. In 1983 the first recording was made of widespread coral bleaching [38]. The extremely high mortality rates (up to 95 %) in combination with persisting disturbances and declined coral growth were projected to delay the recovery for decades [54]. A link between climate change and these bleaching events was however not yet noted, and it took a decade more before ocean warming was linked to coral bleaching [69]. Moreover, it was only in 2017 that the UNESCO World Heritage Centre published the first global assessment about the impact of climate change on coral reefs, after which it became clear that in the three years before, 72 % of the World Heritage reefs had been damaged by coral bleaching [67]. The increasing public attention to causes and consequences of coral degradation is evident from among others the number of studies, restoration projects, the declaration of 'International Year of the Reef 2018' [5], Netflix' documentary 'Chasing Coral' [131] and international collaborations such as the Small Island Developing States (SIDS)[27]. Consequently, restoration as a solution for degradation and coastal hazard risk reduction is gaining ground. Although advertized as an effective measure for coastal protection [62], the actual impact of restorations on the wave attenuation capacity is unknown. Therefore, this research on coral restoration addresses the global demand by tackling one of the more unresolved issues regarding restoration.

Stakeholder's interest
This research could be of relevance for different stakeholders, of which the important actors are elaborated below.

1. *Governments* and *regional authorities* are responsible for the coastal infrastructure that protects coastal communities. They approve and fund large scale restoration measures and are therefore an influential actor in reef restoration activities for coastal hazard risk reduction. This research could substantiate the allocation of funds to regions where restoration could efficiently reduce the runup and show if restoration is efficient at all, to prevent unnecessary expenses on inutile recovery actions.

2. In a recent report the *United Nations* concluded that urgent action is required to combat 'rising sea levels, extreme weather conditions and increasing concentrations of greenhouse gases' [158], in line with Sustainable Development Goal (SDG) 13: 'Take urgent action to combat climate change and its impacts' [109]. They praise the recent development of national adaptation plans, highlighting the importance of mitigating actions and therewith confirming the relevance of this research. Furthermore, as a result of restoration works for coastal protection, new habitat for marine species is created, thereby addressing SDG 14: 'Conserve and sustainably use the oceans, seas and marine resources for sustainable development' [109]. Next to the formulation of the SDG's, the UN also identified 57 *Small Island Developing States (SIDS)* that share similar vulnerabilities: 'small size, remoteness and insularity, disaster proneness and environmental fragility' [27], which impedes economic development. These islands are eager for practical measures to improve coastal safety, to ensure the future habitability of the islands. This research can be the link between the existing knowledge of reef hydrodynamic processes and the practical implementation of restoration measures.

3. *Coastal communities and volunteers* are already much involved in coral restoration actions for conservation of marine resources [6]. However, the flood risk reduction that recovered coral sections could possibly provide is often not taken into account. Therefore, with an indication of efficient coral restoration configurations, these recovery actions would not only benefit marine life but also act as measure to increase coastal safety.

2

Literature review

2.1. The coral reef environment

2.1.1. Morphology

Coral reefs are complex ecosystems comprising of among others algae, coral polyps (the reef-building organisms) and calcium carbonates. They can be found in shallow tropical and subtropical waters, where temperature, light intensity and salinity levels are favourable for reef building corals and its inhabitants [8]. Three main types of coral reefs can be distinguished based on their geomorphological characteristics; fringing reefs, barrier reefs, and atolls [28] (see Figure 2.1).

Reefs are often formed in mid-ocean by volcanic activity, which creates oceanic islands around which corals start to grow, the *fringing reef*. Fringing reefs are identified by their close proximity to the shore, often accompanied by a narrow, shallow lagoon. This renders the system vulnerable to increased water levels and wave heights as no large buffer between the reef crest and land is present [28]. While the coral grows upwards, land subsidence, erosion by wind and wave action and sea level rise increase the space between the reef and the island and a *barrier reef* is formed. Barrier reefs are located further offshore, often at the edge of the continental shelf. The lagoon is both wide and deep and reef dimensions are large, with a length of up to hundreds of kilometers and a width of several kilometers. Similar to the fringing reef, the barrier reef runs (roughly) parallel to the shore. They either encircle an island or form complex chains of structures along coastal stretches [8]. The last successive state of reef evolution is marked by inundation of the island's center, leaving only a coral rim, the *atoll*. The ringshaped coral reefs encircle a deep lagoon [171]. Due to the small size of the coral rim, natural resources are sparse on atoll islands [49]. Furthermore, the low elevation makes the islands susceptible to sea level rise and changes in hydrodynamic forcing [153], which aggravates the pressure on resources.

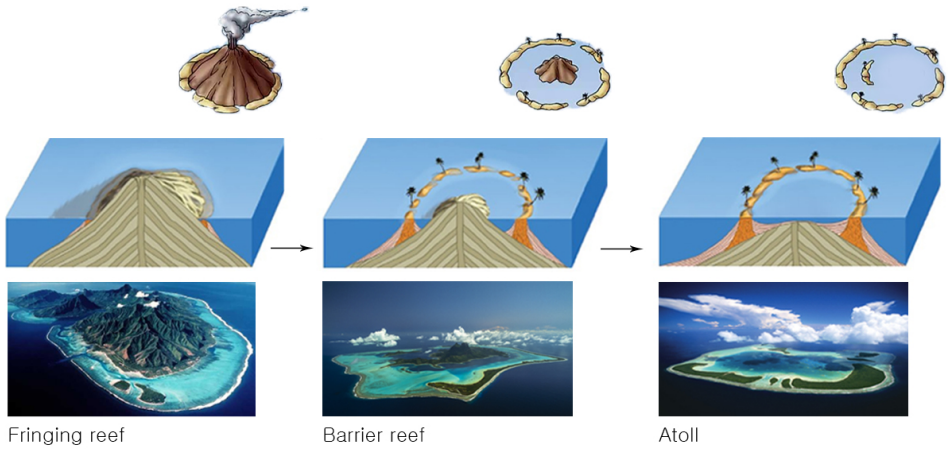

Figure 2.1: Evolution of coral islands. Sources: [107], [9], [170], [3], [4]

2.1.2. Structural zones

Different structural zones can be identified in coral ecosystems, each with specific effects on wave transformation across the reef. Important zones are the forereef, the reef crest, the reef flat and the lagoon [79]. Furthermore, beach characteristics influence the maximum vertical elevation above mean water level that waves reach, the runup. The different zones are indicated in Figure 2.2.

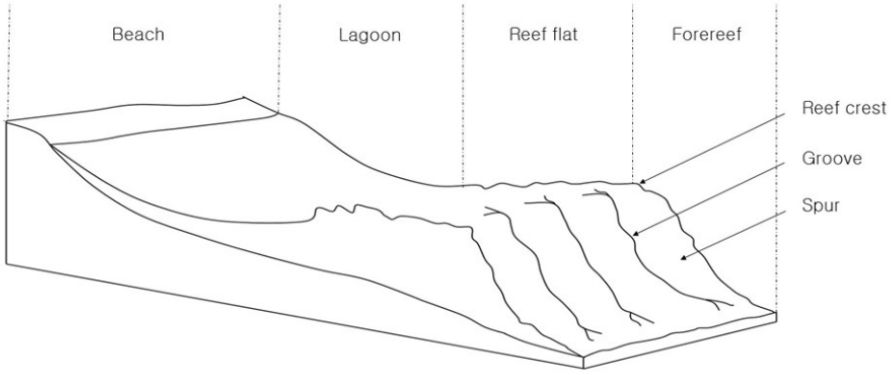

Figure 2.2: Structural zones coral reef

Forereef
The forereef is the slope at the seaward edge of the reef, extending from the low-tide mark into deep water [112], where waves shoal, refract and possibly break. The habitat of the upper 20 m is often characterized by a linear reef with spurs (shore-normal ridge) and grooves (shore-normal patch) [79]. This system of alternating high and low reliefs drives Lagrangian circulation cells, where open ocean, low-sediment, highly nutritious water is transported to the forereef and coral debris and sediment away from the forereef to deeper waters [140]. The spur and groove system is most effective in circulating water and decreasing the bottom shear stress when spurs are located orthogonal to the dominant wave direction and in areas where wave activity is large [140].

Reef crest
The reef crest is the highest part of the reef which is exposed or nearly exposed during low tide. This segment of up to 50 m wide is fully exposed to the incoming wave energy [141]. Habitats at the reef crest adapt to the hydrodynamic conditions on site; in moderate wave action areas corals form a tight colony to withstand the waves, and in severe climates only fast growing algae are present on the calcareous crest [112]. The reef crest is not always present; if not, the forereef is connected to the reef flat.

Reef flat
The reef flat is the shallow zone between the reef crest and shore that is highly variable in character, with widths ranging between 20 meters and a few kilometers, depths of centimeters up to meters and flat to mildly sloping bottoms [112]. The flat is covered with a mixture of coral rock, rubble and sand and is home to many benthic organisms and algae. The limited depth often leads to high temperatures and salinity, which reduces the amount of living corals on the flat [24]. Reef flat characteristics such as the width and roughness highly influence the level of wave dissipation.

Lagoon
Either encircled by atoll rims or barrier reef flats, lagoons are situated in areas well protected from the open ocean environment. Their depths usually vary between 20 to 60 m, while widths range between 2500 m to 100 km [80]. Lagoon depths are usually maintained by a balance between sedimentation and bottom subsidence. Temperatures in the lagoon are relatively high due to the reduced wave action and water flow. Typically, small coral patches and sea grass cover the sandy lagoon beds [66].

Beach
Reef fronted beaches are often characterized by a steep slope and wave exposure during high-tide only [146]. They consist of carbonate sediments that originate from shells and coral detritus [147]. Particularly the beach slope is of importance for wave transformation at the reef fronted beach. Its effect is best investigated using the surf similarity parameter ξ [15], which is a measure of the beach slope relative to the wave steepness:

$$\xi = \frac{tan\alpha}{\sqrt{H/L_0}} \tag{2.1}$$

where $\tan(\alpha)$ is the beach slope and H (wave height) $/L_0$ (offshore wave length) the wave steepness. In case of reflection at the reef beach, the beach toe wave heights are used as input for Equation 2.1. The surf similarity parameter influences among others the breaker type (surging, collapsing, plunging or spilling), the breaking wave height relative to depth ratio (γ_b), the setup, the runup and wave reflection [15]. Typically the ξ-value of the usually steep reef fronted beach is large, leading to plunging or surging waves which limit dissipation, thereby enhancing the runup. Furthermore, steep beaches lead to large reflection of wave heights due to the limited dissipation.

2.1.3. Ecology

A basic understanding of coral reef ecology, in particular factors related to *coral recruitment*, is required to assess the feasibility and effectiveness of restoration operations. Recruitment refers to the settlement of newly formed corals (by reproduction) in the reef community, a critical process for the survival of reef populations [133]. Three phases of recruitment can be distinguished: larval availability, settlement ecology and post-settlement ecology [136]. Although biotic factors greatly influence the recruitment rates of coral, we focus on abiotic factors in this study; the hydrodynamic conditions that could possibly prevent growth, maturation and survival of newly formed corals. Water motion has been shown to have great impact on the transport and dispersal of larvae, as well as on whether larvae can successfully attach to the substratum [129].

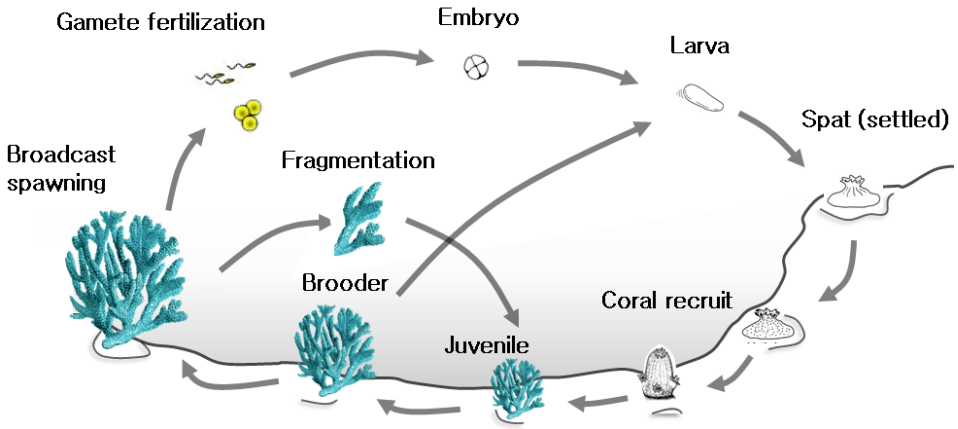

Figure 2.3: Phases of coral recruitment

Larval availability
Larval availability encompasses the processes of fertilization and transport of larvae, see Figure 2.3. Reproduction by corals can be both sexual and asexual. Fragmentation, the physical splitting of coral fragments due to breakage, during storms for instance, is the most important mode of asexual reproduction and vital to the survival of certain coral species [68]. During sexual reproduction, fertilization can appear as brooding (within the maternal polyp) or broadcast spawning (when the gametes are released into the water column) [132]. The frequency and quantity of produced larvae depends on abiotic factors such as coral bleaching, nutrient release and changes in salinity and sedimentation [136] and biotic factors such as the density of spawning adults. After fertilization, larvae are transported away to settling areas on the reef by ocean currents, across both short distances (leading to self-seeding of the coral) and longer distances, connecting coral reefs of adjacent islands. The reef interconnectivity is an important factor in the recolonization of disturbed

coral systems, but also in the conveyance of both nutrients and contaminants [152]. Storlazzi et al. [152] note that reefs with little self-seeding recover quickly from local disturbances as the larvae sources are healthy, whereas high self-seeding reefs are susceptible to local stresses.

Settlement ecology

During settlement, larvae interrupt their transport to select an appropriate settling habitat where they transition from planktonic larvae to benthic juveniles. Two critical stages can be discerned; the transport of larvae to the substratum and the establishment phase that entails both the attachment and metamorphosis of the larvae [7]. In both phases, hydrodynamic forces play an active role.

Transport or delivery to the substratum is mainly accomplished by active downward swimming of the larvae, turbulent transport and gravitational deposition [7]. The relative importance of these transport modes depends on the turbulence intensity; the energy present in the turbulent fluctuations as function of the mean flow. Recent research (Hata et al. [64]) has shown the effectiveness of turbulence and eddying structures in navigating larvae to the settlement site, in comparison with the weak swimming force. Hata et al. [64] urge that complex micro-structures are required for the generation of sufficient turbulence. This positive feedback between structural complexity and settlement of coral species has been documented widely [121][128][58].

During the first encounter with a substratum, larvae examine the adequacy of the location, which is mainly defined by the type, chemistry, surface conditions and flow characteristics [7], before possibly attaching to the substrate's surface. The settling position and success of the attachment depends on the larval adhesive strength and speed. The strength of the attachment acts as a resistive force against the hydrodynamic forces; drag, lift and the acceleration reaction force that is present in accelerating or decelerating flows. The adhesion speed is also of importance; quickly sticking larvae can attach in high velocity regions, whereas larvae with slowly developing adhesive strength have to find sheltered areas where shear forces are low [81].

When corals have successfully attached, the characteristic morphological and biochemical changes of the metamorphosis take place, during which the coral transforms from a larva to a benthic juvenile [133]. The settlement site will be the base from which new coral colonies form during the *post-settlement ecology phase*.

2.2. Reef hydrodynamics

Hydrodynamic processes on reefs cover a range of spatial and temporal scales, from in-canopy fluid motion forced by oscillatory flow [88] to wave, tide or buoyancy driven currents [101]. To analyze the potential of different coral reef restoration configurations as a nature based defense, larger scale hydrodynamic processes that control wave attenuation and runup on coral reef fronted coasts are studied (Section 2.2.1), as well as wave driven flows through the canopy (Section 2.2.2).

2.2.1. Wave transformation at the reef scale

In this section, the wave transformation processes at the reef scale are explored, with special focus on processes that influence runup at the coast. First, general principles of wave generation (Section 2.2.1.1) and wave propagation and dissipation of sea, swell and infragravity waves at coral reefs (Section 2.2.1.2) are outlined to obtain a broad overview of wave transformation processes at reefs. Subsequently, the influence of water level variations (tide, sea level rise, storm surge), incident wave heights and the coral reef morphology (reef slope, reef flat width and elevation) on the different runup components is studied in detail in Section 2.2.1.3.

2.2.1.1 Wave generation

Sea and swell
Waves are generated by the disturbance of the sea surface under sustained winds. Due to the variation in wind force a random wave field (the so-called wind sea) is created that is mathematically described as the superposition of sinusoidal waves with differing amplitudes, frequencies, phases and direction [105]. As dictated by the dispersion relation, waves with larger wavelengths travel faster (frequency dispersion). Furthermore, as the random wave field disintegrates while propagating through the ocean, the directional spreading decreases (directional dispersion) [35]. Therefore, at great distance from the generation area, waves are regular and long-crested, they travel in similar direction and have similar frequencies (swell).

Bound infragravity waves
The phase-coupling (grouping) of two swell waves that have slightly differing frequencies leads to the generation of a third wave, the bound long wave or infragravity wave [120]. Considering a simplified bichromatic wave field, the superposition of two swell waves gives a resonance pattern where amplitudes are locally amplified or damped [21]. A slow and a fast modulation can be observed; a fast modulation on the time scale of the short waves and a slow modulation, the wave group envelope. At the wave group scale, the higher amplitude waves transport more momentum and thus induce a larger water level depression compared to the smaller amplitude waves. This results in varying water level depressions at the time scale of the wave envelope; the bound long wave [21]. On horizontal beds, it travels 180 degrees out of phase with the wave group envelope [95]. This simplification of wave groups consisting of two waves by Longuet-Higgins and Stewart [85] can be extended to the full short wave field that is visible in nature [21].

Free infragravity waves
The sea state at the outer edge of the reef is a mixture of high-frequency sea and swell (SS) and bound infragravity (IG) waves. At the reef, IG waves are released as a result of two distinct processes: (1) due to shoaling and breaking of short period waves and (2) by a moving breakpoint. At the forereef the depth sharply decreases. The equilibrium response of IG waves to the short-wave envelope derived by Longuet-Higgins and Stewart [85] does not hold at this sloping bottom. While moving shoreward on the forereef the phase-lag between the IG waves and the short-wave envelope increases. In the process, energy is transferred from the high-frequency waves to the bound long wave [72]. Ultimately bound long waves are released and propagate across the reef as free long waves, a process that is enhanced by depth-limited short period wave breaking at the forereef and reef crest [18].
Additionally, free IG waves can be generated by the oscillation of the short wave breakpoint [12]. The variation in wave height of incoming short wave groups creates a pattern where higher waves break further offshore in accordance with the depth-limitation set by the breaking criterion. The temporal variation of the breakpoint induces time-varying radiation stress gradients and thus time-varying setups [21]: the "breakpoint generated waves" [12].

2.2.1.2 Wave propagation and transformation at reefs

As waves propagate across the reef they shoal, dissipate energy and transfer energy in between frequencies by non-linear interactions [122].

At the forereef, waves start to interact with the bottom, lose energy due to frictional wave dissipation and shoal until they reach the wave height limit and break. Several empirical and semi-empirical formulations exist to estimate this breaking wave height [74], of which several are elaborated in Section A.1 of Appendix A. The breaking wave height and the location of breaking depends among others on the water level elevation and wave field characteristics [74]. In his laboratory experiments of breaking waves at steep slopes, Jensen [74] concluded that γ (the maximum wave height to depth ratio) is generally between 0.4 and 0.6. As the reef crest is generally the point of maximum bed elevation and thus minimum water depth, the reef crest submergence determines the maximum wave height of waves propagating onto the reef flat. It forms a wave height filter; only waves with a lower wave height than the critical breaking limit propagate onto the reef flat [88]. Overall much dissipation can be attributed to short wave breaking and frictional wave dissipation at the forereef and reef crest [93]. According to Ferrario et al. [50], the average amount of transmitted short wave energy past the reef crest is around 2 %. The resulting abrupt decrease in radiation stress during the localized short wave breaking at the forereef leads to a water level setup shoreward of the breakpoint [166]. This setup allows the propagation of larger waves onto the reef flat [74]. The temporal variation in setup causes the generation of the free IG waves. Gourlay [57] note a minimal influence of reflection at the steep forereef on both the transmittance of wave energy and the setup; their measurements have shown reflection coefficients of around 0.1 (fraction of the incoming wave height), which would result in a setup reduction of only 1 % [57].

On the reef flat, short wave dissipation by bottom friction is substantial and can even be the dominant dissipation mechanism as water depths are usually small and friction coefficients of coral reefs typically large [88]. Whereas offshore most energy is contained in the high frequency band, at the shoreward end of the reef flat a high peak is evident around the lower frequencies [74]. This is a result of wave breaking and frictional dissipation of the short waves and a transfer of energy to the IG motions combined with the limited IG frictional wave dissipation [37]. What is more, the breakpoint-generated free long waves often appear to be the dominant source of IG wave energy across the reef, which leads to a gradual increase of IG wave energy shoreward of the breakpoint and a decrease in short wave energy [122][120][37]. The frictional wave damping of short waves across the reef flat is among others dependent on the reef flat width and canopy roughness.

Waves with a significantly reduced wave height arrive at *the toe of the beach*, where wave breaking dissipation will further reduce the wave energy of both short and IG waves. Frictional wave dissipation is limited due to the marginal roughness of coral sediments. However, wave energy is also converted into potential energy, the runup [150]. Runup is defined as "the height above the stillwater elevation (tide and surge) reached by the swash" [75]. A slowly varying and a fast oscillatory signal can be discerned in the swash motion: the quasi-steady water level elevation by wave setup and the time-varying motions by short and IG wave action. Various formulations exist to predict the runup. Here we outline the theory by Stockdon et al. [150], as she conveniently made a distinction in the runup contributions of setup, IG wave energy and incident wave energy. From statistical analysis of 10 experiments with highly differing conditions, Stockdon et al. [150] derived the following formulation for the elevation of extreme runup, that is defined as the 2 % exceedance value:

$$R_{2\%} = 1.1\left[\langle\eta\rangle + \frac{S}{2}\right] \quad \text{, where} \tag{2.2}$$

$$S = \sqrt{(S_{inc})^2 + (S_{IG})^2} \tag{2.3}$$

$$S_{inc} = 0.75 * \beta * (H_0 L_0)^{1/2} \tag{2.4}$$

$$S_{IG} = 0.06 * (H_0 L_0)^{1/2} \tag{2.5}$$

$$\langle\eta\rangle = 0.35 * \beta_{foreshore} * (H_0 L_0)^{1/2} \tag{2.6}$$

where $R_{2\%}$ is the 2 % exceedance value of the runup, S_{inc} the incident swash height, S_{IG} the infragravity swash height, η the maximum setup at the shoreline, H_0 the offshore significant wave height, L_0 the offshore wave length and β the beach slope [150].

2.2.1.3 Hydrodynamic and morphological factors influencing runup

As mentioned in the paragraph above, extreme water levels at the shoreline are caused by a combination of setup, short wave energy and IG wave energy. Generally the relative contribution of the setup, the short wave energy and the IG wave energy at reef fronted coasts is controlled by the water level, the incident wave conditions and the reef morphology [113]. The main morphological elements are the slope of the forereef, the reef flat width and the roughness [124][57][37]. In this section, for each runup component relevant physics are explained first, after which all hydrodynamic processes and reef morphological characteristics influencing the contribution to the runup of each component are further elaborated. An overview of all factors influencing the setup, IG wave energy and short wave energy is displayed in Figure 2.4 on page 17.

Short wave energy

To investigate processes affecting the short wave energy component of swash at the shoreline, the transformation of sea and swell (SS) across the reef is studied. For straight, parallel contours and normally incident waves, the steady-state wave energy conservation equation that describes the change in energy flux is given by [16][118]:

$$\frac{\partial EC_{gx}}{\partial x} = \langle \epsilon_b \rangle + \langle \epsilon_f \rangle (+\langle N \rangle) \tag{2.7}$$

Here E is the wave energy which can be approximated using linear wave theory (see Equation 2.13). The same holds for C_g, the group velocity. ϵ_b is the time-averaged dissipation rate due to wave breaking and ϵ_f the dissipation rate due to friction. The term N describes the nonlinear interactions that transfer energy from the short wave frequency band to the IG frequency band, a phenomenon first described by Hasselmann [63]. These non-linear transfers appear to be the dominant term in the short wave energy balance during small wave conditions [118]. For hazard risk reduction, these conditions are not normative and therefore the assumption of limited non-linear interactions can often be adopted (N=0) [88]. Several (semi-)empirical formulations exist for the dissipation due to breaking and friction. For the prediction of energy loss due to wave breaking, Battjes and Janssen [16] established the periodic bore model for random breaking waves at a beach. Key elements of this model are the calculation of the fraction of breaking waves as a function of H_{rms} and H_b (maximum wave height determined by the breaking criterion), and the subsequent estimation of the dissipation rate per breaking wave by assuming the formation of a bore [16]. Here we outline the slightly adapted version of this model by Baldock et al. [13] who improved the existing model for breaking waves at steep slopes. He derived the following time-averaged energy dissipation rate by wave breaking:

$$\langle \epsilon_b \rangle = \frac{1}{4} \rho g f_p B Q (H_b^2 + H_{rms}^2) \tag{2.8}$$

where B is a constant of the order one and Q the fraction of breaking waves:

$$Q_b = \exp\left[-\left(\frac{H_b}{H_{rms}} \right)^2 \right] \tag{2.9}$$

The breaking wave height H_b can be approximated with any common expression [13]. Next to wave breaking dissipation, frictional wave dissipation has a significant effect on the wave transformation process, especially at reefs where roughness is large. An often used formulation for the average frictional dissipation per unit area is given by Thornton and Guza [157]:

$$\langle \epsilon_f \rangle = \rho C_f \frac{1}{16\sqrt{\pi}} \left(\frac{2\pi \bar{f} H_{rms}}{sinh(kh)} \right)^3 \tag{2.10}$$

From Equation 2.10 it can be deduced that friction is mainly dependent on the wave height, the water depth, the wave length and the bottom roughness. Where for most coastal environments, both sandy and reef lined, wave breaking is the main dissipation mechanism, Lowe et al. [88] have also observed wave conditions where frictional wave damping was dominant. The important factors influencing this energy decay of short waves

as a result of wave breaking and friction are described below.

Factors influencing the short wave height

1. The *maximum short wave height* is highly controlled by the water level, regardless of whether this water level is a result of tide, sea level rise, surge or wave setup [118]. Higher water levels allow passage of higher short waves onto the reef flat [88]. For very high water levels, short wave energy can even be dominant over IG wave action at the coast [78]. For incident wave heights larger than the wave height dictated by the breaking criterion the surfzone is said to be energy saturated [156]. For saturated surfzones the short wave height at the reef flat is independent of the incident wave conditions and foremost determined by the water level [118]. However, as water levels increase, the maximum allowable wave height exceeds the incident wave conditions, in which case the wave height at the reef is also a function of the incident wave conditions. What is more, the incident wave conditions indirectly do influence the short wave height at the reef, as larger incident wave conditions lead to a larger setup and thus higher water level.

2. *Across the reef flat*, the decay of short wave energy by friction is foremost regulated by the wave height, the water level, the roughness and the reef flat width [118], as can be deduced from Equation 2.10. The frictional dissipation is a function of the near-bottom wave orbital velocity and thus reef flat wave height [88], although this wave height is again controlled by the water level as explained above. Frictional dissipation increases for shallower water depths, larger widths and increased roughness [125], although there is a limit to which reef flat width extension is effective; at some point all short wave energy is dissipated.

3. At sloping reef flats wave breaking continues, although more gradual than at the steep interface of the forereef. This gradual reduction in wave energy and thus small radiation stress gradients lead to a much smaller setup than the setup at the forereef.

Wave setup

Wave setup is the increase in water level elevation (the pressure gradient) that balances the gradient in radiation stress caused by breaking waves, as described by the cross-shore momentum equation. The steady state, depth-integrated, wave-averaged momentum equation reduces to a balance between the radiation stress gradient and the pressure gradient under the assumption of zero time-averaged mass flux and a zero bottom stress [86][32]:

$$\underbrace{\frac{\partial S_{xx}}{\partial x}}_{\text{radiation stress gradient}} + \underbrace{\rho g(h_0+\bar{\eta})\frac{\partial \bar{\eta}}{\partial x}}_{\text{pressure gradient}} = 0 \tag{2.11}$$

where S_{xx} is the cross-shore component of the radiation stress, h_0 the still water depth and $\bar{\eta}$ the time averaged deviation around h_0, the setup (or setdown) [32]. Under the assumption of zero wave orbital motion below $\bar{\eta}$ and expressions for wave orbital velocities derived from linear wave theory (assumptions required to solve Equation 2.11 analytically) S_{xx} can be formulated as:

$$S_{xx} = E\left(2\frac{c_g}{c} - \frac{1}{2}\right) \quad \text{, where} \tag{2.12}$$

$$E = \frac{1}{8}\rho g H^2 \tag{2.13}$$

These formulations are used to analyze the setup at a reef, where two distinct setup zones are visible; at the shoreward end of the forereef (near the reef crest) and at the beach. The rapid reduction in water depth at the forereef causes a strong decay in wave energy due to localized wave breaking, resulting in large radiation stress gradients and thus setup [30]. This setup remains relatively constant throughout the reef flat due to the limited wave breaking at the flat and only gradual wave height reduction by frictional wave dissipation, which leads to marginal radiation stress gradients. An additional water level elevation is apparent at the beach, where waves that arrive at the toe cause a setup against the shore. This setup is easier to approximate as much research has been invested in setup at sandy beaches. As such, the setup at the beach is relatively easy to predict once the wave transformation processes at the reef are established. Therefore below all factors

influencing the setup at the forereef are elaborated.

Factors influencing setup

1. The forereef slope has a strong control on wave dissipation by breaking and friction and therefore setup [57]. At steeper forereef slopes, depth-limited wave breaking is confined to a smaller surfzone width (∂x in Equation 2.11), which leads to large radiation stress gradients and hence setup [32]. Furthermore, on steeper slopes, reduced frictional wave dissipation prior to wave breaking results in larger radiation stress gradients [30]. However, Quataert et al. [125] observe a limit to the increase in setup due to increasing slopes. At very steep slopes (steeper than 1:3), the magnitude of the bed stress decreases significantly as the bed stress is a function of the near-bed velocity in cross-shore direction, which is small in the large water depths of the steep slopes. This reduction in bed stress leads to a reduction in setup [125] [32].

2. The forereef roughness determines both the amount of frictional wave dissipation and the bed stress. As the forereef roughness increases, frictional dissipation prior to wave breaking increases, decreasing the setup [33]. However, enhanced roughness is also predicted to increase bed stresses due to the increased interaction of currents with the rough bottom profile, which enhances the setup [125][33]. Numerical simulations show the increase in bed stress counteracts the diminishing effect of increased frictional wave dissipation on the wave setup, causing Buckley et al. [33] to conclude that increasing the roughness at the forereef has no large net effect on wave setup reduction.

3. Higher water levels increase the maximum wave height of waves passing onto the reef, in accordance with the breaking criterion. This leads to a reduction in radiation stress gradients due to reduced depth-induced wave breaking, which, as dictated by the momentum balance described in Equation 2.11, results in a decrease in setup for larger water depths [125].

4. The setup increases nearly linearly with the incident short wave height due to the increased incoming wave energy. IG wave energy has little effect on the setup as bound long wave energy offshore of the breakpoint contributes only marginally to the wave energy budget [33].

5. Péquignet et al. [118] showed that the setup is not significantly influenced by reef flat width.

IG wave energy

IG wave generation, shoaling, frictional wave dissipation and dissipation by wave breaking are studied to assess the IG wave energy contribution to the runup. As summarized briefly in Section 2.2.1.1 and Section 2.2.1.2, two types of generation mechanisms for IG waves exist, the breakpoint mechanism and the release of shoaling bound long waves. Across reefs infragravity waves are primarily generated by the time-varying breakpoint [160]. They cause an increase in IG wave energy behind the breakpoint (often near the reef crest) and become increasingly dominant across the flat [160].

IG waves lose energy due to frictional dissipation and wave breaking. Where friction is generally negligible on sandy beaches, it is an important, currently assumed to be dominant dissipation mechanism of IG wave energy on coral reefs [122]. van Dongeren et al. [159] describe the bottom friction dissipation rate of the IG waves according to the formulation of Henderson [65]:

$$D_{bot} = f_{cw}\rho\left(\frac{g}{h}\right)^{3/2}\frac{H_{rms}}{\sqrt{8}}\frac{H_{rms,IG}^2}{8} \tag{2.14}$$

Near the shoreline IG wave energy decreases extensively due to wave breaking dissipation [21]. Here IG waves steepen to form a bore and then break [159], or are reflected at the shoreline. Short waves behind the crest of the steepened IG waves travel faster than the ones in the water level depression in front of the IG wave crest, in accordance with the shallow water wave speed of the linear wave theory, resulting in a bore-bore capture of short waves and hence a reduction of the number of short waves [159]. A possible formulation for the wave breaking dissipation rate is given by van Dongeren et al. [159]:

$$D_{br} = \alpha f_{low}\rho g\frac{H_{rms,IG}^2}{4} \tag{2.15}$$

The important factors affecting the phenomena of IG wave generation and dissipation are described below.

1. The relative contribution of the breakpoint generated waves and the released IG waves to the wave energy budget is foremost dependent on the forereef slope. Battjes et al. [18] distinguished two regimes, the mild-slope regime where shoaling waves are dominant and the steep-slope regime where breakpoint generated waves contribute most to the infragravity wave energy at the reef. This is confirmed by results of van Dongeren et al. [159], where the normalized bed slope parameter is found to be an indicator of the generation mechanism:

$$\beta_b = \frac{h_x}{\omega}\sqrt{\frac{g}{h_b}} \tag{2.16}$$

where h_x is the bed slope and h_b the breaking depth. The dominance of breakpoint generated waves on steep slopes can be attributed to the fact that short waves on steep slopes have limited adaptation time to transfer energy to the long wave before they break [161]. The effect and dominance of breakpoint oscillations is further enhanced for steep short waves typical for storm conditions [11]. Observations of IG wave energy at reefs by Pomeroy et al. [122], Buckley et al. [32] and Baldock [10] confirm the prevalence of the breakpoint mechanism and thus the radiation stress forcing. As a consequence, factors that influence the setup also affect the amount of IG wave energy: the water level, forereef slope, forereef roughness and incident wave conditions.

2. Wave reflection of IG waves at the beach is an important source of IG wave energy. van Dongeren et al. [159] describe the reflection R as a function of the beach slope h_x and height of the incoming long wave H_{IG}:

$$R = 0.2\pi\beta_{H_{IG}}^2 \quad \text{, where} \tag{2.17}$$

$$\beta_{H_{IG}} = \frac{h_x}{\omega}\sqrt{\frac{g}{H_{IG}}} \tag{2.18}$$

Therefore, a larger beach slope leads to a larger reflection at the coast.

3. As can be deduced from Equation 2.14, the frictional wave dissipation of IG waves depends foremost on the wave height, the reef flat roughness, the water depth and the reef flat width. IG wave breaking increases with increasing IG wave height and frequency.

Seiching

Amplification of the wave height by resonance at the reef flat is an additional source of energy. Waves can excessively impact the runup under certain conditions that trigger the excitation of resonant modes [37]. The open basin estimate gives an indication of the resonance period at a reef [113]:

$$T_n = \frac{4L}{(2n+1)\sqrt{gh}} \tag{2.19}$$

where L is the reef flat width, n the resonant mode (0,1,2, ..) and h the water depth above the reef flat. The resonance period shows a fluctuation in time due to changing hydrodynamic conditions (water level above the reef). If the incoming wave period matches the natural resonant period a resonance pattern appears with a fixed node at the reef crest and an antinode at the shoreline [116]. However, this pattern only develops when a second condition is met; the forcing frequency must exceed a certain threshold of frictional dissipation characteristics of the reef [123].

The effect of resonance is controlled by the reef's morphological characteristics and hydrodynamic forcing conditions. As short waves experience more frictional wave dissipation, amplification of energetic IG and VLF wave motions is most destructive for reef fronted coastal environments. The resonance period is mainly dictated by the reef flat width; wide reefs with a horizontal bottom promote the excitation of long wave resonance motions. Larger water depths lead to an increase of the natural frequency, but more importantly, a reduction in frictional dissipation which is especially important on wider reefs. Frictional dissipation is increased for a larger reef flat roughness.

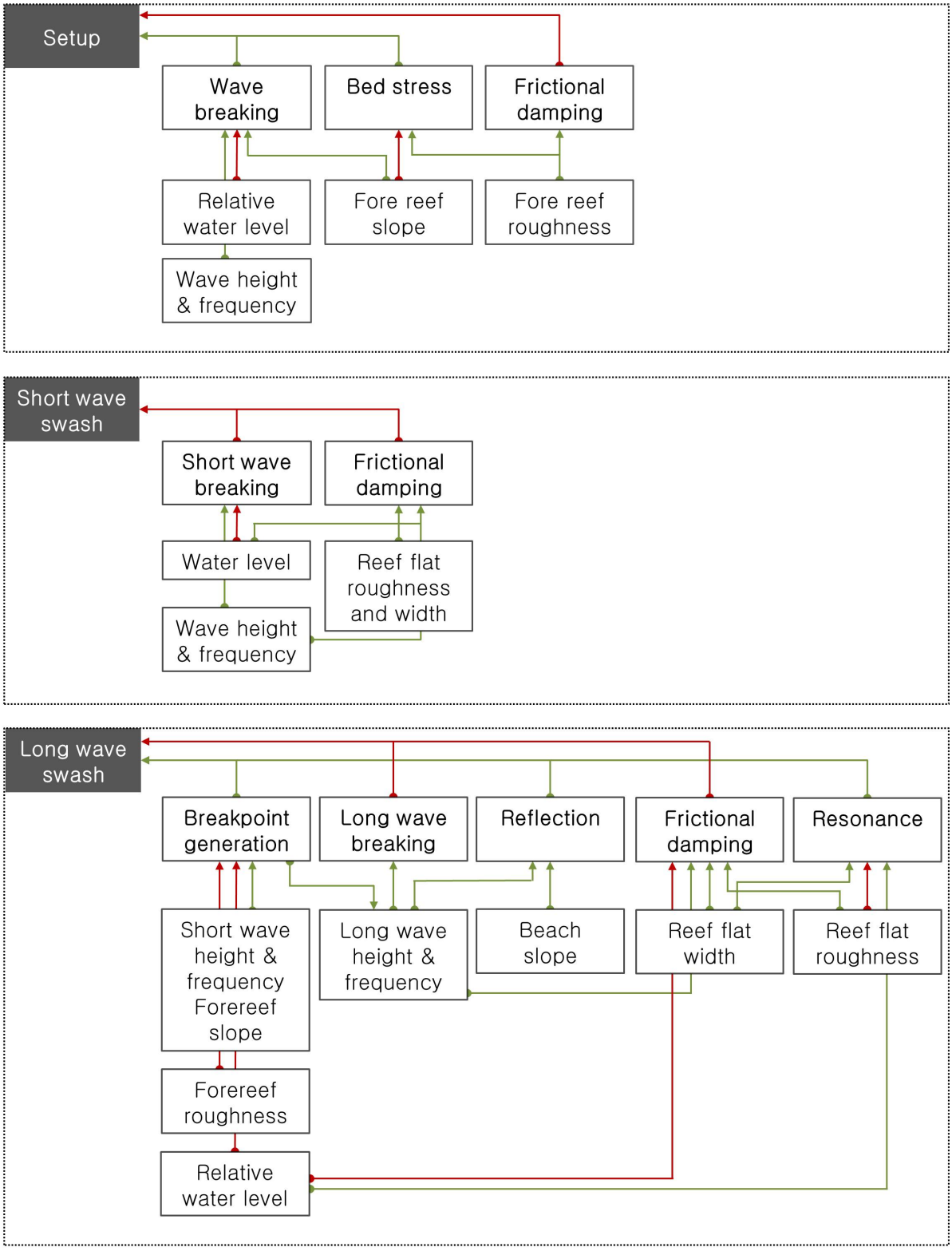

Figure 2.4: Summary of factors influencing the runup that have been described in Section 2.2.1.3, showing all hydrodynamic variables and reef morphological parameters that affect the setup, short wave and long wave component of the runup. Green arrows indicate a positive correlation: an increase in first factor leads to an increase of the next factor. Red arrows indicate a negative correlation.

2.2.2. In-canopy flow

In this section flow through the canopy is explored, as flow structures inside the reef have a significant effect on the survival and growth of benthic organisms, while canopy characteristics in turn have an effect on larger scale hydrodynamics by influencing the resistance encountered by the overlying flow [90][87]. Hydrodynamics at the scale of reef colonies have been described both qualitatively [101][87] and quantitatively [89][129]. A quantitative understanding of canopy flows remains challenging due to among others the limited optical and acoustic access to the interior of the reef [101], the computational effort required to resolve the turbulent flows and the large spatial variation in reef geometries and organisms [87]. To study the hydrodynamics within the reef, we start with a schematization of the canopy. Typically, the reef is depicted as multiple coral branches, where flow through either real coral structures [129] or idealized geometries (arrays of vertical cylinders) [89] is investigated. The flow in and above the canopy can be described by the spatially averaged, Reynolds-averaged Navier-Stokes equations on a horizontal plane [87]:

$$\frac{D\langle u\rangle}{Dt} = \underbrace{-\frac{1}{\rho}\frac{\partial\langle P\rangle}{\partial x}}_{\text{pressure gradient}} + \underbrace{\frac{1}{\rho}\frac{\partial\tau_{xy}}{\partial z}}_{\text{shear stress}} - \underbrace{f_x}_{\text{canopy resistance}} \tag{2.20}$$

Equation 2.20 shows that the acceleration of the canopy flow is driven by the pressure gradient and shear stress and counteracted by the canopy resistance. Below the relative dominance of these terms for different flow regimes is investigated, whereby a distinction between unidirectional and wave-driven flows is made.

2.2.2.1 Unidirectional flow over canopy

When a unidirectional current meets a submerged reef, a boundary layer develops due to the large velocity gradient perpendicular to the canopy as a result of the discontinuity in form drag [87], see Figure 2.5a. This leads to a vertical transfer of momentum and energy from the mean motion to the canopy flow. Momentum can also be horizontally transferred from the mean motion to the turbulent fluctuations around the coral stems, the wake turbulence (see Figure 2.5b).

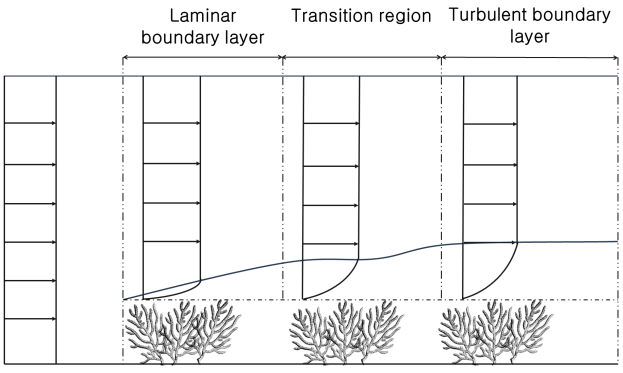

(a) Boundary layer turbulence at a reef

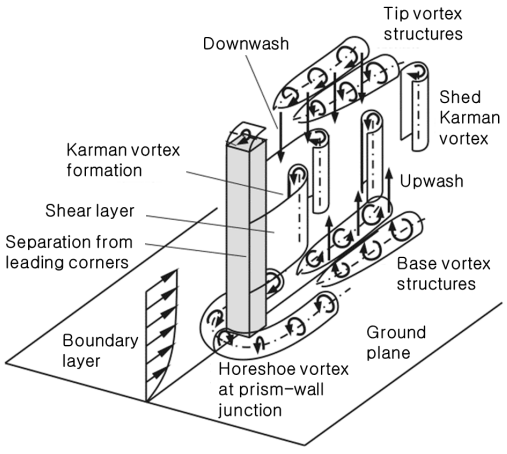

(b) Wake turbulence. Source: McClean and Sumner [97]

The exact in-situ flow structure of a unidirectional current over a canopy mainly depends on the ratio between the water depth (h) and the canopy height (h_c). This ratio controls the driving force of momentum transfer to the canopy [90]. Nepf and Vivoni [111] identify two zones inside the canopy, the upper 'vertical exchange zone' where shear-driven momentum transfer is important, and the lower 'longitudinal exchange zone' where drag by vegetation and the pressure gradient control the momentum transfer. The extend of these zones depends on the ratio h/h_c. In general, three canopy flow regimes with different h/h_c ratios can be discerned; the unconfined flow (water depth much larger than the canopy height), the depth limited flow (water depth above the canopy similar to the canopy height) and the emergent flow (canopy height (almost) reaches water surface) [87].

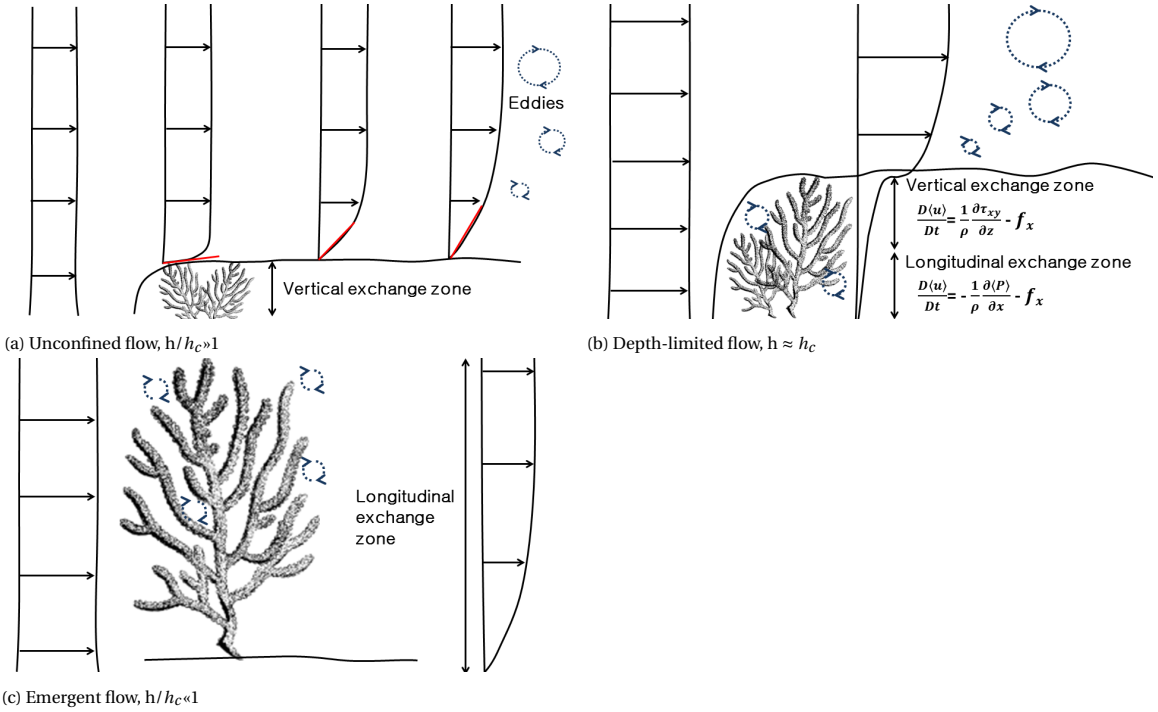

(a) Unconfined flow, h/h_c»1

(b) Depth-limited flow, h ≈ h_c

(c) Emergent flow, h/h_c«1

Figure 2.6: Velocity profiles for different ratios of the water depth over the canopy height for unidirectional currents

In *unconfined flows*, a boundary layer develops as depicted in Figure 2.5a [87]. The shear layer at the top of the reef dominates the turbulent transport [111]. At the reef top velocity gradients are largest, leading to large associated shear stresses at this location. Wake turbulence of individual coral branches is of minor influence on the turbulence budget in unconfined flows [127]. Hence, for unconfined flows the in-canopy flow is driven by a balance between the form drag and shear stress. The 'vertical exchange zone' of the canopy extends throughout its entire height, see Figure 2.6a.
When we decrease the ratio h/h_c, the flow becomes *depth limited*. In this intermediate flow regime two distinct zones are visible (see Figure 2.6b). In the upper layer of the canopy, flow is dominated by vertical exchange as a result of mixing layer (shear) turbulence. Flow in the lower layers is controlled by longitudinal exchange through advection, where turbulence is produced by wakes around the stems [111]. Lastly, for very small ratios of h/h_c, the reef becomes *emergent*. Here only a 'longitudinal exchange zone' is visible. The flow is completely driven by the pressure gradient and all turbulence is generated by wake turbulence [111]. This situation is depicted in Figure 2.6c.

2.2.2.2 Wave-driven flow over canopy

Lowe and Falter [87] list two fundamental differences between unidirectional and wave-driven flows: (1) the latter induces large oscillatory pressure gradients and (2) the flow resistance is larger for wave-driven flows due to the accelerations inside the canopy that add an inertial force. Recent studies have shown the flow enhancement inside the canopy by oscillating (wave-driven) flows in comparison with unidirectional flows. Reidenbach et al. [129] measured an increase of factor 10 to 15 in hydrodynamic forces and peak shear stresses on top of the reef when accounting for wave motions. More generally, Lowe et al. [89] show the dependence of flow enhancement on the wave kinematics and the geometry of the canopy. They derived the following equation that governs the oscillatory canopy flow:

$$\frac{\partial(\hat{U}_w - U_{\infty,w})}{\partial t} = \underbrace{\left(\frac{A_\infty^{rms}}{L_s}\right)|U_{\infty,w}|U_{\infty,w}}_{\text{shear}} - \underbrace{\left(\frac{A_\infty^{rms}}{L_d}\right)|\hat{U}_w|\hat{U}_w}_{\text{drag}} - \underbrace{\frac{C_M\lambda_p}{1-\lambda_p}\frac{\partial \hat{U}_w}{\partial t}}_{\text{inertial force}} \tag{2.21}$$

where:

- $U_{\infty,w}$= the canopy independent velocity

- $\hat{U}_w$= the canopy vertically averaged, unsteady velocity component of the oscillatory flow
- C_M= empirical inertia coefficient
- $\lambda_p = A_p / A_T$ where A_p is the plan area of the canopy element and A_T the total canopy area divided by the number of elements [89]
- $A_\infty^{rms} = U_\infty^{rms}/\omega$ is "the rms wave orbital excursion length of the free-stream potential flow" [89]
- L_s is the canopy shear length scale and L_d is a canopy drag length scale (see Lowe et al. [89])

The dimensionless parameters A_∞^{rms}/L_s, A_∞^{rms}/L_d and $C_M\lambda_p/(1-\lambda_p)$ define the relative importance of respectively the shear, the drag and the inertial force. Based on these three parameters, three regimes can be distinguished: the canopy independent flow, the inertia force dominated flow and the unidirectional limit. For low density canopies with small orbital excursion lengths relative to the canopy drag and shear length scales, the flow is *canopy independent*. Due to the small value of λ_p (canopy density) the inertia is negligible, which can be deduced from Equation 2.21. The shear and drag are small due to the small values of $A_\infty^{rms}/\ L_d$ and $A_\infty^{rms}/\ L_s$. The in-canopy flow is therefore hardly reduced compared to the flow above the canopy and is driven by the oscillatory pressure gradient [89]. When $A_\infty^{rms}/\ L_d$ and $A_\infty^{rms}/\ L_s$ are still small but the canopy density high, the canopy elements interact with the flow and attenuate the canopy flow. The flow is *inertia force dominated*. With increasing A_∞^{rms} the canopy flow decreases due to the increased shear and drag. For very high values of $A_\infty^{rms}/\ L_d$ and $A_\infty^{rms}/\ L_s$ the flow approaches the *unidirectional limit*. A balance exists again between the shear stress and canopy drag [89].

2.2.2.3 Modeling the effect of in-canopy flow characteristics

The in-canopy hydrodynamics have a significant effect on larger scale flow and wave characteristics. In this research, main focus is on the accurate modeling of wave dissipation processes as function of the reef features. Two approaches exist to model the effect of in-canopy hydrodynamics on wave energy dissipation, the *bottom friction approach* and the *cylinder approach* [155]. In the bottom friction approach, vegetation is accounted for in a bottom friction parameter that increases for increasing roughness and structural complexity of the canopy. In this approach, a boundary layer flow as depicted in Figure 2.5a is assumed for all flow regimes and canopy characteristics. In the cylinder approach, the canopy is modeled as a structural element where dissipation is estimated by the actual vegetation induced forces [155], a method first suggested by Dalrymple et al. [41]. This method offers a more physics-based approach to vegetation modeling compared to the bottom friction approach, although the latter is still implemented widely in studies on reef hydrodynamics.

The theory on in-canopy flows is an important factor in the determination of the model with which to represent the wave transformation at the reef scale. If, for instance, the flow is depth limited or emergent, one should wonder whether the physics of a system are accurately captured by a single bottom friction parameter, as complex turbulent structures across the vegetation field are often observed that are generally better captured by the cylinder approach [155]. Hence, the theory on in-canopy flows not only gives insight into the physical processes that induce wave dissipation by the coral canopy, but also gives the theoretical background to the limitations of the bottom friction and canopy model approach.

2.3. Coral restoration techniques

Knowledge of and experience with coral reef restoration is developing fast, mainly due to widespread coral degradation that asks for active intervention. A comprehensive overview of restoration approaches is given by Zimmer [177], where a distinction is made between *Indirect action* (Reef protection), *Reef repair*, *Coral transplantation* and *Artificial reefs*. Below the first two techniques are briefly described, after which a more comprehensive elaboration of the latter two techniques, both coral construction methods, follows. Reason for this is the large scale applicability of coral transplantation and artificial structures which makes them suitable for our research purpose. Important to note is the assumption that by restoring corals we can restore the entire reef ecosystem by assisting natural recovery processes [46]. This assumption is substantiated by the fact that corals are the keystone species in the reef ecosystem as they provide habitat, shelter and accreting elements for the ecosystem [46]. Opel et al. [115] support this notion by confirming the link between the biodiversity and abundance of biotic communities and the coral cover.

2.3.1. Reef protection

Reef protection comprehends the elimination and prevention of anthropogenic disturbances. Possible sources of reef stress due to human activities are among others fresh-water runoff, nutrient loading, vessel grounding and sedimentation [177]. For resilient reefs with manageable damage, elimination of stress factors is sufficient for the reef to grow back to its full potential [48]. However, severe damage requires active intervention in the system, in which case reef protection is supplemented by active restoration techniques. It should be emphasized that before actively intervening in the coral ecosystem, chronic disturbances should be eradicated for a measure to be effective on the long term [135].

2.3.2. Reef repair

Reef repair techniques involve *emergency triage*, the restoration of *structural integrity* and restoration of *topographic complexity* [177]. Storms and other environmental hazards such as vessel grounding, blast fishing and coral mining dislodge and destabilize coral [20], creating a bed of coral rubble and other debris. Edwards et al. [47] call these beds 'killing fields for young coral', as rubble smothers the coral larvae. In sheltered conditions the disturbance of coral rubble is negligible, but under regular wave forcing the rubble beds can have an extensive impact on the health of the ecosystem. Therefore, *(emergency) triage* is often executed whereby loose beds are either removed or stabilized. Stabilization methods range from the placement of plastic mashes to the deployment of limestone boulders [47]. Triage also involves the reattachment of recovered coral heads onto the reef using materials such as epoxy, nails, rod and wire and cement [177].
Irregularities in the reef structure such as fractures and craters, often the result of single-event disturbances such as storms and vessel groundings, should be repaired as the *structural integrity* is important for the reef's coastal protection function [20]. Projects to improve the structural integrity include the filling of craters with gravel, rock, rubble or armouring units and stabilization of cracks by concrete and steel bars [177].
Next to the structural complexity, topographic complexity is an important characteristic of a healthy reef as it influences coral recruitment and biodiversity [177]. Topographic restoration is mainly aimed at improving the substrate for coral recruitment by creating relief, often using concrete or limestone. The surface of the concrete or limestone is shaped by adding small rocks/coarse sediment, drilling holes or by attaching protruding elements, in order to achieve a fitting surface rugosity [177].
All aforementioned physical reef repair techniques have proved valuable but are often inefficient due to the high costs of labour and material.

2.3.3. Reef construction

2.3.3.1 Coral transplantation

Coral transplantation is the most widely applied active restoration technique, whereby coral is collected from a healthy reef, to be either transplanted directly to a degraded reef or to be raised in a nursery and then placed back onto the restoration site [62]. Stages of the transplantation process are the *sourcing* of coral transplants, the *coral culture* and the *attachment of coral transplants* [46].

Sourcing Coral transplants are retrieved from existing reef structures, often as small fragments. These fragments can originate from detached coral branches or from healthy donor colonies. The collateral damage of transplantation can be minimized by applying the first technique of collecting live loose corals [46]. However, living detached coral branches are not always available, or they do not represent the robust species present at a reef. Therefore, one might need to resort to taking transplants from living branching corals, which should be done with caution to prevent degradation of the donor colony [46].

Coral culture During early coral restoration projects, immediate reattachment of corals retrieved from a donor site to the restoration site was advocated [135]. However, when the pitfalls of this technique became apparent (negative impact on both the donor colony and the transplants [135]), concepts surfaced where corals where cultured in a nursery. In general two types of nurseries exist, the in-situ coral farms that are located in sheltered coastal areas and the ex-situ nurseries that are in effect large aquariums in which corals are reproduced [46]. The mid-water nurseries are a cost efficient option and studies by Rinkevich [135][134] show the success of the approach. If located in optimal conditions (sheltered, away from other activities, away from other reef structures), large colonies can grow from the transplants. Ex-situ nurseries, although more expensive, have several advantages over in-situ nurseries. Firstly, the hydrodynamic conditions can be accurately controlled [47] and natural hazards such as storms and warming events are averted [62]. Secondly, innovative techniques used on land based farms can improve growth rates and species diversity. It is even possible to increase the resiliency of corals to climatic threats by using assisted evolution techniques [62]. Therefore, among others Halpern and Teicher [62] argue that ex-situ farming is the method to be used for large scale restoration efforts.

Attachment of transplants The attachment of transplants is a critical factor in the restoration process. Edwards et al. [47] have defined three factors on which attachment properties depend: the hydrodynamic exposure, the size of the transplants and the substrate of the reef. In highly sheltered conditions, attachment is not required as corals will stay in place without a fixation. Under all other conditions, corals are fixed to a substrate with materials ranging from epoxy adhesives to wires, ties and nails [47]. They can be attached to dead coral or coral rock, or artificial substrates such as reef balls (see Section 2.3.3.2). Natural or hand-drilled holes are often used to install the reef transplant, with the use of cement or epoxy adhesive as binder.

2.3.3.2 Artificial reef construction

Artificial reefs are man-made underwater structures which serve as a shelter for waves and currents. Generally, artificial reefs are considered when aforementioned reef restoration options have proved insufficient [177]. Different functions are attributed to the artificial reef structure, among others the provision of substrate for coral and other reef biota, the decrease in wave action and the increase in topographic complexity [46] [177]. Critical notes have also been made. When improperly installed, displaced artificial reef structures can aggravate reef destruction. Furthermore, in theory there is plenty of hard substrate available for corals to grow on which alleviates the need for artificial substrates [46]. What is more, natural recovery processes can be disrupted and naturally occurring species could be displaced. Then again, the immediate decrease in water level above the reef caused by the raised elevation of the structure promotes depth-induced wave breaking which leads to a decrease in wave height. In this way, artificial reefs act as a natural submerged breakwater and improve coastal safety [128]. The most common types of artificial reefs are the ReefBall®, EcoReefs® and Biorock®, see Figure 2.7.

The *ReefBall*® is a hollow concrete module whose pH is similar to water to mimic the structure and characteristics of the marine environment [14]. Their size ranges between 0.3 and 1.5 meters. They are easy to construct, using simple mold constructions and easily accessible products. Furthermore, they can be floated to the restoration site [14].
EcoReefs® are ceramic modules of snowflake pieces that mimic branching corals [103]. The snowflake structure provides a large surface area for coral settlement, which is also enhanced by the micro porous, non-toxic surface of the ceramic [103]. Transplanted corals can be attached by simple ties. Information on EcoReefs® is however sparse compared to the large database of ReefBall® projects.
The *Biorock*® technique mimics the natural mineral accretion process by electrolysis, whereby natural minerals attach to a steel structure and form a hard limestone coating [173]. The composition of the created surface is similar to natural coral reefs, which increases coral recruitment rates. Biorocks are easy to construct.

(a) ReefBall

(b) EcoReefs

(c) Biorock

(d) Corals growing on ReefBall

(e) Corals growing on EcoReefs

(f) Corals growing on Biorock

Figure 2.7: The three promising artificial reef units; depicted in the upper row the modules just after installation, in the bottom row after significant coral recruitment. Sources: a), d): [14] ; b), e): [45] ; c): [100] ; f): [39]

3

Thesis outline and objectives

Based on the defined problem statement (Chapter 1), a literature review was conducted to obtain an overview of the state of the art research (Chapter 2). This facilitates the expression of research objectives that are well suited to tackle the knowledge gaps. Below, the resulting research questions and objectives are stated, after which the thesis outline is explained.

3.1. Research objectives

The prediction of the wave transformation over reef morphologies is complex, however we are starting to understand the reef hydrodynamics and the connection between offshore wave forcing, the reef geomorphology and the resulting runup. Much of this research, however, is dedicated to the fringing reef type, leaving topics such as the predominance of other reef profile shapes and their influence on wave transformation and runup at the reef lined coast relatively unexplored. How to reduce this runup using coral restoration is an even newer field of research. Large knowledge gaps are left to investigate on the topic of coral restoration for coastal protection. Among others, reef hydrodynamic processes resulting from restorations are unidentified, as well as their location of maximum potential, both alongshore and in the cross-shore zone. Consequently, this research was initiated in which the following main question is covered:

> *How can we efficiently decrease runup across various reef morphologies by restoring the coral, taking into account intrinsic reef (hydrodynamic) processes and practical and operational limits of coral restoration techniques?*

Four subquestions are identified that together elucidate the main research question, with corresponding research objectives:

1. *What are the key hydrodynamic processes that drive inundation and flooding of reef fronted coastlines?*
    (a) Analyze results of numerical modeling studies by Pearson [116] and Quataert [124] (1) to inspect the relative importance of hydrodynamic forcing conditions and profile parameters on runup at reef lined coasts and (2) to parametrize wave transformation and flooding processes across coral reefs.
    (b) Establish a reef hydrodynamic model to predict wave transformation and flooding across reef fronted coastlines, in order (1) to verify where along the cross-shore coral restoration can be effective and (2) to predict the drivers of flooding under varying conditions and for varying reef geometries, which helps to determine the restoration strategy.
2. *How can a large number of coral reef bathymetries be classified into a limited amount of reef profile groups, based on the essential morphological features of the reef geometries?*
    (a) Establish a cluster (grouping) model that captures the important geometric characteristics of reef profiles.

   (b) Identify dominant reef profile shapes based on the profile classification results.

3. *How do varying reef geometries influence wave transformation and flooding?*

   (a) Analyze wave transformation characteristics across varying profile shapes.

   (b) Identify reef profile types most vulnerable to flooding and inundation.

4. *What are the hydrodynamic effects of varying coral restoration configurations, across varying reef shapes, and how does this affect their runup reduction potential?*

   (a) Define restoration configurations based on the practical, operational and computational feasibility of the restoration.

   (b) Describe the key alterations to the reef hydrodynamics induced by coral restorations, under varying forcing conditions.

   (c) Identify restoration configurations with runup reduction potential.

3.2. Thesis outline

This thesis is structured on the basis of the four research questions. Below, the thesis chapters and corresponding research questions are indicated. The four main chapters (Chapters 4, 5, 7 and 8) all consist of a separate Conclusion and Discussion section for clarity of the results, which are then shortly summarized in the final Conclusion (Chapter 9).

Part I: System Analysis

Part II: Data analysis and model synthesis

Ch 4. Reef hydrodynamic model - Subquestion 1

Ch 5. Reef profile variability - Subquestion 2

Part III: Numerical Simulations

Ch 6. Methodology

Ch 7. Reef geometry control on nearshore hydrodynamics - Subquestion 3

Ch 8. Effects of coral restoration on reef hydrodynamics and coastal hazards - Subquestion 4

Part IV: Conclusions and Recommendations

II

Data Analysis and Model Synthesis

In order to evaluate the runup reduction potential of restoration configurations at varying coral reef morphologies, an insight into the actual flood vulnerability and drivers of inundation at reef lined coasts is essential, as well as an insight into the predominance of different reef morphologies.

Ch 4. Reef hydrodynamic model

Ch 5. Reef profile classification

4

Reef hydrodynamic model

4.1. Introduction

The hydrodynamic behaviour and flood vulnerability of low-lying reef environments is capricious in nature, due to the large variation in forcing conditions and many non-linear interactions between reef morphology and hydrodynamics, as illustrated by Figure 2.4. For this reason a simplified tool is created, with which the complex water level variations across a variety of reefs can be modeled, in order to predict the dominant drivers of runup at the coast. Based on this knowledge, restoration strategies tailored to the on-site conditions can be designed. Moreover, with this rapidly solving reef hydrodynamic model, it is possible to generate an overview of the flood vulnerability for a large number of coastal sections, giving insight into the locations where the need for restoration is high. In this chapter, the reef hydrodynamic model is elaborated, that is constructed based on a data analysis of fringing reef simulations by Pearson [116] and an evaluation of existing analytical expressions for wave transformation and dissipation.

4.2. Model Formulation

In Figure 4.1 an overview of the reef hydrodynamic model is depicted. The model domain consists of a 1D cross-shore grid that can be generated by the model, based on user specified parameters for the forereef and beach slope, the reef width and the water level above the reef. Alternatively any arbitrary reef profile can be imported as vectors with x-coordinates and corresponding depths.

In summary, the short wave transformation and mean water level variations between the offshore boundary and the beach toe are resolved by the simultaneous integration of the short wave energy balance and the cross-shore momentum balance, according to the equations in the upper part of Figure 4.1, as first described by Battjes and Janssen [16]. The IG wave generation is empirically derived based on the dataset of Pearson [116], while the IG wave propagation is solved by the IG wave energy balance between the reef crest and the beach toe following the approach of van Dongeren et al. [159]. Based on the obtained wave heights and water levels at the beach toe, the runup is predicted using formulations from literature that are validated with the XBeach dataset of Pearson [116]. The model returns the wave breaking -and frictional wave dissipation as a function of the cross-shore distance, the wave energy transformation of short and IG waves across the reef, the setup and an estimate of the runup.

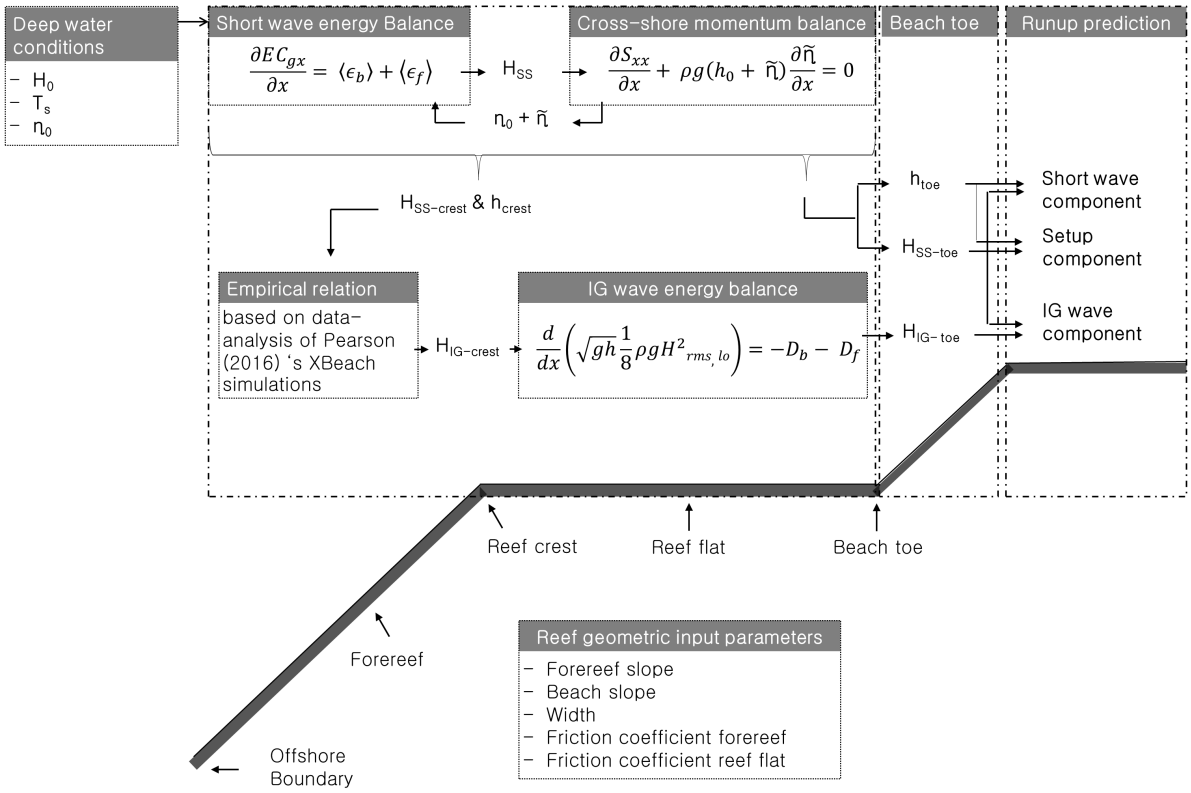

Figure 4.1: Schematization of the simplified reef hydrodynamic model, showing how the runup is calculated based on beach toe wave heights and water levels, which are calculated based on the short wave energy balance, the cross-shore momentum balance, an empirical formulation for the infragravity wave height at the reef crest and the IG wave energy balance between the reef crest and the beach toe. Input parameters are the deep water conditions and the reef geometric parameters, that need to be supplied by the user.

4.2.1. Short wave transformation

The short wave transformation is modeled using Battjes and Janssen [16]'s two step iteration process for solving the wave height and water level variations simultaneously. First, the wave energy balance is solved:

$$\frac{\partial EC_{gx}}{\partial x} = \langle \epsilon_b \rangle + \langle \epsilon_f \rangle \tag{4.1}$$

The radiation stress gradient as a result of the cross-shore wave height variation induces a water level variation:

$$\underbrace{\frac{\partial S_{xx}}{\partial x}}_{\text{radiation stress gradient}} + \underbrace{\rho g(h_0 + \bar{\eta})\frac{\partial \bar{\eta}}{\partial x}}_{\text{pressure gradient}} = 0 \tag{4.2}$$

This water level variation is used to recompute the wave height with Equation 4.1. Below the wave breaking dissipation (ϵ_b) and the frictional wave dissipation (ϵ_f) terms are elaborated.

4.2.1.1 Dissipation by wave breaking

The dissipation by wave breaking is generally solved using parametric wave breaking models, that describe sea state characteristics using time averaged, local parameters [13]; the local wave height H_{rms}, the water depth, the wave frequency and the fraction of breaking waves Q_B. Parametric wave models are computationally efficient and therefore often used [13]. Among others, Battjes and Janssen [16], Baldock et al. [13] and Janssen and Battjes [73] formulated wave breaking models, all with different model assumptions and limitations. In these models, the wave breaking dissipation is foremost dependent on the wave height H_{rms} relative to the maximum breaker height H_b. But while the breaking wave height H_b strongly affects the wave transformation process, its prediction is mainly based on (semi-)empirical formula with limited validity [74]. Overviews of breaking wave characteristics are given by Jensen [74] and Robertson et al. [137]. They underline

that no single value of the wave breaking parameter exists and that knowledge of the local wave climate and bathymetry is of essence for the choice of formulation. Among others Baldock et al. [13], Battjes and Janssen [16], Battjes and Stive [17], Ruessink et al. [143] and Kamphuis [76] studied the maximum wave height to depth ratio (γ) at sandy beaches, which was shown to be dependent on, among others, the wave length, the bottom slope and the wave steepness. Gourlay [56] focused on wave transformation on fringing reefs, for which a single breaking wave parameter was more difficult to parametrize. Consistent with analyses of field and laboratory data for breaking waves on steep reef fronts by Nelson et al. [110], different breaking regimes were established based on which a γ factor could be identified.
To maximize the accuracy of the hydrodynamic model, different parametric wave breaking models (the Battjes and Janssen [16], Baldock et al. [13] and Janssen and Battjes [73] model) and breaker height formulations (by Battjes and Janssen [16], Battjes and Stive [17], Ruessink et al. [143], Kamphuis [76], Massel and Gourlay [93] and Su et al. [154]) are elaborated in Appendix A.1. Their validity is tested by comparing results of the different model formulations to laboratory experiments of Buckley et al. [32]. The results are depicted in Appendix A. The stable wave model of Janssen and Battjes [73] is best able to capture wave dissipation across reefs (see Figure A.2 in Appendix A). For this model, breaker height formulations are less dominant in the prediction of the wave transformation. As the breaker height formulation by Su et al. [154] is especially derived for reef lined coasts, based on the Janssen and Battjes [73] model, this breaker height formulation is recommended.

4.2.1.2 Dissipation by friction

The time-averaged short wave dissipation by friction is modeled according to XBeach [138]:

$$\langle \epsilon_f \rangle = \frac{2}{3\pi} \rho f_w \left(\frac{\pi H_{rms}}{T_{m01} sinh(kh)} \right)^3 \tag{4.3}$$

This formulation is derived from the instantaneous bed shear stress combined with an expression for the third even velocity moment [59]:

$$\langle \epsilon_f \rangle = \langle |\tau u| \rangle = \frac{1}{2} \rho f_w \langle |\tilde{u}|^3 \rangle \tag{4.4}$$

where

$$\langle |\tilde{u}|^3 \rangle = 0.42 * u_{orb}^3 = 0.42 * \left(\frac{\pi H_{rms}}{T_p sinh(kh)} \right)^3 \tag{4.5}$$

4.2.2. IG wave transformation

No simple formulations relating the IG wave height to offshore wave parameters exist. However, much information on the IG wave height transformation at reefs can be gathered from the large XBeach database of Pearson [116], consisting of 1D non-hydrostatic XBeach simulations of a fringing reef, with differing reef widths, forereef slopes, beach slopes, roughness values and hydrodynamic input conditions. From this database, semi-empirical formulations can be deduced.

As was observed by among others Pearson [116], Pomeroy et al. [122], Van Dongeren et al. [160] and Masselink et al. [94], the main input of IG wave energy is generally delivered by the breakpoint mechanism, due to which the IG wave height strongly increases across the forereef. At the reef crest, often a decrease in energy is observed, due to reflection and wave dissipation [162]. Behind this point, frictional wave dissipation generally causes a decay of IG waves across the reef flat [160], although resonant forcing can increase the IG wave energy across the reef flat [119].

The XBeach results for the extreme water level elevations and the influence of different model parameters are depicted in Figure 4.2 (reef crest) and Figure 4.3 (beach toe). Based on Figures 4.2 and 4.3, it is possible to distinguish the factors that influence the IG wave height at the two locations. Note that the IG component of the extreme water level is interpreted as half the IG wave height that is exceeded by 2 % of the waves $H_{2\%}$. In further analyses, no distinction between IG and VLF waves is made (both are infragravity motions).

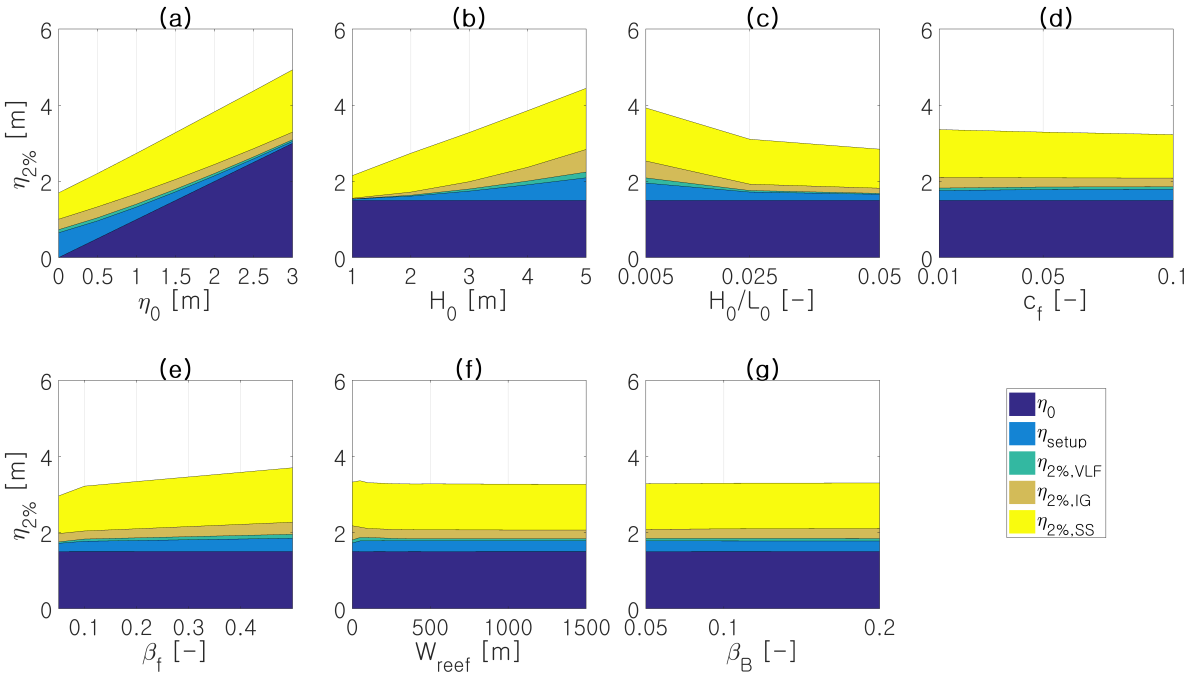

Figure 4.2: Model variables influencing the extreme water level at the reef crest: the water level, the wave height, the wave steepness, the friction coefficient, the forereef slope, the reef width and the beach slope, respectively

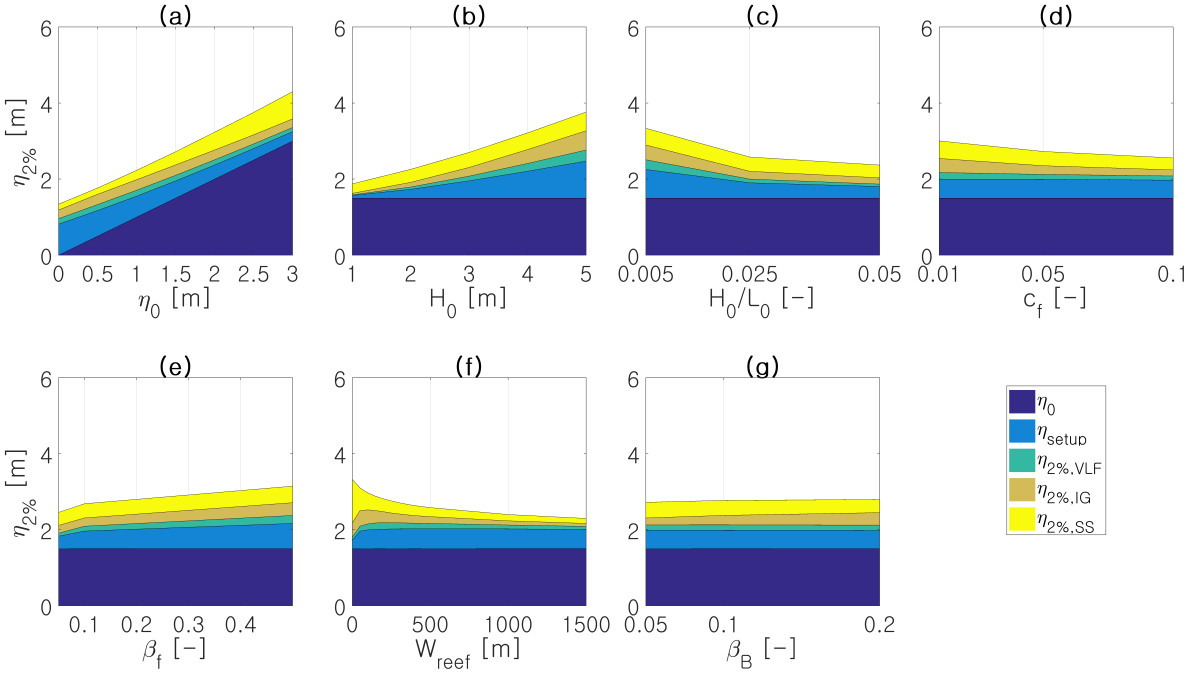

Figure 4.3: Model variables influencing the extreme water level at the beach toe: the water level, the wave height, the wave steepness, the friction coefficient, the forereef slope, the reef width and the beach slope, respectively

The results shown in Figure 4.2 for the IG wave height at the reef crest are in line with the expectations from the literature review. As the water level increases, H_{SS} increases while H_{IG} and the setup decrease due to the reduced breakpoint forcing. Furthermore, as H_0 increases, H_{SS} first increases slightly (here the surfzone is unsaturated), after which it stays constant; now H_{SS} is solely a function of the water depth. An increase in forereef slope results in an increase in H_{IG}, due to the enhancement of the breakpoint mechanism. From Figure 4.3 it is thus clear that the water level above the reef flat (η_0), the incident wave height H_0, the wave

length L_0 and the forereef slope β_f primarily influence the IG wave height at the reef crest, a finding that is supported by Masselink et al. [94]. The IG wave height at the beach toe (see Figure 4.3) is, in addition to the model parameters described above, influenced by the width of the reef and the roughness (due to frictional wave damping) and the beach slope that influences the amount of reflection. As reflected waves are damped while propagating offshore, the effect of reflection is less visible at the reef crest.

Ideally an empirical formulation for the IG wave height at the beach toe as a function of all above mentioned model parameters is found. However, due to non-linear interactions between model parameters it is difficult to find such a formulation. Therefore, the reef hydrodynamic model describes the IG wave generation and transformation in two steps. First, IG waves are 'generated' at the reef crest based on the derived semi-empirical relations, assuming that breakpoint generated waves are dominant and that their approximate wave height is reached at the reef crest. The second step is the propagation and dissipation of the IG waves across the reef flat up to the beach toe.

4.2.2.1 IG wave generation

There are two options to obtain the IG wave height at the reef crest. A first option is finding the best fit between input conditions of the conceptual model and the XBeach simulations and directly using the XBeach IG wave height output. However, a standalone, accessible formulation is preferred for the ease of use and computational speed. Therefore, the four model parameters H_0, η_0, L_0 and β_f are input for the linear regression analysis that is outlined below.

Analyses of the IG wave height at the crest against model parameters show that clear patterns are only found when the IG wave height is normalized by the water level relative to the reef flat η_0. This can be explained by the fact that the water level controls both the wave dissipation, the setup and the breakpoint mechanism; higher water levels lead to increased short wave transmission across the reef but reduced setup and IG wave generation. This opposite influence of η_0 on short and IG wave heights could be the cause of the goodness of fit for normalized IG wave heights compared to non-normalized IG wave heights.

The obtained dimensionless parameter H_{IG}/η_0 (H_{IG} is defined as the significant wave height) is now formulated as a function of the four previously denoted model parameters:

$$\frac{H_{IG-crest}}{\eta_0} = f(\beta_f^a H_0^b \eta_0^{-c} L_0^d) \quad [-] \tag{4.6}$$

In order to obtain a dimensionless combination of the four model parameters, the coefficients b and d should be equal to c. Next to this formulation, we also explore the IG wave generation for filtered wave lengths, as in general the wave length is of large (non-linear) influence on the IG wave height, which complicates the deduction of accurate formulations. The IG wave height at the crest is now formulated for each wave length separately :

$$\frac{H_{IG}}{\eta_0} = f(\beta_f^a H_0^b \eta_0^{-c}) \quad [-] \tag{4.7}$$

in which the coefficient b should be equal to c to preserve the dimensionlessness. The coefficients of Equations 4.6 and 4.7 are found by an optimization algorithm that searches the combination of coefficients that gives the best expression for the IG wave height at the crest. The goodness of fit is evaluated by the coefficient of determination R^2, which is a measure of the prediction accuracy of a fitted function:

$$R^2 = 1 - \frac{\sum_{i=1}^{n}(y_i - \hat{y}_i)^2}{\sum_{i=1}^{n}(y_i - \bar{y}_i)^2} \tag{4.8}$$

where $\hat{y}$ is the fitted value for H_{IG}/η_0 and $\bar{y}$ the mean H_{IG}/η_0 value. Optimization of the R^2 value gives the optimal coefficients. The coefficients of Equation 4.6 are plotted in Figure 4.4 and read:

$$\frac{H_{IG}}{\eta_0} = f(\beta_f^{0.35} H_0^{0.65} \eta_0^{-1.27} L^{0.61}) \quad [-] \tag{4.9}$$

The formulations for filtered wave lengths are visualized in Figure 4.6. The original dataset contains 12 distinct wave periods as input. However, the input wave period is linked to the input wave height, resulting in

filtered wave length plots where only one wave height is simulated. Therefore, based on preliminary results wave length bins are formed that are analyzed separately. Several conclusions can be drawn from Figures 4.4 and 4.6:

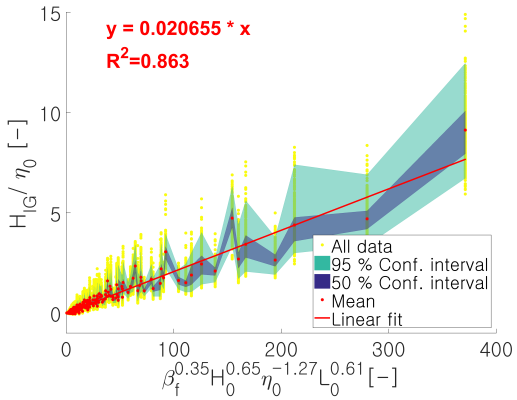

Figure 4.4: Plot of the dimensionless IG wave height calculated by XBeach versus the empirical formulation described by Equation 4.9

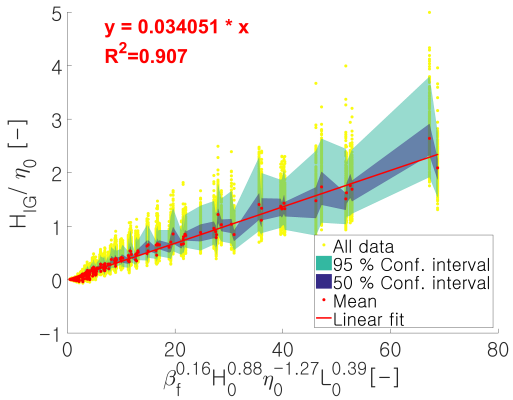

Figure 4.5: Plot of the dimensionless IG wave height calculated by XBeach versus the empirical formulation described by Equation 4.6, with removal of the swell waves

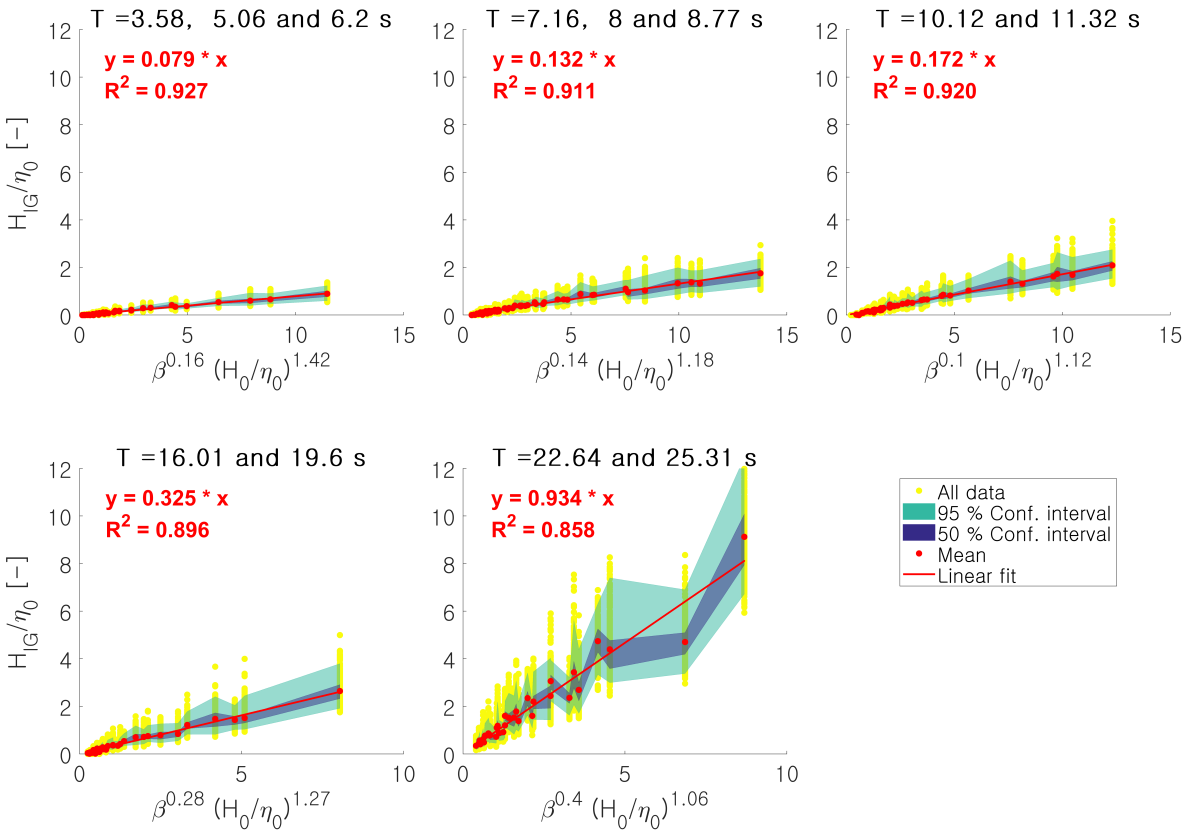

Figure 4.6: Plot of the dimensionless IG wave height calculated by XBeach versus optimized empirical formulations, sorted per wave period

- For smaller wave periods, the IG wave height prediction is more accurate than for larger (swell) period waves (periods between 20 and 25 s). A possible cause for this is the distinction between the wave components. The wave heights of the different wave components (SS, VLF and IG) are determined

based on rather arbitrary, predefined cutoff frequencies that determine which part of the wave energy belongs to which component. As the cutoff frequency between the SS and IG waves maintained by Pearson [116] is 0.04 Hz (25 s), part of the incident short wave energy can be assigned to the IG wave energy, blurring the results. As swell waves are the cause for large scatter in Figure 4.4, the figure is replotted with elimination of the two largest periods, see Figure 4.5. This indeed improves the results.

- The coefficients of the prediction formulations give an insight into the importance of different parameters. The coefficients of Equation 4.9 indicates that the wave height is the primary influencing factor.
- Both Figure 4.4 and 4.6 show a good correlation between the plotted data and the fitted function. However, it is interesting to verify which factors could induce the scatter in the data. To this effect, both figures are replotted with colour filters for η_o, H_0, the steepness, C_f, β_f, β_b and the reef width. The main causes of scatter are found to be the reef width and the roughness, for which the plots can be found in Appendix A, Section A.2. Low values for the friction and the reef width cause larger IG wave heights than predicted. A logical explanation for this is the reflection of IG waves at the beach, which lose energy while propagating in offshore direction by frictional wave damping. If both reef width and roughness are low, the frictional wave damping is reduced resulting in larger IG wave heights at the reef crest than expected.
- The accuracy of the predictions is deemed large enough for implementation of the semi-empirical formulation in the conceptual model. Because the accuracy for smaller wave lengths is higher when filtering on wave length bins, the linear fits that are depicted in Figure 4.6 are used in the conceptual model to describe the IG wave height at the reef crest.

4.2.2.2 IG wave propagation

The obtained IG wave height at the reef crest is the input for the IG wave balance as depicted in Figure 4.1, according to van Dongeren et al. [159]. It is clear that the IG wave height reduces due to friction and wave breaking and increases due to shoaling. Non-linear interactions between short waves and IG waves that lead to further shoaling of the IG waves are not taken into account, which seems a reasonable assumption as most short waves break at the reef crest. The increase of IG waves by non-linear interactions between IG waves of slightly differing frequencies and by resonant forcing are also not described, which could lead to an underestimation of the IG wave height at the beach toe.

At the beach, IG waves are reflected. While propagating seaward, frictional wave damping reduces the IG wave height. The total IG wave height is the summation of incoming and outgoing wave heights, taking into account the phase difference between the two waves [159]. However, it is not possible to accurately capture the phase difference in this simplified model. Furthermore, for the prediction of the runup, the incoming wave heights are required. Therefore, we restrict ourselves to the prediction of incoming IG wave heights.

4.2.3. Runup prediction

Several formulations exist for runup at sandy coastlines (e.g. Holman R. A. and Sallenger [71] Holman [70], Van Gent [163], Gomes da Silva et al. [55]). Research has also been invested in runup at reef fronted coasts (Seelig [144], Nwogu and Demirbilek [113], Quataert [124]), but empirical formulations are lacking. Since runup is used as an indicator for the efficiency of coral restoration, an appropriate formulation is required. Hence different runup relations are investigated using the XBeach database of Pearson [116]. The analysis continues on his observations:

- Stockdon et al. [150] overpredicts the incident swash and underpredicts the setup and IG swash as wave dissipation across the reef and both the setup and IG wave generation at the forereef are not taken into account.
- The formulation for bulk runup described by Van Gent [163], where runup is a function of the wave height at the beach toe, is an improvement in prediction compared to Stockdon et al. [150] but still shows a large scatter.
- Merrifield et al. [98] and Blacka et al. [23] derived semi-empirical formulations based on field measurements at the Marshall Islands and laboratory experiments of the Cook Islands, respectively. Both

obtained promising results, although the applicability of their predictions was limited to the experiment settings. For the large range of modeled conditions by Pearson [116], the formulations show a large scatter.

As no reasonable accuracy is obtained with any of the above described theories, other formulations are tested. For this the approach of Stockdon et al. [150] is adopted, where a distinction is made between the incident swash, the infragravity swash and the setup, as this approach has a better physical basis than the bulk runup description. To distinguish promising formulations from literature, first a preliminary analysis of factors influencing the swash and setup is performed using the XBeach simulations of Pearson [116]. All results are aggregated into Figure 4.7, showing the different runup components and their dependency on the model parameters.

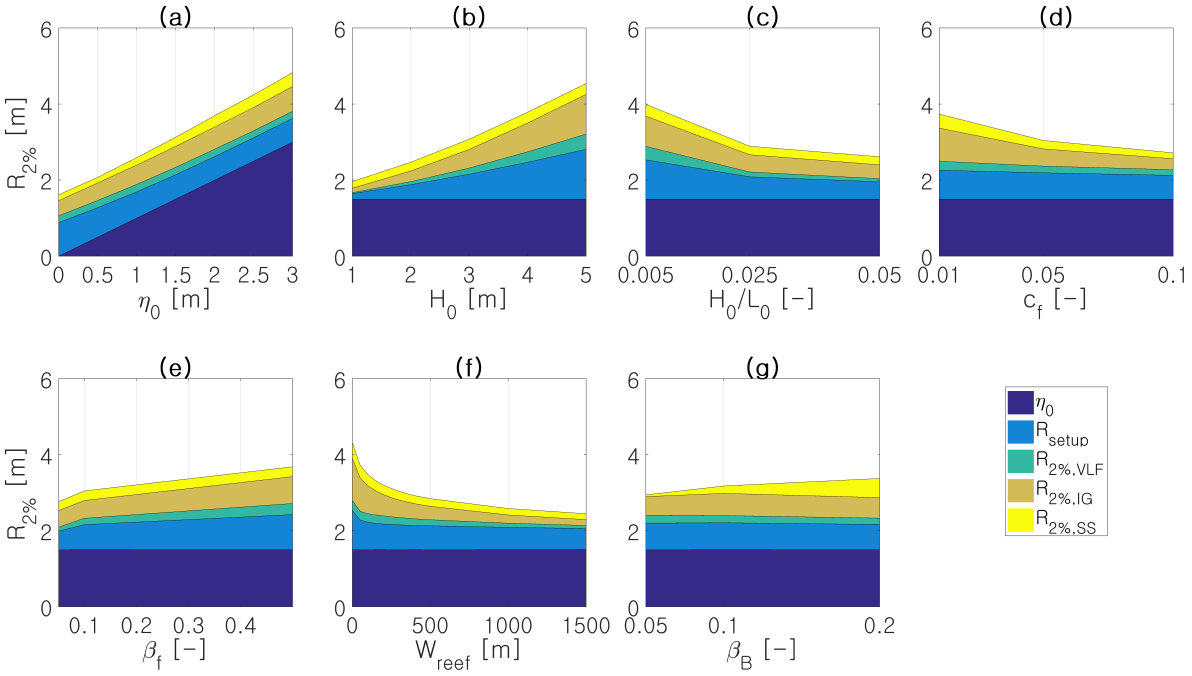

Figure 4.7: Model variables influencing the runup: the water level, the wave height, the wave steepness, the friction coefficient, the forereef slope, the reef width and the beach slope, respectively

Based on Figure 4.7, as well as Figure 2.4 on page 17 (a summary of factors influencing the runup based on the literature review), an inventory can be made of factors influencing the runup and promising empirical formulations:

- The *incident swash*, $R_{2\%,SS}$ is foremost influenced by η_0, H_0, the beach slope, the roughness and the reef width. The formulation of Stockdon et al. [150] (adapted by using reversed shoaling) incorporates these effects, as well as (to a lesser extent) the formulation by van Ormondt [164].
- The *infragravity swash* $R_{2\%,IG+VLF}$ is affected by all model parameters except for the beach slope. This demonstrates the complexity of the IG swash formulation. Formulations by Stockdon et al. [150], Gomes da Silva et al. [55] and van Ormondt [164] are tested. Furthermore, the relation between the IG wave height at the beach toe and the IG swash is examined.
- The *setup* is mainly affected by η_0, H_0, the wave steepness and the forereef slope, in line with theory as the setup is mostly generated at the reef crest. As the wave breaking model by Janssen and Battjes [73] is expected to accurately predict the setup, no additional formulations for the setup are required.

4.2.3.1 Incident swash (S_{inc})

Stockdon (2006)
According to Stockdon et al. [150] the incident swash can be described as:

$$S_{inc} = 0.75 * \beta_b * (H_0 L_0)^{1/2} \tag{4.10}$$

where the incident swash is a function of the beach slope β_b, the offshore wave height H_0 and the deep water wave length L_0. Pearson [116] analyzed this formulation and found a large discrepancy between theoretical S_{inc} values and the XBeach results. Reason for this is the effective dissipation of wave energy at the reef that reduces the short wave height at the beach toe compared to sandy coastlines. This is further substantiated by the observation that the incident swash is dependent on the roughness and reef width (see Figure 4.7).

To incorporate the effect of wave dissipation in the runup prediction, the local wave height at the beach toe is used. As described by Stockdon et al. [150], observations of local wave heights can be used as input for Equation 4.10 when reverse shoaled (see Intermezzo) to an equivalent offshore wave height H_{0-rev}. In this way, variations in roughness, reef width and water level at the beach toe are implicitly taken into account in the prediction of the runup. The theoretical S_{inc} value based on Equation 4.10 is compared to the XBeach output for S_{inc}, as shown in Figure 4.8.

Intermezzo Reverse shoaling involves estimating deep water conditions from measurements at shallow or intermediate depths using linear wave theory. First the wavenumber k and the ratio between the group and phase velocity n at measurement depth h are calculated from the dispersion relation. The deep water wave height is then calculated according to:

$$\frac{H}{H_{0-rev}} = K_{sh} = \sqrt{\frac{1}{tanh(kh)}\frac{1}{2n}} \tag{4.11}$$

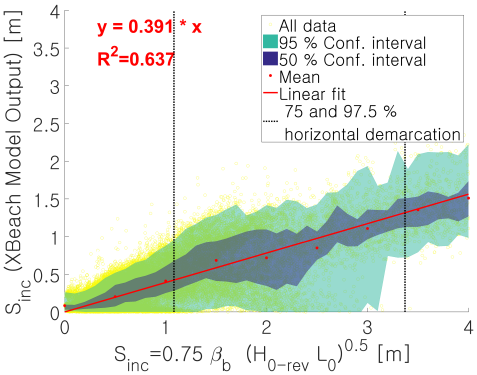

Figure 4.8: Incident swash as a function of the beach slope, the reverse shoaled H_0 and L_0 according to Stockdon et al. [150]

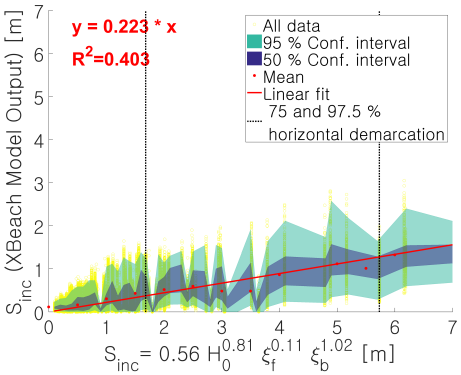

Figure 4.9: Incident swash as a function of H_0, ξ_b and ξ_f according to van Ormondt [164]

As can be deduced from Figure 4.8, the runup formulation by Stockdon et al. [150] using the reverse shoaled wave height H_{0-rev} clearly follows a trend, although the scatter is significant. Figure 4.10 gives more insight into the observed inconsistency of the formulation. For smaller wave lengths, Stockdon et al. [150] gives a good upper limit for the runup. However, the larger the wave length, the more the empirical formulation overpredicts the runup measured by XBeach. Apparently the dependency of the runup prediction on the wave length is too large. Figure 4.7 confirms the small influence of the wave length on the runup height. Another interesting observation is the distinct grouping of model runs with equal beach slope (β_b), indicating that the variation in beach slope is not accurately captured by the model.

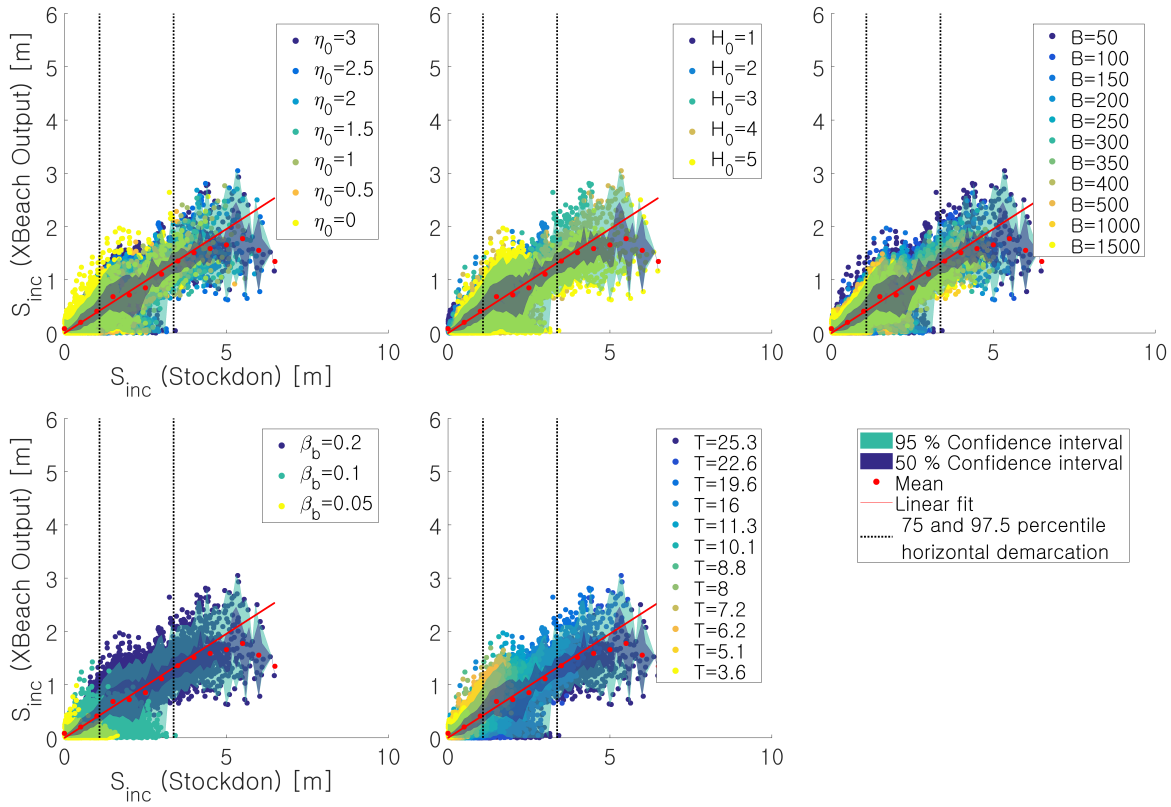

Figure 4.10: Colour maps of model variables influencing the incident swash as formulated by Stockdon et al. [150], depicting the offshore water level η_0, the offshore wave height H_0, the reef width, the beach slope and the wave period

Van Ormondt (2018)

van Ormondt [164] generated an XBeach dataset to find new empirical formulations for runup at reef fronted coasts. In his simulations, the wave height, the wave period, the reef width, the forereef slope and the beach slope were varied while keeping the water level constant during all model runs. Using a regression analysis, he obtained the following formulation for S_{inc}:

$$S_{inc} = 0.56 * H_0^{0.81} * \xi_f^{0.11} * \xi_b^{1.02} \tag{4.12}$$

where

$$\xi_{f,b} = \frac{\beta_{f,b}}{\sqrt{H_0/L_0}} \tag{4.13}$$

The results are shown in Figure 4.9. The obtained formulation shows less correlation between the data and the fitted function than Stockdon et al. [150]'s formulation. This is attributed to two important model deficiencies. First of all, varying water levels are not taken into account, while the water level is a dominant factor in the wave dissipation process [125]. Furthermore, the incident swash is dependent on the offshore wave height, thereby neglecting the interaction between the wave height, the water level and frictional characteristics of the reef that leads to the transformation of shoreward propagating waves.

Model improvement

Figure 4.8 (and to a lesser extent Figure 4.9) shows a trend in the incident swash height, but with large scatter and only moderate correlation between data and fitted trends. Therefore a new relation is formulated based on Figure 4.7 and the conclusions drawn from Figure 4.10. The improved formulation is dependent on the reverse shoaled wave height, the wave length and the beach slope with coefficients that are derived with an optimized linear regression analysis:

$$S_{inc} = f(\beta_b^{1.9} H_0^{0.73} L_0^{0.27})[m] \tag{4.14}$$

The improved model is depicted in Figure 4.11. The correlation value is increased from 0.6 for the original formulation to 0.85 for the optimized formulation. Figure A.6 in Appendix A, Section A.3, shows the influence of model parameters on the final result. The scatter now foremost originates from water level and beach slope variations. For very low water levels at the beach toe, the XBeach model gives larger runup values than predicted. Furthermore, the runup prediction for gentle slopes is less accurate. Separate analyses of simulations with beach slopes of 0.05 and 0.1 show that the runup is hardly dependent on the wave height and wave length for these gentle slopes, which is cause for the observed scatter. However, the model does accurately capture the influence of the offshore wave height, wave length and frictional dissipation across the reef with reasonable accuracy.

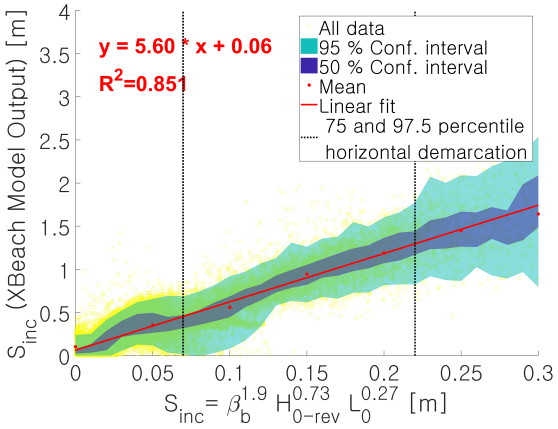

Figure 4.11: An optimization of Stockdon et al. [150]'s formulation for the incident swash, where model parameters to include where obtained from Figure 4.7 and 4.10 and coefficients determined by optimizing the fit between data and the linear regression

4.2.3.2 Infragravity swash (S_{IG})

Several formulations for the infragravity swash component of the runup exist, again mainly for gently sloping sandy beaches (e.g. Stockdon et al. [150], Gomes da Silva et al. [55], Van Ormondt). Their applicability to reefs is explored in the following paragraphs.

Stockdon (2006)
Stockdon et al. [150]'s parametrization links the IG swash to the offshore wave height and wave length:

$$S_{IG} = 0.06 * (H_0 L_0)^{1/2} \tag{4.15}$$

Results of Formulation 4.15 are depicted in Figure 4.12, which shows only a moderate fit with the data. As at most reefs the breakpoint mechanism dominates the IG wave generation, it was expected that just an offshore wave height and wave length only does not accurately capture the IG swash at reef fronted coasts.

Gomes da Silva (2018)
Gomes da Silva et al. [55] provides an improved expression for the IG swash based on field experiments of ten different beaches. By means of a linear regression analysis he obtained the following formulation for the IG swash:

$$S_{IG} = 0.012 * (H_0 L_0 / \beta)^{1/2} \tag{4.16}$$

According to Figure 4.7, the inclusion of the beach slope should not improve the IG swash formulation at reefs. This is clear from the reduction in correlation of Figure 4.13 compared to Figure 4.12.

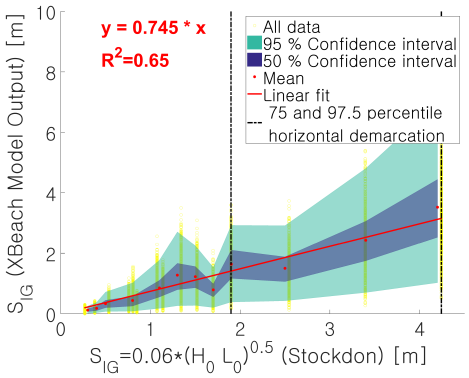

Figure 4.12: IG wave runup component as function of H_0 and L_0 as formulated by Stockdon et al. [150]

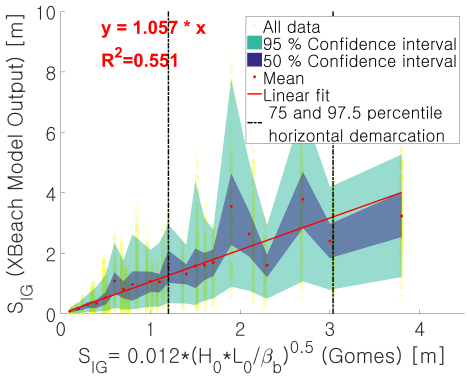

Figure 4.13: IG wave runup component as function of H_0, L_0 and β as formulated by Gomes da Silva et al. [55]

Van Ormondt (2018)
van Ormondt [164] defined the IG swash as:

$$S_{IG} = 0.64 * H_0^{1.06} * \xi_b^{0.42} \tag{4.17}$$

where ξ_b is given by Equation 4.13. The results are depicted in Figure 4.14. Although formulation 4.17 shows a clear trend of increasing S_{IG} with increasing offshore wave height and beach steepness, the correlation is rather low.

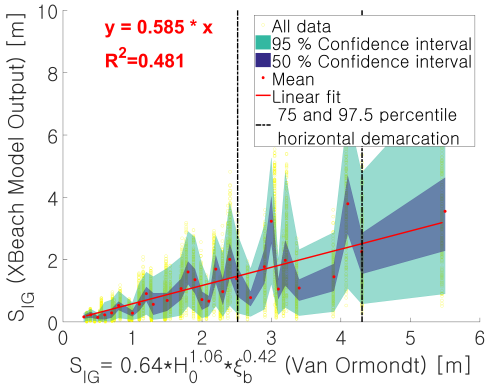

Figure 4.14: IG wave runup component as function of H_0 and ξ_b as formulated by van Ormondt [164]

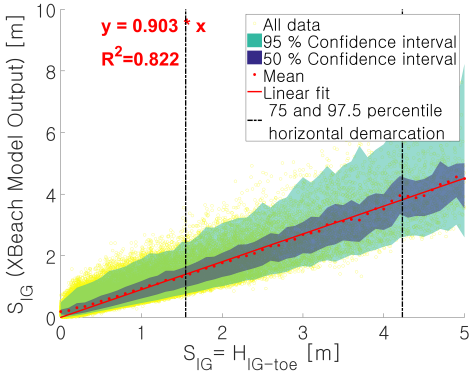

Figure 4.15: IG wave runup component as function of H_{IG} at the beach toe

Model improvement
All three above described formulations are a function of the offshore wave height, the offshore wave length and for the last two cases the beach slope. Varying water levels, the forereef slope and frictional wave damping across the reef are not taken into account, which causes the large scatter in prediction values. Therefore another formulation is desired.

In the conceptual model, the IG wave height at the toe is calculated. Assuming this wave height can be predicted with reasonable accuracy, the infragravity swash can be linked to the IG wave height at the beach toe. In this way, the frictional wave dissipation across the reef and the effect of H_0, η_0 and the forereef slope on the IG wave generation are implicitly taken into account. In Figure 4.15, the runup obtained by XBeach is plotted against the IG wave height at the toe. A significant increase in goodness of fit is clear, although scatter is apparent for lower S_{IG} values. Therefore, the influence of several parameters is investigated (see Figure 4.16).

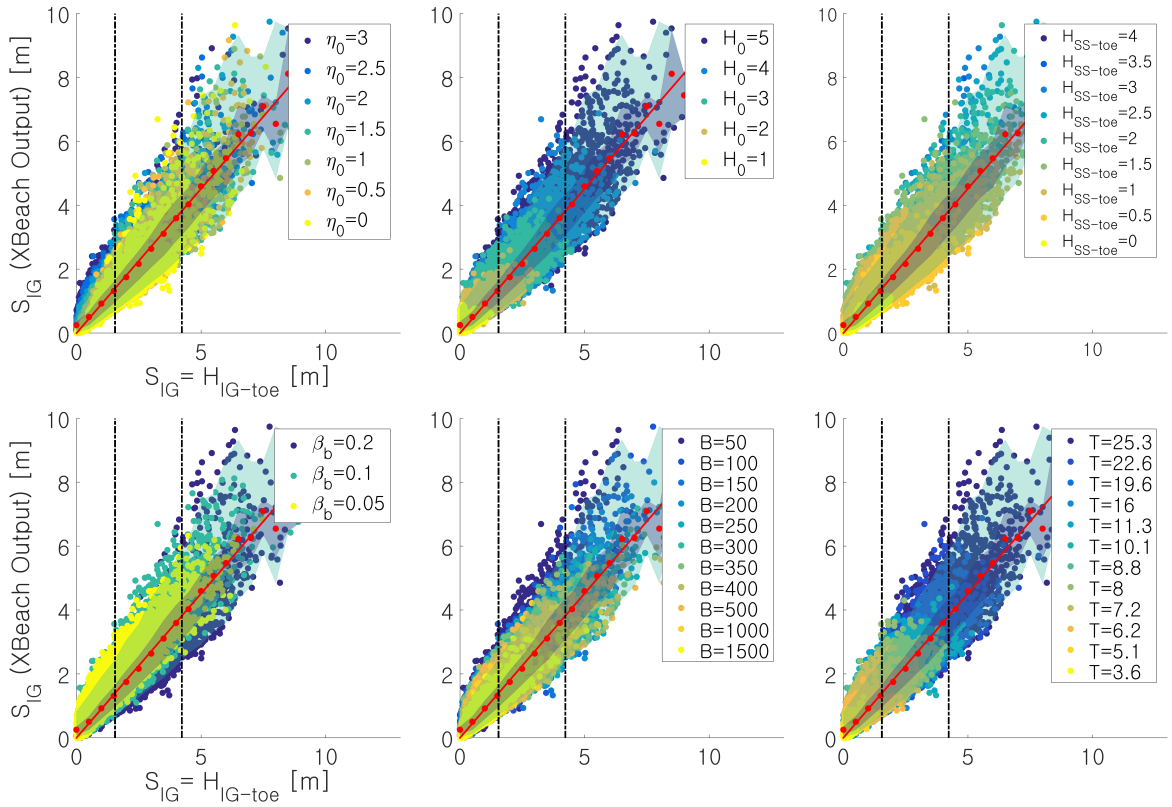

Figure 4.16: IG runup as function of IG wave height at the beach toe, showing the influence of several model parameters: the offshore water level, the offshore wave height, the wave height at the beach toe, the beach slope, the reef width and the wave period, respectively

Figure 4.16 reveals two interesting aspects. Firstly, the incident wave height at the beach toe influences the IG wave runup. This could indicate a transfer of energy from the short waves to the long waves between the beach toe and the swash zone. Secondly, other aspects such as the offshore wave height, the wave length and beach slope are neatly aligned with the solution, showing that for larger wave heights, wave lengths and beach slopes larger IG wave runup is generated. The infragravity swash is thus best modeled as a function of both the infragravity and incident wave height at the beach toe, as depicted in Figure 4.17.

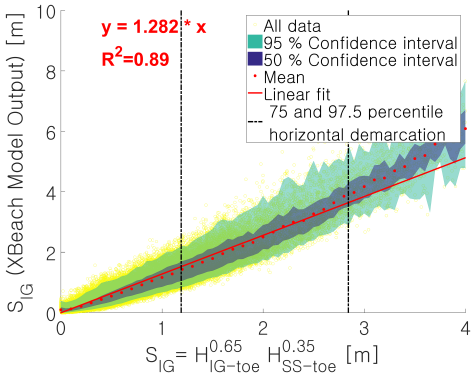

Figure 4.17: The IG swash as a function of both the IG and incident wave height at the beach toe. The coefficients of H_{IG} and H_{SS} are derived from a linear regression analysis

4.3. Discussion

The results of this simple hydrodynamic model are promising, showing that for a first-order assessment, the reef hydrodynamics can be captured by this relatively simple and fast model. The model is, however, subject to limitations and could benefit from additional investigation into its elements.

The short wave transformation and setup, solved by the Janssen and Battjes [73] model, match data of laboratory experiments by Buckley et al. [32], in agreement with model calibration tests of Janssen and Battjes [73] and Su et al. [154], although the number of validation test in this study are sparse. Moreover, on very steep forereef slopes reflection of short waves can occur, a process that is not taken into account in the current formulation. For this reason, wave heights and setup at the reef flat can be overestimated. The inclusion of a (simple) reflection formulation could improve the accuracy of the model on steep slopes.

The formulation for the IG wave height at the reef crest is empirically derived from the dataset of Pearson [116] and therefore calibrated to the modeled conditions of Pearson [116]: forereef slopes between 1:20 and 1:2, wave heights between 1 and 5 m and water levels between 0 and 2 m. Under these conditions, the breakpoint mechanism is assumed to be the main source of IG wave energy, as the normalized bed slope parameter (see Equation 2.16) is large, which indicates a surf-zone forcing regime [159]. Hence, the applicability of this formulation, which shows a large correlation (0.9) with the fitted data, is limited to cases where breakpoint forcing is dominant. An extension of the model parameter space would increase the accuracy and reliability of the empirical formulation.

The IG propagation across the reef is modeled according to van Dongeren et al. [159], where IG wave heights reduce shoreward of the reef crest by frictional wave damping and wave breaking. This evolution of the IG wave height is supported by observations of IG wave dynamics of Van Dongeren et al. [160]. For certain hydrodynamic conditions, however, an increase in IG wave energy across the reef is observed. Péquignet et al. [118] note an increase in IG wave energy due to resonant forcing, whereas Pearson [116] shows examples of increasing IG wave heights possibly due to the ongoing process of short wave breaking that transfers energy to the IG waves. It is difficult to capture the additional energy sources as they highly depend on the forcing conditions and profile parameters. However, it can be assumed that there is a correlation between among others the location of the breakpoint, which is determined by the height of the incoming short waves and the water level, that indicates whether there is an ongoing transfer of energy from the short waves to the IG waves across the reef flat, an interesting topic of further research. Resonant forcing can also be predicted based on theory of Nwogu and Demirbilek [113], which could be implemented as a warning when the combination of reef dimensions and hydrodynamic forcing come close to the resonant forcing mode.

The derived runup formulations show a significant improvement of the predictive skill compared to the existing formulas. For coral reefs, it is deemed imperative to base the runup on beach toe wave parameters instead of offshore wave characteristics, due to the variety of processes that affect wave heights and water levels while traveling across the reef. However, this does require an additional step of solving the wave transformation across the reef to be able to use the derived runup formulations. The predictive skill of these formulations is therewith also dependent on the predictive skill of the hydrodynamic model.

4.4. Conclusion

In this chapter, a fast model for a rapid, first-order assessment of reef hydrodynamics is proposed. Its goal is twofold: (1) to use as a screening tool on a large set of reef profiles before using more complex, process-based models like XBeach on a small subset, defined based on the simple model, and (2) to gain more insight into the drivers of runup at reef lined coasts. Based on relatively simple formulations, incoming wave heights and water levels are predicted. These formulations are gathered based on an evaluation of existing wave models and a data-analysis on XBeach simulations of fringing reefs [116]. Subsequently, runup formulations based on beach toe wave heights have been derived that show a good correlation with the XBeach data [116]. A significant increase in goodness of fit compared to existing formulations for runup at sandy coastlines is observed. In Figure 4.18, an overview of the chosen formulations and model characteristics is depicted. Additional validation steps are required, and implementation of additional processes such as reflection and resonance could be useful to obtain more exact results.

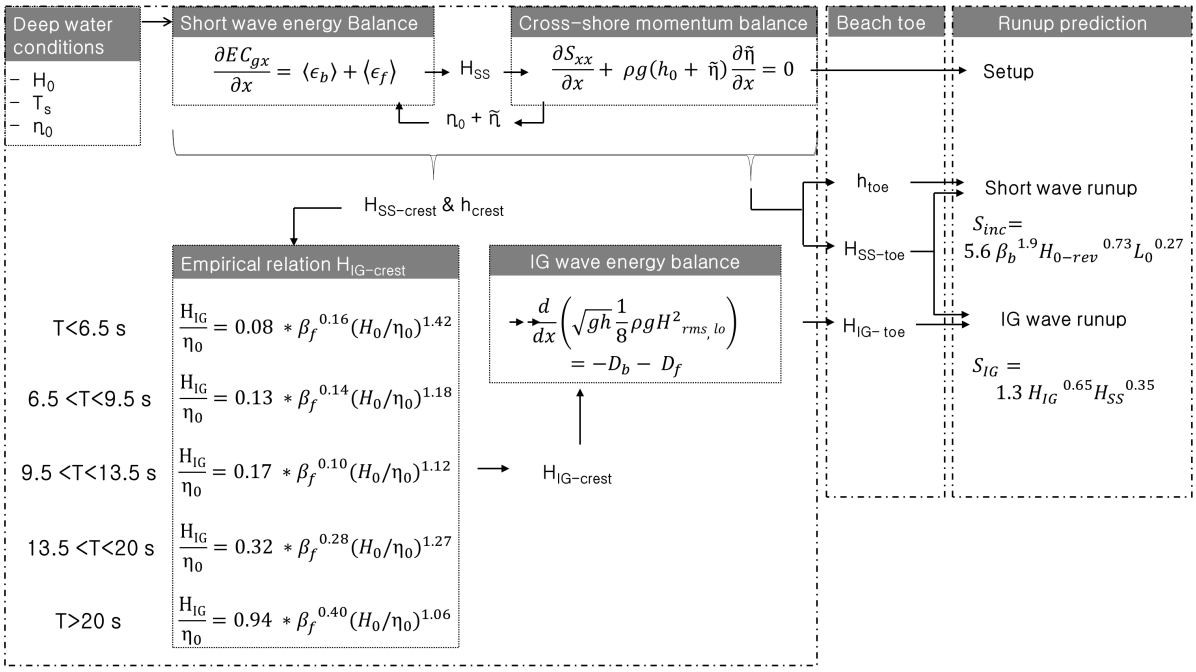

Figure 4.18: Schematization of the simplified reef hydrodynamic model including the derived model formulations, showing how the runup is calculated based on beach toe wave heights and water levels, which are calculated based on the short wave energy balance, the cross-shore momentum balance, an empirical formulation for the infragravity wave height at the reef crest and the IG wave energy balance between the reef crest and the beach toe. Input parameters are the deep water conditions and the reef geometric parameters, that need to be supplied by the user.

5

Reef profile classification

The coral reef morphology is highly variable in character, displaying a variety of topographic structures with different length scales. Costa et al. [40] investigated the influence of this varying reef morphology for coral reefs along the northeast coast of Brazil. She observed a strong control of the reef geometry on the wave propagation and dissipation. However, little is known about the natural reef profile variability worldwide. Therefore, 30.000 US reef profiles were made available to be classified using a clustering algorithm. A cluster algorithm can efficiently process and translate large amounts of data into a structured, compact overview of representative dataset characteristics. In this way, it is possible to find the dominant reef profiles and an estimate of their frequency of occurrence. These reef profiles then serve as input for the subsequent numerical modeling study, to explore the effects of varying geometries on wave transformation and dissipation. Elements of the cluster analysis are elaborated in this chapter.

5.1. Dataset

Clustering activities start with the acquisition and preprocessing of data. Only with a proper understanding and preparation of the data, data modeling is meaningful [165]. Therefore dataset characteristics are briefly described in this section.

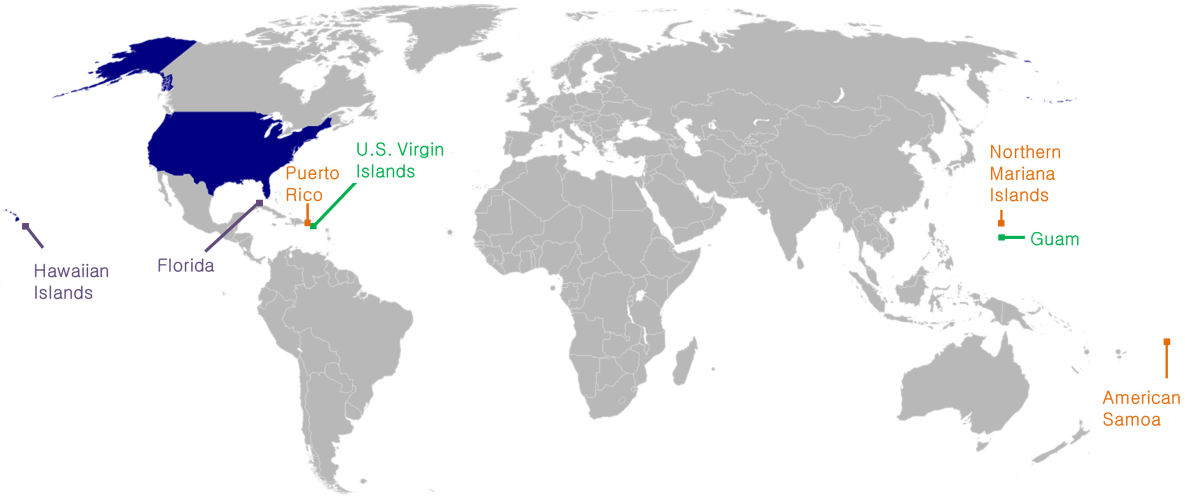

Figure 5.1: An overview of the geographic positions that are represented by the reef profile dataset

The dataset consists of depth profiles of reefs in United States territory, of which the locations are shown in Figure 5.1. The depth profiles are measurements of the depth at cross-shore intervals of 2 meter, starting at a height of 20 meter above the mean water level and extending to a depth of 30 meter below mean water level.

Table 5.1: Characteristics of the reef profile dataset denoted per geographic area, giving the number of surveyed profiles for each region and the types of reef present at each location

	Hawaiian Islands	**Florida**	**Puerto Rico**	**US Virgin Islands**	**Northern Mariana Islands**	**Guam**	**American Samoa**
Nr of profiles [-]	13404	6039	5531	1664	1035	1295	1198
Type of reef	Barrier Fringing Atoll	Barrier	Barrier Fringing	Barrier Fringing	Barrier Fringing	Fringing	Barrier Fringing

The dataset characteristics are noted in Table 5.1. Figure 5.1 and Table 5.1 are used to evaluate (1) whether the deduction of general reef characteristics based on the dataset is possible and (2) if there are factors that degrade the clarity and relevance of the results.

As can be deduced from Figure 5.1, the islands of the US territory are scattered across the world, which is favourable for the geographic representation of the dataset. This large geographical spread also indicates that a large variation in reef length scales and shapes is likely, which asks for a cluster algorithm that is well adapted to capture the complex profile variations.

Table 5.1 shows two interesting characteristics of the dataset. Firstly, in contrast to barrier and fringing reefs, data on atoll islands are sparse as the surveyed islands of the US territory are relatively large. Even the dataset of the Hawaiian islands covers only the eight larger islands (Oahu, Niihau, Molokai, Maui, Lanai, Kauai, Kahoolawe and Big Island) where few profiles can be regarded as atoll profiles. The underrepresentation of atoll islands should be kept in mind in the evaluation of the cluster analysis results. Secondly, the number of surveyed profiles varies significantly among the different topographic regions. As shown in Table 5.1, the datasets of the Hawaiian Islands and Florida are much larger in size than the dataset of American Samoa. However, as the size of each subset is largely proportional to the surface area of the geographic region it represents, the dataset in its entirety is deemed suitable as input for the cluster analysis.

5.2. Clustering techniques

Clustering is a technique in which a large, unstructured dataset, as visualized in the left image of Figure 5.2, is classified into groups (clusters) that show similar characteristics. In general, a dataset consists of different observations that are described with predefined cluster variables, as also illustrated by Figure 5.2. This gives a square matrix where rows are the different observations (e.g. different reef profiles) and columns the characteristics with which to describe an observation (e.g. the depth at different cross-shore locations). The objective of a cluster algorithm is to find groups in which the observations are strongly related (similar) to each other and unrelated (dissimilar) to observations that belong to other groups. Different methods exist to determine this (dis)similarity between observations, which are elaborated in the next section. Furthermore, there are different ways to characterize the dataset of the US reefs (or define the cluster variables), which are elaborated in Section 5.2.2.

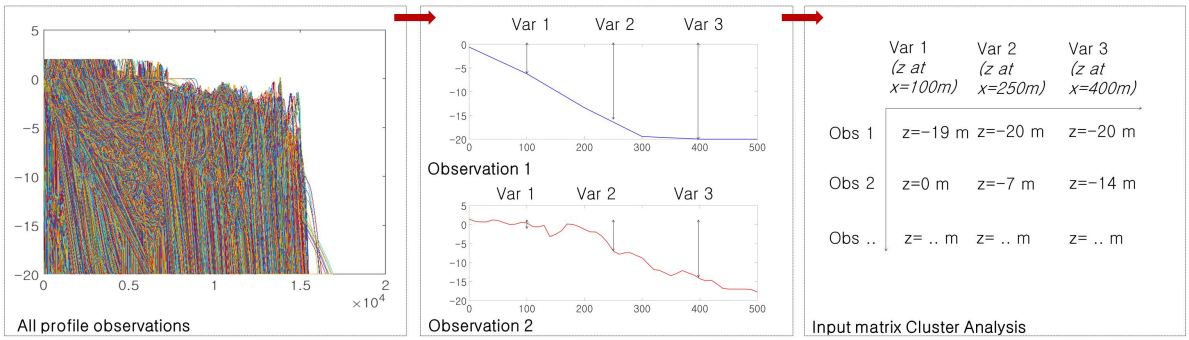

Figure 5.2: The input for the cluster analysis: the large dataset that is composed of multiple observations (the reef profiles), which are characterized by a set of variables, in this case the depth at different cross-shore locations

5.2.1. Cluster methods

Different algorithms exist to classify the reef profiles. Which model is best applicable depends on the dataset and research objective. It is often difficult to determine the cluster method a priori when processing large, multi-dimensional datasets where the full dataset is difficult to visualize. Therefore, testing with different models is advised. Three methods are chosen to evaluate: the k-means model, the Gaussian Mixture Model and the Maximum Dissimilarity algorithm. These models are widely used and have clear, distinctive features. Below, the models are elaborated, while overviews of k-means and the Gaussian Mixture model are given in Figures 5.3 and 5.4.

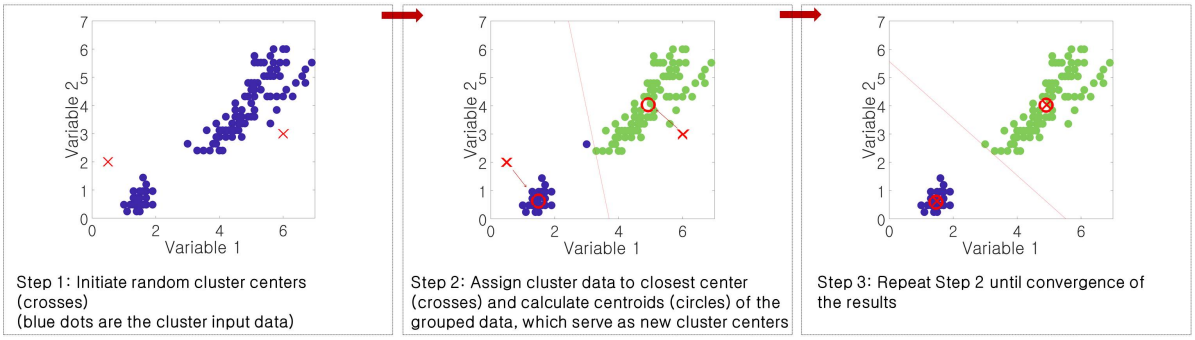

Figure 5.3: The clustering steps of the k-means algorithm

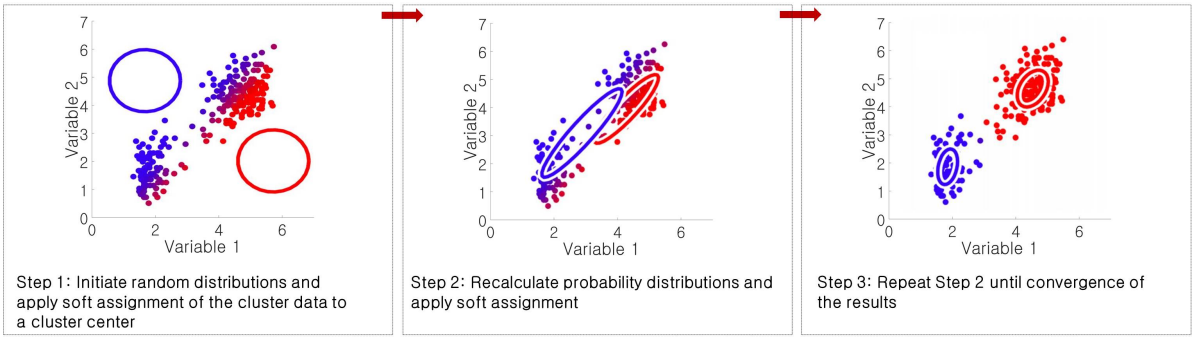

Figure 5.4: The clustering steps of the Gaussian Mixture Model, adapted from Bishop [22]: Pattern recognition and machine learning, Figure 9.8

5.2.1.1 K-means cluster algorithm (KMA)

The k-means clustering algorithm is an algorithm that aims to assign all observations of a dataset to a predefined number of cluster centers k. The algorithm is initialized with a set of k mean values as cluster centers (Step 1). In Step 2, all observations are assigned to one of the cluster centers based on minimization of the Euclidean Distance between the observation variables and cluster centers. The Euclidean Distance is defined as the straight-line distance between two points in space. As k-means minimizes the distance between cluster centers and observations, spherical groups are created. The centroids of the clustered observations serve as cluster center for the next iteration step. This process is continued until convergence of the results (MacKay [91]).

5.2.1.2 Gaussian Mixture Model (GMM)

As an alternative to the heuristic based (e.g. KMA) and distance based (e.g. MDA) clustering techniques, clustering algorithms based on probability models have been developed, the mixture models [25]. A mixture model assumes that the dataset originates from k probability distributions that are defined by a mean, a covariance and a mixing coefficient that determines its weighing in the full probability distribution. The cluster centers (of a predefined quantity k) are now defined by the different probability distributions. A Gaussian

mixture model assumes a Gaussian probability distribution:

$$G(X|\mu,\Sigma) = \frac{1}{\sqrt{(2\pi)^d|\Sigma|}} \exp\left\{-\frac{1}{2}(X-\mu)'\Sigma^{-1}(X-\mu)\right\} \tag{5.1}$$

in which the parameters μ (mean vector with length d equal to the number of variables) and Σ (the covariance matrix of dimensions d x d) are unknown . The clustering algorithm is initialized by random values for μ_k, Σ_k and mixing coefficients π_k. While k-means employs a hard clustering assignment, where in each iteration, all observations belong 100 % to a certain cluster center, the Gaussian mixture model applies a soft assignment, where an observation belongs to a cluster center with a certain probability. In an iterative procedure, the conditional probability of an observation belonging to a cluster is calculated, after which μ_k, Σ_k and π_k are updated. The intermediate results are evaluated based on the log-likelihood function while the process continues until convergence of the log-likelihood function. This results in cluster groups with parabolic shapes. A more elaborate description of the Gaussian Mixture Model is given by Reynolds [130].

5.2.1.3 Maximum Dissimilarity Algorithm (MDA)

The Maximum Dissimilarity Algorithm is an efficient algorithm that creates a subset V_N of the full dataset of M observations that should represent the variability of the full dataset. The size of the subset N is predefined. The subset vectors are chosen based on the maximum dissimilarity between the observations and the subset members [114]. First, an initialization subset vector V_1 is required. A good initialization vector is the observation with the largest total distance to other observations [114]. This vector is transferred from the observation matrix to the subset matrix, as is done for each new subset member. The next subset member V_2 is the observation vector with the largest Euclidean distance to subset member V_1. Subset members V_3 to V_N are selected based on the maximum distance between observations and any of the subset vectors [34].

5.2.2. Cluster variables

A cluster algorithm requires M observations of N variables as input. The variables describe characteristics of the observations. There are different ways to characterize the dataset described in Section 5.1.

1. Morphological parameters of the reef

A sophisticated method of characterizing the dataset is to establish general reef parameters for each reef profile (e.g. reef flat width, forereef slope) that serve as input variables for the cluster analysis. de Souza Pereira et al. [43] show good results with the clustering of Brazilian beach profiles based on beach morphodynamic parameters. However, the automatic determination of general reef parameters for a large number of reefs is not straightforward. Moskalik et al. [104] describe a method to classify different sections of bathymetric profiles based on mathematical decompositions. This is, however, beyond the scope of this research. Cluster analysis based on morphological reef parameters is more suitable for smaller datasets than the current US reef profile dataset, such that profile parameters can be visually identified.

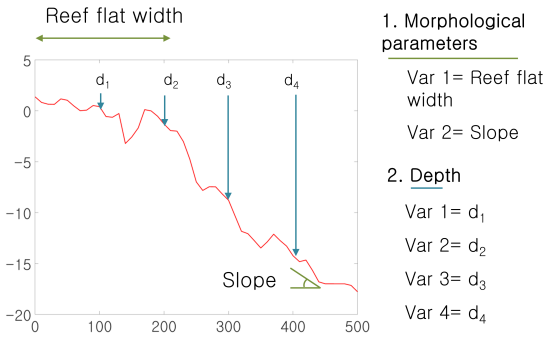

Figure 5.5: An example of a reef profile in which two definitions for the cluster variable are indicated: (1) the reef width and the reef slope (morphological reef parameters) and (2) the depth at different cross-shore locations (x=100 m, x=200 m, x=300 m and x=400 m)

2. Depth

An obvious cluster variable is the depth at different cross-shore locations as it is easily obtained from the profile dataset (see Figure 5.5). Costa et al. [40] successfully classified 180 beach profiles based on similarity between depth profiles. There are however downsides to this approach. Firstly, the translation of a depth profile in cross-shore direction leads to large Euclidean differences between profiles while they show similar characteristics. Also, larger scale topographic regions such as reef crests are problematic. These characteristic features are undetectable when using the depth as cluster variable (except for when there are many reef crests at approximately the same cross-shore location which is unlikely). Already shorter distance cross-shore

translations of reef crests will result in a large dissimilarity between two profiles that are actually much alike. What is more, the cluster centers show a tendency towards reefs with larger lengths. As cluster algorithms require square matrices as input, all reefs are extended to the length of the longest reef by adding deep water depth values to the vector. Because of this, observation vectors of short reefs are by definition fairly similar as the bulk of the vector consists of the same value. Therefore, variations between shorter reef profiles will be resolved less than variations in longer profiles.

5.3. Methodology

To transform the large, complex reef profile dataset into a clear overview of reef profile characteristics, several cluster variables and cluster methods are examined to establish the optimal cluster algorithm. For this, first a cluster method is chosen with which to investigate the different ways to define the cluster variables. The Gaussian Mixture model has been deemed suitable for this as recent research on profile classification showed the good performance of the Gaussian Mixture model in grouping ocean temperature profiles, which are similar to our reef profiles [96]. In total, three different ways of defining the cluster variable are explored, which are illustrated in Figure 5.6: the depth at regular cross-shore intervals, the normalized depth and the depth at seaward increasing interval spacing. Additionally, two types of filtering are applied on the cluster input data while using the depth at regular cross-shore intervals as cluster variable. For filter option (1), data are filtered on the geographic region, after which the cluster analysis is applied on the different geographic regions separately. For filter option (2), the input data are divided into bins with similar length, after which clustering is applied on the different bins. In total, this gives five cluster variable options to examine.

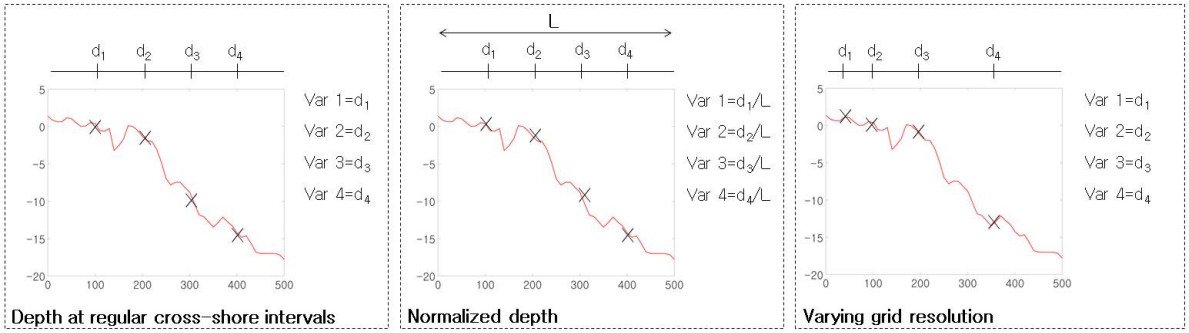

Figure 5.6: Three ways to define the cluster variables; the depth at regular cross-shore intervals, the depth at seaward increased spacing and the normalized depth

For all five approaches, the depth files are first adapted to increase the accuracy and topographic representation of the dataset. All bed level variations above +2 m are filtered out as they will not influence the wave propagation and dissipation but do steer cluster centers in the wrong direction. Furthermore, large water depths are less important for wave transformation processes, hence depths below - 20 m are also removed from the dataset.

Once the cluster variable is established, the three different cluster methods (k-means, maximum dissimilarity and the Gaussian Mixture model) are compared on their ability to represent the reef profile dataset with distinct geometric reef profiles. All tests are run for a relatively small amount of cluster centers (20 to 21 centers), to obtain a clear image of the cluster centers that can be visually inspected and compared. Three indicators are used to evaluate the performance of the different cluster variables and methods:

1. The *distribution of profiles across the cluster centers.* The objective is to find geometrically distinct profiles that represent a substantial part of the dataset. Therefore, groups of approximately equal size are preferred. We are not looking for profile outliers that have a very distinct geometry but represent only a few reef profiles.
2. The average *root mean square error* (RMSE) per cluster center. The RMSE gives an indication of the profile variability within a clustered profile group. A low RMSE, or low variance, implies that profiles

within a cluster center are very similar, which supports the validity of the cluster center to represent all profiles in a group.

3. The *Davies-Bouldin index*. The Davies-Bouldin index is an internal evaluation scheme to investigate how well profiles fit to their assigned cluster center and not to others. The lowest, nonnegative D-B index indicates the best performance [42].

Ultimately, once both the cluster variable and cluster method is set, both the input (e.g. number of cluster centers) and the results of the cluster analysis are further refined to obtain a good overview of the reef profile shapes and the frequency of occurrence of different reef types.

5.4. Results

In this section, first the results of the analyses of possible cluster variables and cluster methods are presented, after which the final steps to obtain the representative profiles are elaborated.

5.4.1. Results cluster variables

Five different cluster variables are investigated, of which an overview of the results is given in Table 5.2. These results are explained in the next paragraphs.

Table 5.2: A summary of the performance of the five cluster variables in finding geometrically distinct representative reef profiles. The distribution of the number of profiles across the cluster centers is judged with a grade between - - and ++, where - - indicates that profiles are distributed very irregularly across the cluster centers. The weighted average root mean square error (RMSE) is the weighted average of the RMSE's of all cluster centers, taking into account the number of profiles that belong to the cluster centers. The Davies-Bouldin index is an evaluation scheme to identify how well profiles fit in the cluster center and not to other cluster centers. A lower DB index indicates a better performance of the cluster algorithm.

	Distribution profiles across centers [- - to ++]	Weighted average RMSE [-]	Davies-Bouldin index [-]
Regular depth	- -	3.33	1.49
Normalized depth	-	3.76	4.32
Varying grid resolution	+	2.63	1.67
Geographic filtering	-	3.78	5.03
Length filtering	++	2.73	1.67

Regular depth The depth at regular intervals is taken as cluster variable. The results of the Gaussian Mixture model with this cluster variable are displayed in Figure 5.7 and the accompanying Table 5.3. This table shows the size of the represented dataset (number of profiles that belong to the cluster) and the average root mean square error (RMSE) for the five shortest and the five longest cluster centers (the full table is displayed in Appendix B). From Table 5.3 it is clear that cluster centers with a larger length represent a smaller number of profiles with a higher accuracy (low RMSE) than the smaller length-scale cluster centers. This difference in resolution is also illustrated by Figures 5.9 and 5.8, from which it is clear that much profile variability of shorter profiles is lost.

Table 5.3: Cluster center characteristics; the size of the represented profile dataset, the average of the RMSE of all profiles in a cluster center (RMSE 100) and the average of the 95 percentile lowest RMSE's (RMSE 95), thereby removing the influence of extreme outliers

Cluster nr	1	2	3	4	5	16	17	18	19	20
Size	11969	5704	4154	1201	1262	182	125	147	112	12
RMSE 100	3.87	3.58	3.80	3.48	3.07	2.18	2.11	1.53	1.20	1.12
RMSE 95	3.64	3.39	3.62	3.31	2.92	2.13	2.08	1.42	1.16	1.08

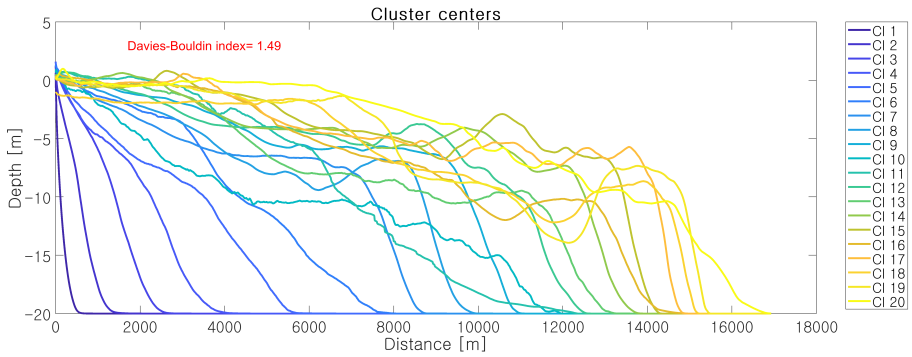

Figure 5.7: Results of the cluster analysis with the GM model, with 20 cluster centers and the depth at regular cross-shore intervals as cluster variable. The Davies-Bouldin index, an internal evaluation scheme to show whether cluster centers are well-defined (a lower index indicates a better performance), is printed in red in the left upper corner.

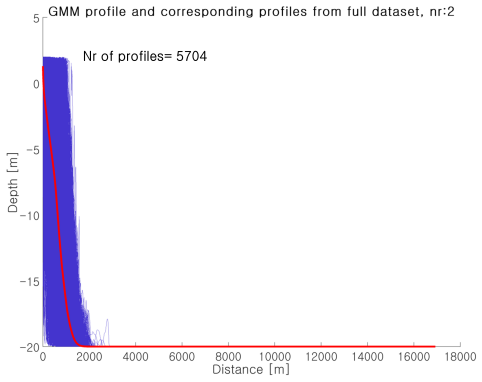

Figure 5.8: Results of the cluster analysis with the GM model, with 20 cluster centers and the depth at regular cross-shore intervals as cluster variable, for cluster number 2

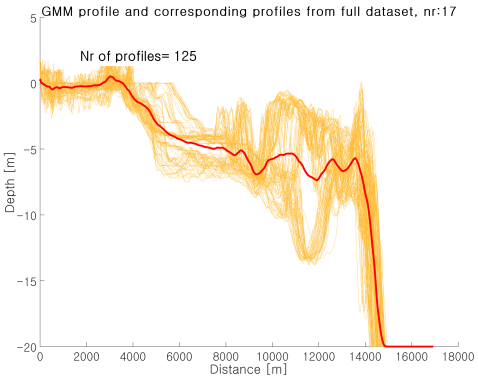

Figure 5.9: Results of the cluster analysis with the GM model, with 20 cluster centers and the depth at regular cross-shore intervals as cluster variable, for cluster number 17

Normalization The profile lengths (defined as the cross-shore distance between profile data points at +2 m and -20 m relative to the mean water level) are normalized, making all lengths equal to one. Information on the original length of the profile is added as variable with a weighing equal to the weighing of the depth vector. The results are depicted in Figure B.2 on page 124 (Appendix B). The advantage of the normalization is that profiles with the same shape but with different length scales are grouped together. To a certain extent this approach agrees with our goal of finding geometrically distinct reef profiles. Various topographic shapes appear when using normalized profiles as input variable. However, Table B.2 shows that 10 of the 20 cluster centers represent less than 100 profiles, indicating that the assignment of cluster centers is rather arbitrary. This is quantified by the Davies-Bouldin index, which is much higher than for the regular profiles, indicating that the cluster centers are ill-defined. Furthermore, the shorter profiles are again misrepresented, as they are grouped into a large cluster with a high RMSE.

Varying grid resolution Regular intervals in cross-shore direction steer the solution towards longer reefs, decreasing the resolution of smaller reefs. This accounts for both regular and normalized depths. With a varying grid resolution depth variables are not equally spaced but determined at locations with increased spacing in offshore-direction. This gives more weight to depths closer to the coast than to depths further offshore. As can be deduced from Figure B.3 and Table B.3 in Appendix B, this does improve the resolution of the shorter profiles compared to the regular depth intervals and the normalized profiles. The profiles are now distributed more fairly across the cluster centers and the variability within the cluster group is significantly reduced for the shorter profiles. The Davies-Bouldin index is however not lowered, indicating that cluster centers are defined less clear due to the decreased number of input variables.

Geographic filtering By geographic filtering of the dataset and performing cluster analysis for each region separately, profiles with the same age and thus similar characteristics are grouped together. Cluster analysis on these groups would thus result in more clearly defined cluster centers. However, many regions show overlapping profile features, resulting in similar cluster centers (see Figure B.4 in Appendix B). Furthermore, geographic regions with a larger profile variability, especially a variation in length, still show the tendency of cluster centers to longer profiles (see Figures B.6 and B.7 in Appendix B for an illustration of this). Therefore, geographic filtering does not significantly improve the cluster results.

Length binning The profile dataset is grouped into length bins, with increasing bin size for larger reefs. For a first estimate of the effect of length filtering, the following length bins are created:
(0-250 m, 250-500 m, 500-1000 m, 1000-2000 m, 2000-4000 m, 4000-17000 m)
As shorter profiles are more suitable for restoration purposes than the very long profiles, the length bins are chosen such that the resolution is improved for shorter profiles. From Figure B.5 and Table B.5 it is clear that profiles are now more equally distributed across the cluster centers and that length filtering gives a favourable RMSE value and Davies-Bouldin index.

Comparison Two promising options to characterize the reef profile dataset emerge for the preliminary analysis: the varying grid resolution and the filter technique of dividing the cluster input data into length bins and subsequent cluster analysis with the regular depth as cluster variable. As can be deduced from Table 5.2 they score very similar on the defined performance indicators. However, the advantage of length filtering over the varying grid resolution is that with length filtering, all data points are retained, while with the varying grid size, cluster variables are removed from the dataset to obtain the desired gradual increase in cross-shore spacing between depth variables. This leads to very schematic overviews of the longer profiles. Therefore, the analysis continues with the supervised classification of filtering the length before applying the cluster analysis.

5.4.2. Results cluster methods

The three cluster methods are evaluated for depth profiles that are filtered on their length. The results are displayed in Figures B.5, B.8 and B.9 in Appendix B, Section B.2, and summarized in Table 5.4. A quick scan of results with the Maximum Dissimilarity Algorithm learns that, although the technique can serve as an input reduction tool, clustering with MDA to obtain a concise overview of possible profiles is not accurate, which is apparent from the uneven distribution of profiles across cluster centers, the high RMSE value and the bumpy shapes of the cluster centers. This makes sense, as the MDA looks for the most diverse profiles without regard for the probability of occurrence. Interestingly, k-means performs better than the Gaussian Mixture model on the defined performance indicators (see Table 5.4), although the difference in performance is not very significant. However, because the k-means algorithm is computationally more efficient than the Gaussian Mixture model, k-means is used in the final cluster algorithm.

Table 5.4: A summary of the performance of the three cluster methods in finding geometrically distinct representative reef profiles. The distribution of the number of profiles across the cluster centers is judged with a grade between - - and ++, where - - indicates that profiles are distributed very irregularly across the cluster centers. The weighted average root mean square error (RMSE) is the weighted average of the RMSE's of all cluster centers, taking into account the number of profiles that belong to the cluster centers. The Davies-Bouldin index is an evaluation scheme to identify how well profiles fit in the cluster center and not to other cluster centers. A lower DB index indicates a better performance of the cluster algorithm.

	Distribution profiles across centers [- - to ++]	Weighted average RMSE [-]	Davies-Bouldin index [-]
k-means	++	2.40	1.41
Gaussian Mixture Model	++	2.73	1.67
Maximum Dissimilarity	- -	5.71	1.66

5.4.3. Representative profiles

The results of the cluster variables and cluster methods have shown that to abstract geometrically distinct representative reef profiles from a large reef profile dataset, the best results are obtained by dividing the full

profile dataset into several length bins and applying the k-means algorithm on the different length bins separately. The analysis continues on these observations, further exploring the optimal *length bin borders*, the *number of clusters centers* and the *method to extract the final representative profiles*. The steps that are executed are elaborated below.

Determination of the length bins The profiles are sorted into length bins by inspecting the borders of different cluster centers for large length bin widths, determining the length-bin borders in such way that cluster centers are not divided in two by the border (see Figure B.10 in Appendix B for an illustration of this). Five length bins are distinguished.

Determination of the number of clusters To ensure that the topographic variability of the dataset is retained, a large number of cluster centers is desired. However, for a compact overview of dataset characteristics, few cluster centers are preferred. Based on several test runs with different numbers of clusters, it was concluded that 10 to 15 cluster centers per length bin are a good balance between topographic variability and compactness of the results. The exact number of clusters is decided by evaluating the Davies-Bouldin index for the different numbers of cluster centers.

Extraction of representative profiles As the cluster centers are imaginary profiles that are not per se visible in nature, they are converted to real profiles. This is done by extracting the profile that is most similar to the cluster center by means of the minimum Euclidean distance. However, the results also show significant variability within each cluster center. To capture this behaviour, additional clustering per cluster center was performed, which did not lead to the desired improved topographic representation. By trial and error it was concluded that the profiles similar to the 12.5, 25, 75 and 87.5 percentile do capture the smaller scale profile variations, while still accurately representing the cluster center subset, see Figure B.11 in Appendix B for an illustration of this. Here the profiles in a cluster center are labeled to one of the five representative profiles based on the minimum Euclidean distance. Thus, in total five real profiles are extracted per cluster center. The final results are displayed in Figures B.12 to B.21 in Appendix B, where for each length bin the cluster centers are depicted separately, showing all profiles belonging to the cluster center, the confidence intervals and the representative profiles.

Deduction of general profile characteristics All results are examined to deduce general profile characteristics. Based on careful visual inspection, it appears that ten profile shapes are adequate to represent (almost) all representative profiles. Profiles that are irreducible to simple generalizations are labeled as 'Not assigned' in Table 5.5. The profile shapes are depicted in Figure 5.10. Table 5.5 gives an estimate of the frequency of occurrence of the ten profile shapes (ordered from high to low prevalence). This table is constructed by labeling all representative profiles as one of the ten reef types and summing up the size of the dataset that corresponds to the representative profiles.

Table 5.5: Reef types and their frequency of occurrence

Type	0	1	2	3	4	5	6	7	8	9	10
Description	Not assigned	Straight	Typical	Barrier	Convex	Three-slope	Concave	Two-slope	Two-slope forereef	Lagoon	Offshore crest
Nr. of profiles	631	9288	5543	4020	3413	3110	2264	768	762	211	148
Freq. of occurrence	0.02	0.31	0.18	0.13	0.11	0.10	0.08	0.03	0.03	0.01	0.00

The ten profiles are shortly described as:

1. The '**straight**' reef type with a constant slope.
2. The '**typical fringing reef**' type where a distinct reef flat is apparent, followed by a relatively steep forereef slope.
3. The '**barrier**' type, which shows a reef flat, followed by a mildly sloping region, a trough and then a crest.

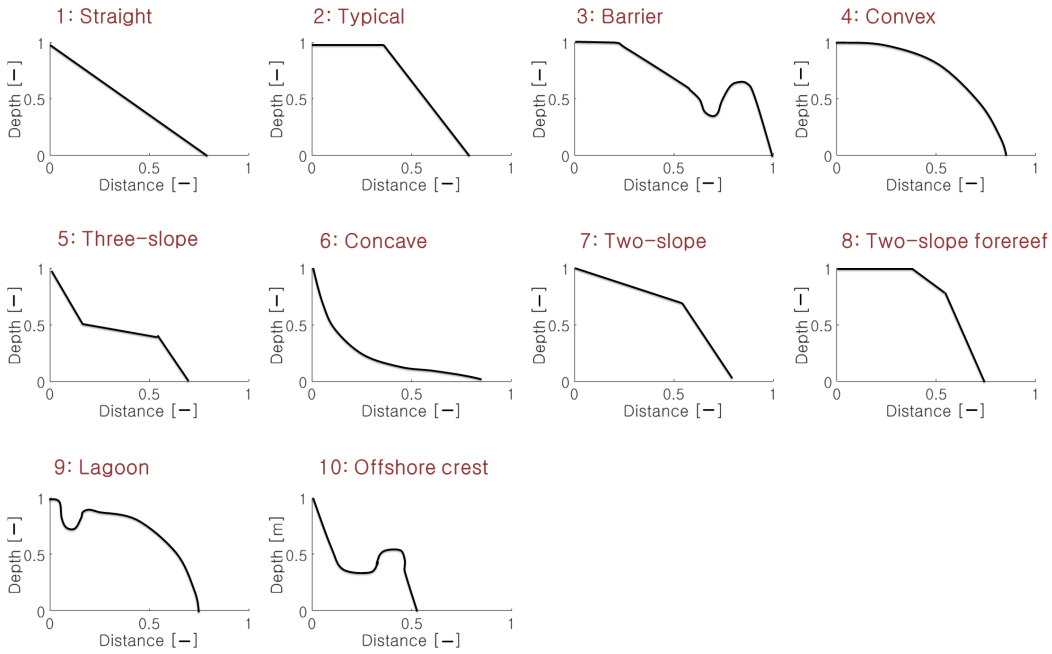

Figure 5.10: The ten governing reef types of the US reefs, based on the inspection of cluster analysis results

4. The '**convex**' profile where the transition between the reef flat and the forereef is gradual, with an increasing slope in offshore direction.

5. The '**three-slope**' profile, where two distinct, sharp increases in depth are connected by a flat or mildly sloping shelf at depths significantly below the mean water level.

6. The '**concave**' reef type, where the slope is steep nearshore and gradually flattens in offshore direction.

7. The '**lagoon**' type, with a lagoon close to shore followed by a convex depth profile.

8. The '**two-slope**' profile, in which two regions can be discerned; a mildly sloping part closer to shore, followed by a steeper forereef.

9. The '**two-slope forereef**', where the steep forereef is connected to the reef flat by an intermediate slope region.

10. The '**offshore crest**', where a steep slope is interrupted by a clear bump in the profile.

Some critical notes can be made on these results, which are shortly described below.

- The cluster algorithm is not adequately fit to distinguish smaller scale reef features such as lagoons and reef crests, as even shorter cross-shore translations of these features results in a large dissimilarity between two profiles. Therefore, the estimation of the number of lagoon-type reefs is most probably underpredicted.

- Typical reefs with a short reef flat (widths up to 50 m) are hard to distinguish as the profiles seem similar to the straight reef profile. For this reason, the number of typical fringing reef-type profiles is likely underpredicted. Furthermore, as a cluster center is the centroid of all observations in a clustered group, the shape of the cluster center tends to become more gradual than is observed in nature. Figure 5.11 gives an illustration of this. For this reason, even if many profiles in a clustered group are regarded as the typical reef profile, the cluster center can look differently. This problematic issue is partly resolved by extracting the real profiles from the dataset instead of using the cluster centers directly.

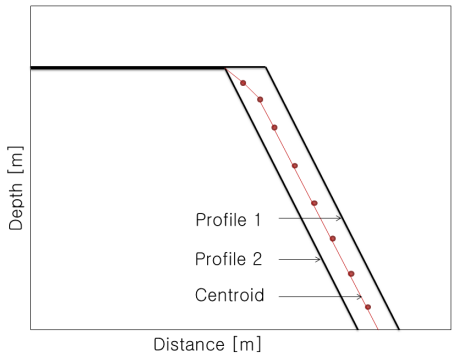

Figure 5.11: An illustration of how cluster center shapes seem smoother than the observations belonging to the cluster

- To calculate how many reef profiles each shape represents (Table 5.5), all reef profiles in a clustered group are labeled to one of the five representative profiles. In this way, outliers are also labeled to the reef shape to which it is most similar to, while in effect they look not much alike the particular reef shape. Therefore, the numbers denoted in Table 5.5 mainly serve as a first order estimate of the frequency of occurrence of different reef types.

Selection of reef shapes for the modeling study In the final step, the profiles to be used as input for the subsequent modeling steps are determined by inspecting the profile shapes depicted in Figure 5.10 and the reef type characteristics denoted in Table 5.5.

From Table 5.5 it is clear that profiles shapes 7 to 10 (two- slope, two-slope forereef, lagoon and offshore crest) are rare shapes, with a frequency of occurrence of less than 3 percent. Next to that, the two-slope forereef profile is similar to the typical profile and the convex profile, adding limited value when modeling this profile. Therefore these shapes are excluded from the modeling studies.

Because of computational constraints, the full length of the barrier reef is difficult to model. As the shoreward region of the barrier reef looks much alike the 'typical' fringing reef, the typical reef is assumed to also represent the barrier reef type, leaving five reef types. These five shapes are observed to verify whether they will distinctly affect the wave transformation process. While the straight, typical fringing, convex and three-slope profile show distinct features, the concave profile is similar to the straight profile, showing only a difference in shape at larger depths where wave dissipation is less affected by the profile shape. The shallower foreshore of the concave profile compared to the straight profile will lead to a reduction in the short wave height and possibly in setup and infragravity wave height as well, but this change in wave transformation is expected to be small compared to the difference in wave characteristics between other profiles. Therefore, the concave profile is also excluded from the modeling study. This leaves four dominant profiles: the straight, the typical fringing, the convex and the three-slope shape, which account for 70 % of all the reefs surveyed in this study. Of these four dominant reef types, the general characteristics are established and their natural variability is denoted in Table 5.6, based on inspection of all representative profiles that are labeled to a certain reef type. Figure 5.12 gives an overview of the characteristics mentioned in this table. Figure 5.12 and Table 5.6 will help to select the input reef profiles for the modeling study that is described in the next chapter.

Table 5.6: The natural variability of the different reef shape types

Type	1	2	3	4
Description	Straight	Typical	Convex	Three-slope
Characteristic 1	Reef slope: 0.01-0.7	Reef flat width: 50-4000 m	Reef width: 300-3000 m	Nearshore slope: 0.02-0.1
Characteristic 2		Forereef slope: 0.01-0.5		Flat width: 500-1000 m
Characteristic 3				Flat depth: -4 to -10 m
Characteristic 4				Offshore slope: 0.01-0.2

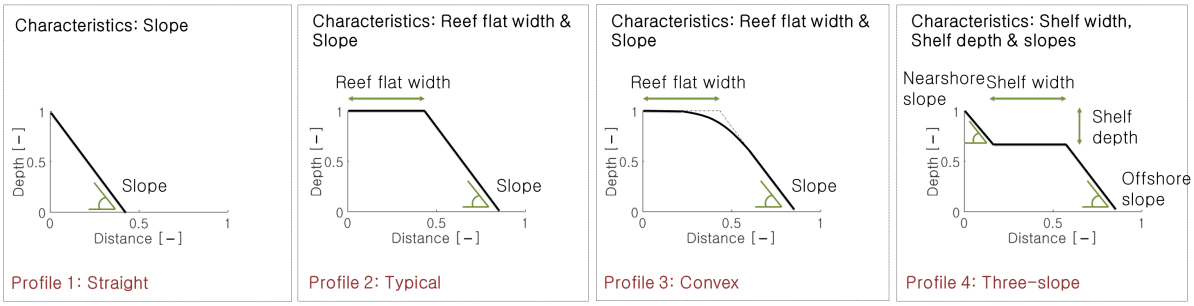

Figure 5.12: The characteristics of the 4 dominant reef shapes denoted in Table 5.6 visualized

5.5. Conclusion and Discussion

Several clustering methods have been applied to different cluster variables extracted from the reef profile dataset of US reefs. The supervised classification technique of grouping reefs based on lengths and subsequent cluster analysis with the k-means model on the separate subgroups returns cluster centers that give a good overview of the larger scale reef characteristics. The following extraction of five representative profiles per cluster center gives insight into the smaller scale profile variability, albeit with some limitations. The inspection and labeling of all representative profiles leads to the distinction of 10 dominant reef shapes and a first order estimate of their frequency of occurrence. Four of these profiles have been deemed suitable for subsequent modeling studies as their frequency of occurrence is relatively high and their features distinct from each other: the straight, the typical fringing reef, the convex and the three-slope profile. Together, these reefs represent 70 % of the reefs surveyed in this study. The natural variability of these shapes is denoted, which will be used to select the input bathymetries for the numerical simulations in the next chapter, which will be based on the schematized reef shapes.

The insight gained into the reef profile variability is the foundation for subsequent modeling steps. But of equal importance is the increase in knowledge about the predominance of different reef shapes. Often, a reef shape is assumed without a specification of its frequency of occurrence (e.g. Gourlay [56] and Buckley et al. [33]), which can now be substantiated based on the cluster analysis results. Furthermore, reef shapes have been identified that have been granted little attention in research, while often observed in nature. This gives rise to new lines of research.

It should be emphasized that the obtained reef shapes are a highly schematized version of the reef profiles. The actual reef profiles often consist of smaller scale undulations, which could in turn also affect the wave transformation process. Furthermore, the calculated frequency of occurrence is only a first order estimate and could be analyzed in more depth.

III

Numerical Simulations

Numerical simulations have been carried out to assess the effect of varying reef geometries and restoration configurations on wave transformation and flooding of reef fronted coastlines

Ch 6. Methodology

Ch 7. Reef geometry control on nearshore hydrodynamics

Ch 8. Effects of coral restoration on reef hydrodynamics and coastal hazards

6

Methodology

To gain insight into the effect of both varying reef profile shapes and restoration configurations on wave transformation and flooding at low-lying reef coastlines, a numerical hydrodynamic model needs to be set up. The model should accurately capture the dominant physics of the reef system, while minimizing the computational effort to obtain satisfactory results. In this chapter, we explain the method to establish a well-functioning hydrodynamic model, elaborating on the choice of model, the model setup with which to generate reliable results and post-processing methods.

6.1. Hydrodynamic model

Typical observations of reef hydrodynamics include significant low-frequency wave motions, a distinct setup across the reef flat, sea-swell wave breaking, reflection and wave transformation at the steep reef interface and substantial frictional wave dissipation. Buckley et al. [31] studied the skill of different nearshore wave models (XBeach [138], SWASH (Simulating WAves till SHore) [175] and SWAN (Simulating WAves Nearshore) [26]) in predicting wave transformation across steep reef environments by comparing numerical model outcomes to laboratory observations. They concluded that the reef-specific processes are accurately captured by both XBeach (see Roelvink et al. [138]) and SWASH (see Zijlema et al. [175]), models that have been validated for reef-lined coasts (e.g. Zijlema [174], Pomeroy et al. [122], Quataert et al. [125]). Of course, other models exist with similar characteristics, however as the aforementioned models are developed by Deltares, the TU Delft and UNESCO-IHE, all Dutch-based institutions, these models are selected for further inspection. Below, the choice of model, including the important model options, is elaborated by examining the required *wave resolution*, the *numerical efficiency*, the *dimensional space* and the method of *vegetation modeling*.

Wave process resolution A choice must be made between the short wave-resolving models, where individual short waves are modeled (both SWASH and XBeach non-hydrostatic mode are capable of this), and short wave-averaging (long wave -resolving) models (XBeach-surfbeat mode), in which short wave height variations on the wave group scale are solved. Van Dongeren et al. [160] showed the good predictive skill of the XBeach-surfbeat (XB-SB) model, a long wave-resolving model, in simulating the IG wave dynamics at reefs, both the generation mechanism and decay due to frictional wave dissipation, as well as the runup and rundown of infragravity waves. Lashley et al. [83] investigated the validity of this short-wave averaged model to predict wave transformation and wave runup at reef coasts by comparing the XB-SB model to the short wave-resolving nonhydrostatic XBeach model (XB-NH). They concluded that XB-NH systematically underpredicts the setup across the reef while accurately representing H_{rms}, in contrast to the XB-SB model where the setup is accurately predicted while the wave energy on the reef flat is overestimated. Furthermore, Lashley et al. [83] observed that both the XB-SB and XB-NH model accurately capture the extreme runup under various hydrodynamic conditions (while the short wave runup component is not included in the XB-SB model), as the runup was dominated by low-frequency waves. The shortcoming of the XB-SB model to not include the short wave runup component was highlighted by Gawehn [52], who, in contrast to Lashley et al. [83], concluded that a short-wave resolving model is key to accurately predict the runup. As the different runup components (the setup, short, IG and VLF wave components) are of interest in this research, here also a short wave-resolving model is adopted.

Resolved physics Since the initiation of short wave-resolving model development, Boussinesq type models have been the primary focus of attention [176]. In contrast to the shallow water equations, the Boussinesq type equations include frequency dispersion and non-linear wave field evolution [176]. Among others, Nwogu and Demirbilek [113] validated a Boussinesq type model with laboratory data of fringing reefs, showing that the model accurately captures nonlinear wave-wave interactions and runup. However, Zijlema et al. [176] argue that their non-hydrostatic model (SWASH) is even more skilled to model wave transformation processes on the scale of individual short waves, by incorporating an efficient numerical scheme with an improved description of the wave breaking process. The early version of SWASH [176] was thereafter incorporated in the XB-NH model, making the two models, when used in 1D, highly similar.

Dimensional space Van Dongeren et al. [162] investigated low-frequency dynamics across a fringing reef using both a 1D and 2D XBeach model, to test the predictive skill of the differing model settings. With the two-dimensional model, wave-driven circulation cells were observed that induce a reduction in setup, which in turn leads to realistic friction coefficients that were used to calibrate the model with field data of the Ningaloo reef. These wave-driven flows are not captured by the 1D model, rendering the model more sensitive to calibration options. However, the 1D model was concluded to be able to capture the important hydrodynamic processes. As 2D models are computationally more expensive and require significantly more time to construct, the 1D model is assumed to sufficiently capture the desired phenomena.

As can be concluded of previous paragraphs, a 1D, non-hydrostatic phase-resolving model meets our modeling requirements, making both XB-NH and SWASH equally suited. However, as this research continues on work by among others Pearson [116], Gawehn [52] and Quataert [124], who successfully used the XB-NH model to simulate wave transformation and runup on reef lined coasts, the XB-NH model is chosen.

Vegetation modeling Wave dynamics are considerably affected by the coral canopy, as was discussed in Section 2.2.2, Chapter 2. There are two options to model this canopy in XBeach. Firstly, a canopy flow model can be implemented, in which flow through the canopy is solved, based on which the canopy drag force is determined that causes the dissipation of waves [142]. Secondly, the dissipation by vegetation can be captured by adjusting the bottom friction coefficients. Rooijen et al. [142] studied the skill of a canopy flow model coupled to the XBeach non-hydrostatic model and concluded that the accuracy of the wave height prediction is increased compared to the bottom friction approach, although similar results can be obtained by the calibration of friction coefficients. A disadvantage of the canopy model is that much information about the coral canopy structure is required, which is often not available, making the bottom friction approach easier to implement. Furthermore, the canopy flow model is less validated than the bottom friction approach [142]. As this research does not focus on individual coral species but on the overall effects of frictional wave damping across restored coral sections, the bottom friction approach is deemed better suited.

6.2. Input selection

To capture the effect of the reef geometry on wave hydrodynamics, different *bathymetries* are selected to serve as input for the modeling study. Furthermore, to assess whether coral restoration enhances coastal safety by reducing the runup, various *restoration configurations* are modeled. This leads to a wide variety of bathymetric inputs, that are all subjected to different *hydrodynamic forcing conditions*. Below, the chosen parameter space of the bathymetric and hydrodynamic input is elaborated. In the decision of the parameter space to be modeled, a trade-off must be made between the computational costs (storage and run durations) and the required variation in input conditions to be able to make conclusions on the effects of differing geometries and restoration configurations on nearshore hydrodynamics.

6.2.1. Bathymetry

The bathymetric input is selected based on the results of the cluster analysis, in which four dominant reef shapes are established (see Figure 5.12), of which the observed natural variability in profile characteristics is denoted in Table 5.6. For each reef shape, a number of parameter variations is modeled to include the natural variability of the profile shape. This number is limited to reduce the model input, as the primary research interest is the effect of the different restoration configurations, which requires numerous simulations in itself. Nevertheless, the selected profile variations should give a good first impression of the reef geometry control.

The four profile shape configurations are elaborated below. All profiles are modeled for a 1:12 beach slope, adopted from Lashley et al. [83].

Typical fringing reef profile The typical fringing reef profile is described by its reef flat width and forereef slope. The effects of varying reef profile parameters on wave transformation and runup have been extensively studied by Pearson [116]. For this reason, only four profile variations are modeled, varying the slope (0.1 and 0.5) and the width (100 and 250 m), in which the smaller widths are chosen for computational efficiency.

Convex profile In effect, the convex profile is a variation of the typical fringing reef profile, in which the sharp transition between the forereef and the reef flat has been smoothed. To investigate the difference between the smoothened convex profile and the typical profile, the convex profile is modeled for a single slope of 0.1 and two reef widths (100 and 250 m). The convex profile, relative to the typical reef profile, is illustrated in Figure 6.1.

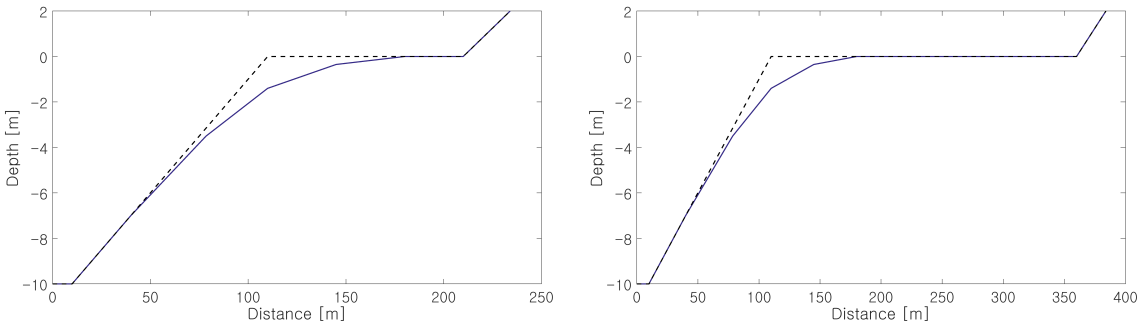

Figure 6.1: Input geometries of the convex reef profile

Straight profile As can be deduced from Figure 5.12 and Table 5.6, the straight profile is described with one characteristic, the slope, which is observed to range from a value of 0.01 to 0.7. To capture this variability, the straight profile is modeled with three different slopes: 0.025, 0.1 and 0.5.

Three-slope profile The three-slope profile, in which a sharp nearshore slope is followed by a shelf, shows a large natural variability, with varying shelf widths, shelf depths, and differing nearshore and offshore slopes. As shelfs at larger depths have little influence on wave transformation, and as the depth at which coral restorations can be executed (see Section 6.2.2) is between 2 and 7 m, a shelf depth of 5 m is chosen. Shelf widths of 100 and 250 are modeled to be able to compare the influence of the shelf width to the reef flat width. Both offshore and nearshore slopes are set at 0.1 in order to compare the effect of the three-slope profile to the straight profile.

6.2.2. Restoration configurations

For each profile type, different restoration configurations are designed, based on restrictions of coral restoration works and the existing reef morphology. Several restrictions have been set for coral restoration based on consultation of the United States Geological Survey (USGS), a US scientific agency, which are elaborated below.

Restoration depth Restorations are mostly performed at depths between two to seven meters. The upper boundary is set by ecological constraints; coral cannot grow in very shallow areas as seawater temperatures rise quickly for low water depths, which the coral cannot survive. The lower boundary is set by operational constraints, as coral restoration works at large depths are expensive and less efficient as both frictional and wave breaking dissipation are smaller at larger water depths.

Restoration height As discussed in Section 2.3, two types of restoration exist, the natural restoration (coral transplantation, commonly referred to as green restoration) and the artificial restoration (artificial reef construction, also referred to as grey restoration). The former is assumed to create an increase in bed level of 0.25 meters, whereas the artificial reef is assumed to increase the bed level by 1.25 m.

Restoration width The effects of reef restorations are modeled for three different reef widths: 5, 10 and 25 meter. The width of the restored area is constricted due to the costs. The artificial reef widths are restricted to 5 and 10 meter as costs of this restoration technique are higher than for the natural restoration.

Restoration location Restorations at different cross-shore locations are investigated, of which the exact locations are displayed in Figure 6.2. These locations are chosen based the restoration depth constriction. It should be noted that restorations at the reef flat (for the typical reef and the convex reef) are only modeled for water depths above 2 m, as restored sections at the reef flat that are often exposed to shallow water depths are not viable. Furthermore, simulating restorations that reach above mean water level increases the chance of computational instabilities.

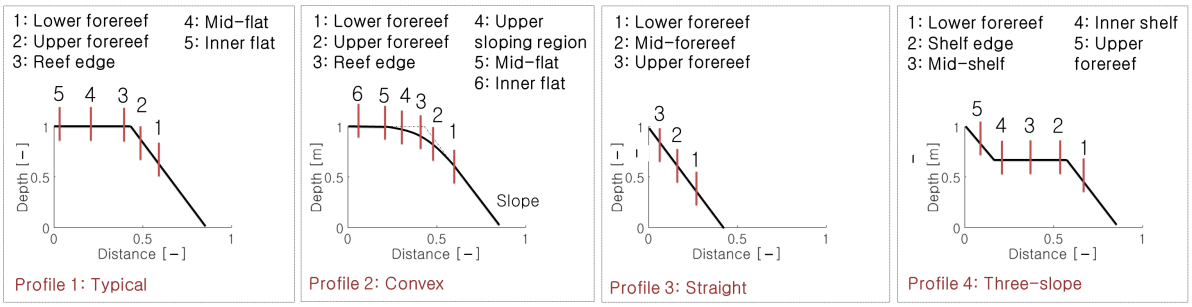

Figure 6.2: Restoration locations across the different reef shapes

Restoration roughness Restorations significantly increase the bottom roughness. Appropriate values for the friction coefficient are determined based on the paper of Storlazzi et al. [151], were different friction coefficients were established for different percentages of coral cover. Here, a friction coefficient of 0.1 is assumed for restored areas (50 % coral cover) and 0.01 for the other parts of the reef (no coral cover).

6.2.3. Hydrodynamic conditions

To investigate the effect of the reef geometry control and restoration works under varying forcing conditions, different water levels, wave heights and wave periods are imposed on the model.

Offshore water level The water level is a critical parameter in reef hydrodynamics. It controls among others the frictional wave damping, wave breaking dissipation, the IG wave generation and the setup. To account for varying tides, possible sea level rise and other water level variations, different water levels relative to the beach toe are modeled. Reasonable values for water level variations are deduced from Kolijn [82], who concluded that reef water levels of 68 investigated reef sites often range between 0 and +2.5 m relative to the reef flat, with tidal excursions of 0.5 to 1 m. For the purpose of restoration for coastal protection, shallow water depths are not of interest as runup at the coast is expected to be small. Therefore offshore water levels of 0.5, 1 and 2 m are modeled.

Offshore wave height Coral restorations are expected and designed to increase coastal safety for moderate storm events. Wave heights corresponding to these storm events vary significantly across reef lined islands. The database of Kolijn [82] showed that significant wave heights of random measured storm events vary between approximately 1 and 4.5 meters, while Quataert et al. [125] observed maximum wave heights of 6 m. Therefore, offshore wave heights of 2, 4 and 6 meters are modeled.

Offshore wave period As can be concluded from the data analysis (Chapter 4) on XBeach simulations by Pearson [116] of fringing reefs, the wave period strongly affects reef hydrodynamics and runup in particular. The effect of the wave period is best included by incorporating different values for the wave steepness, that is defined as:

$$s_0 = \frac{H_0}{L_0} = \frac{H_0}{\frac{gT_0^2}{2\pi}} \tag{6.1}$$

The wave steepness is a measure of the sea state. A low wave steepness (0.01) indicates a swell event, whereas a high steepness (0.05) corresponds to locally generated storms. Therefore, values of 0.01 and 0.05 are modeled for the wave steepness, which corresponds to the following wave periods:

Table 6.1: Wave periods corresponding to different combinations of wave heights and wave steepness factors

		H (m)		
		2	4	6
Steepness	0.01	11.32	16.02	19.6
(-)	0.05	5.06	7.16	8.77

6.3. Model setup

The setup of the one-dimensional, non-hydrostatic XBeach model, that is run for different input bathymetries and forcing conditions, requires attention to the *computational grid*, the generation of *boundary conditions*, the important *parameter settings* and the *output selection*.

6.3.1. Computational grid

A computational grid is constructed in consideration of several factors. Firstly, XBeach-NH does not solve the exact dispersion relation, but an approximation of it. This approach was shown to approximate linear wave theory well for values of kh (=2*π/L * h, where L is the wave length and h the depth) below 1 [149] (shallow water). Therefore, depths should not be larger than this limit. Hence, the offshore depth is determined by the dispersion relation as well as the wave height to depth ratio, as waves should not enter the domain and break instantly.

The grid size determines what part of the high-frequency end of the spectrum is captured by the model. The grid points per wave length are set at 64. At each location, the maximum grid size is determined based on the local wave length and the number of grid points required per wave length. XBeach determines the time step required for Courant number stability based on the grid size, from which it follows that small grid sizes drastically increase simulation times due to the small allowed time steps.

Along the beach, grid resolution is high until the maximum expected runup, which is assumed to be two times the incoming offshore wave height, based on maximum runup heights observed by Pearson [116]. From this point up to the beach crest, grid resolution decreases again for computational efficiency. Behind the beach crest, a negative slope is applied to prevent eventual overtopping volumes from flowing back to the sea. Overtopping reduces the runup and therefore scatters the results. To monitor whether overtopping occurs and runup is underpredicted, overtopping volumes are measured with a discharge meter on top of the beach crest.

6.3.2. Boundary conditions

At the offshore boundary, a wave time series is imposed that should represent the deep-water sea state. This time series is computed by XBeach based on the JONSWAP spectrum, requiring the significant wave height and frequency, the spectral shape and the directional wave spreading coefficient as main input. The wave height and period are varied, the spectral shape is set at 3.3 (the default value for wind seas) and the directional wave spreading at 100.000 (the value to indicate zero directional wave spreading). In our case, several unique time series of half an hour are created, implicating that the longest possible wave in our domain has a wave period of half an hour. The model run duration is set at three hours, to be able to make a fair estimate of the runup ($R_{2\%}$) value. In three hours, approximately a thousand peaks of 10 s waves can be captured,

enough to accurately predict the $R_{2\%}$ value. The resolution decreases for longer period waves, making the prediction of the IG and VLF component of the runup less accurate. For each combination of hydrodynamic input parameters, the time series is computed by XBeach and reused in all simulations with equal hydrodynamic forcing, to be able to systematically compare results of different reef geometries and restorations. For all simulations, an equal spin-up time of one hour was incorporated, based on the analysis of spinup times of reefs with differing reef widths by Pearson [116], who concluded that reefs up to 1500 m in width require a spinup time of less than an hour. During this time, waves that are generated at the offshore boundary will have traveled across the domain, ensuring that everywhere on the reef wave energy is present.

6.3.3. Parameter settings

All parameter settings of XBeach are mentioned in the 'params' file, of which an example can be found in Appendix C. Most parameters are set at their default value. Roelvink et al. [139] note that the most sensitive parameter is the maximum breaker steepness (*maxbrsteep*), the parameter that determines where the non-hydrostatic correction is turned off, defined as the wave height to water depth ratio. Its optimal value is found at 0.4.

6.3.4. Output selection

Different parameters can be selected as output by XBeach. For global output, output is given at each x-grid location at a user specified output time interval. Point output gives output at specified output locations, for which the output time can be reduced without increasing the storage too much. Point output is specified at the following locations:

- Offshore
- At 5 meters below the beach toe elevation
- At the reef crest/ shelf edge (if present)
- At the mid-flat/ mid-shelf (if present)
- At the inner edge of the shelf (if present)
- At the beach toe
- At 0.5 m seaward of a restoration
- Halfway the restoration
- At 0.5 m shoreward of the restoration

The water level, bed level and velocity are given as output parameters, based on which wave heights (different components and a distinction between incoming and outgoing wave heights) and the setup can be determined. Runup is determined by a runup gauge, while a discharge meter at the top of the beach records whether overtopping occurs.

6.4. Post-processing methods

The XBeach output is post-processed to obtain the $R_{2\%}$ value, the runup components, the SS, IG and VLF wave height components (the total, the incoming and outgoing wave heights) and the setup. The $R_{2\%}$ value, the runup with a 2 % exceedance value, as well as the $R_{2\%}$ value of the SS, IG, VLF and setup component of the runup, are calculated based on water level time series of the runup. The setup component is obtained by extracting the offshore water level from the mean water level. The SS, VLF and IG runup components are obtained from the detrended water level time series by spectral composition, where the cutoff frequencies of 0.04 (cutoff between SS and IG waves) and 0.004 (cutoff between IG and VLF waves) determine which part of the variance spectrum belongs to which component. The total water level results are sorted in ascending order to select the 2 % exceedance value.

At each cross-shore location, wave height components can be discerned based on spectral analysis of local water level time series. Furthermore, water level time series can be splitted into incoming and outgoing water level time series based on the method of Guza et al. [60], using water level elevations and velocities.

7

Reef geometry control on nearshore hydrodynamics

7.1. Introduction

The control of the typical fringing reef geometry (e.g. slope of the forereef, reef flat width) on wave transformation and dissipation has been intensively studied (e.g. Gourlay [56], Nwogu and Demirbilek [113], Pomeroy et al. [122] and Cheriton et al. [37]). To a lesser extent, profiles with a slight deviation from the typical fringing reef profile have been modeled as well (e.g. Massel and Gourlay [93], Costa et al. [40] and Kench and Brander [78]). The reef profile classification of US reefs demonstrated the presence of other prominent reef shapes than the typical fringing reef, which show a relatively high frequency of occurrence and expectedly distinct hydrodynamic behaviour: the straight reef profile, the convex shape and the three-slope profile. Therefore, numerical simulations have been carried out to investigate the effect of varying reef geometries on wave transformation and runup at the coast. The input selection and model setup have been described in Chapter 6 (Methodology). Below, the XBeach results of the geometry control are elaborated for each profile shape.

7.2. Results

In this section, wave transformation and runup are analyzed for the four reef shapes. First, an analysis of typical fringing reef wave characteristics is made, as these observations can be supported by literature and the conceptual model results (Chapter 4). Next, the hydrodynamics of the convex, straight and three-slope profile are analyzed and compared to the typical fringing reef profile.

For each profile shape, the wave height transformation across the different profile configurations (differing widths and slopes) is depicted for one hydrodynamic condition, for which median input conditions are chosen: a wave height of 4 m, a water level of 1 m and a wave steepness of 0.05 (wind-sea) (Figures 7.1, 7.3, 7.6 and 7.8). Next to that, the influence of varying hydrodynamic conditions and profile parameters on runup is illustrated for each profile shape (Figures 7.2, 7.4, 7.7 and 7.9).

7.2.1. Typical fringing reef profile

The results of the XBeach simulations for the four typical fringing reef profile configurations are depicted in Figure 7.1. This figure gives insight into the IG and VLF wave generation at the reef crest, reflection against the reef crest, wave dissipation across the reef flat and the frequency shift throughout the domain, as well as the influence of differing dimensions of the typical fringing reef profile on the final runup height. The observations that are elaborated below are in line with the literature review and conceptual model results.

Waves are generated at the offshore boundary, where a unimodal JONSWAP spectrum is imposed in which most energy is contained in the SS band. At the steep interface of the forereef, a second spectral peak appears near the lower frequencies, the infragravity motions that are found to be primarily generated by the breakpoint generation mechanism on steep (>1:20) forereef slopes [30][94]. This generation mechanism is

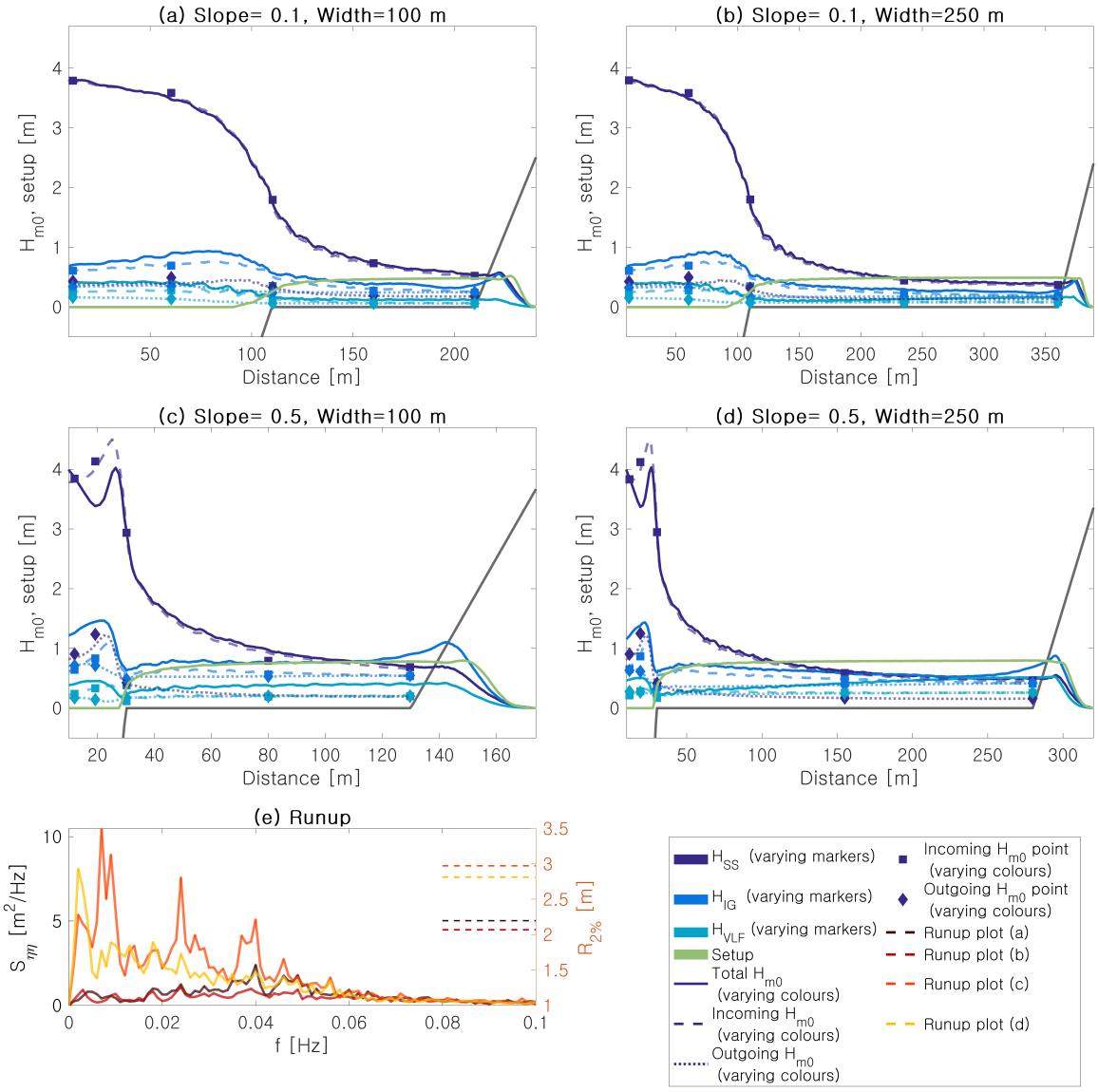

Figure 7.1: Wave transformation ((a) - (d)) and runup (e) across four typical fringing reef profile configurations. The colours depict the different wave components (short, infragravity and very-low frequent waves) and the setup. The marker shapes depict either incoming or outgoing waves calculated from point output data of XBeach. The different line plots depict either total, incoming or outgoing wave heights obtained from the global XBeach data. The difference between point output data and global data is attributed to the output resolution of the global data (output is generated every 2 seconds), which is smaller than the point output data (output is generated every second).

thoroughly analyzed in Section 4.2.2, from which it was concluded that the height of the IG waves is primarily dependent on the forereef slope, the water level, the wave height and the wave period, in accordance with the recent study of Masselink et al. [94]. This conclusion is supported by subplots (a) and (c) of Figure 7.1, from which it is clear that the IG wave height increases with increasing forereef slope. The VLF motions show similar patterns, with a drastic increase in wave height for the 1:2 slope, in accordance with the study by Gawehn et al. [53] who noted the VLF wave height increase as a result of the breakpoint mechanism. Interestingly, the VLF motions show divergent growth patterns across the reef flat for the different geometries. For the 1:2 slope (subplots (c) and (d)), a progressively increasing VLF wave height across the reef flat is observed, with increasing wave heights for larger widths. Across the 1:10 slope (subplots (a) and (b)), VLF wave heights are progressively damped. Gawehn et al. [53] studied growth patterns of VLF waves across a fringing reef flat at Roi Namur, where VLF waves were found to either show resonant, standing, progressive growing

or progressive dissipative behaviour. For water depths larger than 0.5 m, they mainly observed VLF waves that are growing in amplitude shoreward of the reef crest, which could explain the observed behaviour of the VLF waves in subplots (c) and (d), supported by the fact that the frictional coefficients are low and the setup across this profile large. The progressive dissipative behaviour is spotted in subplots (a) and (b), where incoming VLF waves as well as the setup are lower.

Across the reef flat both low and high frequency waves are dissipated by frictional wave damping and wave breaking dissipation. Close to shore, the peak of the energy is fully shifted to the lower frequencies, the short waves being largely dissipated. The influence of the reef flat width is evident from the larger SS and IG wave dissipation across reefs with equal forereef slope but larger reef widths. Furthermore, as the wave breaking zone is more confined for steeper slopes, radiation stress gradients increase and hence the setup, which follows from the comparison of setups of subplots (a) and (c) (and (b) and (d)). The increase in setup leads to an increase in maximum stable short wave height across the reef flat, leading to larger short wave heights at the beach toe for steeper forereef slopes.

At the steep forereef and the relatively steep beach, waves are reflected. Reflection increases for lower frequency waves and steeper bed slopes [15]. This is supported by the plotted incoming and outgoing wave heights for the different topographies. The steeper forereef configurations (subplot (c) and (d)) drastically increase the reflection of IG waves that are generated just offshore of the reef edge, which is apparent from the large outgoing wave heights at the forereef. Even shorter period waves are reflected off of this steep bed. This does not occur for the more gentle slopes of subplots (a) and (b). The reflection of IG waves and VLF motions at the beach is also significant, which leads to an overall increase in IG and VLF wave heights across the reef flat.

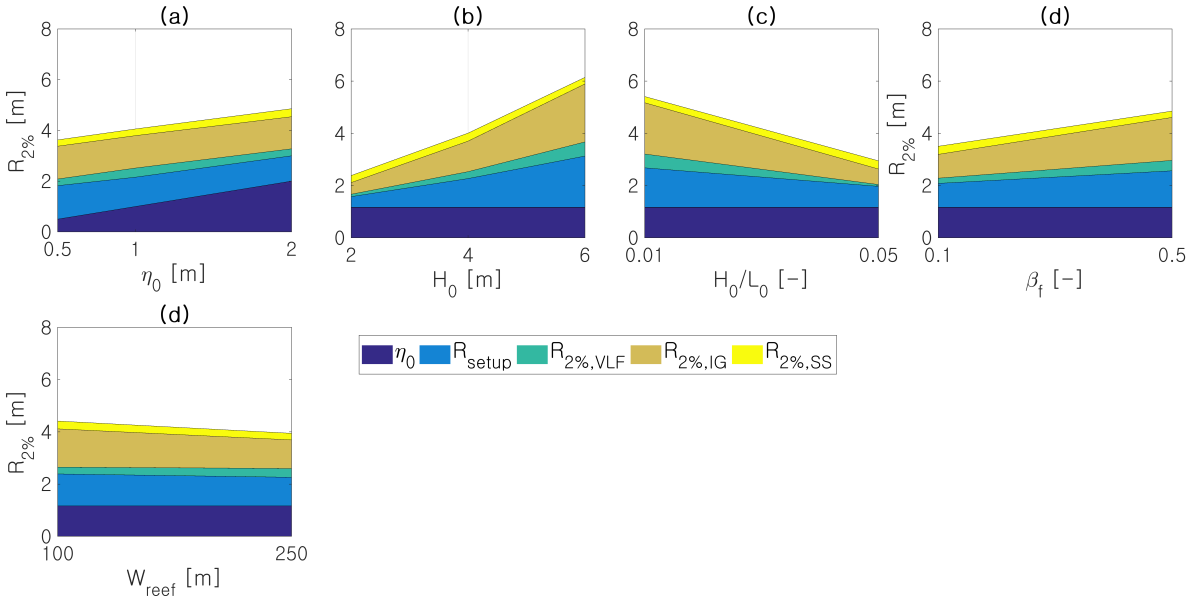

Figure 7.2: The effect of varying hydrodynamic conditions and profile parameters of the typical fringing reef on the different runup components: the water level, wave height, wave steepness, forereef slope and reef width, respectively

In subplot (e) of Figure 7.1 the runup spectra are depicted for the four different geometries under one hydrodynamic forcing condition, while in Figure 7.2, the effect of varying boundary conditions and profile parameters on runup is displayed. The runup at the typical fringing reef profile has been extensively inspected in Section 4.2.3 (see Figure 4.7), of which the observations are confirmed by Figure 7.1 and 7.2: Larger wave heights, lower steepness values and larger forereef slopes drastically increase the setup, the IG and the VLF wave components of the runup, while larger reef widths slightly decrease both the SS, IG and VLF component of the runup. For similar XBeach simulations of a fringing reef, Pearson et al. [117] noted a larger dependence of runup on the reef width, which is to be expected due to the higher modeled friction coefficients.

7.2.2. Convex profile

Two configurations of the convex profile are modeled, which are displayed in Figure 7.3. In general, the mechanisms underlying the hydrodynamics of the convex profile are similar to the typical fringing reef profile, such as the IG generation by the breakpoint, the distinct setup zone, the wave height decay across the reef flat and the shift of the energy peak from the high frequencies to the lower frequencies. Below, most important observations that distinguish the convex reef from the typical fringing reef profile are elaborated.

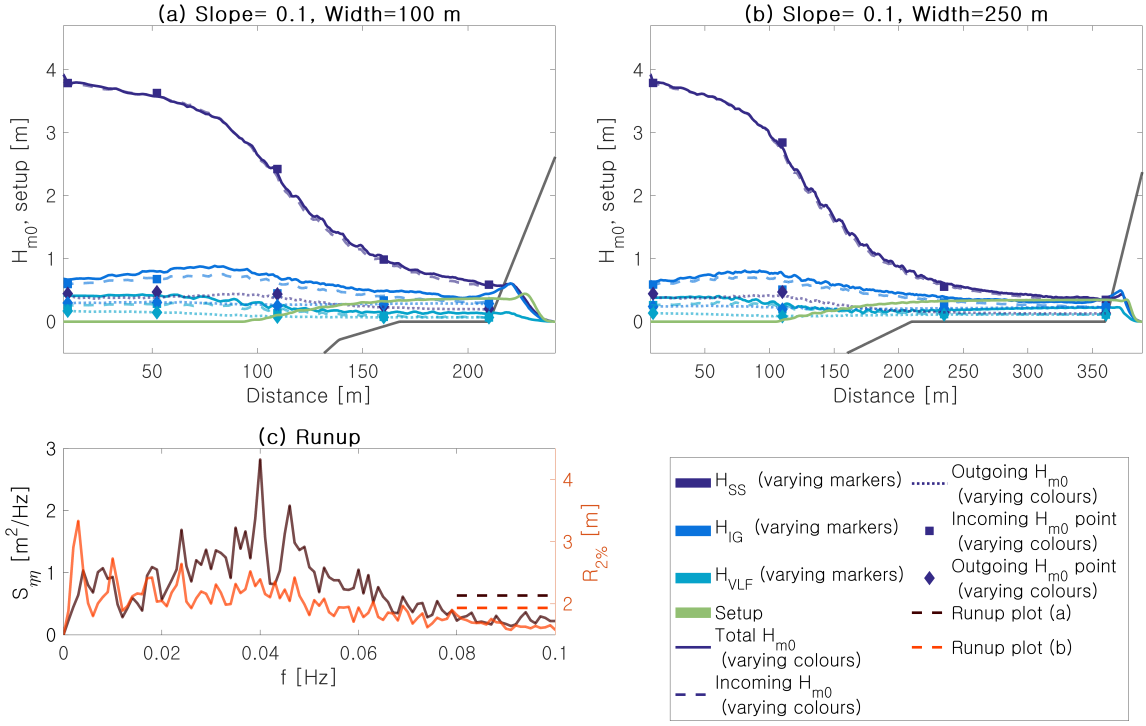

Figure 7.3: Wave transformation ((a) - (b)) and runup (c) across two convex reef profile configurations. The colours depict the different wave components (short, infragravity and very-low frequent waves) and the setup. The marker shapes depict either incoming or outgoing waves calculated from point output data of XBeach. The different line plots depict either total, incoming or outgoing wave heights obtained from the global XBeach data. The difference between point output data and global data is attributed to the output resolution of the global data (output is generated every 2 seconds), which is smaller than the point output data (output is generated every second).

The main characteristic of the convex profile is the smoothed reef edge, where the depth decreases gradually compared to the typical fringing reef profile. The gradual shoreward decrease of the depth causes a gradual decay of the incident short wave height, which induces lower radiation stress gradients than the typical fringing reef profile, hence a significantly lower setup of the water level across the flat. As a result of reduced frictional wave dissipation across the flat, due to larger water depths at the reef edge of the convex profile, beach toe SS wave heights are larger at the convex profile.

The maximum incoming IG wave height of the convex profile (offshore of the reef crest) is approximately equal to the typical fringing reef profile (see Figures 7.1 and 7.3). Shoreward of the reef edge, however, IG wave heights are larger for the convex reef. This could be caused by several factors. Firstly, the steeper reef interface of the typical fringing reef profile leads to larger reflections of the IG and VLF motions, which can result in larger total IG wave heights offshore of the reef crest for the typical fringing reef and lower IG wave energy across the flat. Furthermore, the smooth convex profile leads to a more gradual decay of IG waves, that slowly adapt to the decreasing depths, whereas IG waves have been noted to dissipate energy at the steep reef edge of the typical fringing reef profile, possibly due to wave breaking [162]. Also, frictional wave dissipation is larger for the shallow water depths above the reef flat of the typical reef. These three factors are assumed to cause the IG wave height of the convex profile to be slightly larger than the typical fringing reef profile values. The very-low frequency motions across the convex reef show a similar, progressively damped behaviour as

the 1:10 sloped typical fringing reef profile.

Total runup values for the two convex profiles under one forcing condition, which are displayed in subplot (c) of Figure 7.3, are lower than for the two typical fringing reef profiles with similar slope (1:10) and widths. The runup spectra, however, show an increase in low frequency runup at the convex coast compared to runup at the typical fringing reef. In Figure 7.4 the different runup components, under varying forcing conditions, are displayed to investigate the cause of the total runup decrease. In order to make a fair comparison between the convex profile and the typical fringing reef profile, Figure 7.2 is replotted after filtering out slope values of 0.5 (see Figure 7.5). From the inspection of Figures 7.4 and 7.5, it is clear that the decrease in runup is the result of a decrease in setup, whereas the contribution of the IG component slightly increases for the convex profile, which is the result of both slightly larger IG and SS beach toe wave heights for the convex profile. Runup at the convex profile responds less to water level variations than the typical fringing reef profile due to the smoothed profile, where the setup does not decrease significantly with increasing water levels. To the other boundary conditions (the wave height and the steepness) and profile parameters (the reef width), the runup at the convex profile responds similarly to the typical fringing reef profile.

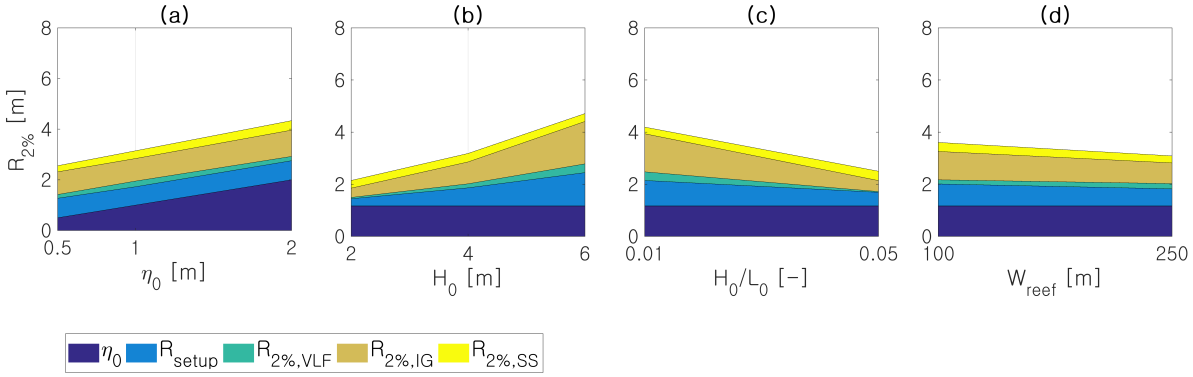

Figure 7.4: The effect of varying hydrodynamic conditions and profile parameters of the convex reef on the different runup components: the water level, wave height, wave steepness and reef width, respectively

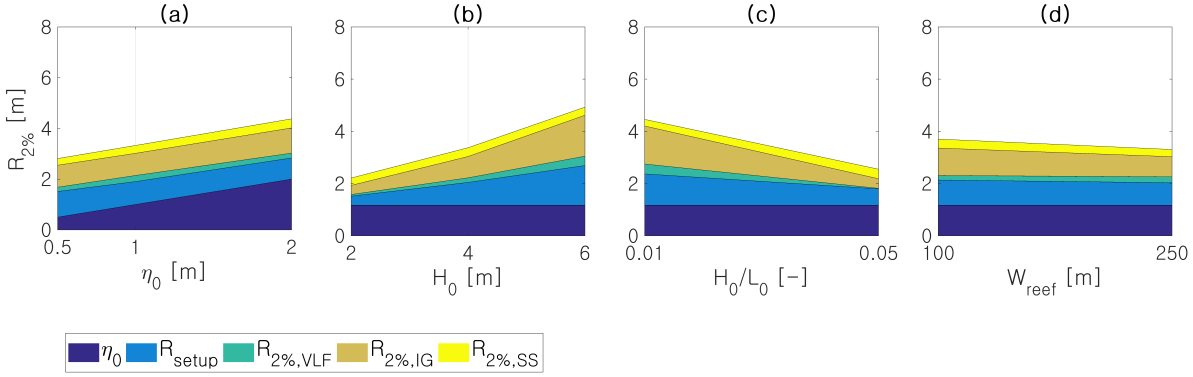

Figure 7.5: The effect of varying hydrodynamic conditions and profile parameters of the typical fringing reef on the different runup components, filtered for a slope of 0.1

7.2.3. Straight profile

The physics of the straight reef profile are distinctly different from the typical fringing reef profile. Without the reef flat acting as a buffer between the wave breaking point and the swash zone, large runup values are registered as waves break close to shore and plunge at the steep beach. The wave transformation and runup across the straight profile are displayed in Figure 7.6 for the three different slopes.

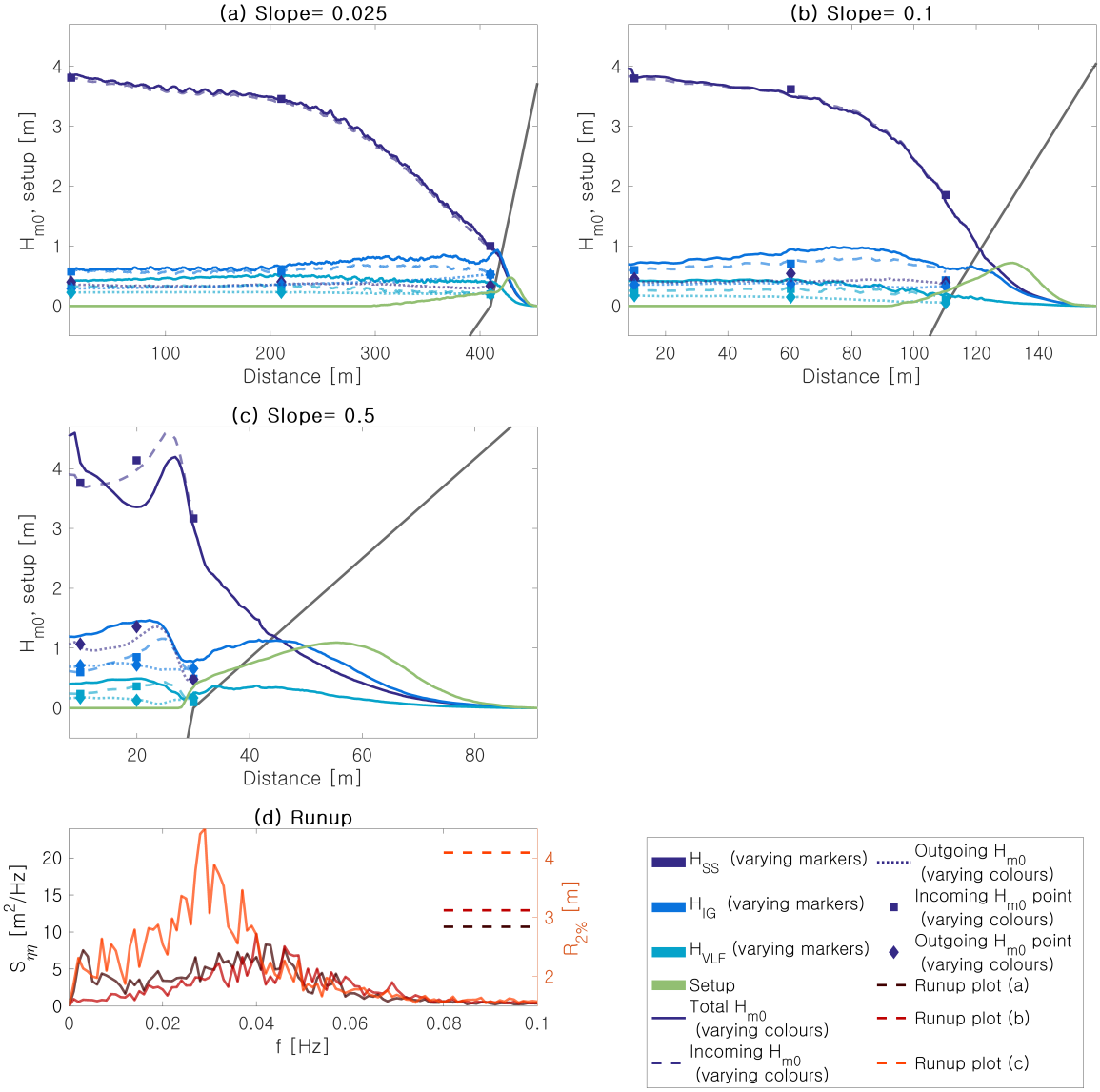

Figure 7.6: Wave transformation ((a) - (b)) and runup (c) across three straight reef profile configurations. The colours depict the different wave components (short, infragravity and very-low frequent waves) and the setup. The marker shapes depict either incoming or outgoing waves calculated from point output data of XBeach. The different line plots depict either total, incoming or outgoing wave heights obtained from the global XBeach data. The difference between point output data and global data is attributed to the output resolution of the global data (output is generated every 2 seconds), which is smaller than the point output data (output is generated every second).

The transformation of incident short waves across straight profiles (with slopes of 0.1 and 0.5) is similar to wave transformation over the typical fringing reef up to the point of the reef crest. However, for straight profiles, waves encounter the beach immediately after. The rapid wave breaking dissipation leads to a large setup against the shore, with values that exceed the maximum setup at the typical reef, allowing waves to travel further up the coast. This is apparent from the distance between the beach toe (y=0 in Figure 7.6) and the point where wave energy and setup are zero; this point has shifted onshore for the straight profile. Across the straight profile with a slope of 0.025, incident waves decay more gradually due to the gentle slope, resulting in a much smaller setup.

The IG wave transformation plots across the straight and typical fringing reef profiles show, again, similar patterns and magnitudes offshore of the reef edge. For the straight profile slopes of 0.1 and 0.5, the IG wave energy increases up to a point shoreward of the breakpoint location, where they lose energy, presumingly

due to wave breaking. Behind this point, IG wave energy increases again, possibly due to transfer of energy between SS and IG waves, as was observed in Section 4.2.3, where an energy transfer between SS and IG was apparent between the beach toe and the swash zone. At the gentle straight slope of 0.025, the peak in IG wave energy is less pronounced, as expected since the breakpoint generation mechanism is more effective for steeper slopes [94]. The reflection of IG waves at the steep interfaces of the straight profile is similar to the typical fringing reef profile with a short reef flat length.

The incoming VLF motions across the straight profiles with slopes of 0.025 and 0.1 show characteristics similar to the typical fringing reef profile. The offshore present VLF motions are dissipated across the reef, with no apparent energy input. For the steep slope of 0.5, an increase in VLF motions is visible, similar to the typical fringing reef profile. The reflection of VLF motions at the beach is, interestingly, largest for the gently sloping profile (slope of 0.025). An explanation for this could be the rapid steepening of VLF waves at the steep slopes which causes wave breaking, whereas VLF waves are dissipated across the gentle straight slope, after which large part of their energy is reflected at the beach.

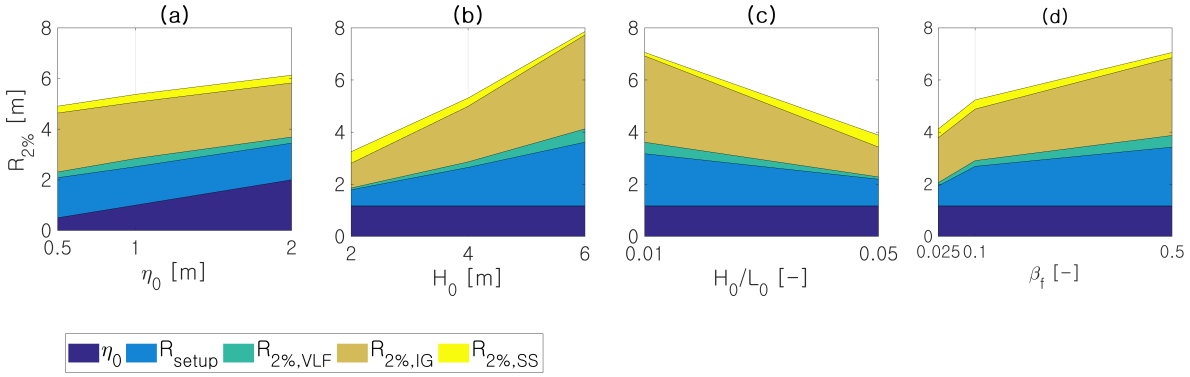

Figure 7.7: The effect of varying hydrodynamic conditions and profile parameters of the straight reef on the different runup components: the water level, wave height, wave steepness and forereef slope, respectively

As can be deduced from subplot (d) of Figure 7.6, runup is larger for steeper straight reefs. Interestingly, the runup spectra in this figure show the high VLF wave energy present at the 1:40 sloping profile. The exact cause for this cannot be extracted from the current results. It could be a related to the nearshore wave steepness, or to limited breaking of VLF waves, or an other mechanism. Runup at the straight profile greatly exceeds the runup of the typical fringing reef profile (see Figures 7.6 and 7.1). The increase in runup is the result of large IG wave heights and an increase in setup, which is evident from Figure 7.7. The relation between runup heights and offshore wave parameters (wave height, water level and wave steepness) show patterns that are similar to the typical fringing reef profile.

7.2.4. Three-slope profile

In Figure 7.8, the wave transformation and runup across two three-slope configurations are depicted. Incident short waves are dissipated across the shelf as a result of wave breaking and frictional wave damping. Wave height reduction at the inner shelf edge (located at a depth of 5 m) relative to the offshore wave height is 25 and 30 % for shelf widths of 100 and 250 m, respectively. Past the inner shelf point, the depth decreases quickly on the 1:10 nearshore slope. This induces large radiation stress gradients and hence setup against the shore. This setup is approximately equal to the setup of the straight profile, as only the largest waves break at the outer shelf edge. The setup is expected to decrease compared to the straight profile for larger wave heights and lower water levels, as these waves will be dissipated more across the shelf.

The IG wave height plots show interesting patterns. The IG wave height first increases slightly at the outer shelf edge, where the largest incoming short waves break and generate IG waves. Across the shelf, the IG wave height slightly reduces, presumably as a result of frictional wave damping. At the nearshore reef slope, the breakpoint mechanism again induces low frequency motions, which is apparent from the sudden increase in IG motions at the location of rapid short wave dissipation. Where at the inner shelf edge the IG wave height

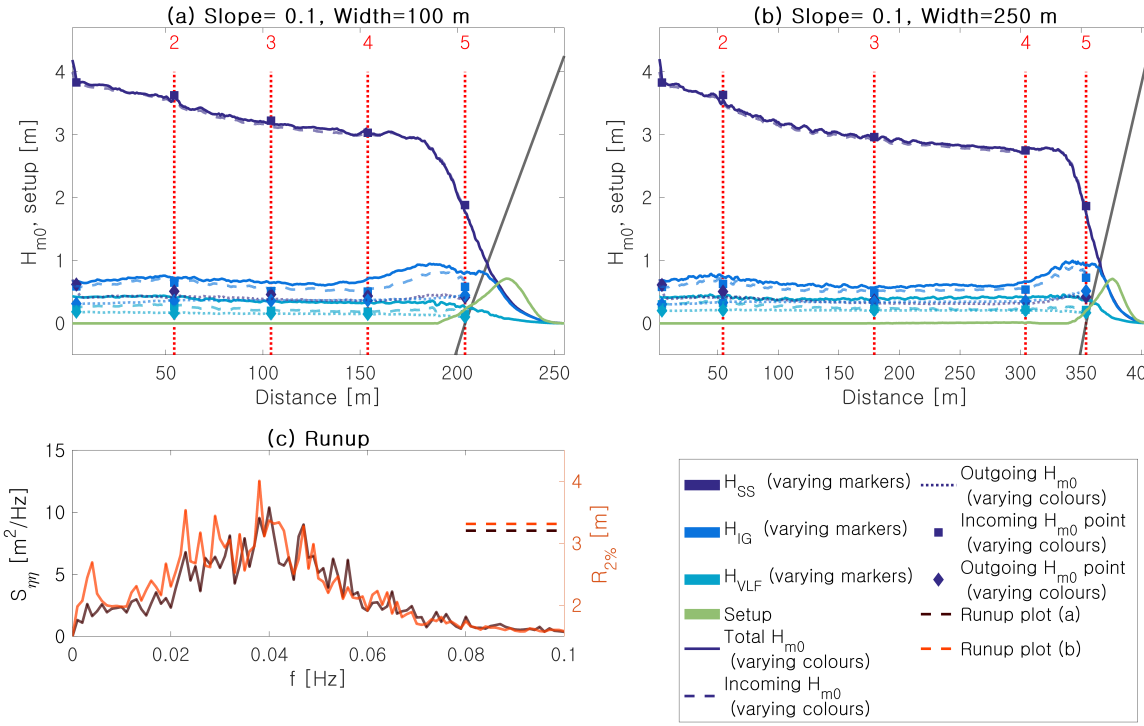

Figure 7.8: Wave transformation ((a) - (b)) and runup (c) across two three-slope reef profile configurations. In subplots (a) and (b), the colours depict the different wave components (short, infragravity and very-low frequent waves) and the setup. The marker shapes depict either incoming or outgoing waves calculated from point output data of XBeach. The different line plots depict either total, incoming or outgoing wave heights obtained from the global XBeach data. The difference between point output data and global data is attributed to the output resolution of the global data (output is generated every 2 seconds), which is smaller than the point output data (output is generated every second). Vertical, red dotted lines and corresponding numbers indicate locations: (2) the outer shelf edge, (3) the mid-shelf, (4) the inner shelf edge and (5) the beach toe. Runup spectra are plotted in subplot (c) on the left y-axis, total runup values ($R_{2\%}$) on the right y-axis.

is smaller than at the same depth of the straight profile, the IG wave height across the three-slope profile increases drastically behind this point, reaching similar IG wave height values at the beach toe. VLF motions are constant across the shelf, with no significant source of energy at the offshore edge, and shoal at the beach, possibly with energy input from the short waves. Reflection at the straight profile is larger than at the three-slope profile, leading to larger outgoing waves for the straight profile.

In Figure 7.8 both the runup spectra and total runup values are plotted for one hydrodynamic forcing condition. Against expectations, this runup is slightly larger than the runup at the straight reef profile, due to an increase in IG and VLF wave energy near the shore. On top of that, the IG and VLF components of the runup are larger for larger shelf widths (for the hydrodynamic input conditions used in Figure 7.8). The comparison of Figure 7.9 (three-slope profile) and 7.7, where the results of the straight profile are filtered for slopes of 1:10, gives more insight into the mechanisms responsible for driving the runup:

- Runup at the three-slope profile is on average smaller than runup at the straight profile. This is mainly caused by a large reduction in runup at the three-slope profile for low steepness values and large (6 meter) wave heights. For each subplot depicting the influence of a parameter variation, the average runup across all other modeled conditions is calculated. A significant increase in runup across a certain parameter therefore also increases the average runup in other subplots.

- The setup and IG components of the runup are on average smaller for the three-slope profile. The decrease in setup at the shore is expected, as wave dissipation across the shelf width reduces the radiation stress gradients. Decreased IG wave heights are assumed to be caused by the IG wave dissipation across the shelf and SS wave dissipation that reduces the breakpoint forcing near the shore. Under certain hydrodynamic conditions, however, such as the condition depicted in Figure 7.8, IG and VLF

wave runup increases for the three-slope profile relative to the straight profile. Infragravity wave growth mechanisms should be investigated to verify whether this could be the cause for the observed increase in runup.

- The runup at the three-slope profile reacts differently to changes in hydrodynamic forcing than the straight profile, especially to incident short wave heights. The larger the incoming SS wave height, the larger the breakpoint forcing at the outer edge of the shelf, but also the larger both the SS and IG dissipation across the shelf. For this reason, the increase in IG wave height for increasing input wave heights is much smaller at the three-slope profile than at the straight profile.

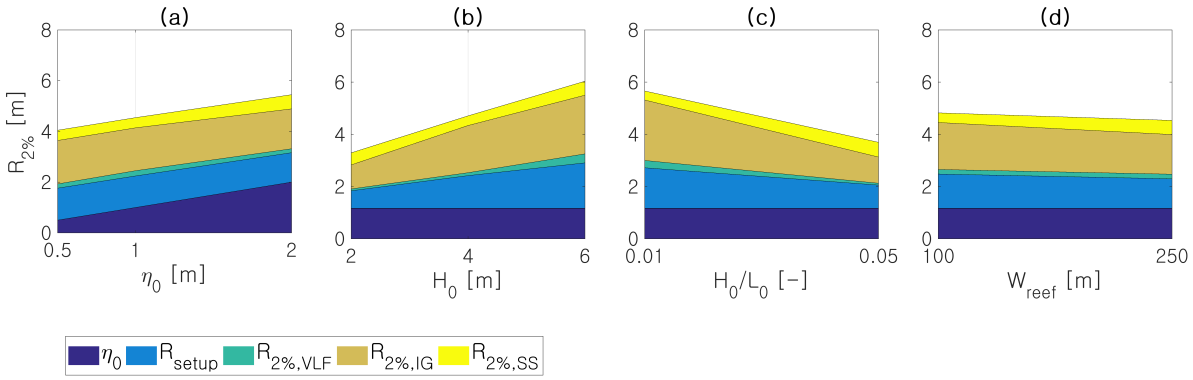

Figure 7.9: The effect of varying hydrodynamic conditions and profile parameters of the three-slope reef on the different runup components: the water level, wave height, wave steepness and reef width, respectively

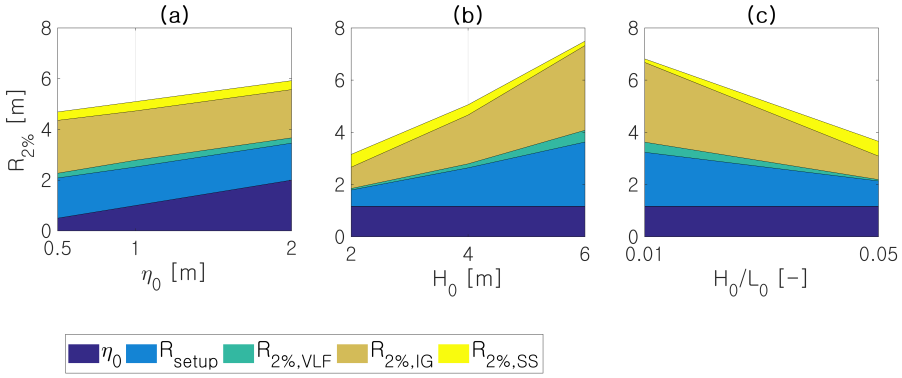

Figure 7.10: The effect of varying hydrodynamic conditions and profile parameters of the straight reef, filtered for a slope of 1:10, on the different runup components

7.3. Discussion

A first insight is gained into the reef geometry control on nearshore hydrodynamics by modeling different shapes with varying profile dimensions, under different forcing conditions. The understanding of wave dynamics across reef types other than the fringing reef, which have not been explored in detail yet, can help point out important drivers of flooding at varying coastal sections. This enables the determination of coastal management strategies adapted to the local situation. Furthermore, a first indication of hydrodynamic conditions responsible for flood hazards along different reef lined coasts is given. Some reservations, however, should be made as to the applicability of the results.

Firstly, the range of analyzed profile shapes is limited as coral restorations are the main interest of this research. This limits the validity of the observed relations between profile parameters and reef hydrodynamics.

Furthermore, in Figures 7.1, 7.3, 7.6 and 7.8, two output signals are depicted, the global output where at each cross-shore grid location water levels are outputted at a time interval of 2 seconds, and the point output, where water level time series are saved at a limited number of predefined locations with a time interval of 1 s. Point output time series are therefore more accurate, and as a difference between point output and global output wave heights is observed, it is recommended to rerun global output data with an increased resolution. Moreover, the division of wave energy into either SS, IG or VLF bands is rather arbitrary, decided by predefined cutoff frequencies between the different wave height components (0.04 and 0.004 Hz), without much regard for actual wave types present in a spectrum. Therefore, energy of long-period short waves can end up in the IG wave component, the energy of IG waves can be attributed to VLF motions and vice versa, scattering the results and making it more difficult to determine forcing mechanisms. A solution for this is a more careful analysis of actual wave spectra for different hydrodynamic conditions and at different cross-shore locations, in order to obtain more physics-based cut-off frequencies.

With the XBeach non-hydrostatic mode, it is not possible to directly determine whether wave dissipation occurs by frictional wave damping or wave breaking dissipation, which is of interest to fully understand the wave transformation process. Via a force balance analysis the frictional wave damping can be separated from the wave breaking dissipation by elaborating the momentum balance terms. This is strongly recommended for future research on the topic of reef geometry control on nearshore hydrodynamics. Moreover, the XBeach model is run for only one (low) friction coefficient, limiting information on the effect of frictional wave damping. Therefore, it is recommended to rerun the XB non-hydrostatic model with different friction coefficient values to discover the effect of frictional wave damping on reef hydrodynamics. With a very low friction coefficient, wave breaking dissipation can be discerned from frictional wave damping.

An interesting area of further research is the generation and dissipation of IG and VLF waves. IG and VLF wave generation is strongly linked to the short wave dissipation process, as energy input is strong at locations of rapid short wave breaking dissipation. At each reef profile, a distinct peak in IG and VLF energy is present around the breakpoint location. A more detailed analysis and parametrization of this process would thus be interesting, linking the maximum IG wave height just behind the breakpoint, instead of at the reef crest as was done in Section 4.2.2 (Chapter 4), to offshore wave parameters, short wave dissipation processes and profile parameters. In this way, possibly a semi-empirical formulation can be found that is valid across a variety of profiles where the breakpoint forcing is dominant. The dissipation of IG and VLF energy is another interesting topic of research. At the convex and typical fringing reef profiles, the IG and VLF wave energy is strongly damped across the reef edge. An elaboration of the energy balance at this location, as was done by Van Dongeren et al. [162], could highlight most important dissipation processes. Finally, the transformation of IG and VLF waves across the reef flat and shelf show interesting patterns, of which growth mechanisms can be explored on the basis of research by Gawehn et al. [53].

In Section 4.2.3, it was concluded that beach toe wave parameters and water levels can be used to give a reasonable estimate of runup at the reef fronted coast. Formulations were derived based on XBeach simulations of a fringing reef [116], which showed a large increase in goodness of fit compared to existing runup formulations for sandy beaches. The runup results across the various modeled reef shapes can be used to validate the derived expressions and verify whether they can predict runup at other reef shapes such as the straight and three-slope profile.

7.4. Conclusion

Wave transformation and flooding of reef fronted coastlines is greatly affected by the reef profile shape and profile dimensions. Short wave dissipation and setup over various reef shapes show clear patterns, where a narrow surfzone (steep slope) leads to a large setup and the degree of wave breaking and frictional wave dissipation (reef flat / shelf width and submergence) determines the SS beach toe wave heights and the resulting setup between the beach toe and the shore. The generation of IG and VLF waves is highly dependent on the forereef slope. The IG and VLF propagation is, however, more complex, showing both progressive growing and progressive dissipative behaviour across the different shapes.

The typical fringing reef is characterized by IG and VLF wave generation at the forereef, which is stronger for

steeper profiles, SS and IG wave dissipation across the flat (stronger for wider reef flat) and a distinct setup across the reef flat that is again stronger for steeper forereef slopes. VLF waves show a progressive growing behaviour across the profiles with a 1:2 slope, with larger beach toe VLF wave heights measured for larger widths. At the 1:10 slope, VLF waves show a progressive dissipative behaviour.

The smoothed reef edge of the convex profile reduces radiation stress gradients and hence setup relative to the typical fringing reef profile, but also decreases the frictional wave dissipation and thus increases beach toe SS wave heights. The input of energy from short waves to the IG motions is similar for the two profiles, but IG wave dissipation is larger across the typical fringing reef type. Runup at the convex profile coast is lower than at the typical fringing reef profile due to the large reduction in setup, although the IG wave component of the runup has slightly increased.

Of the four modeled shapes, the straight profile is most vulnerable to coastal flooding, due to the large setup near the shore and significant IG generation by the breakpoint mechanism, as no reef flat is present to damp part of the incoming short wave energy. Mildly sloping straight profiles are much less susceptible to flooding due to the increased frictional wave dissipation across the profile and diminished breakpoint generation, which leads to much lower setup and IG wave runup contributions at the gently sloping (1:40) straight profile. Interestingly, the reflection of VLF motions at this gentle profile is large, leading to a slightly higher VLF runup component than for the 1:10 profile.

Short wave dissipation across the shelf of the three-slope profile reduces the setup and the beach toe SS wave heights relative to the straight profile. On average, the short wave dissipation reduces the breakpoint forcing near the shore and hence the IG wave heights. However, under certain conditions, IG and VLF wave runup is larger at the three-slope profile than at the straight profile. A possible explanation for this is the generation of IG and VLF waves at the outer edge of the shelf in combination with a progressive growing behaviour across the shelf, which leads to a larger runup at the coast. This effect depends highly on the incoming SS wave heights.

8

Effects of coral restoration on reef hydrodynamics and coastal hazards

8.1. Introduction

Coral restoration is promising from both an ecological and coastal safety perspective. Coral transplantation and artificial reefs significantly improve biodiversity and help coral reefs to recover from stress events [102]. The increased bed elevation and enhanced friction coefficients of recovered sections are expected to cause an increase in frictional wave damping, while the reduced depth above the restored corals might intensify the wave breaking dissipation. However, little research has been invested in the actual hydrodynamic effects of these restorations. Therefore, numerical simulations, as described in the methodology (Chapter 6), have been executed to assess the effect of different restoration configurations under varying hydrodynamic forcing conditions, to be able to describe their influence on wave transformation and, most importantly, the potential for flood risk reduction.

8.2. Results

In this section, general observations of hydrodynamics across the restored reefs are described (Subsection 8.2.1), after which we elaborate on the effect of varying boundary conditions and restoration configurations on wave transformation and runup (Subsection 8.2.2). The section is concluded with an overview of the bulk results, to properly illustrate the runup reduction potential of different restorations across the different reef profile types (Subsection 8.2.3).

8.2.1. General overview

In Chapter 7 the general hydrodynamics across the different reef shapes are described. Coral restorations alter the hydrodynamics across the reef, of which the general effects are described in this section. For conciseness, the results are elaborated for one hydrodynamic forcing condition (a wave height of 4 m, a water level of 2 m and an offshore wave steepness of 0.05), a reef width of 100 m, a slope of 1:10 and a restoration width of 10 m. The influence of varying boundary conditions and profile parameters is discussed in Section 8.2.2. The observations below follow from a careful analysis of the wave height transformation across all restoration locations of the different reef shapes. The full wave height transformation plots are depicted in Appendix D (Figures D.1 to D.19), of which an example is depicted in Figure 8.1 (lower forereef restoration of the typical fringing reef). For each plot, the main results are summarized in a table (e.g. Table 8.1) to substantiate the observations, denoting the wave transmission across the restoration (the wave height just shoreward of the restoration divided by the wave height just seaward of the restoration), the setup across the restoration, the beach toe wave heights and the runup components. In the Intermezzo on page 78, the values denoted in the different tables are explained.

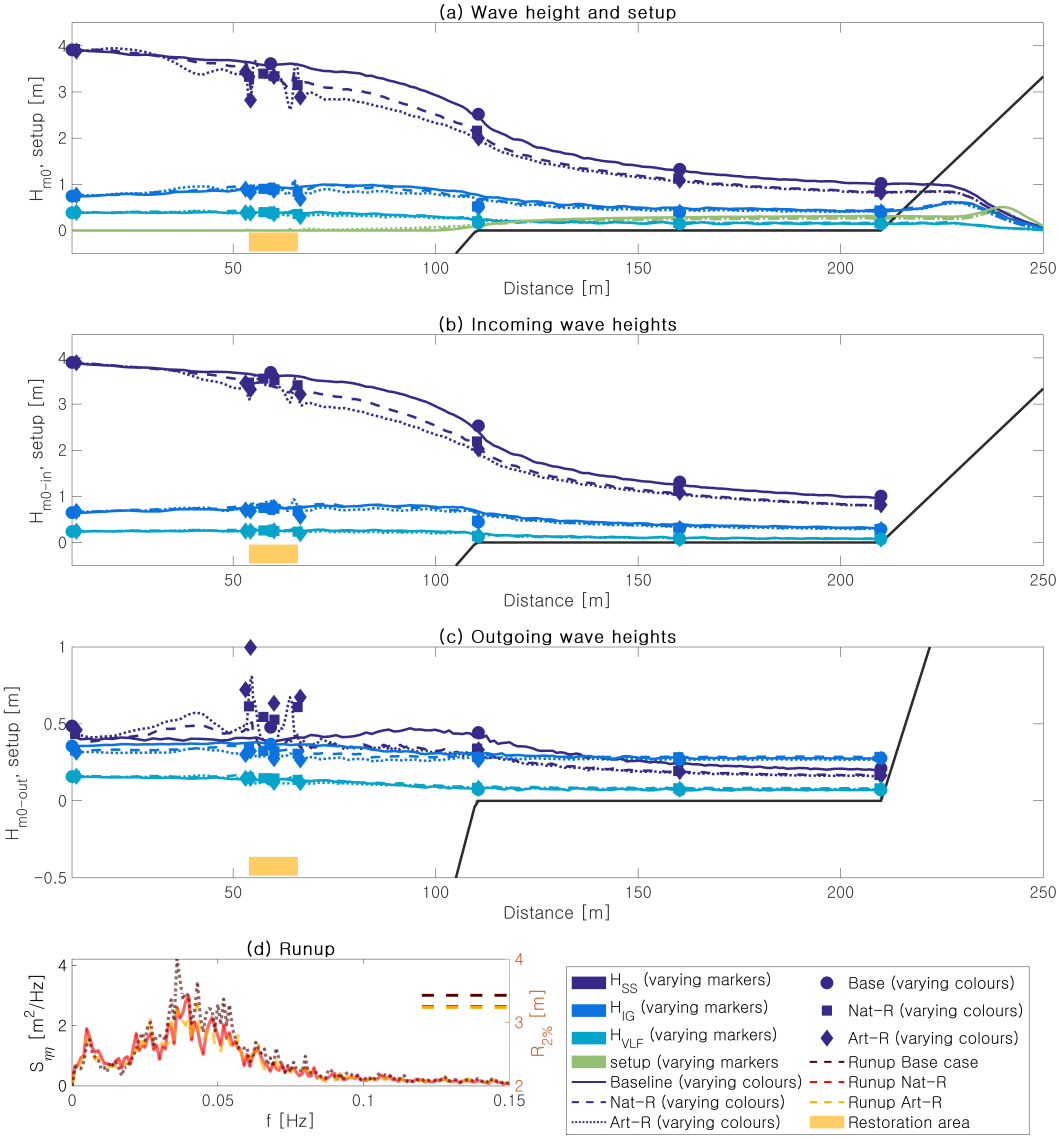

Figure 8.1: Example of result: Wave transformation and runup across a restoration at the **lower forereef of the typical fringing reef**, displaying the total (subplot a), the incoming (subplot b) and the outgoing (subplot c) SS, IG and VLF waves, as well as the runup (subplot d)

Intermezzo summarizing tables

For each restoration, wave transformation and reflection characteristics are summarized in two tables, one for wave transformation and runup (e.g. Table 8.1) and one for reflection (e.g. Table 8.3), which should be interpreted as follows:

- 'Baseline' refers to the scenario without a restoration, 'Natural' to coral transplantation (commonly referred to as green restoration) and 'Artificial' to artificial reef construction (commonly referred to as grey restoration).
- Values inside parentheses indicate the relative (natural or artificial restoration versus baseline) reduction (green) or increase (red) in wave transmission, beach toe wave heights and runup.
- Wave transmission is defined as the wave height just shoreward of the restoration divided by the wave height just seaward of the restoration.
- Reflection at the restoration is defined as the outgoing wave height just seaward of the restoration divided by the outgoing wave height just shoreward of the restoration. This is unlike the common expression for reflection, where the incoming wave height is divided by the outgoing wave height. However, as reflection occurs at various locations at a reef (forereef, beach), this value will not give too much insight into the effect of the restoration, whereas the chosen reflection parameter can indicate whether outgoing wave heights decrease or increase across the restoration and hence whether reflection at the exact location of the restoration occurs.

8.2.1.1 Typical fringing reef

For the typical fringing reef, five restoration locations are investigated: the lower forereef, the upper forereef, the reef edge, the mid-flat and the inner reef flat (typical fringing reef restorations 1 to 5 in Figure 6.2 on page 62, respectively). The full wave transformation plots are displayed in Figures D.1 to D.5 in Appendix D. Below, the results are summarized in Tables 8.1 to 8.8 and important observations are noted.

Table 8.1: Summary of wave transformation characteristics across the **lower forereef restoration of the typical fringing reef profile** (restoration 1 in Figure 6.2), displaying the wave transmission across the restoration (ratio of wave heights shoreward versus seaward of the restoration), the setup across the restoration, the wave heights and total setup at the beach toe and the runup components. Other table characteristics are noted in the Intermezzo on page 78.

	Wave transmission restoration [-]			**Beach toe wave heights [m]**			**Runup [m]**		
	Baseline	*Natural*	*Artificial*	*Baseline*	*Natural*	*Artificial*	*Baseline*	*Natural*	*Artificial*
SS	0.99	0.96 *(-3%)*	0.89 *(-10%)*	0.96	0.80 *(-17%)*	0.79 *(-18%)*	0.50	0.48 *(-4%)*	0.47 *(-7%)*
IG	1.01	1.06 *(+5%)*	0.92 *(-9%)*	0.32	0.31 *(-3%)*	0.29 *(-9%)*	0.42	0.38 *(-10%)*	0.38 *(-10%)*
VLF	1.01	0.99 *(-2%)*	0.86 *(-15%)*	0.09	0.09 *(-2%)*	0.08 *(-8%)*	0.02	0.01 *(-26%)*	0.01 *(-29%)*
	Across restoration [m]			**Beach toe [m]**					
	Baseline	*Natural*	*Artificial*	*Baseline*	*Natural*	*Artificial*	*Baseline*	*Natural*	*Artificial*
Setup	0.00	0.00	0.01	0.31	0.26 *(-16%)*	0.26 *(-14%)*	0.63	0.51 *(-19%)*	0.51 *(-19%)*
Total							1.57	1.38 *(-12%)*	1.37 *(-13%)*

Table 8.2: Summary of wave transformation characteristics across the **upper forereef restoration of the typical fringing reef profile** (restoration 2 in Figure 6.2), displaying the wave transmission across the restoration (ratio of wave heights shoreward versus seaward of the restoration), the setup across the restoration, the wave heights and total setup at the beach toe and the runup components. Other table characteristics are noted in the Intermezzo on page 78.

	Wave transmission restoration [-]			**Beach toe wave heights [m]**			**Runup [m]**		
	Baseline	*Natural*	*Artificial*	*Baseline*	*Natural*	*Artificial*	*Baseline*	*Natural*	*Artificial*
SS	0.93	0.89 *(-4%)*	0.71 *(-24%)*	0.96	0.81 *(-16%)*	0.79 *(-18%)*	0.50	0.49 *(-3%)*	0.48 *(-4%)*
IG	1.01	0.99 *(-1%)*	0.64 *(-37%)*	0.32	0.29 *(-8%)*	0.24 *(-24%)*	0.42	0.36 *(-14%)*	0.31 *(-27%)*
VLF	0.96	0.99 *(+3%)*	0.62 *(-36%)*	0.09	0.08 *(-9%)*	0.07 *(-22%)*	0.02	0.02 *(-)*	0.02 *(-)*
	Across restoration [m]			**Beach toe [m]**			**Runup [m]**		
	Baseline	*Natural*	*Artificial*	*Baseline*	*Natural*	*Artificial*	*Baseline*	*Natural*	*Artificial*
Setup	0.00	0.00	0.14	0.31	0.30 *(-3%)*	0.33 *(+8%)*	0.63	0.55 *(-13%)*	0.58 *(-9%)*
Total							1.57	1.42 *(-10%)*	1.39 *(-12%)*

Forereef restorations Two restorations at the forereef have been investigated, (1) a restoration at the lower forereef, that is constructed at depths between four to seven meters relative to the reef crest (Table 8.1) and (2) a restoration at the upper forereef, that is applied at depths of 2 m below the reef crest going downwards (Table 8.2). The most offshore restoration (lower forereef) induces wave breaking at a significant distance from the baseline scenario breakpoint. The wave transmission across the restoration is slightly lower than wave transmission across this region for the baseline scenario, see columns 1 to 3 of Table 8.1. This is caused by a combination of reflection at the restoration, as outgoing wave heights seaward of the restoration are larger than just shoreward of the restoration (see Table 8.3), and wave dissipation across the restoration, which is apparent from the slight increase in setup across the restoration. The reduction of SS wave heights reduces the setup across the reef by decreasing radiation stress gradients at the reef edge, which again reduces beach toe wave heights as they are limited by the depth above the reef flat. The additional setup of waves breaking close to shore is now also decreased, effectuating a reduction in runup by

Table 8.3: Reflection at the lower forereef restoration of the typical fringing reef: The outgoing wave heights seaward of the restoration divided by the outgoing wave heights shoreward of the restoration. If larger than one, reflection at the outer edge of the restoration is assumed to occur. See the Intermezzo on page 78 for further clarification of the table.

	Reflection at restoration		
	Baseline	*Natural*	*Artificial*
SS	0.99	1.23	1.29
IG	1.03	1.12	1.15
VLF	1.04	1.13	1.21

the restoration. IG and VLF motions are slightly reduced by the restoration, although to a much smaller extent than the upper forereef restoration. A possible explanation for the IG and VLF wave height reduction is the decreased breakpoint forcing [122], that is among others dependent on the incoming SS wave height, by SS wave dissipation seaward of the breakpoint. Moreover, the analysis of IG wave runup at reef fronted coasts, described in Section 4.2.3 of Chapter 4, showed the significant input of energy from the SS waves to the IG waves between the beach toe and the coast. Therefore, a reduction in SS waves is expected to bring about a reduction in nearshore IG wave heights and runup, as depicted in Tables 8.1 and 8.2.

The upper forereef restoration is characterized by inducing wave breaking near the breakpoint of the baseline scenario, which is apparent from the low wave transmission coefficient of the baseline scenario (see Table 8.2); wave heights are already decreasing substantially in this region without the restoration present. The upper forereef restoration further lowers the wave transmission of both SS, IG and VLF waves, with a larger relative reduction than the lower forereef restoration. There are two causes for this. Firstly, the upper forereef restoration is more effective in reflecting waves offshore, which can be deduced from the reflective values denoted in Table 8.4. Secondly, the dissipation of short and infragravity wave energy is enhanced for shallower water depths. Vetter et al. [166] showed the good predictive skill of the steady state cross-shore momentum balance in predicting setup across the reef flat, where the setup is governed by both the gradients in radiation stress and the water depth. This explains the increase in setup by the artificial restoration, where increased radiation stress gradients are combined with the small depth above the restoration. As the depth above the natural restoration is larger and radiation stress gradients smaller, the setup of the natural restoration is similar to the baseline scenario. Again, due to a reduction of SS wave heights at the beach toe, the additional setup near the shore is decreased, which, in combination with a reduction of IG and VLF components, leads to a reduction in runup.

Table 8.4: Reflection at the upper forereef restoration of the typical fringing reef: The outgoing wave heights seaward of the restoration divided by the outgoing wave heights shoreward of the restoration. If larger than one, reflection at the outer edge of the restoration is assumed to occur. See the Intermezzo on page 78 for further clarification of the table.

	Reflection at restoration		
	Baseline	*Natural*	*Artificial*
SS	0.92	1.19	1.50
IG	1.09	1.12	1.58
VLF	1.24	1.18	1.76

Restorations at the reef flat Three restorations at the reef flat have been examined, one at the reef flat, one at the mid-flat and one at the inner edge of the reef flat.

Table 8.5: Summary of wave transformation characteristics across the **reef edge restoration of the typical fringing reef profile** (restoration 3 in Figure 6.2), displaying the wave transmission across the restoration (ratio of wave heights shoreward versus seaward of the restoration), the setup across the restoration, the wave heights and total setup at the beach toe and the runup components. Other table characteristics are noted in the Intermezzo on page 78.

	Wave transmission restoration [-]			**Beach toe wave heights [m]**			**Runup [m]**		
	Baseline	*Natural*	*Artificial*	*Baseline*	*Natural*	*Artificial*	*Baseline*	*Natural*	*Artificial*
SS	0.76	0.66 *(-14 %)*	0.38 *(-50 %)*	0.96	0.79 *(-18 %)*	0.73 *(-24 %)*	0.50	0.48 *(-4 %)*	0.44 *(-13 %)*
IG	0.76	0.63 *(-16 %)*	0.40 *(-47 %)*	0.32	0.27 *(-15 %)*	0.20 *(-38 %)*	0.42	0.36 *(-13 %)*	0.29 *(-31 %)*
VLF	0.83	0.71 *(-15 %)*	0.57 *(-31 %)*	0.09	0.08 *(-12 %)*	0.08 *(-10 %)*	0.02	0.01 *(-22 %)*	0.02 *(+4 %)*
	Across restoration [m]			**Beach toe [m]**					
	Baseline	*Natural*	*Artificial*	*Baseline*	*Natural*	*Artificial*	*Baseline*	*Natural*	*Artificial*
Setup	0.12	0.22 *(+88 %)*	0.62 *(+435 %)*	0.31	0.35 *(+12 %)*	0.65 *(+110 %)*	0.63	0.59 *(-6 %)*	0.89 *(+40 %)*
Total							1.57	1.45 *(-7 %)*	1.63 *(+4 %)*

The most extreme case is the restoration directly at the edge of the reef flat (see Table 8.5). Here, setup is greatly increased across the restoration due to the increase in radiation stress gradients, combined with a significant reduction in the water depth. This effect, that is similar to the effect of a reef crest, was also noted by Yao et al. [172], who concluded that the reef-submergence parameter

Table 8.6: Reflection at the reef edge restoration of the typical fringing reef: The outgoing wave heights seaward of the restoration divided by the outgoing wave heights shoreward of the restoration. If larger than one, reflection at the outer edge of the restoration is assumed to occur. See the Intermezzo on page 78 for further clarification of the table.

	Reflection at restoration		
	Baseline	*Natural*	*Artificial*
SS	1.17	1.18	2.70
IG	1.04	0.96	1.31
VLF	1.07	0.91	0.92

was the main controlling parameter on the setup, based on laboratory data of a fringing reef. For this reason, setup across the artificial reef, that has a lower submergence, is much larger than across the natural restoration. The short wave heights are significantly reduced due to the short wave breaking dissipation and significant reflection at the outer edge of the reef, which can be deduced from Table 8.6. In contrast to observations of Péquignet et al. [119] and Franklin et al. [51], who noted the increase in IG motions behind the reef crest as a result of resonant mode forcing, IG waves are reflected at the reef edge (see Table 8.6), dissipated across the restoration, and further dissipated across the reef flat, which leads to a reduction of IG beach toe wave heights. Van Dongeren et al. [162] investigated the dissipation of IG waves across a fringing reef and concluded that IG waves can lose energy either by frictional wave damping, IG bore dissipation and work done by short waves. Van Dongeren et al. [162] also point out that in shallower water depths, IG wave dissipation is larger due to the increased bottom dissipation, which could explain the increased dissipation across the rough, increased bed elevations of the restorations. The small VLF motions are not much affected by the restoration. In summary, the large increase in setup for the artificial restoration leads to a higher runup than the baseline scenario, whereas the natural restoration slightly decreases the runup as a results of the SS and IG wave height reductions.

Table 8.7: Summary of wave transformation characteristics across the **mid-flat restoration of the typical fringing reef profile** (restoration 4 in Figure 6.2), displaying the wave transmission across the restoration (ratio of wave heights shoreward versus seaward of the restoration), the setup across the restoration, the wave heights and total setup at the beach toe and the runup components. Other table characteristics are noted in the Intermezzo on page 78.

	Wave transmission restoration [-]			**Beach toe wave heights [m]**			**Runup [m]**		
	Baseline	*Natural*	*Artificial*	*Baseline*	*Natural*	*Artificial*	*Baseline*	*Natural*	*Artificial*
SS	0.92	0.84 *(-9 %)*	0.58 *(-36 %)*	0.96	0.80 *(-17 %)*	0.64 *(-34 %)*	0.50	0.49 *(-2 %)*	0.46 *(-9 %)*
IG	0.96	0.86 *(-11 %)*	0.66 *(-31 %)*	0.32	0.29 *(-10 %)*	0.19 *(-41 %)*	0.42	0.37 *(-12 %)*	0.27 *(-35 %)*
VLF	1.02	0.86 *(-16 %)*	0.65 *(-36 %)*	0.09	0.08 *(-9 %)*	0.06 *(-34 %)*	0.02	0.01 *(-16 %)*	0.01 *(-28 %)*
	Across restoration [m]			**Beach toe [m]**					
	Baseline	*Natural*	*Artificial*	*Baseline*	*Natural*	*Artificial*	*Baseline*	*Natural*	*Artificial*
Setup	0.01	0.04 *(+351 %)*	0.13 *(+1604 %)*	0.31	0.31 *(-1 %)*	0.41 *(+34 %)*	0.63	0.56 *(-11 %)*	0.61 *(-4 %)*
Total							1.57	1.44 *(-8 %)*	1.35 *(-14 %)*

Table 8.8: Summary of wave transformation characteristics across the **inner flat restoration of the typical fringing reef profile** (restoration 5 in Figure 6.2), displaying the wave transmission across the restoration (ratio of wave heights shoreward versus seaward of the restoration), the setup across the restoration, the wave heights and total setup at the beach toe and the runup components. Other table characteristics are noted in the Intermezzo on page 78.

	Wave transmission restoration [-]			**Beach toe wave heights [m]**			**Runup [m]**		
	Baseline	*Natural*	*Artificial*	*Baseline*	*Natural*	*Artificial*	*Baseline*	*Natural*	*Artificial*
SS	0.95	0.87 *(-8 %)*	0.66 *(-30 %)*	0.96	0.84 *(-12 %)*	0.67 *(-31 %)*	0.50	0.54 *(+7 %)*	0.51 *(+1 %)*
IG	0.99	0.87 *(-11 %)*	0.73 *(-26 %)*	0.32	0.31 *(-3 %)*	0.26 *(-20 %)*	0.42	0.40 *(-5 %)*	0.28 *(-33 %)*
VLF	1.06	0.98 *(-7 %)*	0.77 *(-28 %)*	0.09	0.09 *(-2 %)*	0.08 *(-12 %)*	0.02	0.03 *(+53 %)*	0.02 *(+14 %)*
	Across restoration [m]			**Beach toe [m]**					
	Baseline	*Natural*	*Artificial*	*Baseline*	*Natural*	*Artificial*	*Baseline*	*Natural*	*Artificial*
Setup	0.00	0.01	0.06	0.31	0.30 *(-4 %)*	0.35 *(+15 %)*	0.63	0.60 *(-4 %)*	0.58 *(-9 %)*
Total							1.57	1.57 *(-0 %)*	1.38 *(-12 %)*

The effects of a restoration at the mid-flat and the inner flat are less pronounced than the restoration at the reef edge and can be explained on the basis of the cross-shore momentum balance. Again, reflection (see Table 8.9) and dissipation across the restoration causes a decrease in both SS, IG and VLF wave heights (see Tables 8.7 and

Table 8.9: Reflection at the mid-flat restoration of the typical fringing reef: The outgoing wave heights seaward of the restoration divided by the outgoing wave heights shoreward of the restoration. If larger than one, reflection at the outer edge of the restoration is assumed to occur. See the Intermezzo on page 78 for further clarification of the table.

	Reflection at restoration		
	Baseline	*Natural*	*Artificial*
SS	1.08	1.01	1.53
IG	1.00	0.90	0.98
VLF	0.93	0.97	1.16

8.8). Further seaward, however (at the mid-flat restoration), incoming wave heights are larger as less energy has been dissipated, causing the setup across more seaward located restorations to be larger due to the larger radiation stress gradients. This effect is only observed for the artificial restoration; here the setup at the beach toe is 0.41 m (an increase of 34 % relative to the baseline scenario) for the mid-flat restoration and 0.35 m (an increase of 15 % relative to the baseline scenario) for the inner flat restoration. The additional setup at the shore is however smaller for the mid-flat restoration as the inner flat restoration is located close to the nearshore breakpoint, increasing radiation stress gradients. Therefore, the runup reduction is larger for the mid-flat restoration, due to a decrease in the SS, IG and setup component. Ideally, a reef flat restoration is located somewhere in between the mid-flat restoration and the inner flat restoration, where wave heights have already been naturally dissipated across the reef, minimizing the additional setup across the restoration, but not too close to the inner surf zone where radiation stress gradients are again increased by the restoration.

8.2.1.2 Convex reef

In Chapter 7, it was shown that the convex reef profile has a similar effect on the reef hydrodynamics as the typical fringing reef profile, the large difference being the reduction in setup across the reef flat due to the smoother gradients in bathymetry, which increases the width of the surf zone. This effect is partly nullified by the increase in setup between the nearshore breakpoint and the shore, as SS beach toe wave heights are larger for the convex profile. It is expected that restorations across the convex profile show hydrodynamic patterns similar to restorations at the typical fringing reef profile. In Appendix D all results are depicted. Below, the particularities of the convex reef restorations are summarized.

In general, mechanisms of wave transformation across convex profile restorations are similar to the typical fringing reef restoration. SS, IG and VLF wave heights are reduced across the restoration by reflection and dissipation, for which wave transmission is lower for restorations in lower water depths (see Tables D.1 and D.3 in Appendix D for comparison, in which the SS wave transmission reduction over the artificial reef is 16 and 39 % for the lower forereef restoration (restoration 1 as established in Figure 6.2) and the upper slope restoration (restoration 4 as established in Figure 6.2), respectively). The IG wave reduction is largest for restorations that are located shoreward of the breakpoint, where the IG motions have gained energy and are attenuated by friction, wave breaking and reflection. This is clear from the beach toe IG wave heights that are reduced by the artificial restoration with 24, 32, 40, 47, 45 and 28 % for restorations 1 to 6, respectively (see Tables D.1 to D.5 in Appendix D). Here the reduction across the inner flat restoration seems smaller as the restoration is located right at the beach toe.

Table 8.10: Summary of wave transformation characteristics across the **reef edge restoration of the convex reef profile** (restoration 3 in Figure 6.2), displaying the wave transmission across the restoration (ratio of wave heights shoreward versus seaward of the restoration), the setup across the restoration, the wave heights and total setup at the beach toe and the runup components. Other table characteristics are noted in the Intermezzo on page 78.

	Wave transmission restoration [-]			**Beach toe wave heights [m]**			**Runup [m]**		
	Baseline	*Natural*	*Artificial*	*Baseline*	*Natural*	*Artificial*	*Baseline*	*Natural*	*Artificial*
SS	0.87	0.77 *(-12 %)*	0.53 *(-40 %)*	1.13	0.92 *(-18 %)*	0.82 *(-27 %)*	0.51	0.52 *(+1 %)*	0.49 *(-5 %)*
IG	0.93	0.84 *(-9 %)*	0.55 *(-41 %)*	0.40	0.35 *(-12 %)*	0.24 *(-40 %)*	0.50	0.45 *(-9 %)*	0.36 *(-28 %)*
VLF	0.82	0.71 *(-14 %)*	0.55 *(-33 %)*	0.10	0.09 *(-9 %)*	0.07 *(-28 %)*	0.02	0.02 *(+27 %)*	0.02 *(-15 %)*
	Across restoration [m]			**Beach toe [m]**			**Runup [m]**		
	Baseline	*Natural*	*Artificial*	*Baseline*	*Natural*	*Artificial*	*Baseline*	*Natural*	*Artificial*
Setup	0.04	0.11 *(+151 %)*	0.35 *(+715 %)*	0.24	0.25 *(+5 %)*	0.42 *(+71 %)*	0.62	0.54 *(-12 %)*	0.67 *(+9 %)*
Total							1.64	1.54 *(-6 %)*	1.53 *(-7 %)*

Similar to the restorations across the typical fringing profile, the increase in setup across the reef flat is largest for the artificial restoration that is located closest to the breakpoint (Restoration 3, see Table 8.10). The increase in setup across the reef flat is 71 % at this location, which leads to an increase in the setup component of the runup. At locations further offshore (Restoration 2) and onshore (Restoration 4 to 6) this effect decreases, and setup at the beach decreases as beach toe wave heights have been decreased by the restoration.

8.2.1.3 Straight profile

All restorations across the straight profile show similar characteristics and are comparable to the forereef restorations of the typical fringing reef. In Table 8.11, wave transformation characteristics of the upper forereef restoration of the straight profile are displayed. As the hydrodynamic effects of the other two restorations are explained by the same mechanisms, their characteristics are summmarized in Tables D.6 and D.7 in Appendix D.

Table 8.11: Summary of wave transformation characteristics across the **upper forereef restoration of the straight reef profile** (restoration 3 in Figure 6.2), displaying the wave transmission across the restoration (ratio of wave heights shoreward versus seaward of the restoration), the setup across the restoration, the wave heights and total setup at the beach toe and the runup components. Other table characteristics are noted in the Intermezzo on page 78.

	Wave transmission restoration [-]			**Beach toe wave heights [m]**			**Runup [m]**		
	Baseline	*Natural*	*Artificial*	*Baseline*	*Natural*	*Artificial*	*Baseline*	*Natural*	*Artificial*
SS	0.93	0.88 *(-5 %)*	0.70 *(-24 %)*	2.46	2.26 *(-8 %)*	1.99 *(-19 %)*	0.60	0.55 *(-8 %)*	0.53 *(-12 %)*
IG	1.07	1.02 *(-4 %)*	0.63 *(-41 %)*	0.75	0.66 *(-12 %)*	0.54 *(-28 %)*	0.66	0.46 *(-31 %)*	0.43 *(-34 %)*
VLF	0.98	0.91 *(-7 %)*	0.67 *(-32 %)*	0.19	0.16 *(-18 %)*	0.13 *(-31 %)*	0.05	0.03 *(-41 %)*	0.02 *(-59 %)*
	Across restoration [m]			**Beach toe [m]**			**Runup [m]**		
	Baseline	*Natural*	*Artificial*	*Baseline*	*Natural*	*Artificial*	*Baseline*	*Natural*	*Artificial*
Setup	0.00	0.00	0.14	0.08	0.12 *(+36 %)*	0.19 *(+127 %)*	0.95	0.75 *(-21 %)*	0.74 *(-23 %)*
Total							2.26	1.79 *(-21 %)*	1.72 *(-24 %)*

Incident short and IG wave heights are reduced across the restoration, for which wave transmission is again reduced for lower water depths. The reduction in beach toe wave heights then induces a significant decrease in setup against the shore, which combined with the large decrease in IG wave heights leads to a sharp reduction in runup. The largest runup reduction across the straight reef (the upper forereef artificial restoration, with a reduction of 24 %) is much larger than the largest reduction of the typical fringing profile runup (mid-flat artificial restoration, reduction of 14 %). The effect of the restoration across the straight profile is much stronger than across the typical fringing reef and convex profile due to (a) the large decrease in setup and IG wave heights as a result of the SS wave dissipation and reflection and thereby a smoothing of the radiation stress gradients and the diminished input of energy from SS waves to the IG waves, and (b) the significant reflection of IG and VLF waves across the restoration (see Figures D.12 to D.14).

8.2.1.4 Three-slope profile

At the three-slope profile, five different restoration locations have been modeled: at the offshore lower forereef, at the edge of the shelf, at the mid-shelf, at the inner edge of the shelf and at the nearshore upper forereef slope (restorations 1 to 5 in Figure 6.2, respectively). The three-slope profile restorations show interesting hydrodynamic patterns that induce a large reduction in runup, of which the mechanisms are elaborated below.

Table 8.12: Summary of wave transformation characteristics across the **shelf edge restoration of the three-slope reef profile** (restoration 2 in Figure 6.2), displaying the wave transmission across the restoration (ratio of wave heights shoreward versus seaward of the restoration), the setup across the restoration, the wave heights and total setup at the beach toe and the runup components. Other table characteristics are noted in the Intermezzo on page 78.

	Wave transmission restoration [-]			**Beach toe wave heights [m]**			**Runup [m]**		
	Baseline	*Natural*	*Artificial*	*Baseline*	*Natural*	*Artificial*	*Baseline*	*Natural*	*Artificial*
SS	0.97	0.95 *(-2 %)*	0.90 *(-8 %)*	2.50	2.17 *(-13 %)*	2.05 *(-18 %)*	0.60	0.39 *(-35 %)*	0.43 *(-29 %)*
IG	0.95	0.92 *(-3 %)*	0.75 *(-21 %)*	0.84	0.58 *(-30 %)*	0.51 *(-39 %)*	0.83	0.39 *(-52 %)*	0.38 *(-53 %)*
VLF	0.98	0.94 *(-4 %)*	0.80 *(-19 %)*	0.23	0.17 *(-28 %)*	0.16 *(-30 %)*	0.06	0.02 *(-68 %)*	0.01 *(-83 %)*
	Across restoration [m]			**Beach toe [m]**			**Runup [m]**		
	Baseline	*Natural*	*Artificial*	*Baseline*	*Natural*	*Artificial*	*Baseline*	*Natural*	*Artificial*
Setup	0.00	0.00	0.02	0.06	0.05 *(-23 %)*	0.08 *(+27 %)*	0.95	0.62 *(-35 %)*	0.61 *(-36 %)*
Total							2.45	1.43 *(-42 %)*	1.44 *(-41 %)*

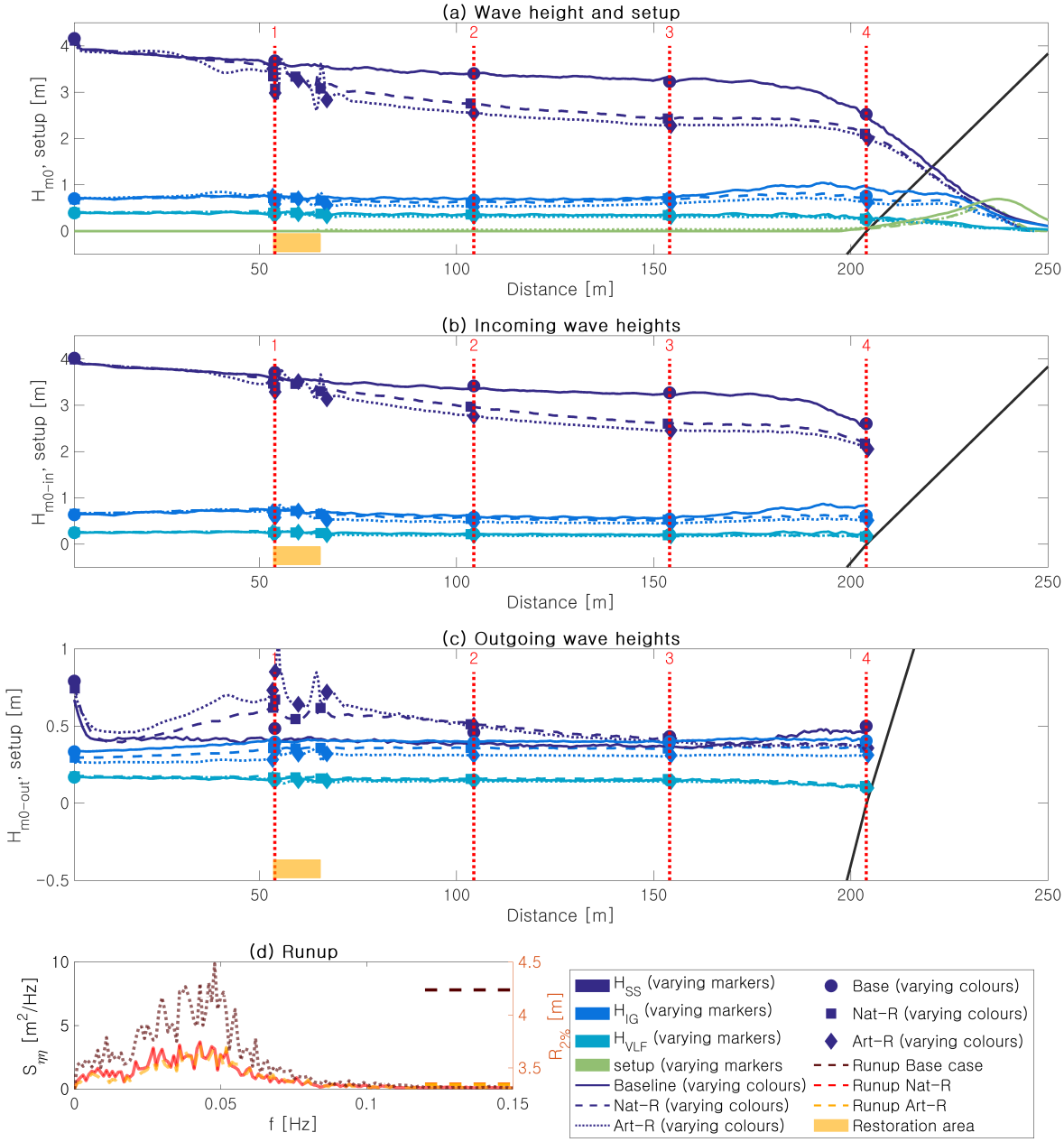

Figure 8.2: Wave transformation and runup across a restoration at the shelf edge of the three-slope profile, displaying the total (subplot a), the incoming (subplot b) and the outgoing (subplot c) SS, IG and VLF waves, as well as the runup (subplot d). Locations 1 to 4 indicate the shelf edge, the mid-shelf, the inner shelf and the beach toe, respectively.

Shelf restorations The restorations at the outer forereef and across the shelf show a similar effect on reef hydrodynamics as they are all located at approximately the same depth. Incident, incoming short waves are reduced in height across the restoration, partly due to reflection (see Figure 8.2), partly due to dissipation across the restoration that decreases the depth just up to the depth of breaking for the largest waves. The reflection at the restoration causes the overall wave energy to reach the inner shelf edge to be significantly reduced. Across the nearshore surfzone, the transfer of energy from the short waves to the IG waves is now limited as a result of the dissipation of SS waves, decreasing the IG wave heights near the shore and hence runup component. The setup across the restoration is minimal due to the relatively large depth, and setup near the shore is reduced by the dissipation and reflection of SS waves. The IG and VLF components of the runup are significantly decreased by the restorations. This is assumed to be caused by the IG and VLF wave dissipation and reflection across the restoration, which reduces the wave transmission across restorations

relative to the baseline scenario (see Table 8.12).

Interesting patterns are observed for the outgoing wave heights, which are depicted in Figure 8.2. Outgoing SS wave heights seaward of the restoration increase up to the restoration location, after which they gradually decrease shoreward of the restoration (see Figure 8.2 and Table 8.12 illustrating the wave transformation across the outer shelf edge restoration, and Figures D.15 to D.19 in Appendix D for other shelf restorations). This could indicate a reflection of SS waves at both the outer edge and the inner edge of the restoration. Outgoing IG wave heights are larger shoreward of the restoration than seaward. This could also indicate the (partial) reflection of IG waves at the inner edge of the restoration back to the coast, of which the effect is strongest for the artificial restoration at the shelf edge. This again affects the calculated incoming wave heights shoreward of the restoration, as the inward reflected IG waves cannot be discerned from the incoming IG waves.

Upper forereef restoration The restoration at the upper forereef is again much comparable to the upper forereef restoration of the straight profile. SS and IG wave heights across the restoration are significantly reduced prior to the nearshore breakpoint location, leading to a large reduction in the SS, IG and setup component of the runup (see Figure D.19 and Table D.11 in Appendix D).

Restorations across the three-slope show a large decrease in runup (around 40 %), which is much larger than the runup reduction across the other profiles. Although the dissipation mechanisms and reflection are hard to separate based on current results, it seems that reflection at the outer edge of the restoration is the main contributor to the reduction in SS wave heights (based on the comparison of total, incoming and outgoing wave heights), as a result of which the wave energy reaching the shore is diminished, reducing both the setup and IG runup components.

8.2.2. Varying boundary conditions

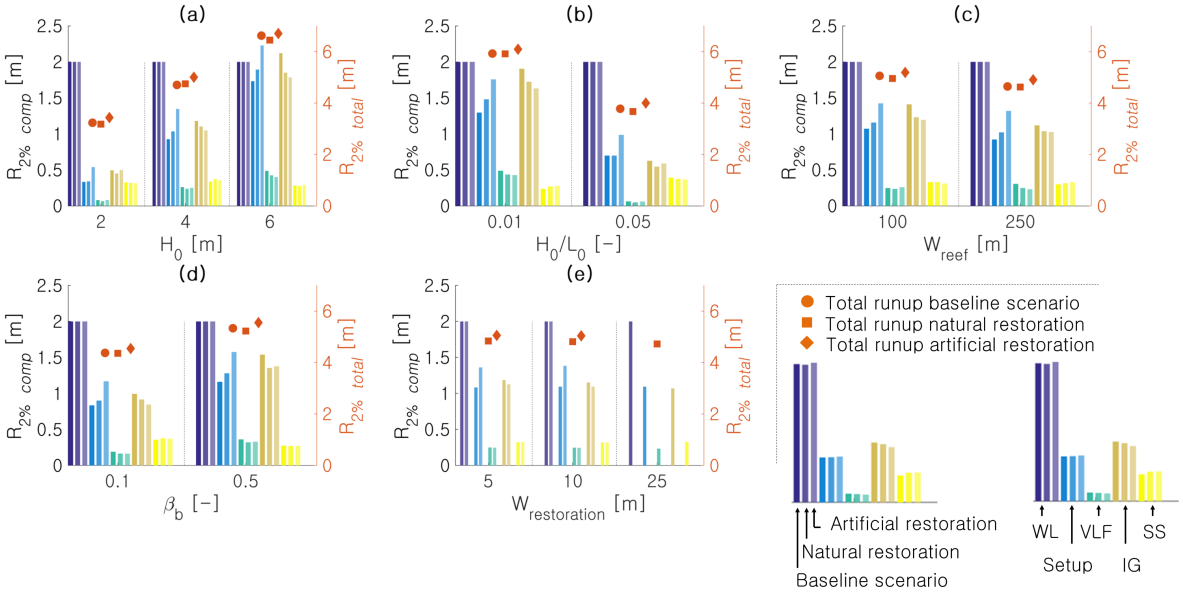

Figure 8.3: An example of the runup plots depicting the influence of varying boundary conditions and profile parameters. Indicated in different colours, from left to right the offshore water level, the setup, the VLF, the IG and the SS wave height component), for (from left to right) the baseline scenario, the natural restoration and the artificial restoration (indicated by differences in transparency). The total runup is indicated by orange round (baseline), square (natural restoration) and diamond (artificial restoration) markers, whose magnitude is given on the right y-axis

In the previous section, the wave transformation was described for one hydrodynamic forcing condition. However, the boundary conditions greatly influence the effect of a restoration. Among others, water level and wave height variations move the breakpoint location, which in turn affects radiation stress gradients induced by the restoration. Profile parameters influence the IG and VLF generation, which again regulates the efficiency of the restoration, as wave damping is larger for larger wave heights. For each restoration location, a

figure such as Figure 8.3 is constructed, in which the runup components of the baseline scenario, the natural restoration and the artificial restoration are plotted, for variations in water level, wave height, steepness, restoration width and corresponding profile parameters. All results can be found in Appendix D, Section D.2. In this section, most important effects of varying forcing conditions and profile parameters observed in Figures D.20 to D.26 in Section D.2 of Appendix D are summarized and illustrated.

Restoration width In contrast to what can be expected, the restoration width does not significantly affect the runup, as can be deduced from Figures D.20 to D.26 in Section D.2 of Appendix D. IG wave heights are slightly reduced by restorations with larger widths, but other components remain relatively constant across the modeled restoration width variations. This could be an indication that the frictional wave dissipation across the relatively short restored section is low. Secondly, as wave reflection is an important aspect of the restoration, and as wave reflection is relatively independent of the restoration width, this could support the notion that the restoration width hardly affects the efficiency of the restoration.

Setup and SS wave heights The setup component of the runup is strongly affected by coral restorations, of which the effect varies again strongly with varying boundary conditions, profile parameters and the restoration location. For the straight and the three-slope profile the impact of a restoration on setup is clear, as the smoothing of radiation stress gradients and reduction of SS beach toe wave heights induces a reduction in setup across almost all modeled variations (see subfigures (c) and (d) of Figure 8.4). For the typical fringing reef profile and the convex reef, it is more difficult to distinguish clear trends in setup variations across varying hydrodynamic forcing and profile parameters. Reason for this is that two distinct setup zones can be discerned for these profiles, at *the reef flat* and at *the beach*, that react differently to coral restorations.

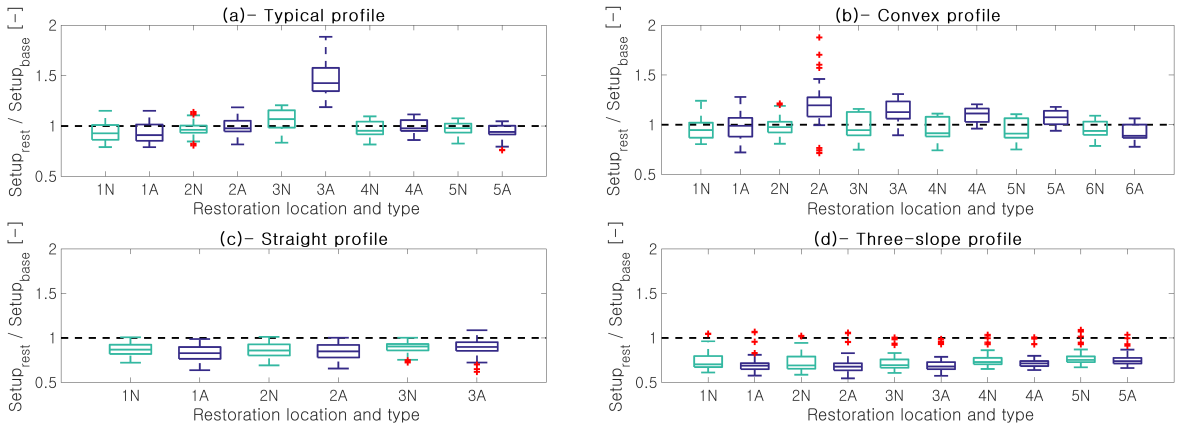

Figure 8.4: Setup component of the runup, for each restoration location (denoted by the numbers 1-6 at the x-axis) and for each restoration type (natural (N) restoration or an artificial (A) reef restoration, also indicated at the x-axis). For each restoration location and type, the setup component of the runup of the restoration scenario relative to the baseline scenario is calculated, for all hydrodynamic forcing conditions and reef parameters. This results in box plots where for each restoration type (location and restoration height), the 25, 50 and 75 percentile are plotted as blue (artificial restoration) or turquoise (natural restoration) boxes, the upper and lower extreme data points that are not considered outliers as coloured horizontal lines and the outliers as red pluses. The larger the spread in data, the more the setup is influenced by variations in hydrodynamic and profile forcing parameters. Furthermore, y-values below 1 indicate that setup is reduced by the restoration, whereas y-values above one indicate an enhancement of the setup by the restoration

For restorations at the reef flat, *setup across the reef flat* is increased by the restoration due to the local SS wave dissipation across the shallow restoration. The effect of forereef restorations on setup across the reef flat is dependent on the location of the breakpoint. For restorations located far offshore of the breakpoint (restoration 1 in Figure 8.4), setup across the flat is decreased as radiation stress gradients are smoothed. The location of the breakpoint, however, changes with the hydrodynamic forcing conditions. For larger wave heights and lower water depths, the breakpoint moves seaward and vice versa. This gives rise to different effects of restorations that are located on the upper forereef part, effectuating both a reduction and enhancement of the setup depending on the hydrodynamic forcing, as depicted in Figure 8.4, Restorations 2A and 2N.
At the beach, an *additional water level setup* is apparent that is largely dependent on the beach toe SS wave heights, as was shown in Section 4.2.3. As wave dissipation is largest for lower water levels and large wave

heights (see Section 4.2.1), the SS wave height reduction is largest for these conditions and hence the reduction in additional setup at the beach. This effect is illustrated in Figure 8.5, where the reduction in SS beach toe wave heights is largest for restorations on the reef flat, and larger for the artificial restoration than for the natural restoration. The sum of the reef flat setup and the beach setup then determines the setup component of the runup. As can be deduced from the above mentioned observations, the effects of the restoration are contradictory. On the one hand, setup across the reef generally increases as a result of a restoration, after which a reduction in SS wave heights across the restoration leads to a reduction in setup at the beach. The setup component of the runup is therefore reduced under certain circumstances and increased under other.

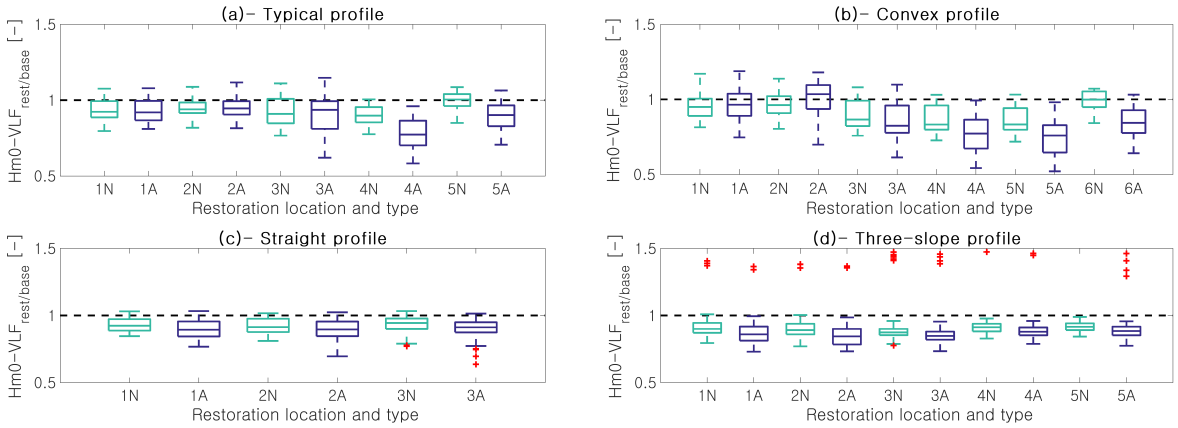

Figure 8.5: SS wave height at the beach toe, for each restoration location (denoted by the numbers 1-6 at the x-axis) and for each restoration type (natural (N) restoration or an artificial (A) reef restoration, also indicated at the x-axis). For each restoration location and type, the SS wave height at the beach toe of the restored reef relative to the baseline scenario is calculated, for all hydrodynamic forcing conditions and reef parameters. This results in box plots where for each restoration type (location and restoration height), the 25, 50 and 75 percentile are plotted as blue (artificial restoration) or turquoise (natural restoration) boxes, the upper and lower extreme data points that are not considered outliers as coloured horizontal lines and the outliers as red pluses. The larger the spread in data, the more the SS wave reduction is influenced by variations in hydrodynamic and profile forcing parameters. Furthermore, y-values below 1 indicate that the SS wave height is reduced by the restoration, whereas y-values above one indicate an enhancement of the SS wave height by the restoration

IG and VLF wave heights The effect of coral restorations on IG and VLF wave heights shows clear trends among the model variations, as can be deduced from Figures 8.6 and 8.7.

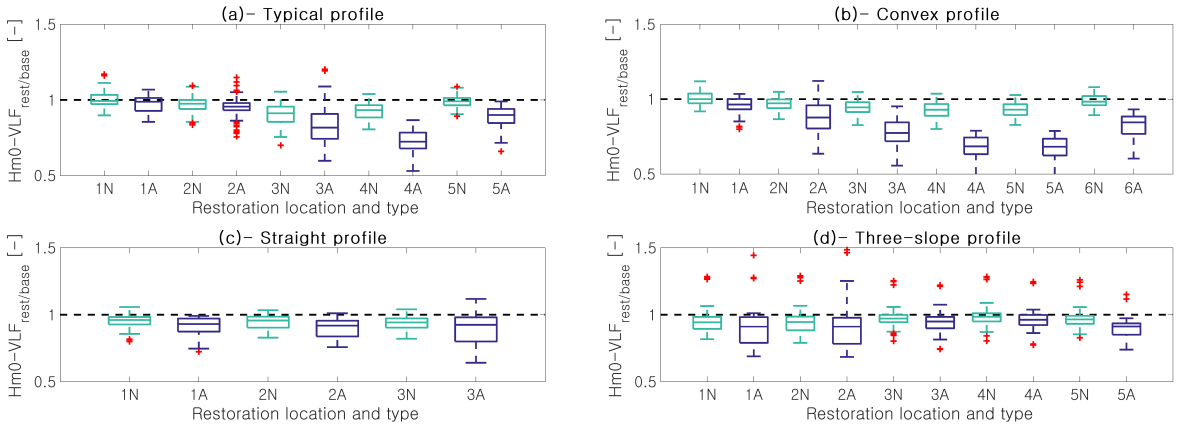

Figure 8.6: IG wave height at the beach toe, for each restoration location (denoted by the numbers 1-6 at the x-axis) and for each restoration type (natural (N) restoration or an artificial (A) reef restoration, also indicated at the x-axis). For each restoration location and type, the IG wave height at the beach toe of the restored reef relative to the baseline scenario is calculated, for all hydrodynamic forcing conditions and reef parameters. This results in box plots where for each restoration type (location and restoration height), the 25, 50 and 75 percentile are plotted as blue (artificial restoration) or turquoise (natural restoration) boxes, the upper and lower extreme data points that are not considered outliers as coloured horizontal lines and the outliers as red pluses. The larger the spread in data, the more the IG wave reduction is influenced by variations in hydrodynamic and profile forcing parameters. Furthermore, y-values below 1 indicate that the IG wave height is reduced by the restoration, whereas y-values above one indicate an enhancement of the IG wave height by the restoration

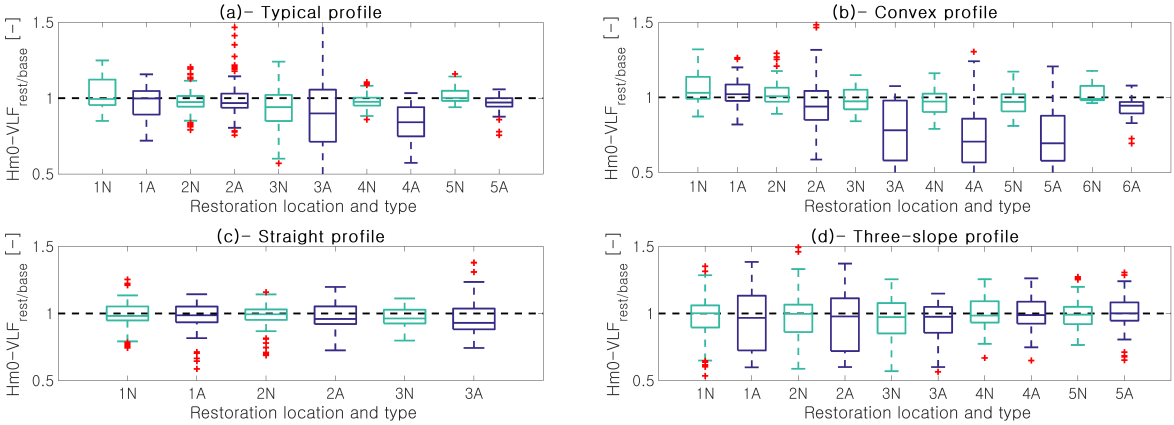

Figure 8.7: VLF wave height at the beach toe, for each restoration location (denoted by the numbers 1-6 at the x-axis) and for each restoration type (natural (N) restoration or an artificial (A) reef restoration, also indicated at the x-axis). For each restoration location and type, the VLF wave height at the beach toe of the restored reef relative to the baseline scenario is calculated, for all hydrodynamic forcing conditions and reef parameters. This results in box plots where for each restoration type (location and restoration height), the 25, 50 and 75 percentile are plotted as blue (artificial restoration) or turquoise (natural restoration) boxes, the upper and lower extreme data points that are not considered outliers as coloured horizontal lines and the outliers as red pluses. The larger the spread in data, the more the IG wave reduction is influenced by variations in hydrodynamic and profile forcing parameters. Furthermore, y-values below 1 indicate that the IG wave height is reduced by the restoration, whereas y-values above one indicate an enhancement of the IG wave height by the restoration

The efficiency of the restoration is strongly linked to the generation of IG and VLF waves by the breakpoint mechanism. As was explained in Section 2.2.1.1 and again highlighted in Chapter 7, the breakpoint mechanism is most strong for low water levels, large wave heights and large forereef slopes. Next to that, wave dissipation and reflection is largest for low water levels and large wave heights. Both mechanisms are clearly observed in Figures D.20 to D.26 in Appendix D, where the IG and VLF wave height reduction by the restoration is large for restoration locations that are located shoreward of the breakpoint and under the above mentioned hydrodynamic forcing conditions (large wave heights and forereef slopes and low water levels). Restorations that are located seaward of the breakpoint location reduce incoming SS wave heights and thereby the IG waves that are generated by the breakpoint mechanism. The reduction of the beach toe IG wave heights across various restoration locations is illustrated in Figure 8.6, whereas the reduction of the beach toe VLF wave heights is displayed in Figure 8.7.

8.2.3. Bulk results

In the previous sections, the main mechanisms that lead to either an increase or reduction of the different runup components are elaborated. In this section, a final overview is given of the *hydrodynamic effects of a restoration* and the *flood risk reduction potential* across the different restoration locations and reef shapes.

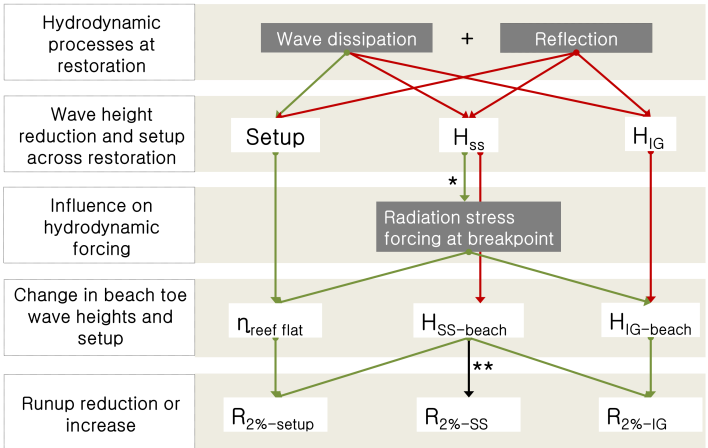

Figure 8.8: Hydrodynamic effects of a restoration. Green arrows indicate a positive correlation (e.g. when wave dissipation across the restoration increases, setup across the restoration increases). Red arrows indicate a negative correlation (e.g. when wave dissipation across the restoration increases, the SS wave height behind the restoration decreases). *: H_{SS} reduction only affects radiation stress forcing of setup and IG waves when located seaward of the breakpoint. **: $H_{SS-beach}$ only minor influence on SS runup.

In Figure 8.8, an overview of the *hydrodynamic effects of a restoration* is given. Across the restoration, wave dissipation and reflection cause a decrease in infragravity (IG and VLF) and SS waves and an increase in setup. The SS wave reduction then affects the radiation stress forcing at the breakpoint if the restoration is located seaward of the breakpoint. If so, SS wave height reduction across the restoration causes a decrease in radiation stress gradients at the breakpoint and thus setup. As the SS wave height is the controlling parameter of the IG generation by the breakpoint forcing, an SS wave height reduction also causes a reduction in IG waves when the restoration is located seaward of the breakpoint. The beach toe wave heights determine the runup, in which the SS beach toe wave height affects the setup and IG wave component of the runup by reducing radiation stress gradients and limiting the transfer of energy from SS to IG waves, respectively. The SS runup component is relatively stable, likely as a result of the depth limitation on the SS wave height.

In Figure 8.9 a final overview of the *runup reduction potential* is given for each profile shape. This figure gives insight into *profile shapes with the most promising runup reduction potential*, *restoration locations that induce the largest reduction in runup* and the *variability of the runup reduction under varying forcing conditions*.

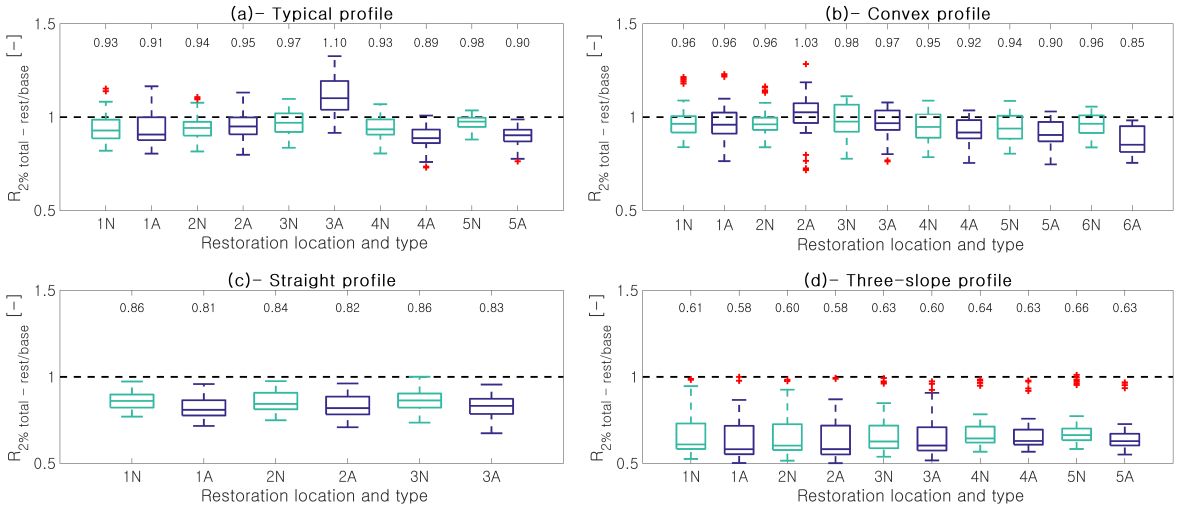

Figure 8.9: The total runup reduction plotted for (a) the typical fringing reef profile, (b) the convex profile, (c) the straight profile and (d) the three-slope profile. In each subplot, for each restoration location (denoted by the numbers 1-6 at the x-axis) and for each restoration type (natural (N) restoration or an artificial (A) reef restoration, also indicated at the x-axis), the runup reduction is calculated, for all hydrodynamic forcing conditions and reef parameters. This results in box plots where for each restoration type (location and restoration height), the 25, 50 and 75 percentile are plotted as the blue (artificial reef) and green (natural restoration) box, the extreme data points that are not considered outliers as coloured horizontal lines and the outliers as red pluses. Above the box plots, the exact median values are printed.

Profile shape From Figure 8.9 it is evident that restorations across the three-slope profile are most efficient in reducing the runup (with approximately 40 % on average). The depth induced wave breaking outside the baseline scenario surfzone, at relatively large depths, and the significant reflection at the outer edge of the restoration causes a significant reduction in short wave heights, accompanied by a marginal increase in setup. This again diminishes both the breakpoint forcing of IG waves at the nearshore slope and the setup against the shore. To a lesser extent, a similar effect is discerned across the straight profile (subfigure (c) in Figure 8.9), in which the reduced SS beach toe wave heights cause a significant decrease in runup (15 to 19 % reduction on average). Runup reduction at the typical fringing reef profile and convex reef is much smaller (between 5 % and 15 % reduction) due to the increase in setup across the restoration. What is more, there are several conditions (large incident SS wave height, low water depths), under which the restoration increases the runup, which is apparent from the 75 runup percentile depicted in Figure 8.9 that is above 1 for many restoration locations. Clearly, profile shapes that are naturally more susceptible to flooding (the straight and three-slope profile) benefit most from the coral restoration.

Restoration locations The effect of the restoration location varies across the different profile shapes. For the straight and three-slope profile, the restoration location does not influence the runup reduction potential significantly, as they are all located at larger depths away from the breakpoint location. This is different for

the convex and typical fringing reef profile, where restorations located in the vicinity of the baseline scenario breakpoint enhance radiation stress gradients and can therefore increase the setup with up to 70 %. Restorations close to shore and at the lower forereef of the typical and convex profile do have a favourable effect on flood risk. Clearly, restorations at the typical and convex profile must be designed with more care for the prevailing hydrodynamic conditions on site, to prevent the unwanted increase in runup by the restoration.

Varying forcing conditions In Figure 8.9, the influence of varying model parameters can be gathered from the boxplots. The straight profile shows the least variation in runup reduction for varying forcing conditions. At this profile, a reduction in runup is achieved under all conditions and at all locations. For the typical fringing reef and convex profile, the reduction of the runup is highly dependent on the restoration location and on the forcing conditions; the boxplots show a large spread with values both below and above one. This is due to contradictory effects of the restoration at these profiles. As can be deduced from Figures D.20 and D.21, typical fringing reef restorations mostly increase the setup across the reef flat but reduce SS and IG wave heights. Hydrodynamic forcing conditions determine which mechanism is dominant. Across the three-slope profile, restorations induce a reduction in runup across all locations, although the boxplots show a large scatter in reduction values. As can be deduced from Figures D.25 and D.26, the restorations across the three-slope profile respond strongly to wave height and water level modulations, as expected as larger wave heights and lower water levels will significantly increase dissipation and reflection across the relatively deep restorations at the shelf.

8.3. Discussion

The results on the effects of coral restoration for coastal protection seem promising, as a reduction in runup can be accomplished for each reef profile shape, the efficiency dependent on the location of the restoration. This gives hopeful ground for future research, as much is left to discover about the effect of coral restorations. Some caveats must be made, however, on the predictive capability of these results.

Restoration schematization Coral restorations are modeled as bed elevations with enhanced friction coefficients. In nature, coral transplantations and artificial reef restorations are not impermeable, allowing some water to flow through the canopy, which could induce a reduction in setup and reduced reflective values compared to the impermeable bed case. Another schematization assumption is that the existing reef is of poor quality, with sufficiently low bed elevations to be schematized as a flat bed with a low roughness, on which restorations are imposed. If large coral colonies are present at the reef, the effect of the coral restoration is diminished, as reflection and wave breaking are expected to be the main cause of the runup reduction, which is partly taken over by existing reef communities. Hence, the schematization of the coral canopy as an impermeable wave blocker at an otherwise flat bed defines the upper limit of the runup reduction potential.

Model limitations The reef is schematized as a 1D system, solving only variations in cross-shore direction. The assumption of limited along shore variation in waves and currents is viable for the middle section of long stretches of restorations. On the lateral edges of the domain, however, 2D effects such as wave induced currents become important, creating circulation cells at the boundaries of the restoration that alter the hydrodynamics across the reef. Moreover, circulation cells induced by low-crested breakwaters have shown to be a contributor to coastal erosion [126]. These effects will not be captured by the 1D model.

Model processing There are several limitations regarding the processing of XBeach data. Firstly, as was mentioned before, the distinction between SS, IG and VLF waves is based on cutoff frequencies that determine which part of the energy spectrum is attributed to which wave component. Next to this, the total wave heights are splitted into incoming and outgoing wave heights based on theory by Guza et al. [60]. It is, however, not possible to distinguish whether the incoming waves are in fact incident incoming waves or waves that are reflected off of the inner edge of a restoration in the direction of the shore, which is presumed to happen at the three-slope reef.

Hydrodynamic forcing conditions Variations in model forcing conditions and profile parameters are modeled to capture some of the variability observed in nature. An important phenomenon is resonance at the

reef, a mechanism that can be responsible for a significant enhancement of the runup and that is a function of both hydrodynamic and morphological parameters [53] [117]. An indication of this hydrodynamic phenomenon was only observed across the steep (1:2 slope) fringing reef (see Figure 7.1), where VLF waves showed a slightly progressively growing pattern across the reef flat, attaining their maximum height near the coast and minimum height at the reef edge, although wave heights were very small. The resonant forcing across these reefs is in accordance with the study of Pearson [116], who noted that resonance occurs mainly on narrow reef flats. The effect of a restoration on the resonant forcing is difficult to gather from the current dataset, although it is clear from Figure 8.3 that outgoing wave heights can be slightly larger shoreward of the restoration than seaward of the restoration, an indication that waves are reflected off of the beach and then again reflected shoreward off of the restoration. A reflection basin could be detrimental for coastal safety, although an increase in runup by wave motions has not been observed in this dataset. Therefore a study on resonant forcing by restorations, searching for parameter combinations that can excite resonance as a result of a restoration, would be highly interesting to observe this effect and identify under which conditions these restorations become problematic.

Wave dissipation processes Based on the XBeach non-hydrostatic model, it is not possible to determine whether the wave height reduction is the effect of either frictional wave damping, wave breaking dissipation, a transfer of energy between frequencies or reflection. A detailed analytical analysis of wave dissipation processes across the restoration would thus be of large interest to accurately describe the wave transformation processes across the restoration.

Coral ecology In this research, focus is on the hydrodynamic effects of coral restorations, with limited attention to the ecological response of restored sections. For this, a canopy model as described by Rooijen et al. [142] is more appropriate, with which in canopy flow and shear stresses can be modeled, which coupled to ecological growth properties and constrictions of coral can give an insight into the growth potential and longevity of the restored sections at different locations. Based on the current study, it can be concluded that restorations in zones of rapid wave dissipation and hence high bottom stresses (such as the reef edge restoration of the typical fringing reef) are not favourable from a hydrodynamic point of view. From an ecological point of view, these zones are also troublesome, as bottom stresses are often too high for large canopies to develop. For this reason, the reef edge of a fringing reef is often formed by a calcareous crest as corals cannot grow at this exposed site. Hence, most questionable locations from an ecological point of view are already omitted by their enhancement of the flood risk. Outside the region of rapid wave dissipation (reef edge), wave action across the increased bed elevations of the restorations induces significant flow through the coral canopy, transporting nutrients to the coral and flushing debris, which is ecologically favourable.

Feasibility of upscaling coral restoration In this study, it is assumed that large stretches of coral reef can be restored. Little attention has been paid to the actual feasibility of this. It needs to be investigated whether the large scale implementation of coral transplantation or artificial reef construction is possible, and if the benefits of coral restoration outweigh the costs.

8.4. Conclusion

For four reef profile shapes, restorations have been designed and modeled to assess their effect on wave transformation and flood risk reduction. A first insight is gained into profiles and locations with restoration potential, as well as mechanisms responsible for the reduction in runup.

Restoration potential is distinctly different among varying profile shapes. The typical fringing reef and the convex reef feature a reef flat that acts as a natural wave attenuator, diminishing the flood risk reduction effect of the coral restoration. The straight and three-slope profile are relatively unprotected from wave action, rendering them vulnerable to coastal flooding, but also responsive to restoration measures. Runup reductions of up to 40 % are observed for the three-slope profile and up to 20 % for the straight profile, while runup reduction across the typical and convex reef are stalled at approximately 5 %. For each profile shape, both the most promising and the least promising restoration locations are indicated in Figures 8.10 to 8.13, in which the reduction of different runup components is illustrated.

In general, the main mechanisms responsible for runup reduction are the reflection and dissipation of SS and IG wave heights across the restoration. The reduction of SS waves can cause the setup and IG wave runup to decrease due to the reduced radiation stress gradients and breakpoint forcing, as well as a diminished transfer of energy from short waves to the infragravity waves. Under certain conditions, runup can be increased by a restoration as a result of a large increase in setup, which is often observed for artificial restorations across the typical and convex reef. Possibly, runup could be enhanced due to resonant forcing, but this phenomenon has not been observed in the current dataset. The significant reflection off of the restoration is an interesting characteristic, as this reduces the overall wave energy shoreward of the restoration and thereby the runup. Therefore, dense coral canopies or artificial structures are wanted as a low permeability maximizes the reflection.

The results of this chapter show promising terrain for restoration measures. Based on the gained insight into the hydrodynamic effects of restorations, optimal coral restoration strategies can be formulated, although model limitations and restrictions on the validity of the results need to be kept in mind. The study has given ground for many future areas of study, on the topic of among other reflection and dissipation processes across the restoration, resonance excitement by restorations and the effect of hydrodynamics on coral ecology.

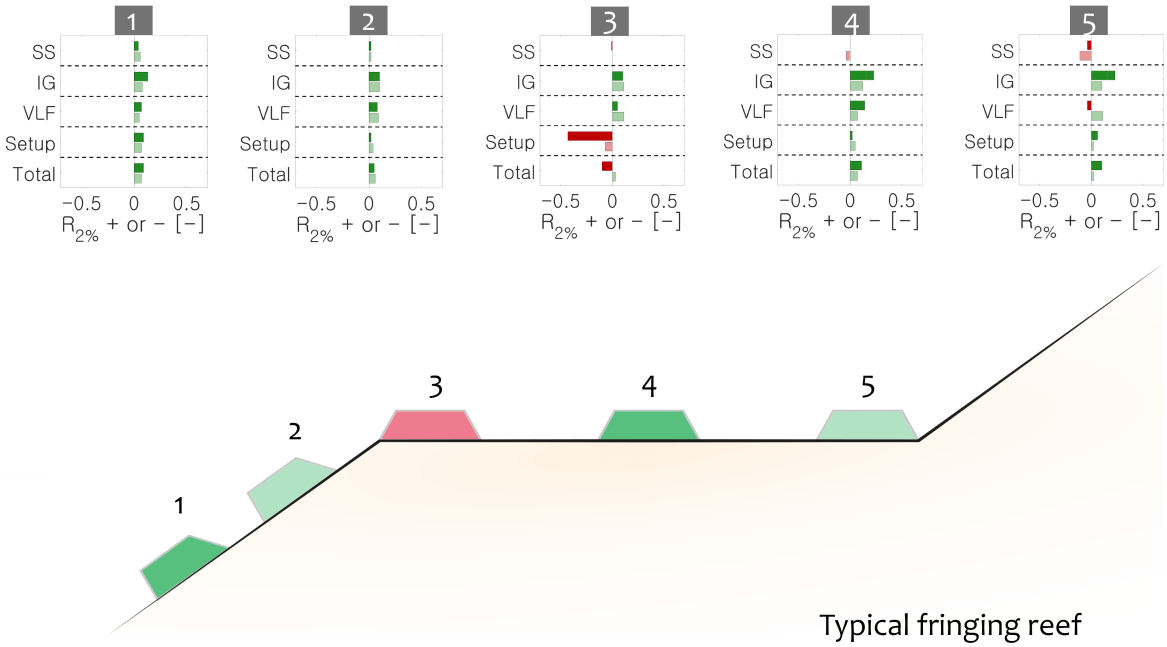

Figure 8.10: Final overview of the runup reduction at the five restoration locations of the typical profile. In subfigures 1 to 5, the relative runup reduction is depicted for the five restorations, in which the dark red and green colors indicate the artificial reef restoration, and light red and green the natural restoration. At the depicted reef profile, restorations are coloured according to how well they reduce the runup (green is positive, red is negative impact)

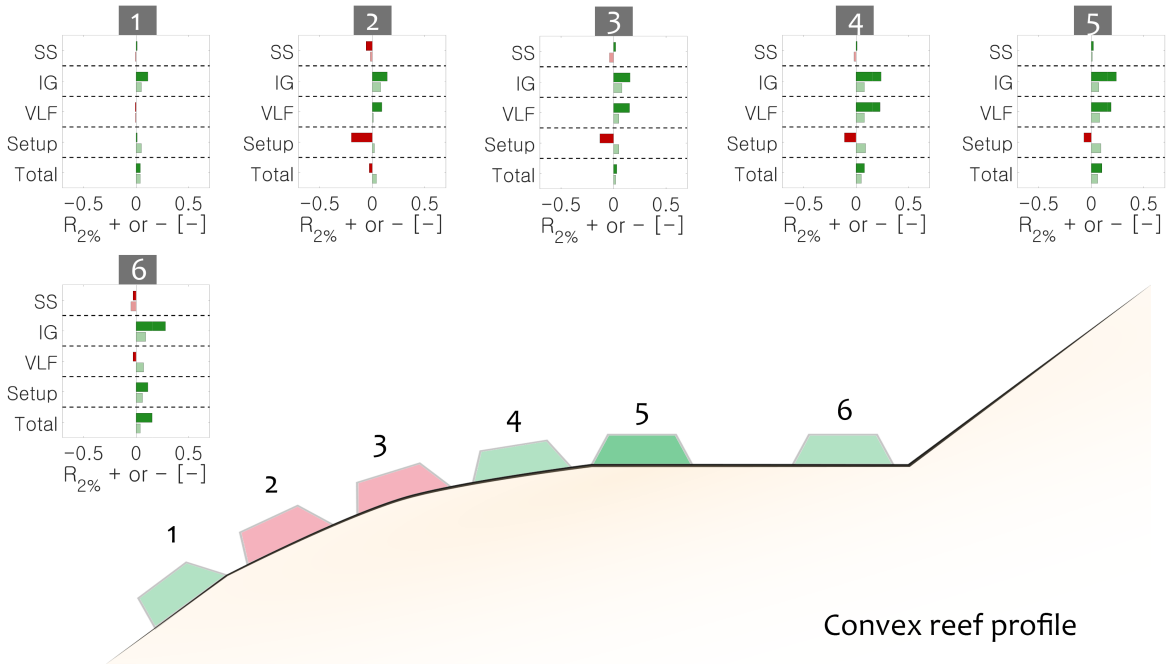

Figure 8.11: Final overview of the runup reduction at the six restoration locations of the convex profile. In subfigures 1 to 6, the relative runup reduction is depicted for the six restorations, in which the dark red and green colors indicate the artificial reef restoration, and light red and green the natural restoration. At the depicted reef profile, restorations are coloured according to how well they reduce the runup (green is positive, red is negative impact)

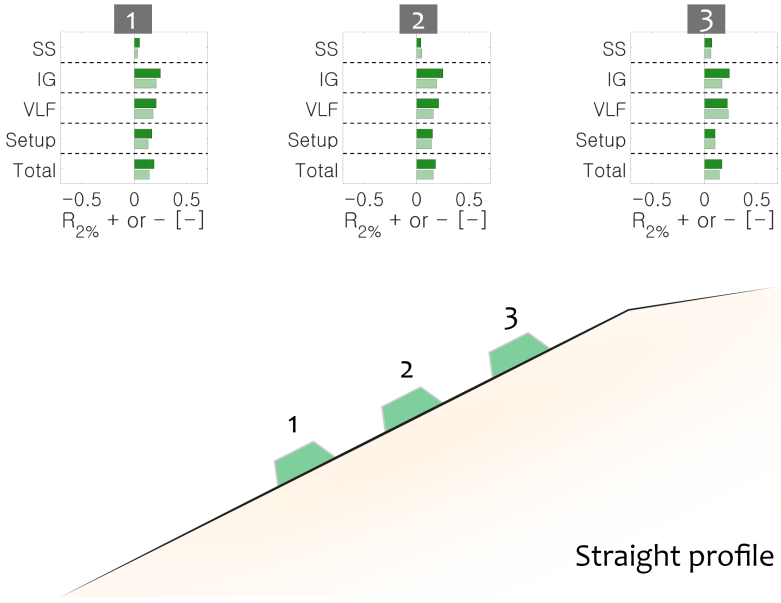

Figure 8.12: Final overview of the runup reduction at the three restoration locations of the straight profile. In subfigures 1 to 3, the relative runup reduction is depicted for the three restorations, in which the dark red and green colors indicate the artificial reef restoration, and light red and green the natural restoration. At the depicted reef profile, restorations are coloured according to how well they reduce the runup (green is positive, red is negative impact)

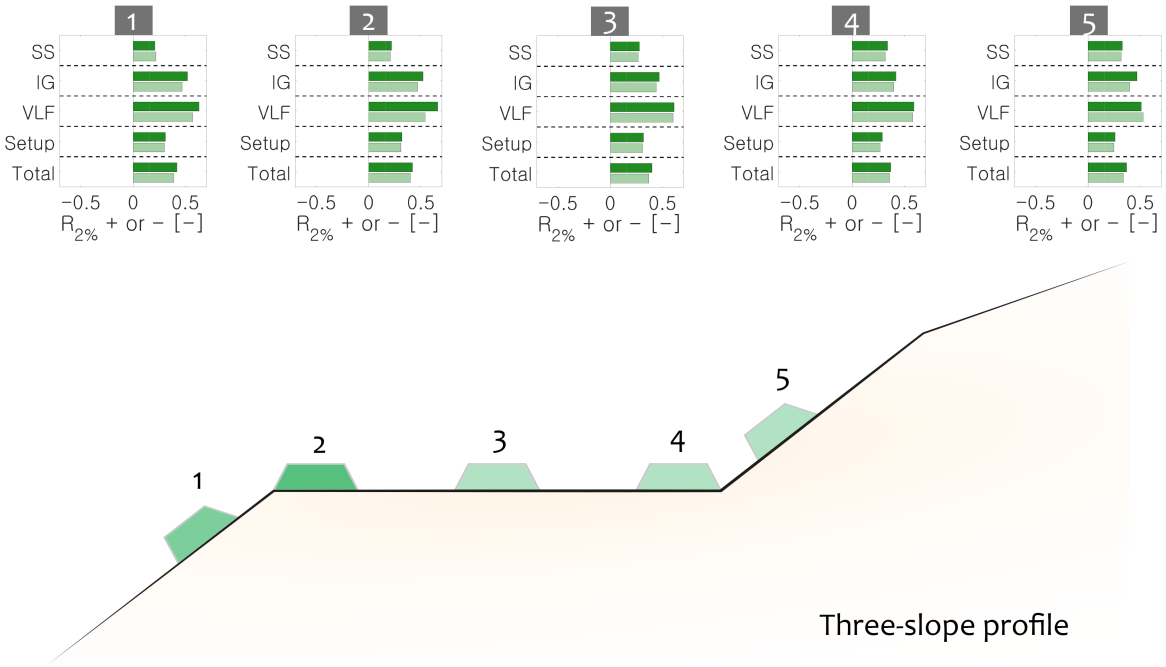

Figure 8.13: Final overview of the runup reduction at the five restoration locations of the three-slope profile. In subfigures 1 to 5, the relative runup reduction is depicted for the five restorations, in which the dark red and green colors indicate the artificial reef restoration, and light red and green the natural restoration. At the depicted reef profile, restorations are coloured according to how well they reduce the runup (green is positive, red is negative impact)

IV

Conclusions and Recommendations

9

Conclusions

This research explores the hydrodynamic effects of coral restorations at various reef morphologies. Four main lines of study can be distinguished: the general reef hydrodynamics, the reef profile variability, the wave transformation and flooding across different reef shapes and finally the flood risk reduction of restorations across various reef morphologies. A simple wave transformation model was developed based on an evaluation of existing wave dissipation models and a data-analysis on XBeach simulations of a fringing reef. A cluster analysis was performed to gain insight into the reef profile variability. Furthermore, an XBeach non-hydrostatic model was set up to discover the effect of different restoration configurations and reef profile shapes on nearshore hydrodynamics.

9.1. Key findings

The main findings of this research are illustrated below on the basis of the research questions outlined in Chapter 3.

What are the key hydrodynamic processes that drive inundation and flooding of reef fronted coastlines?

The runup at a reef fronted coast is highly dependent on local geometric conditions and hydrodynamic forcing, showing little correlation to existing formulations for runup at sandy coastlines (e.g. Stockdon et al. [150] and Gomes da Silva et al. [55]). New formulations for the SS and IG component of the runup at the reef beach have been identified, based on beach toe wave heights and water levels, as the many non-linear interactions between reef geometry and hydrodynamics make the prediction of the runup based on offshore wave parameters highly inaccurate. Beach toe SS wave heights and setup can be reasonably predicted with the parametric wave model of Janssen and Battjes [73]. IG waves at relatively steep reefs (>1:20) are foremost generated by the breakpoint mechanism [122][94], which is dependent on the wave height, water level, forereef slope and wave length, as was also concluded by Masselink et al. [94]. The IG beach toe wave heights are modeled to be generated at the reef crest based on an empirical parametrization of the breakpoint forcing, after which they are dissipated by frictional wave damping and breaking, neglecting work done by short waves [162].

Newly derived runup formulations show the important drivers of runup. The IG runup is mainly dependent on IG and SS beach toe wave heights (see Figure 4.17), indicating a significant transfer of energy from the short waves to the IG waves between the beach toe and the shore. The short wave runup is highly correlated with the SS beach toe wave height, wave length and the beach slope (see Figure 4.11). The setup is calculated using the Janssen and Battjes [73] model, where setup is defined by the steady state, inviscid cross-shore momentum balance, which was shown to predict setup across the reef well by Vetter et al. [166]. This can also be deduced from the comparison of the parametric wave model with observations of Buckley et al. [32] (see Figure A.2). Two distinct setup zones can be discerned, one across the reef flat (if present), which increases for larger input wave heights and forereef slopes and lower water levels, and an additional setup at the beach. This additional setup is foremost a function of beach toe wave heights, which are again dependent on the amount of dissipation across the reef and the water level.

How can a large number of coral reef bathymetries be classified into a limited amount of reef profile groups, based on the essential morphological features of the reef geometries?

Over 30.000 bathymetric profiles of coral reefs across the world have been classified based on the similarity between their depths at a large number of cross-shore locations, similar to the study of Costa et al. [40]. The reef profiles are grouped into bins with similar lengths to ensure a clear resolution of reefs with different length scales. The k-means algorithm is used to allocate the reef profiles in a length bin to different clusters. For each clustered group, 5 representative profiles are extracted that were shown to capture the variability within the clustered profile group. All representative profiles are then categorized based on their reef shape, from which ten distinct shapes were discerned (see Figure 5.10). Four profiles with distinct hydrodynamic behaviour and relatively large frequency of occurrence were then extracted for subsequent modeling steps: the typical fringing reef, the convex reef, the straight reef and the three-slope reef (see Figure 5.12). These reef shapes represent 70 % of the surveyed reef profiles.

How do varying reef geometries influence wave transformation and flooding?

The reef profile shape heavily influences wave transformation and flooding of the reef fronted coasts. The forereef slope controls (1) the radiation stress gradients that cause a setup across the reef and (2) the breakpoint forcing of IG waves. Both mechanisms are enhanced for larger forereef slopes, thereby enhancing the IG and setup component of the runup. The dissipation of both low and high frequency motions across the reef is dependent on the natural wave attenuation capacity of the profile: the reef flat width and level of submergence of the typical fringing and convex reef, the shelf width and submergence of the three-slope profile and the forereef length of gently sloping straight reefs. Waves are dissipated by wave breaking at the outer edge of the reef flat or shelf, while frictional dissipation further decreases wave heights. Dissipation is largest across the typical fringing reef flat due to the shallow water depths, which enhance both wave breaking and frictional wave damping. Slightly larger beach toe wave heights are recorded for the convex profile, while straight profile beach toe wave heights greatly exceed wave heights of the typical profile. Dissipation across the shelf again lessens beach toe wave heights of the three-slope profile compared to the straight reef. The reduction of SS waves at the beach effectuates a reduction in additional setup against the shore and a weakened transfer of energy from the short waves to the IG waves between the beach toe and the shore. This significantly reduces the IG and setup component of the runup. Of the four modeled shapes, the straight profile is most vulnerable to coastal flooding, due to large setup near the shore and significant IG generation by the breakpoint mechanism, as no reef flat or shelf is present to damp part of the incoming short wave energy.

What are the hydrodynamic effects of varying coral restoration configurations, across varying reef shapes, and how does this affect their runup reduction potential?

Nineteen restoration locations across four reef profile shapes have been investigated on their effect on wave transformation and runup. Forcing conditions (wave height, water level, wave steepness) and profile parameters (reef width, forereef slope, restoration width and height) were varied for different model runs. From the observations of hydrodynamics across all restorations, general mechanisms of runup reduction were identified. Generally, the outward reflection of both short and infragravity (IG and VLF) motions reduces wave energy reaching the shore. The dissipation of SS and IG waves across the restoration is substantial, with largest dissipation rates noted for restorations in shallow water depths. The reduction in SS wave heights leads to an increase in setup across the restoration. If, however, the restoration is located seaward of the baseline scenario breakpoint, the SS wave reduction decreases the radiation stress forcing at the breakpoint and hence the setup across the reef flat. Furthermore, as the SS wave height is the controlling parameter of the IG generation by the breakpoint forcing, an SS wave height reduction also causes a reduction in IG wave height (when the restoration is located seaward of the breakpoint). The reduction of SS beach toe wave heights reduces the additional setup near the shore and IG wave component of the runup. Naturally, the dissipation of IG waves also leads to a reduction in IG wave runup.

Restoration potential is distinctly different among varying reef profile shapes. The typical fringing reef and the convex reef feature a reef flat that acts as a natural wave attenuator, diminishing the flood risk reduction effect of the coral restoration. The straight and three-slope profile are relatively unprotected from wave action, rendering them vulnerable to coastal flooding, but also responsive to restoration measures. Average

runup reductions of approximately 40 % are observed for the three-slope profile due to the significant reflection of waves at the shelf restorations. At the straight profile, runup is reduced with up to 20 %, while runup reduction across the typical and convex reef are stalled at approximately 5 %.

The optimal restoration location is different for each reef type. For the straight and three-slope profile, the restoration location does not influence the runup reduction potential significantly, as they are all located at larger depths away from the breakpoint location. This is different for the convex and typical fringing reef profile, where restorations located in the vicinity of the baseline scenario breakpoint enhance radiation stress gradients and can therefore increase the setup with up to 70 %. Therefore, restorations at the upper forereef and reef edge of the typical and convex profile are deemed unsuitable. Restorations closer to shore and at the lower forereef do have a favourable effect on flood risk. Clearly, restorations at the typical and convex profile must be designed with more care for the prevailing hydrodynamic conditions on site, to prevent the unwanted increase in runup by the restoration.

9.2. Advances

A new, simple wave transformation model is described that gives a fair approximation of wave transformation and runup at reef fronted coastlines. The novelty of this model lies in its ease of use, the computational efficiency and the fact that it is purpose-built for reefs. It is accessible for a wide range of stakeholders involved in coastal management and protection of reef lined areas. Moreover, it enables the quick calculation of large numbers of profiles.

Not before has such a large dataset of reef profiles been grouped. We now know what the actual reef bathymetries look like that make up the reef coastline. The schematization of the clustered profile groups then enables the efficient modeling of different reef geometries, extending knowledge of reef hydrodynamics across a wider range of profiles than the typical fringing reef profile.

Coral restorations are often executed for ecological reasons. Coral restoration for coastal protection is, however, marginally investigated. With this research, it is shown that coral restorations have the potential of creating a positive impact on coastal flood risk reduction. A first guideline on how to optimize the effect of a restoration is given, by exploring different restoration locations at various reef morphologies and under varying forcing conditions.

9.3. Limitations

Important model and research limitations and assumptions have been described in the Discussion section of Chapters 4, 5, 7 and 8. The main limitations are in summary:

- Limited validation of reef hydrodynamic model.
- Validity of derived empirical expressions for IG generation and runup restricted by model limitations of Pearson [116].
- Reef profile grouping based on depth observations requires thorough supervision of the classification process and additional steps to obtain clear results.
- 1D XBeach modeling approach neglects 2D effects such as horizontal circulation cells and longshore currents.
- Limited variation in reef profile parameters (forereef slope, reef flat/shelf width).
- Limited variation in restoration locations and hydrodynamic forcing conditions. Significant resonant forcing not observed for modeled parameters.
- Schematization of a restored reef as a flat bottom with low roughness on which an impermeable bed elevation with increased friction coefficients is imposed.

In spite of these limitations, the concept of coral restoration is believed to be a promising technique to reduce coastal hazards. Furthermore, the reef hydrodynamic model, although not perfect, gives a good first order assessment of reef hydrodynamics.

10

Recommendations

This study can give fruitful grounds for future research, for which we can make several recommendations.

1. **Collect field, laboratory and numerical data to validate and extend the current simple reef hydrodynamic model**
   As coral restoration projects are executed all around the world's reefs, often without knowledge of hydrodynamic effects of the restoration, there is much potential for a fast, easy to use model to predict the wave transformation and runup across various reef shapes, with and without restorations. However, more research is required for the model to be implemented as a trustworthy tool. Several elements of the model could be topic of further research:

   (a) *Validate short wave transformation model of Janssen and Battjes [73] across different reef shapes with field and numerical data*
   Various field campaigns have been executed to measure wave transformation at reefs [125]. Therefore, suitable datasets need to be identified, as well as numerical data to support the validity of the short wave transformation model.

   (b) *Improve and extend semi-empirical relations for breakpoint forcing of IG waves and runup with numerical simulations*
   The empirical parametrization of IG wave heights and runup based on XBeach simulations of Pearson [116] has shown good results for the typical fringing reef. Interestingly, the numerical simulations executed in this study show that the breakpoint forcing of IG waves is dominant across a range of profiles. This suggests that it is possible to derive empirical formulations for IG wave heights at reef profiles other than the typical fringing reef. Furthermore, the XBeach simulations of varying reef shapes and restoration configurations can be used to further investigate the relation between beach toe wave heights and runup, and verify whether the obtained relations hold for other reef profile shapes.

   (c) *Implement additional processes in simple reef hydrodynamic model*
   Several processes can be implemented to further advance the model, such as reflection at the forereef and beach and resonance across the reef flat. Furthermore, observed effects of the coral restoration can be incorporated in the simple reef hydrodynamic model.

2. **Convert the updated reef hydrodynamic model into an interactive tool accessible to people with different backgrounds and education**
   As coral restorations are executed by a variety of actors, ranging from well informed employees of federal institutions to local populations committed to the reef's health, it would be of great use to turn the reef hydrodynamic model into a simple to use tool that can be distributed widely. It can also be used as an awareness tool, giving insight into the threats to coastal safety of unhealthy reefs.

3. **Carry out model runs with more variations in reef profile shapes, profile dimensions and other model parameters**
   This study has focused on the effects of coral restoration on a limited number of reef profile shapes and

dimensions. Much more knowledge can be gained about the reef geometry control on nearshore hydrodynamics by increasing the variation in profile dimensions. Furthermore, the reef is modeled with one low friction coefficient. By modeling different roughness values, the effect of frictional dissipation across varying reef profiles can be studied.

4. **Improve the understanding of hydrodynamic and ecological effects of coral restoration**

   (a) *Carry out laboratory experiments to validate the effect of a restoration on nearshore hydrodynamics*
   In this research, the effect of a restoration is investigated using numerical simulations. However, no data are available to calibrate the results. Moreover, the flow through the canopy and its influence on the overlying flow is a difficult subject to model. Furthermore, reflection against a porous restoration is different than against an impermeable bed elevation. Therefore, laboratory experiments of different reef restoration configurations can prove highly valuable.

   (b) *Carry out additional model runs with more variation in restoration configurations*
   In this study, a limited number of different restoration widths, heights and locations is investigated. It would be interesting to increase the number of parameter variations. Furthermore, the effect of the restoration roughness on wave dissipation is an interesting topic of study.

   (c) *Investigate wave dissipation processes across the restoration*
   Based on current model results, it is hard to determine whether wave dissipation occurs as a result of wave breaking or frictional wave dissipation. Therefore, an interesting line of research is the elaboration of the momentum balance across the restoration, to determine the contribution of each dissipation process. This requires careful attention, as the multiple locations of reflection at the reef complicate the establishment of the momentum balance terms.

   (d) *Investigate resonance excitement by coral restoration*
   Coral restorations can create a basin in which resonance is enhanced. This enhancement of low frequency motions was, however, not observed in the current dataset. This gives interesting grounds for further research, searching if conditions exist under which resonance negatively affects the runup reduction potential of a restoration.

   (e) *Investigate ecological aspects of coral reef restoration*
   In this research, little attention has been paid to the link between hydrodynamics and ecology, while it's a highly interesting and important topic. If corals cannot survive at the designated restoration location, restoration efforts are useless. This will depend among others on the in situ bed shear stresses, the presence of wave induced currents to transport among others nutrients and coral larvae to the restoration site, and the sea temperature.

   (f) *Carry out case studies with coral restoration*
   In a field experiment, all effects of a restoration can be monitored. Not only its effect on wave transformation and runup reduction, but also the effect on the surrounding ecology. Case studies can also show whether restoration projects are financially viable and if upscaling of the restoration techniques is indeed possible.

   (g) *Build a database of restoration works*
   Countless local restoration projects are being executed to combat the worldwide degradation of reefs. It would be highly valuable if all these efforts were to be monitored and gathered in a large database. With simple checklists that volunteers, agencies and other actors can fill in, they can help making restoration efforts more efficient. The database can be consulted to find out how to execute your restoration. This, of course, along with consulting the simple reef hydrodynamic model to ensure your restoration also aids the protection of the coast.

5. **Establish partnerships with restoration foundations**
   Different platforms exist for coral restoration, such as the Coral Restoration Foundation [2] and the Coral Restoration Consortium [1]. Their large network connects experts and managers to share lessons learned from coral restoration works. To raise awareness on coral restoration for coastal protection, their network can be of invaluable worth.

The knowledge gained about coral restoration to reduce coastal hazards is only the tip of the iceberg. Everyone is invited to further explore this highly relevant field of study, to protect vulnerable, reef fronted coastal areas and keep them habitable for future generations.

Bibliography

[1] Coral Restoration Consortium. URL http://reefresilience.org.

[2] Coral Restoration Foundation. URL https://www.coralrestoration.org/.

[3] Formation of Coral Atoll. *Encycl. Br.* URL https://kids.britannica.com/students/assembly/view/180109.

[4] Magma Plumes, Hot Spot Volcanoes & Coral Reef Evolution. URL https://www.youtube.com/watch?v=5xeXTbXnG24.

[5] International Year of the Reef 2018, 2018. URL https://www.iyor2018.org/.

[6] Volunteer for Coral Reef Conservation, 2018. URL https://www.volunteerworld.com/en/volunteer-abroad/coral-reef.

[7] Avigdor Abelson and Mark Denny. Settlement of marine organisms in flow. 28(1997):317–339, 2012.

[8] Swati Abhinav, Vivek and Chopra. Coral Reef Geology, 2018. URL https://www.britannica.com/science/coral-reef.

[9] Philippe Bacchet. Tetiaroa atoll, 2016. URL https://welcome-tahiti.com/tetiaroa-atoll-rich-in-biodiversity-and-histoiry/.

[10] T. E. Baldock. Dissipation of incident forced long waves in the surf zone-Implications for the concept of "bound" wave release at short wave breaking. *Coast. Eng.*, 60(1):276–285, 2012. ISSN 03783839. doi: 10.1016/j.coastaleng.2011.11.002. URL http://dx.doi.org/10.1016/j.coastaleng.2011.11.002.

[11] T. E. Baldock and D. A. Huntley. Long-wave forcing by the breaking of random gravity waves on a beach. *Proc. R. Soc. A Math. Phys. Eng. Sci.*, 458(2025):2177–2201, 2002. ISSN 13645021. doi: 10.1098/rspa.2002.0962.

[12] T. E. Baldock, D. A. Huntley, P. A.D. Bird, T. O'Hare, and G. N. Bullock. Breakpoint generated surf beat induced by bichromatic wave groups. *Coast. Eng.*, 39(2-4):213–242, 2000. ISSN 03783839. doi: 10.1016/S0378-3839(99)00061-7.

[13] T.E. Baldock, P. Holmes, S. Bunker, and P. Van Weert. Cross-shore hydrodynamics within an unsaturated surf zone. *Coast. Eng.*, 34(3-4):173–196, 1998. ISSN 03783839. doi: 10.1016/S0378-3839(98)00017-9. URL http://linkinghub.elsevier.com/retrieve/pii/S0378383998000179.

[14] Todd Barber and Kathy Kirbo. ReefBall: What is a ReefBall. URL http://rbfdevsite.com/reef-ball-description/.

[15] J. A. Battjes. Surf Similarity. *Coast. Eng. Proc.*, 14(8):1420–1426, 1974. ISSN 09570233. doi: 10.1088/0957-0233/14/8/331. URL http://www.bioone.org/doi/abs/10.2112/05A-0002.1.

[16] J. A. Battjes and J. P. F. M. Janssen. Energy Loss and Set-Up Due to Breaking of Random Waves. *Coast. Eng. 1978*, (1):569–587, 1978. ISSN 1098-6596. doi: 10.1061/9780872621909.034. URL http://ascelibrary.org/doi/10.1061/9780872621909.034.

[17] J. A. Battjes and M.J.F. Stive. Calibration and verification of a dissipation model for random breaking waves. *Coast. Eng.*, pages 649–660, 1985.

[18] J A Battjes, H J Bakkenes, T T Janssen, and A R Van Dongeren. Shoaling of subharmonic gravity waves. 109(March 2003):1–15, 2004. doi: 10.1029/2003JC001863.

[19] Michael W. Beck, Iñigo J. Losada, Pelayo Menéndez, Borja G. Reguero, Pedro Díaz-Simal, and Felipe Fernández. The global flood protection savings provided by coral reefs. *Nat. Commun.*, 9 (1), 2018. ISSN 20411723. doi: 10.1038/s41467-018-04568-z. URL http://dx.doi.org/10.1038/s41467-018-04568-z.

[20] MW (World Bank) Beck and G-M Lange. Managing Coasts with Natural Solutions: Guidelines for Measuring and Valuing the Coastal Protection Services of Mangroves and Coral Reefs. (January):167, 2016. URL https://www.wavespartnership.org/en/knowledge-center/managing-coasts-natural-solutions.

[21] Xavier Bertin, Anouk de Bakker, Ap R. van Dongeren, Giovanni Coco, Gael André, Fabrice Ardhuin, Philippe Bonneton, Frédéric Bouchette, Bruno Castelle, Wayne C. Crawford, Mark Davidson, Martha Deen, Guillaume Dodet, Thomas Guérin, Kris Inch, Fabien Leckler, Robert McCall, Héloïse Muller, Maitane Olabarrieta, Dano Roelvink, Gerben Ruessink, Damien Sous, Éléonore Stutzmann, and Marion Tissier. Infragravity waves: From driving mechanisms to impacts. *Earth-Science Rev.*, 177(January): 774–799, 2018. ISSN 00128252. doi: 10.1016/j.earscirev.2018.01.002. URL https://doi.org/10.1016/j.earscirev.2018.01.002.

[22] Christopher M Bishop. *Pattern recognition and machine learning*. springer, 2006.

[23] Matt J Blacka, Francois Flocard, Kristen D Splinter, Ronald J Cox, and Others. Estimating wave heights and water levels inside fringing reefs during extreme conditions. In *Australas. Coasts Ports Conf. 2015 22nd Australas. Coast. Ocean Eng. Conf. 15th Australas. Port Harb. Conf.*, page 83. Engineers Australia and IPENZ, 2015.

[24] Heidi Block. Coral reef zonation.

[25] Hans H Bock. PROBABILISTIC MODELS IN CLUSTER ANALYSIS. *Comput. Stat. Data Anal.*, 23:5–28, 1996.

[26] NRRC Booij, Roeland C Ris, and Leo H Holthuijsen. A third-generation wave model for coastal regions: 1. Model description and validation. *J. Geophys. Res. Ocean.*, 104(C4):7649–7666, 1999.

[27] Lino Briguglio. Small Island Developing States and Their Economic Vulnerabilities. *Pergamon World Dev.*, 23(9):1615–1632, 1995. ISSN 0305750X. doi: 10.1016/0305-750X(95)00065-K.

[28] Andrew Bruckner. Reef types; Coral Reef Ecology Curriculum. (2012), 2014.

[29] John F. Bruno and Elizabeth R. Selig. Regional decline of coral cover in the Indo-Pacific: Timing, extent, and subregional comparisons. *PLoS One*, 2(8), 2007. ISSN 19326203. doi: 10.1371/journal.pone.0000711.

[30] M. L. Buckley, Ryan J. Lowe, J. E. Hansen, Ap R. van Dongeren, and Curt D. Storlazzi. Mechanisms of Wave-Driven Water Level Variability on Reef-Fringed Coastlines. *J. Geophys. Res. Ocean.*, 123(5):3811–3831, 2018. ISSN 21699275. doi: 10.1029/2018JC013933. URL http://doi.wiley.com/10.1029/2018JC013933.

[31] Mark Buckley, Ryan Lowe, and Jeff Hansen. Evaluation of nearshore wave models in steep reef environments. (June), 2014. doi: 10.1007/s10236-014-0713-x.

[32] Mark L. Buckley, Ryan J. Lowe, Jeff E. Hansen, and Ap R. Van Dongeren. Dynamics of Wave Setup over a Steeply Sloping Fringing Reef. *J. Phys. Oceanogr.*, 45(12):3005–3023, 2015. ISSN 0022-3670. doi: 10.1175/JPO-D-15-0067.1. URL http://journals.ametsoc.org/doi/10.1175/JPO-D-15-0067.1.

[33] Mark L. Buckley, Ryan J. Lowe, Jeff E. Hansen, and Ap R. Van Dongeren. Wave Setup over a Fringing Reef with Large Bottom Roughness. *J. Phys. Oceanogr.*, 46(8):2317–2333, 2016. ISSN 0022-3670. doi: 10.1175/JPO-D-15-0148.1. URL http://journals.ametsoc.org/doi/10.1175/JPO-D-15-0148.1.

[34] Paula Camus, Fernando J. Mendez, Raul Medina, and Antonio S. Cofiño. Analysis of clustering and selection algorithms for the study of multivariate wave climate. *Coast. Eng.*, 58(6):453–462, 2011. ISSN 03783839. doi: 10.1016/j.coastaleng.2011.02.003.

[35] Mercè Casas-Prat, Xiaolan L. Wang, and Joan P. Sierra. A physical-based statistical method for modeling ocean wave heights. *Ocean Model.*, 73(November):59–75, 2014. ISSN 14635003. doi: 10.1016/j.ocemod.2013.10.008.

[36] Herman Cesar, Lauretta Burke, and Lida Pet-Soede. The Economics of Worldwide Coral Reef Degradation. *Econ. Reef Degrad.*, page 18, 2003. URL www.icran.org.

[37] Olivia M. Cheriton, Curt D. Storlazzi, and Kurt Rosenberger. Observations of wave transformation over a fringing coral reef and the importance of low-frequency waves and offshore water levels to runup, overwash, and coastal flooding. pages 1–15, 2016. ISSN 21699275. doi: 10.1002/2016JC012335.Received.

[38] M.A. Coffroth, H.R. Lasker, and J.K. Oliver. Coral Mortality Outside of the Eastern Pacific During 1982-1983: Relationship to El Niño. *Elsevier Oceanogr. Ser.*, 52:141–182, jan 1990. ISSN 0422-9894. doi: 10.1016/S0422-9894(08)70035-7. URL https://www.sciencedirect.com/science/article/pii/S0422989408700357.

[39] Lisa Collins. Bio Rock. URL https://www.gonewest.com/biorock/.

[40] Mirella B.S.F. Costa, Moacyr Araújo, Tereza C.M. Araújo, and Eduardo Siegle. Influence of reef geometry on wave attenuation on a Brazilian coral reef. *Geomorphology*, 253:318–327, 2016. ISSN 0169555X. doi: 10.1016/j.geomorph.2015.11.001. URL http://dx.doi.org/10.1016/j.geomorph.2015.11.001.

[41] R. A. Dalrymple, J. T. Kirby, and P. A. Hwang. Wave Diffraction Due to Areas of Energy Dissipation. *J. Waterw. Port, Coastal, Ocean Eng.*, 110(1):67–79, 1984. ISSN 0733-950X. doi: 10.1061/(ASCE)0733-950X(1984)110:1(67).

[42] David L Davies and Donald W Bouldin. A cluster separation measure. *IEEE Trans. Pattern Anal. Mach. Intell.*, (2):224–227, 1979.

[43] Pedro de Souza Pereira, Lauro Júlio Calliari, and Rodrigo do Carmo Barletta. Heterogeneity and homogeneity of Southern Brazilian beaches: A morphodynamic and statistical approach. *Cont. Shelf Res.*, 30 (3-4):270–280, 2010. ISSN 02784343. doi: 10.1016/j.csr.2009.11.007.

[44] Zeki Demirbilek, Okey G Nwogu, Donald L Ward, and Alejandro Sánchez. Wave transformation over reefs: Evaluation of one-dimensional numerical models. Technical report, ENGINEER RESEARCH AND DEVELOPMENT CENTER VICKSBURG MS COASTAL AND HYDRAULICS LAB, 2009.

[45] EcoReefs. EcoReefs Facebook. URL https://www.facebook.com/EcoReefs/photos/a.175662215837350/184090081661230/?type=3{&}theater.

[46] Alasdair Edwards and Edgardo Gomez. Reef Restoration Concepts and Guidelines: making sensible management choices in the face o f uncertainty. *Coral Reef Target. Res. Capacit. Build. Manag. Progr.*, 2007.

[47] Alasdair Edwards, James Guest, Shai Shafir, David Fisk, Edgardo Gomez, Baruch Rinkevich, Andrew Heyward, Makoto Omori, Kenji Iwao, Rommi Dizon, Aileen Morse, Charlie Boch, Sandrine Job, Lucia Bongiorni, Gideon Levy, Lee Shaish, and Susan Wells. *Reef Rehabilitation Manual*. 2010. ISBN 9781921317057. URL http://scholar.google.com/scholar?hl=en{&}btnG=Search{&}q=intitle:Reef+Rehabilitation+manual{#}4.

[48] Carla I. Elliff and Iracema R. Silva. Coral reefs as the first line of defense: Shoreline protection in face of climate change. *Mar. Environ. Res.*, 127:148–154, 2017. ISSN 18790291. doi: 10.1016/j.marenvres.2017.03.007. URL http://dx.doi.org/10.1016/j.marenvres.2017.03.007.

[49] Jeannie Evers. Atoll, 1012. URL https://www.nationalgeographic.org/encyclopedia/atoll/.

[50] Filippo Ferrario, Michael W. Beck, Curt D. Storlazzi, Fiorenza Micheli, Christine C. Shepard, and Laura Airoldi. The effectiveness of coral reefs for coastal hazard risk reduction and adaptation. *Nat. Commun.*, 5(May):1–9, 2014. ISSN 20411723. doi: 10.1038/ncomms4794. URL http://dx.doi.org/10.1038/ncomms4794.

[51] Gemma Franklin, Ismael Mariño-Tapia, and Alec Torres-Freyermuth. Effects of reef roughness on wave setup and surf zone currents. *J. Coast. Res.*, 165(March):2005–2010, 2013. ISSN 0749-0208. doi: 10.2112/SI65-339.1. URL http://www.bioone.org/doi/10.2112/SI65-339.1.

[52] Matthijs Gawehn. Incident, infragravity and very low frequency wave motions on an atoll reef platform. 2015.

[53] Matthijs Gawehn, Ap R. van Dongeren, Arnold Van Rooijen, Curt D. Storlazzi, Olivia M. Cheriton, and Ad Reniers. Identification and classification of very low frequency waves on a coral reef flat. (November), 2016. doi: 10.1002/2016JC011834.Received.

[54] Peter W. Glynn. Coral Mortality and Disturbances to Coral Reefs in the Tropical Eastern Pacific. *Elsevier Oceanogr. Ser.*, 52:55–126, jan 1990. ISSN 0422-9894. doi: 10.1016/S0422-9894(08)70033-3. URL https://www.sciencedirect.com/science/article/pii/S0422989408700333.

[55] Paula Gomes da Silva, Raúl Medina, Mauricio González, and Roland Garnier. Infragravity swash parameterization on beaches: The role of the profile shape and the morphodynamic beach state. *Coast. Eng.*, 136(December 2017):41–55, 2018. ISSN 03783839. doi: 10.1016/j.coastaleng.2018.02.002.

[56] M. R. Gourlay. Wave transformation on a coral reef. *Coast. Eng.*, 23(1-2):17–42, 1994. ISSN 03783839. doi: 10.1016/0378-3839(94)90013-2.

[57] M. R. Gourlay. Wave set-up on coral reefs. 2. Set-up on reefs with various profiles. *Coast. Eng.*, 28(1-4): 17–55, 1996. ISSN 03783839. doi: 10.1016/0378-3839(96)00009-9.

[58] F Guichard, E Bourget, and J L Robert. Scaling the influence of topographic heterogeneity on intertidal benthic communities: alternate trajectories mediated by hydrodynamics and shading. *Mar Ecol Prog Ser*, 217:27–41, 2001. ISSN 01718630. doi: 10.3354/meps217027.

[59] R. T. Guza and E. B. Thornton. VELOCITY MOMENTS IN NEARSHORE. *J. Waterw. Port, Coastal, Ocean Eng.*, 111(2):235–256, 1985.

[60] R T Guza, E. B. Thornton, and R A Holman. Swash on steep and shallow beaches. *Coast. Eng. Proc.*, (19):708–723, 1984.

[61] J.A. Hall, S Gille, J Obeysekera, W. Sweet, K. Knuuti, and J. Marburger. Regional Sea Level Scenarios for Coastal Risk Management: Managing the Uncertainty of Future Sea Level Change and Extreme Water Levels for Department of Defense Coastal Sites Worldwide. (April):224pp., 2016. doi: 10.13140/RG.2.2.31307.39208.

[62] Gator Halpern and Sam Teicher. Coral Farming, 2018. URL http://www.coralvita.co/coral-farming/.

[63] Klaus Hasselmann. On the non-linear energy transfer in a gravity-wave spectrum Part 1. General theory. *J. Fluid Mech.*, 12(4):481–500, 1962.

[64] Tom Hata, Joshua S. Madin, Vivian R. Cumbo, Mark Denny, Joanna Figueiredo, Saki Harii, Christopher J. Thomas, and Andrew H. Baird. Coral larvae are poor swimmers and require fine-scale reef structure to settle. *Sci. Rep.*, 7(1):1–9, 2017. ISSN 20452322. doi: 10.1038/s41598-017-02402-y.

[65] Stephen M. Henderson. Observations of surf beat forcing and dissipation. *J. Geophys. Res.*, 107(C11): 3193, 2002. ISSN 0148-0227. doi: 10.1029/2000JC000498. URL http://doi.wiley.com/10.1029/2000JC000498.

[66] T.P. Henkel. Coral Reefs, 2010. URL https://www.nature.com/scitable/knowledge/library/coral-reefs-15786954.

[67] Scott F. Heron, Mark C. Eakin, and Fanny Douvere. Impacts of Climate Change on World Heritage Coral Reefs: A First Global Scientific Assessment. 2017.

[68] RC Highsmith. Reproduction by Fragmentation in Corals. *Mar. Ecol. Prog. Ser.*, 7(4):207–226, 1982. ISSN 0171-8630. doi: 10.3354/meps007207. URL http://www.int-res.com/articles/meps/7/m007p207.pdf.

[69] Ove Hoegh-Guldberg. Climate change, coral bleaching and the future of the world's coral reefs. *Mar. Freshw. Res.*, 50(8):839–866, 1999. ISSN 13231650. doi: 10.1071/MF99078.

[70] R. A. Holman. Extreme value statistics for wave run-up on a natural beach. *Coast. Eng.*, 9(6):527–544, 1986. ISSN 03783839. doi: 10.1016/0378-3839(86)90002-5.

[71] Holman R. A. and A. H. Sallenger. Setup and Swash on a Naturla Beach. *J. Geophys. Res.*, 90(945-953): 945–953, 1985.

[72] T. T. Janssen. Long waves induced by short-wave groups over a sloping bottom. *J. Geophys. Res.*, 108 (C8):3252, 2003. ISSN 0148-0227. doi: 10.1029/2002JC001515. URL http://doi.wiley.com/10.1029/2002JC001515.

[73] T T Janssen and J A Battjes. A note on wave energy dissipation over steep beaches. *Coast. Eng.*, 54: 711–716, 2007. doi: 10.1016/j.coastaleng.2007.05.006.

[74] Morten Sand Jensen. Breaking of Waves over a Steep Bottom Slope. 2004.

[75] Chris Jones, Ida Brøker, Kevin Coulton, Jeff Gangai, Darryl Hatheway, Jeremy Lowe, Ron Noble, and Rajesh Srinivas. Wave run-up and overtopping. Technical report, 2005.

[76] J W Kamphuis. Incipient wave breaking. *Coast. Eng.*, 15(3):185–203, 1991.

[77] Jeff Kart. Startup Creating More Resilient Coral To Replace Reefs Wrecked By Climate Change. *Forbes*, 2018. URL https://www.forbes.com/sites/jeffkart/2018/07/22/startup-creating-more-resilient-coral-to-replace-reefs-wrecked-by-climate-change/{#}2b89c1315a14.

[78] Paul S. Kench and Robert W. Brander. Wave Processes on Coral Reef Flats: Implications for Reef Geomorphology Using Australian Case Studies. *J. Coast. Res.*, 221:209–223, 2006. ISSN 0749-0208. doi: 10.2112/05A-0016.1. URL http://www.bioone.org/doi/abs/10.2112/05A-0016.1.

[79] M. S. Kendal, M. E. Monaco, K. R. Buja, J. D. Christensen, C. R. Kruer, M. Finkbeiner, and R.A Warner. Methods Used to Map the Benthic Habitats of Puerto Rico NOAA National Ocean Service Center for Coastal Monitoring and Assessment Biogeography Team. page 45, 2001. URL http://biogeo.nos.noaa.gov/projects/mapping/caribbean/startup.htm.

[80] Cuchlaine Audrey Muriel King and Maurice L. Schwartz. Lagoon Geography, 2019. URL https://www.britannica.com/science/lagoon-geography.

[81] M. A.R. Koehl and M. G. Hadfield. Soluble settlement cue in slowly moving water within coral reefs induces larval adhesion to surfaces. *J. Mar. Syst.*, 49(1-4):75–88, 2004. ISSN 09247963. doi: 10.1016/j.jmarsys.2003.06.003.

[82] Danker J Kolijn. Effectiveness of a multipurpose artificial underwater structure as a coral reef canopy Effectiveness of a multipurpose artificial underwater structure as a coral reef canopy. (August), 2014.

[83] Christopher H. Lashley, Dano Roelvink, Ap van Dongeren, Mark L. Buckley, and Ryan J. Lowe. Non-hydrostatic and surfbeat model predictions of extreme wave run-up in fringing reef environments. *Coast. Eng.*, 137(October 2017):11–27, 2018. ISSN 03783839. doi: 10.1016/j.coastaleng.2018.03.007. URL https://doi.org/10.1016/j.coastaleng.2018.03.007.

[84] Jessica S Levy, Kayla J Ripple, and R S Winters. Lessons learned for increased scalability for in situ coral restoration efforts. *Coral Restoratin Found.*, pages 1–17, 2018.

[85] M S Longuet-Higgins and R W Stewart. Radiation stress and mass transport in gravity waves, with application to 'surf beats'. *J. Fluid Mech.*, 13(4):481–504, 1962. doi: 10.1017/S0022112062000877.

[86] M S Longuet-Higgins and R W Stewart. Radiation stresses in ˜vater waves; with applications a physical discussion,. *Deep Sea Res.*, 11:529–562, 1964.

[87] Ryan J. Lowe and James L. Falter. Oceanic Forcing of Coral Reefs. *Ann. Rev. Mar. Sci.*, 7(1):43–66, 2015. ISSN 1941-1405. doi: 10.1146/annurev-marine-010814-015834. URL http://www.annualreviews.org/doi/10.1146/annurev-marine-010814-015834.

[88] Ryan J. Lowe, James L. Falter, Marion D. Bandet, Geno Pawlak, Marlin J. Atkinson, Stephen G. Monismith, and Jeffrey R. Koseff. Spectral wave dissipation over a barrier reef. *J. Geophys. Res. C Ocean.*, 110 (4):1–16, 2005. ISSN 01480227. doi: 10.1029/2004JC002711.

[89] Ryan J. Lowe, Jeffrey R. Koseff, and Stephen G. Monismith. Oscillatory flow through submerged canopies: 1. Velocity structure. *J. Geophys. Res. C Ocean.*, 110(10):1–17, 2005. ISSN 01480227. doi: 10.1029/2004JC002788.

[90] Ryan J. Lowe, Uri Shavit, James L. Falter, Jeffrey R. Koseff, and Stephen G. Monismith. Modeling flow in coral communities with and without waves: A synthesis of porous media and canopy flow approaches. *Limnol. Oceanogr.*, 53(6):2668–2680, 2008. ISSN 00243590. doi: 10.4319/lo.2008.53.6.2668.

[91] D J C MacKay. An Example Inference Task: Clustering. *Inf. Theory, Inference Learn. Algorithms*, pages 284–292, 2003. ISSN 0028-0836. doi: 10.1038/nature10736.

[92] S R Massel. ON THE LARGEST WAVE HEIGHT IN WATER OF CONSTANT DEPTH. *Ocean Eng.*, 23(7): 553–573, 1996.

[93] S. R. Massel and M. R. Gourlay. On the modelling of wave breaking and set-up on coral reefs. *Coast. Eng.*, 39(1):1–27, 2000. ISSN 03783839. doi: 10.1016/S0378-3839(99)00052-6.

[94] Gerd Masselink, Megan Tuck, Robert McCall, Ap R. van Dongeren, Murray Ford, and Paul Kench. Physical and Numerical Modeling of Infragravity Wave Generation and Transformation on Coral Reef Platforms. 2019.

[95] Gerhard Masselink. Group bound long waves as a source of infragravity energy in the surf zone. *Cont. Shelf Res.*, 15(13):1525–1547, 1995. ISSN 02784343. doi: 10.1016/0278-4343(95)00037-2.

[96] G Maze, H Mercier, and C Cabanes. Profile classification models. pages 48–56, 2017.

[97] J F McClean and D Sumner. An experimental investigation of aspect ratio and incidence angle effects for the flow around surface-mounted finite-height square prisms. *J. Fluids Eng.*, 136(8):81206, 2014.

[98] M. A. Merrifield, J. M. Becker, M. Ford, and Y. Yao. Observations and estimates of wave-driven water level extremes at the Marshall Islands. *Geophys. Res. Lett.*, 41(20):7245–7253, 2014. ISSN 19448007. doi: 10.1002/2014GL061005.

[99] M Miche. Undulatory movement of the sea. *Ann. des ponts chaussées, Paris*, 1944.

[100] Larissa Miller. No Title. URL https://www.piyogapants.com/blogs/news/piyoga-bio-rock-build-in-gili-trawangan.

[101] Stephen G. Monismith. Hydrodynamics of Coral Reefs. *Annu. Rev. Fluid Mech.*, 39(1):37–55, 2007. ISSN 0066-4189. doi: 10.1146/annurev.fluid.38.050304.092125. URL http://www.annualreviews.org/doi/10.1146/annurev.fluid.38.050304.092125.

[102] Phanor H. Montoya-Maya, Kaylee P. Smit, J. Burt April, and Sarah Frias-Torres. Large-scale coral reef restoration could assist natural recovery in Seychelles, Indian Ocean. *Nat. Conserv.*, pages 442–446, 2016. ISSN 18448143. doi: 10.3897/natureconservation.16.8604.

[103] Michael Moore and Mark Erdmann. EcoReefs: A New Tool for Coral Reef Restoration. *Conserv. Pract.*, 3(3):41–43, 2002.

[104] Mateusz Moskalik, Jaroslaw Tegowski, Piotr Grabowiecki, and Monika Zulichowska. Principal component and cluster analysis for determining diversification of bottom morphology based on bathymetric profiles from Brepollen (Hornsund, Spitsbergen). *Oceanologia*, 56(1):59–84, 2014. ISSN 23007370. doi: 10.5697/oc.56-1.059. URL http://dx.doi.org/10.5697/oc.56-1.059.

[105] Walter Heinrich Munk, G R Miller, F E Snodgrass, and N F Barber. Directional recording of swell from distant storms. *Phil. Trans. R. Soc. Lond. A*, 255(1062):505–584, 1963.

[106] Robert Bruce Nairn. *PREDICTION OF CROSS-SHORE SEDIMENT TRANSPORT AND BEACH PROFILE EVOLUTION*. PhD thesis, 1990.

[107] Ishita Nanda. Coral Reefs: Wonder of the Ocean World. URL `http://faculty.montgomerycollege.edu/gyouth/FP{_}examples/student{_}examples/ishita{_}nanda/Types.html`.

[108] Siddharth Narayan, Michael W. Beck, Borja G. Reguero, Iï¿½igo J. Losada, Bregje Van Wesenbeeck, Nigel Pontee, James N. Sanchirico, Jane Carter Ingram, Glenn Marie Lange, and Kelly A. Burks-Copes. The effectiveness, costs and coastal protection benefits of natural and nature-based defences. *PLoS One*, 11(5):1–17, 2016. ISSN 19326203. doi: 10.1371/journal.pone.0154735.

[109] United Nations. *Sustainable Development Goals Report 2016*. UN, 2016.

[110] R C Nelson, E J Lesleighter, and Others. Breaker height attenuation over platform coral reefs. In *1985 Australas. Conf. Coast. Ocean Eng.*, page 605. Institution of Engineers, Australia, 1985.

[111] H. M. Nepf and E. R. Vivoni. Flow structure in depth-limited, vegetated flow. *J. Geophys. Res. Ocean.*, 105(C12):28547–28557, 2000. ISSN 01480227. doi: 10.1029/2000JC900145. URL `http://doi.wiley.com/10.1029/2000JC900145`.

[112] NOAA. What are Coral Reefs, 2018. URL `https://www.coris.noaa.gov/about/what{_}are/`.

[113] Okey Nwogu and Zeki Demirbilek. Infragravity Wave Motions and Runup over Shallow Fringing Reefs. *J. Waterw. Port, Coastal, Ocean Eng.*, 136(6):295–305, 2010. ISSN 0733-950X. doi: 10.1061/(ASCE)WW.1943-5460.0000050. URL `http://ascelibrary.org/doi/10.1061/{%}28ASCE{%}29WW.1943-5460.0000050`.

[114] Derrick Jan Carl Olij. Wave climate reduction for medium term process based morphodynamic simulations with application to the Durban Coast. page 131, 2015.

[115] Ann H. Opel, Colleen M. Cavanaugh, Randi D. Rotjan, and Joey Pakes Nelson. The effect of coral restoration on Caribbean reef fish communities. *Mar. Biol.*, 164(12):1–16, 2017. ISSN 00253162. doi: 10.1007/s00227-017-3248-0.

[116] S. G. Pearson. Predicting Wave-Induced Flooding on Low-Lying Tropical Islands. page 232, 2016. doi: uuid:c3988f4b-99f8-4936-9504-261b32bb0cd1. URL `http://resolver.tudelft.nl/uuid:c3988f4b-99f8-4936-9504-261b32bb0cd1`.

[117] S. G. Pearson, Curt D. Storlazzi, Ap R. van Dongeren, M. F.S. Tissier, and Ad Reniers. A Bayesian-Based System to Assess Wave-Driven Flooding Hazards on Coral Reef-Lined Coasts. *J. Geophys. Res. Ocean.*, 122(12):10099–10117, 2017. ISSN 21699291. doi: 10.1002/2017JC013204.

[118] A. C. Péquignet, J. M. Becker, M. A. Merrifield, and S. J. Boc. The dissipation of wind wave energy across a fringing reef at Ipan, Guam. *Coral Reefs*, 30(SUPPL. 1):71–82, 2011. ISSN 07224028. doi: 10.1007/s00338-011-0719-5.

[119] A. Christine N. Péquignet, Janet M. Becker, Mark A. Merrifield, and Jérôme Aucan. Forcing of resonant modes on a fringing reef during tropical storm Man-Yi. *Geophys. Res. Lett.*, 36(3):20–23, 2009. ISSN 00948276. doi: 10.1029/2008GL036259.

[120] Anne Christine N. Péquignet, Janet M. Becker, and Mark A. Merrifield. Energy transfer between wind waves and low-frequency oscillations on a fringing reef, Ipan, Guam. *J. Geophys. Res. Ocean.*, 119(10):6709–6724, 2014. ISSN 21699291. doi: 10.1002/2014JC010179.

[121] S. Perkol-Finkel, N. Shashar, and Y. Benayahu. Can artificial reefs mimic natural reef communities? The roles of structural features and age. *Mar. Environ. Res.*, 61(2):121–135, 2006. ISSN 01411136. doi: 10.1016/j.marenvres.2005.08.001.

[122] Andrew Pomeroy, Ryan J. Lowe, Graham Symonds, Ap R. Van Dongeren, and Christine Moore. The dynamics of infragravity wave transformation over a fringing reef. *J. Geophys. Res. Ocean.*, 117(11): 1–17, 2012. ISSN 21699291. doi: 10.1029/2012JC008310.

[123] Andrew Pomeroy, Ap R. van Dongeren, Ryan J. Lowe, Jaap Van Thiel de Vries, and Dano Roelvink. Low frequency wave resonance in fringing reef environments. *Coast. Eng.*, pages 1–10, 2012.

[124] Ellen Quataert. Wave runup on atoll reefs. (January):89, 2015.

[125] Ellen Quataert, Curt D. Storlazzi, Arnold Van Rooijen, Olivia M. Cheriton, and Ap R. Van Dongeren. The influence of coral reefs and climate change on wave-driven flooding of tropical coastlines. *Geophys. Res. Lett.*, 42(15):6407–6415, 2015. ISSN 19448007. doi: 10.1002/2015GL064861.

[126] Roshanka Ranasinghe and Ian L Turner. Shoreline response to submerged structures: a review. *Coast. Eng.*, 53(1):65–79, 2006.

[127] Michael R Raupach and R H Shaw. Averaging procedures for flow within vegetation canopies. *Boundary-layer Meteorol.*, 22(1):79–90, 1982.

[128] Borja G. Reguero, Michael W. Beck, Vera N. Agostini, Philip Kramer, and Boze Hancock. Coral reefs for coastal protection: A new methodological approach and engineering case study in Grenada. *J. Environ. Manage.*, 210:146–161, 2018. ISSN 10958630. doi: 10.1016/j.jenvman.2018.01.024. URL https://doi.org/10.1016/j.jenvman.2018.01.024.

[129] Matthew A. Reidenbach, Jeffrey R. Koseff, and M. A.R. Koehl. Hydrodynamic forces on larvae affect their settlement on coral reefs in turbulent, wavedriven flow. *Limnol. Oceanogr.*, 54(1):318–330, 2009. ISSN 00243590. doi: 10.4319/lo.2009.54.1.0318.

[130] Douglas Reynolds. Gaussian Mixture Models, 2009.

[131] Larissa Rhodes. Chasing Coral, 2017.

[132] RH Richmond and CL Hunter. Reproduction and recruitment of corals: comparisons among the Caribbean, the Tropical Pacific, and the Red Sea. *Mar. Ecol. Prog. Ser.*, 60:185–203, 1990. ISSN 0171-8630. doi: 10.3354/meps060185. URL http://www.int-res.com/articles/meps/60/m060p185.pdf.

[133] Robert Richmond. Reproduction and Recruitment in Corals: Critical Links in the Persistence of Reefs. (January 1997), 1997. doi: 10.1007/978-1-4615-5995-5. URL http://link.springer.com/10.1007/978-1-4615-5995-5.

[134] Baruch Rinkevich. Management of coral reefs: We have gone wrong when neglecting active reef restoration. *Mar. Pollut. Bull.*, 56(11):1821–1824, 2008. ISSN 0025326X. doi: 10.1016/j.marpolbul.2008.08.014. URL http://dx.doi.org/10.1016/j.marpolbul.2008.08.014.

[135] Baruch Rinkevich. Rebuilding coral reefs: Does active reef restoration lead to sustainable reefs? *Curr. Opin. Environ. Sustain.*, 7:28–36, 2014. ISSN 18773435. doi: 10.1016/j.cosust.2013.11.018. URL http://dx.doi.org/10.1016/j.cosust.2013.11.018.

[136] Raphael Ritson-Williams, Suzanne Arnold, Nicole Fogarty, Robert S. Steneck, Mark Vermeij, and Valerie J. Paul. New perspectives on ecological mechanisms affecting coral recruitment on reefs. *Smithson. Contrib. Mar. Sci.*, (38):437–457, 2009. ISSN 01960768. doi: 10.5479/si.01960768.38.437. URL https://repository.si.edu/handle/10088/11216.

[137] Bryson Robertson, K R Hall, Richard G Zytner, and Ioan Nistor. Breaking waves : review of characteristic relationships. *Coast. Eng.*, 55(1), 2013. doi: 10.1142/S0578563413500022.

[138] Dano Roelvink, Ad Reniers, A P Van Dongeren, Jaap van Thiel de Vries, Robert McCall, and Jamie Lescinski. Modelling storm impacts on beaches, dunes and barrier islands. *Coast. Eng.*, 56(11-12):1133–1152, 2009.

[139] J. A. Roelvink, A. Dastgheib, T. Spencer, I. Moller, E. Christie, M. Berenguer, D. Sempere, K. van der Meer, J.W. Seyyedabdolhossein, M. Nederhoff, and W. Vermin. Resilience-Increasing Strategies for Coasts - Toolkit - Improvement of physical pro- cesses XBeach improvement & validation; wave dissipation over vegetated marshes and flash flood module, Technical report. 2015.

[140] Justin S. Rogers, Stephen G. Monismith, Robert B. Dunbar, and David Koweek. Hydrodynamics of spur and groove formations on a coral reef. *J. Geophys. Res. Ocean.*, 120(1):145–160, 2015. ISSN 21699291. doi: 10.1002/2014JC010464.

[141] S.O. (NOAA CRCP) Rohmann. A Classification Scheme for Mapping the Shallow-water Coral Ecosystems of Southern Florida. (June):1–14, 2008.

[142] A A Van Rooijen, R J Lowe, M Ghisalberti, J Hansen, R T Mccall, and A R Van Dongeren. Physical and Numerical Modelling of Wave Transformation through a Coastal Canopy. In *Australas. Fluid Mech. Conf.*, number December, 2016.

[143] B. G. Ruessink, D. J.R. Walstra, and H. N. Southgate. Calibration and verification of a parametric wave model on barred beaches. *Coast. Eng.*, 48(3):139–149, 2003. ISSN 03783839. doi: 10.1016/S0378-3839(03)00023-1.

[144] William N Seelig. Laboratory study of reef-lagoon system hydraulics. *J. Waterw. port, coastal, Ocean Eng.*, 109(4):380–391, 1983.

[145] Lee Shaish, Gideon Levy, Gadi Katzir, and Baruch Rinkevich. Coral reef restoration (Bolinao, Philippines) in the face of frequent natural catastrophes. *Restor. Ecol.*, 18(3):285–299, 2010. ISSN 10612971. doi: 10.1111/j.1526-100X.2009.00647.x.

[146] Andrew D. Short. Australian Beach Systems—Nature and Distribution. *J. Coast. Res.*, 221(1):11–27, 2006. ISSN 0749-0208. doi: 10.2112/05A-0002.1. URL `http://www.bioone.org/doi/abs/10.2112/05A-0002.1`.

[147] Andrew D. Short. Coastal Processes and Beaches. *Nat. Educ. Knowl.*, 2012.

[148] S R Singamsetti and H G Wind. Breaking waves. In *Charact. shoaling Break. Period. waves Norm. Incid. to Pl. beaches constant slope*, page 142. 1980.

[149] P.B. Smit, G.S.Stelling, D. Roelvink, J. van Thiel de Vries, R. McCall, A. van Dongeren, C. Zwinkels, and R. Jacobs. XBeach : Non-hydrostatic model Delft University of Technology and Deltares. 2010.

[150] Hilary F. Stockdon, Rob A. Holman, Peter A. Howd, and Asbury H. Sallenger. Empirical parameterization of setup, swash, and runup. *Coast. Eng.*, 53(7):573–588, 2006. ISSN 03783839. doi: 10.1016/j.coastaleng.2005.12.005.

[151] Curt Storlazzi, Borja Reguero, Erik Lowe, James Shope, Ann Gibbs, Mike Beck, and Barry Nickel. RIGOROUSLY VALUING THE ROLE OF CORAL REEFS IN COASTAL PROTECTION: AN EXAMPLE FROM MAUI, HAWAII, U.S.A. (035):665–674, 2017.

[152] Curt D Storlazzi, van Ormondt M, Y-L Chen, and EPL Elias. Modeling Fine-Scale Coral Larval Dispersal and Interisland Connectivity to Help Designate Mutually-Supporting Coral Reef Marine Protected Areas : Insights from Maui Nui , Hawaii. *Front. Mar. Sci.*, 4(December):1–14, 2017. doi: 10.3389/fmars.2017.00381.

[153] Curt D. Storlazzi, Stephen B. Gingerich, Ap Van Dongeren, Olivia M. Cheriton, Peter W. Swarzenski, Ellen Quataert, Clifford I. Voss, Donald W. Field, Hariharasubramanian Annamalai, Greg A. Piniak, and Robert McCall. Most atolls will be uninhabitable by the mid-21st century because of sea-level rise exacerbating wave-driven flooding. *Sci. Adv.*, 4(4):1–10, 2018. ISSN 23752548. doi: 10.1126/sciadv.aap9741.

[154] Shih-Feng Su, Alex Sheremet, and Jane McKee Smith. PARAMETRIC WAVE-BREAKING ON STEEP REEFS. 2009.

[155] Tomohiro Suzuki. *Wave Dissipation Over Vegetation Fields*. 2011. ISBN 9789491211447.

[156] E. B. Thornton and R. T. Guza. Energy saturation and phase speeds measured on the natural beach. *J. Geophys. Res.*, 87(C12):9499–9508, 1982. ISSN 01480227. doi: 10.1029/JC087iC12p09499.

[157] Edward B Thornton and R T Guza. Transformation of wave height distribution. *J. Geophys. Res. Ocean.*, 88(C10):5925–5938, 1983.

[158] United Nations. The Sustainable Development Goals Report. *United Nations Publ.*, pages 1–56, 2017. ISSN 2518-3958. doi: 10.18356/3405d09f-en.

[159] A. van Dongeren, J. Battjes, T. Janssen, J. van Noorloos, K. Steenhauer, G. Steenbergen, and A. Reniers. Shoaling and shoreline dissipation of low-frequency waves. *J. Geophys. Res. Ocean.*, 112(2):1–15, 2007. ISSN 21699291. doi: 10.1029/2006JC003701.

[160] A Van Dongeren, Ryan J Lowe, A Pomeroy, DM Trang, D Roelvink, G Symonds, and Ranasinghe Roshanka. Modelling Infragravity Waves and Currents Across a Fringing Coral. *Coast. Eng.*, pages 1–10, 2012. ISSN 2156-1028. doi: 10.9753/icce.v33.currents.29.

[161] Ap van Dongeren, Henk Jan Bakkenes, and Tim Janssen. Generation of long waves by short wave groups. In *Coast. Eng. 2002 Solving Coast. Conundrums*, pages 1093–1105. World Scientific, 2003.

[162] Ap R. Van Dongeren, Ryan J. Lowe, Andrew Pomeroy, Duong Minh Trang, Dano Roelvink, Graham Symonds, and Roshanka Ranasinghe. Numerical modeling of low-frequency wave dynamics over a fringing coral reef. *Coast. Eng.*, 73:178–190, 2013. ISSN 03783839. doi: 10.1016/j.coastaleng.2012.11.004. URL http://dx.doi.org/10.1016/j.coastaleng.2012.11.004.

[163] Marcel R. A. Van Gent. Wave Runup on Dikes with Shallow Foreshores. *J. Waterw. Port, Coastal, Ocean Eng.*, 127(5):254–262, 2001. ISSN 0733-950X. doi: 10.1061/(ASCE)0733-950X(2001)127:5(254).

[164] M van Ormondt. A new empirical run-up equation, 2018.

[165] Juha Vesanto and Esa Alhoniemi. Clustering of the Self-Organizing Map. *IEEE Trans. NEURAL NETWORKS*, 11(3):586–600, 2000.

[166] O. Vetter, J. M. Becker, M. A. Merrifield, A. C. Pequignet, J. Aucan, S. J. Boc, and C. E. Pollock. Wave setup over a Pacific Island fringing reef. *J. Geophys. Res. Ocean.*, 115(12):1–13, 2010. ISSN 21699291. doi: 10.1029/2010JC006455.

[167] Kevin J.E. Walsh, Kathleen L. McInnes, and John L. McBride. Climate change impacts on tropical cyclones and extreme sea levels in the South Pacific - A regional assessment. *Glob. Planet. Change*, 80-81: 149–164, 2012. ISSN 09218181. doi: 10.1016/j.gloplacha.2011.10.006. URL http://dx.doi.org/10.1016/j.gloplacha.2011.10.006.

[168] Lorraine Whitmarsh. Behavioural responses to climate change: Asymmetry of intentions and impacts. *J. Environ. Psychol.*, 29(1):13–23, 2009. ISSN 02724944. doi: 10.1016/j.jenvp.2008.05.003. URL http://dx.doi.org/10.1016/j.jenvp.2008.05.003.

[169] Christian Wild, Ove Hoegh-Guldberg, Malik S. Naumann, M. Florencia Colombo-Pallotta, Mebrahtu Ateweberhan, William K. Fitt, Roberto Iglesias-Prieto, Caroline Palmer, John C. Bythell, Juan Carlos Ortiz, Yossi Loya, and Robert Van Woesik. Climate change impedes scleractinian corals as primary reef ecosystem engineers. *Mar. Freshw. Res.*, 62(2):205–215, 2011. ISSN 13231650. doi: 10.1071/MF10254.

[170] Art Wolfe. Bora-Bora, French Polynesia. URL https://artwolfe.com/showcase/bora-bora-french-polynesia/.

[171] Colin D Woodroffe and Naomi Biribo. *Atolls*, pages 51–71. Springer Netherlands, Dordrecht, 2011. ISBN 978-90-481-2639-2. doi: 10.1007/978-90-481-2639-2_4. URL https://doi.org/10.1007/978-90-481-2639-2{_}4.

[172] Yu Yao, Wenrun He, Ruichao Du, and Changbo Jiang. Study on wave-induced setup over fringing reefs in the presence of a reef crest. *Appl. Ocean Res.*, 66:164–177, 2017.

[173] Neviaty P Zamani, Ramadian Bachtiar, Hawis H Madduppa, Jhoni Wahyu Adi, Jeddah Isnul, Muhamad Iqbal, and Beginer Subhan. Study on Biorock®Technique Using Three Different Anode Materials (Magnesium, Aluminum, and Titanium). *J. Ilmu dan Teknol. Kelaut. Trop.*, 2(1), 2010.

[174] Marcel Zijlema. MODELLING WAVE TRANSFORMATION ACROSS A FRINGING REEF USING SWASH. *Coast. Eng. Proc.*, (2007):1–12, 2012.

[175] Marcel Zijlema, Guus Stelling, and Pieter Smit. SWASH: An operational public domain code for simulating wave fields and rapidly varied flows in coastal waters. *Coast. Eng.*, 58(10):992–1012, 2011. ISSN 0378-3839. doi: https://doi.org/10.1016/j.coastaleng.2011.05.015. URL http://www.sciencedirect.com/science/article/pii/S0378383911000974.

[176] Marcel Zijlema, Guus Stelling, and Pieter Smit. Simulating nearshore wave transformation with non-hydrostatic wave-flow modelling. pages 1–11, 2011.

[177] Beth Zimmer. Coral reef restoration: an overview. In *Coral reef Restor. Handb.*, pages 39—-59. CRC press, 2006.

A

Reef hydrodynamic model formulations

A.1. Wave breaking formulations

The nearshore dissipation process of wave breaking is solved using parametric wave breaking models, that require a formulation for the breaker height, that is the maximum stable wave height. Below, three common parametric wave breaking formulations are elaborated, after which several breaker height formulations are highlighted. In Section A.1.3, results of the reef hydrodynamic model with different wave breaking models and breaker height formulations are compared to laboratory experiments of Buckley et al. [32], in order to determine the wave breaking dissipation model that is best suited to capture the wave breaking across steep coral reefs.

A.1.1. Parametric wave breaking models

Parametric wave breaking models describe sea state characteristics using time averaged, local parameters [13]: the local wave height H_{rms}, the water depth, the wave frequency and the fraction of breaking waves Q_B.

A.1.1.1 Battjes and Janssen [16]

The basis of many parametric wave breaking models is the model by **Battjes and Janssen [16]**. By making the analogy with a turbulent bore the energy dissipation is predicted, assuming the wave height is Rayleigh distributed with a cutoff function for the maximum possible wave height [16]:

$$p(H) = \begin{cases} 1 - \exp\left(-\frac{1}{2} H^2 / \hat{H}^2\right), & \text{for } 0 \leq H < H_b \\ 1, & \text{for } H_b \leq H \end{cases}$$

This leads to an expression where the dissipation is dependent on the fraction of breaking waves Q_b, the mean frequency $\bar{f}$ and the breaking wave height H_b:

$$\langle \epsilon_b \rangle = \frac{\alpha}{4} Q_b \bar{f} \rho g H_b^2 \tag{A.1}$$

where Q_b is obtained by solving the implicit function:

$$\frac{1 - Q_b}{\ln Q_b} = -(\frac{H_{rms}}{H_b})^2 \tag{A.2}$$

Various formulations for the breaking wave height H_b exist, of which an overview is given in Section A.1.2. The model was validated with flume experiments carried out on both a plane beach and bar-trough beach profile, with a slope of 1:20 and different forcing conditions. The model shows good agreement with the test results and has proved to be very successful in the estimation of nearshore wave processes on mildly sloping beaches [73].

A.1.1.2 Baldock et al. [13]

On steep slopes, the dissipation term of the Battjes and Janssen [16] model is insufficient to balance the shoaling of incoming waves [73], requiring an additional cutoff function to account for very shallow waters. To accurately model breaking waves on steep slopes, Baldock et al. [13] modified the roller model of Battjes and Janssen [16] by adapting the wave height distribution function. Instead of the truncated Rayleigh distribution, the full Rayleigh distribution is used:

$$\mathrm{p(H)} = \frac{2H}{H_{rms}^2} \exp\left[-\left(\frac{H}{H_{rms}}\right)^2\right] \tag{A.3}$$

which leads to an explicit formulation for Q_b and $\langle \epsilon_b \rangle$:

$$Q_b = \exp\left[-\left(\frac{H_b}{H_{rms}}\right)^2\right] \tag{A.4}$$

$$\langle \epsilon_b \rangle = \frac{\alpha}{4} \rho g f_p Q (H_b^2 + H_{rms}^2) \tag{A.5}$$

Any breaker height formulation can serve as input for H_b. Experimental flume tests on a 1:10 beach profile were carried out to support the model, showing that indeed a better fit was found for the inner surf zone, where waves are still found to be Rayleigh distributed and do not follow the cutoff function of Battjes and Janssen [16] ($H/H_{rms} = H_b/H_{rms}$ [13]). On mildly sloping beaches, the Baldock et al. [13] model gave similar results to the Battjes and Janssen [16] model.

A.1.1.3 Janssen and Battjes [73]

Janssen and Battjes [73] observed an algebraic inconsistency in the model of Baldock et al. [13] formulation (see Janssen and Battjes [73] for a detailed description). By eliminating this inconsistency, they obtained an improved (explicit) expression for the wave breaking dissipation:

$$\langle \epsilon_b \rangle = \frac{3\sqrt{\pi}}{16} B f \rho g \frac{H_{rms}^3}{h} \left[1 + \frac{4}{3\sqrt{\pi}} \left((H_b/H_{rms})^3 + \frac{3}{2}(H_b/H_{rms})\right) \exp\left[-(H_b/H_{rms})^2 - \mathrm{erf}(H_b/H_{rms})\right]\right] \tag{A.6}$$

Predictions of the Janssen and Battjes [73] model show a good fit with observations of the wave transformation on steep beaches measured by Baldock et al. [13]. Especially the physics of the inner surf zone, where wave heights can exceed the breaker height, are more accurately captured by the robust model, including 'shore breaks', waves that break very near or at steep beaches. The physics of shore breaks are similar to the reef break, where waves break at the edge of the reef, and therefore the accurate prediction of shore breaks could also improve predictions of the wave transformation across the reef.

A.1.2. Breaker height formulations

The parametric wave breaker models are calibrated with two variables, α and γ, which determine the wave breaking height. Often α is set to one, after which γ is empirically fitted to the data (e.g. Battjes and Stive [17] and Ruessink et al. [143]). Massel and Gourlay [93] treat both α and γ values as variables. Below common breaker formulations with distinct characteristics are shortly described.

- Battjes and Janssen [16] adopted a modified version of Miche [99]'s breaker height criterion, ensuring that in shallow water H_b reduces to γ*h:

$$H_b = 0.142 * L_b * \tanh\left(\frac{\gamma}{0.88} \frac{2\pi h_b}{L_b}\right) \tag{A.7}$$

  A constant γ of 0.8 gave the best fit with the experimental setup as described in Section A.1.1.1.

- Battjes and Stive [17] improved the formulation for γ in Equation A.7 by calibration tests of both laboratory and field data with different profile shapes (plane, bar-trough and concave beaches, slope between 1:20 and 1:40) and hydrodynamic forcing conditions. They defined γ as a function of the wave

steepness, while keeping α equal to one. Nairn [106] further improved this formulation by adding experimental data of the Pacific coast of Thornton and Guza [157]. He found the following relation:

$$\gamma = 0.39 + 0.57 \tanh(33 * s_0) \tag{A.8}$$

Now the wave breaking height is not only a function of the wave length and water depth, but also of the wave steepness.

- Ruessink et al. [143] came up with again a different formulation for the γ-value in Equation A.7 based on field experiments of different beaches (Duck, NC, USA, Egmond and Terschelling, The Netherlands) and additional verification using existing laboratory data of among others Battjes and Janssen [16]. Without a physical explanation but with a better fit than Equation A.8 they defined γ as:

$$\gamma = 0.76 * kh + 0.29 \tag{A.9}$$

where γ is a function of the wave number and local water depth.

- Kamphuis [76] formulated a breaker parameter that is dependent on both the wave length, the water depth and the slope (β), for both regular and irregular waves, based on 225 hydraulic test results with beach slopes between 1:10 and 1:40. It is a modification of Miche [99]'s breaking criterion. For regular waves, the formulation reads:

$$H_b = 0.127 * \exp(4\beta) L_p \tanh\left(\frac{2\pi h_b}{L_b}\right) \tag{A.10}$$

- Massel and Gourlay [93] studied the wave transformation across reefs, for which they fitted experimental data of several fringing reefs to the bore model of Battjes and Janssen [16]. Both α and γ were considered as free coefficients. They formulate two different breaker heights, one at the steep forereef and one at the reef flat. The reef-face is modeled according to Singamsetti and Wind [148], who performed laboratory tests with beach slopes ranging from 0.025 to 0.2:

$$H_b = 0.937 * h_b * \beta^{0.155} \left(\frac{H_0}{L_0}\right)^{-0.130} \tag{A.11}$$

Wave breaking at the reef top, where the slope is often smaller than 0.025, is modeled as:

$$H_b = h \left(\frac{\sqrt{1 + 0.01504 h_*^{-2.5}} - 1}{0.1654 h_*^{-1.25}} \right)^2 \tag{A.12}$$

where:

$$h_* = \frac{h}{g T^2} \tag{A.13}$$

This formulation is based on the study by Massel [92] on breaking wave heights at constant depths, using a large dataset of different field observations of reefs as well as shallow water wave experiments in a flume.

The α value was found to be a function of the non-linearity parameter as formulated by Gourlay [56]:

$$F_c = \frac{g^{1.25} * H^{0.5} * T^{2.5}}{h_e^{1.75}} \tag{A.14}$$

where h_e is the water depth at the reef edge. This parameter was proposed to distinguish different wave transformation regimes: for small values of F_{co} spilling waves are observed, whereas plunging waves

are apparent when F_{co} is larger than 150-200. For different reef configurations, different α-values are found. For a reef with a 1:4.5 slope, they obtained the following fit:

$$\alpha = \begin{cases} 0, & \text{if } F_{c0} \leq 100 \\ 0.0156(F_{c0} - 100)^{0.576}, & \text{if } F_{c0} > 100 \end{cases}$$

For a reef with a 1:1 slope, α was defined as:

$$\alpha = \begin{cases} 0, & \text{if } F_{c0} \leq 100 \\ 0.0252(F_{c0} - 100)^{0.517}, & \text{if } F_{c0} > 100 \end{cases}$$

As the formulation of Massel and Gourlay [93] is especially calibrated to reef profiles, this formulation seems favourable. However, the α and γ values are only fitted to three different test cases, which makes the larger scale applicability questionable.

- Su et al. [154] performed a similar analysis to Massel and Gourlay [93], deriving empirical coefficients for an existing bore model using experimental data of Demirbilek et al. [44]. Based on the Janssen and Battjes [73] bore model, the best fit between observed and modeled wave height transformation was found, evaluating different existing formulas for γ (e.g. Battjes and Stive [17], [106], and Ruessink et al. [143]). They conclude that γ is not related to the offshore wave steepness, but found a good fit for γ related to kh:

$$\gamma = 0.431 + 1.032\frac{\beta}{kh} \tag{A.15}$$

Furthermore, they support Massel and Gourlay [93]'s observation that α is related to the non-linearity parameter F_c, resulting in:

$$\alpha = 1.245 + 9.65 * 10^{-5} * F_c \tag{A.16}$$

A.1.3. Breaker formulation results

All roller models and breaker formulations are formulated based on different assumptions and model calibration data, resulting in models with different ranges of validity. Both the parametric breaker model by Baldock et al. [13] and Janssen and Battjes [73] are adapted for steep slopes, which makes them favourable for implementation in the reef hydrodynamic model. Next to that, they are explicitly formulated, which makes them much faster to solve than the Battjes and Janssen [16] model. For this reason, only the two explicit models are tested.

Breaker height formulations by Su et al. [154] and Massel and Gourlay [93] are validated for reef lined coasts, whereas other formulations are calibrated on field data of sandy coastlines. Based on Figures A.1 and A.2, it is determined whether the range of validity of the models can be extended to the reef environment. Here, the results of the reef hydrodynamic model using different formulations are depicted, as well as results of laboratory experiments by Buckley et al. [32] with the following input conditions:

- $H_{rms,0}$= 4.32 m
- T_p= 13.56 s
- Water level above reef flat = 1.44 m
- Forereef slope= 1:5 and reef width = 500 m

Both parametric wave models of Baldock et al. [13] and Janssen and Battjes [73] give a good global prediction of the wave breaking process across the coral reef. Near the reef crest, the wave height prediction is rather difficult due to the large gradients in bathymetry. However, at the reef flat, the wave height is accurately represented, and as beach toe wave heights are input for the runup prediction formulas, it is most important that these wave heights are similar to the observed wave height values. The magnitude of the setup is also accurately captured by both models. Breaker height formulations have a large influence on the wave breaking process depicted in Figure A.1. To have a stable wave breaking model, Janssen and Battjes [73]'s model is chosen. The breaker height formulation of Su et al. [154] is implemented as this formulation is derived for reef environments and shows a good agreement with the results.

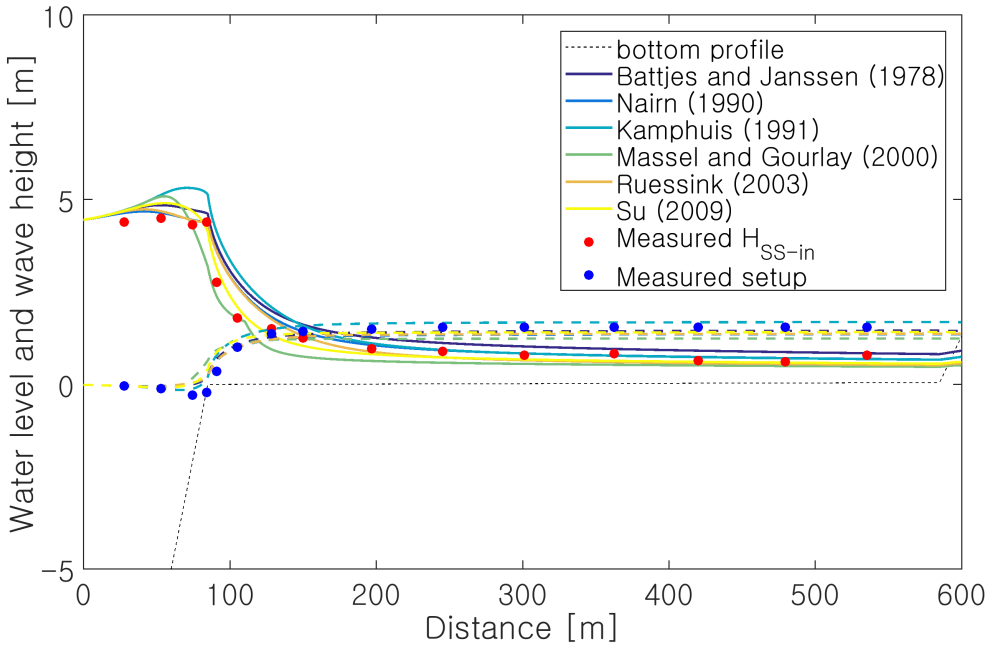

Figure A.1: The wave height transformation of incoming short waves, depicted by the coloured solid lines, and the setup, depicted by the coloured dashed line, for various breaker height formulations, for the parametric wave breaking model of Baldock et al. [13]

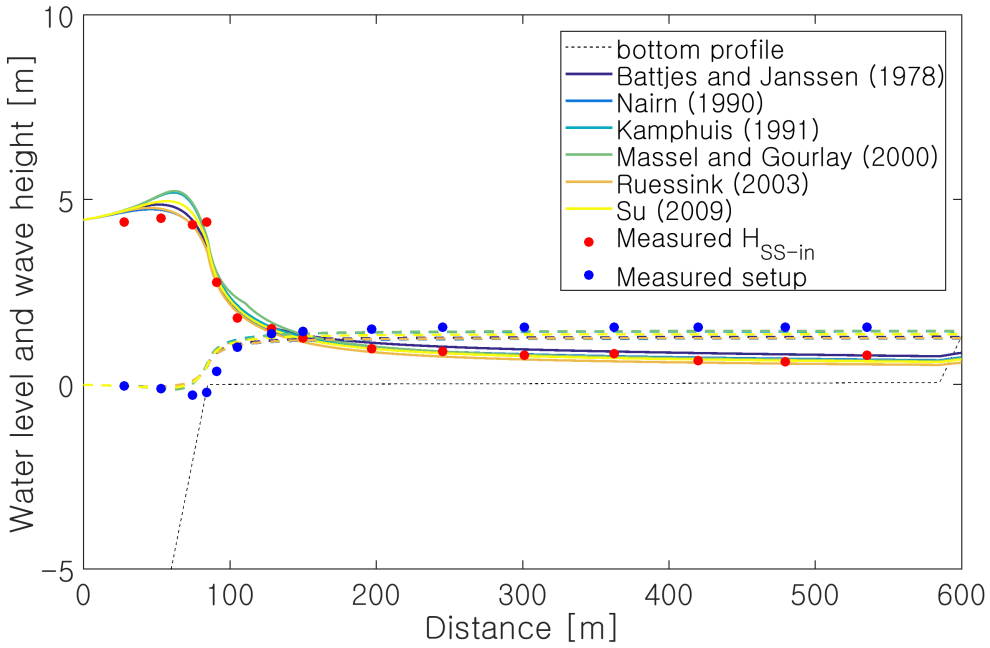

Figure A.2: The wave height transformation of incoming short waves, depicted by the coloured solid lines, and the setup, depicted by the coloured dashed line, for various breaker height formulations, for the parametric wave breaking model of Janssen and Battjes [73]

A.2. Influence of model parameters on IG wave height variability

Different model parameters influence the IG wave height at the reef crest, some of which are not taken into account in the derived empirical formulation based on linear regression analysis. Figures A.3 to A.4 support observations denoted in Section 4.2.2.1 of Chapter 4. From these figures, it is clear that the friction coefficient and the reef width are important causes for scatter in the formulation for the IG wave height.

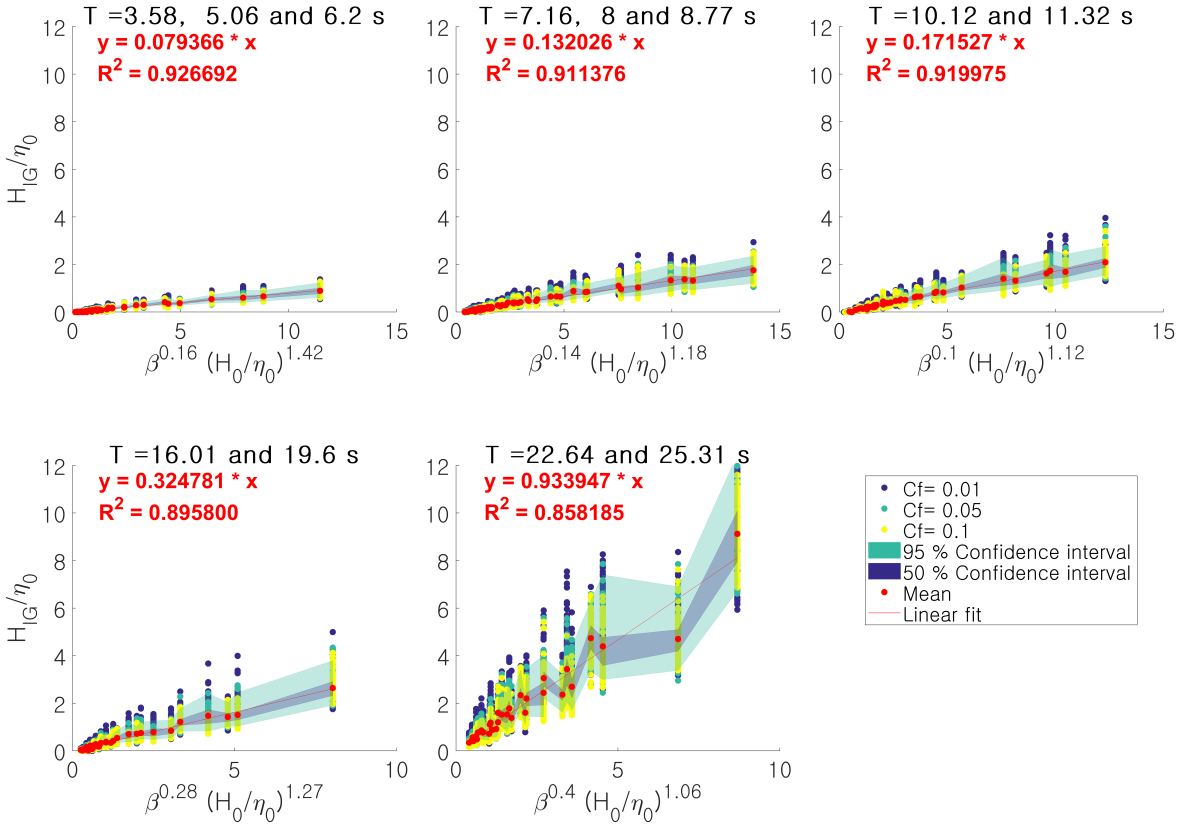

(a) Filtered on the reef roughness

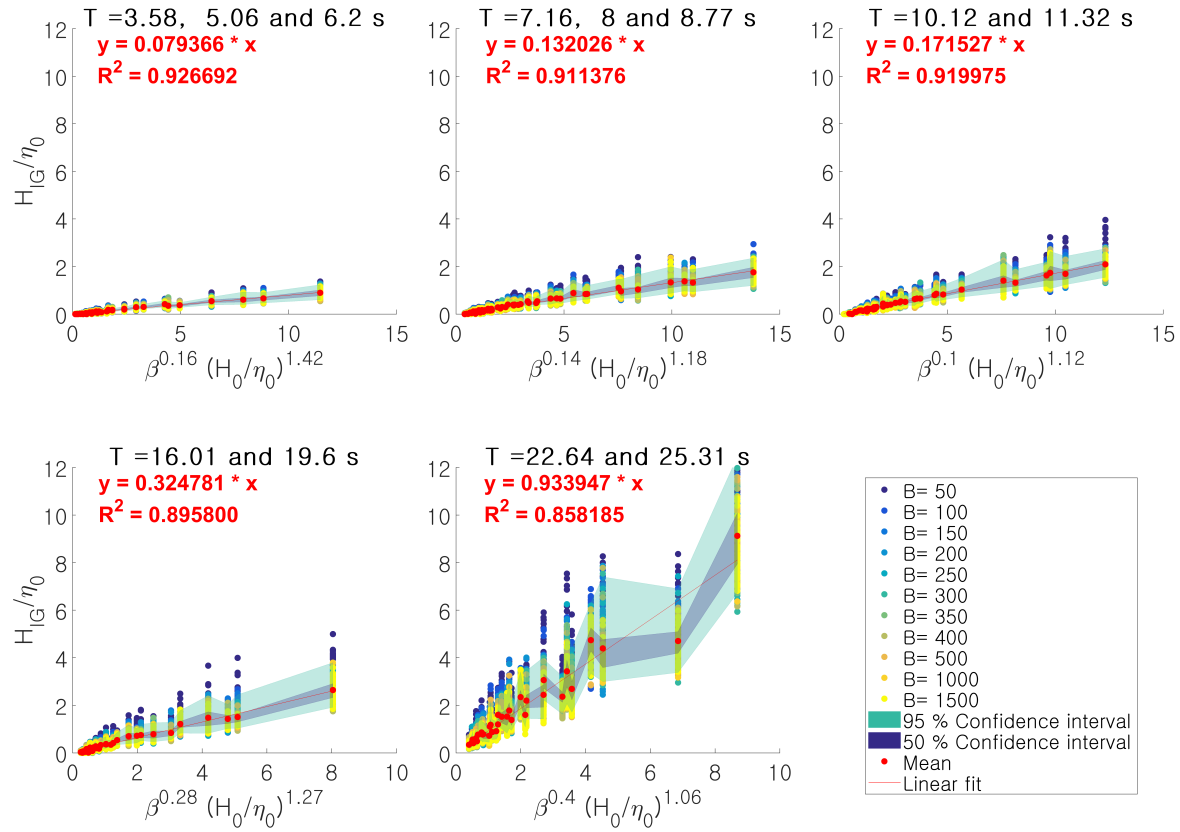

(b) Filtered on the reef width

Figure A.3: Plots of the dimensionless IG wave height calculated by XBeach versus optimized empirical formulations, sorted per wave period group, filtered on (a) the reef roughness and (b) the reef flat width

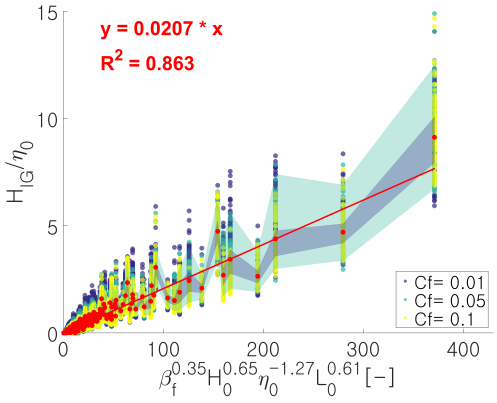

Figure A.4: Plot of the dimensionless IG wave height calculated by XBeach versus optimized empirical formulation, filtered on the roughness

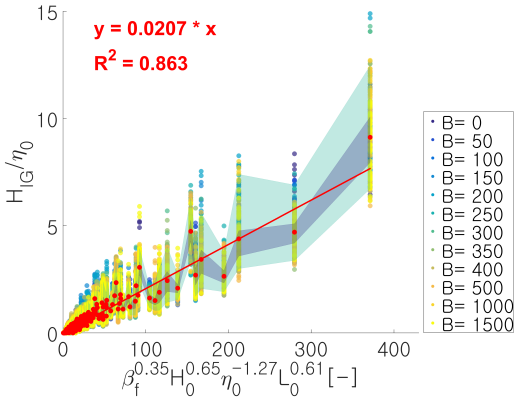

Figure A.5: Plot of the dimensionless IG wave height calculated by XBeach versus optimized empirical formulation, filtered on the reef flat width

A.3. Runup prediction

In Section 4.2.3 of Chapter 4, a runup formulation is derived for the incident swash at the reef beach. Although the goodness of fit is significantly increased compared to existing formulations, the formulation still shows significant scatter. Based on Figure A.6, the sources of scatter can be determined, as is done in Section 4.2.3.

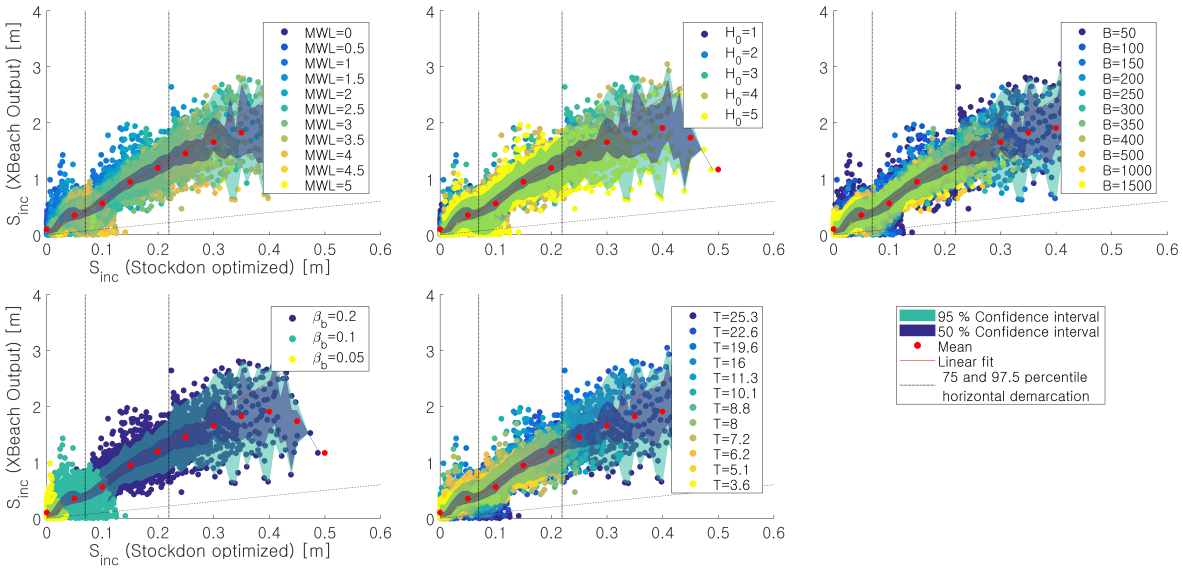

Figure A.6: Colour maps of model variables influencing the optimized incident swash formulation, where the influence of the mean water level at the beach toe, the offshore wave height, the reef width, the beach slope and the period is depicted

B

Cluster Analysis

B.1. Analysis of cluster variables

The cluster analysis starts with the analysis of different cluster variables with one cluster method (the Gaussian Mixture model). In Figures B.1 to B.5 and Tables B.1 to B.5 the results for model runs with different cluster variables are shown: the regular depths, the normalized depths, the varying grid resolution, geographic filtering and the length binning. Based on these results, conclusions on the method to define the cluster variable are denoted in Section 5.4.1 of Chapter 5.

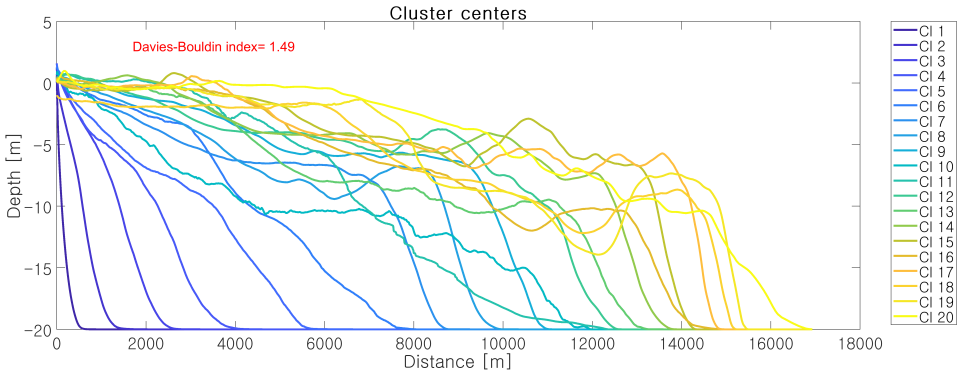

Figure B.1: Results of the cluster analysis with the GM model, with 20 cluster centers and regular depths as cluster variables

Table B.1: Cluster center characteristics of the GM model in combination with the regular depth as cluster variable; the size of the represented profile dataset, the average of the RMSE of all profiles in a cluster center (RMSE 100) and the average of the 95 percentile lowest RMSE's (RMSE 95), thereby removing the influence of extreme outliers

Cluster nr	1	2	3	4	5	6	7	8	9	10
Size	11969	5704	4154	1201	1262	1273	805	790	556	595
RMSE 100	3.87	3.58	3.80	3.48	3.07	3.53	2.93	3.31	2.06	1.91
RMSE 95	3.64	3.39	3.62	3.31	2.92	3.37	2.78	3.09	2.00	1.85

Cluster nr	11	12	13	14	15	16	17	18	19	20
Size	399	70	393	253	164	182	125	147	112	12
RMSE 100	2.08	2.87	2.13	2.24	1.56	2.18	2.11	1.53	1.20	1.12
RMSE 95	1.99	2.80	2.04	2.18	1.52	2.13	2.08	1.42	1.16	1.08

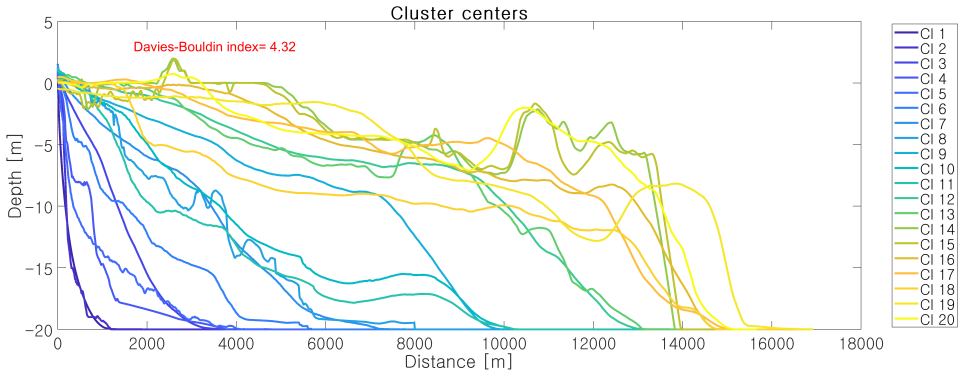

Figure B.2: Results of the cluster analysis with the GM model, with 20 cluster centers and normalized depths as cluster variables

Table B.2: Cluster center characteristics of the GM model in combination with the normalized depth as cluster variable; the size of the represented profile dataset, the average of the RMSE of all profiles in a cluster center (RMSE 100) and the average of the 95 percentile lowest RMSE's (RMSE 95), thereby removing the influence of extreme outliers

Cluster nr	1	2	3	4	5	6	7	8	9	10
Size	15893	10	7346	27	39	78	3211	8	1390	205
RMSE 100	4.08	3.44	4.15	4.96	5.10	6.03	4.09	5.01	3.07	5.31
RMSE 95	3.80	3.44	3.94	4.59	4.83	5.89	3.94	5.01	2.93	5.12

Cluster nr	11	12	13	14	15	16	17	18	19	20
Size	146	934	10	1	2	322	113	92	254	79
RMSE 100	5.71	2.74	3.43	0.04	0.18	2.58	2.63	6.09	1.55	3.24
RMSE 95	5.59	2.63	3.43	0.04	0.18	2.53	2.51	5.86	1.46	3.16

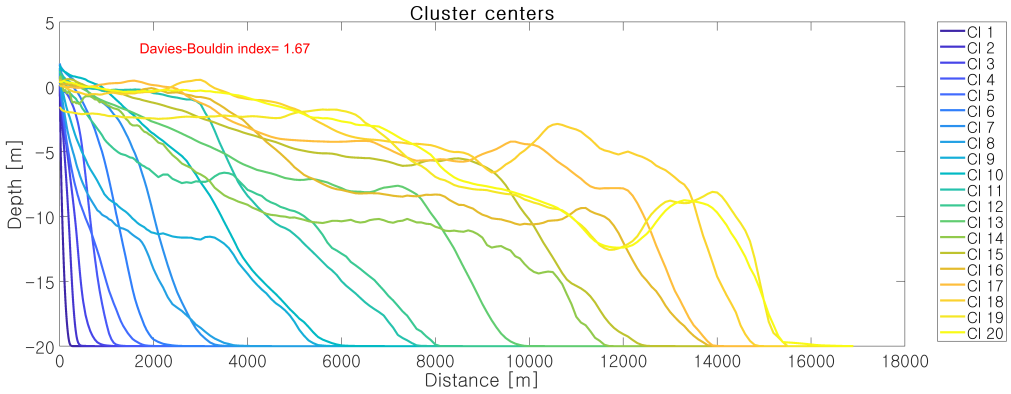

Figure B.3: Results of the cluster analysis with the GM model, with 20 cluster centers and irregularly spaced depths as cluster variables

Table B.3: Cluster center characteristics of the GM model in combination with the depth at varying distances as cluster variable; the size of the represented profile dataset, the average of the RMSE of all profiles in a cluster center (RMSE 100) and the average of the 95 percentile lowest RMSE's (RMSE 95), thereby removing the influence of extreme outliers

Cluster nr	1	2	3	4	5	6	7	8	9	10
Size	5211	3854	3678	2666	1798	2409	2404	1571	1018	1504
RMSE 100	3.58	2.49	2.79	2.58	2.95	2.33	2.48	3.39	3.40	2.66
RMSE 95	3.40	2.34	2.64	2.47	2.76	2.24	2.37	3.20	3.21	2.55

Cluster nr	11	12	13	14	15	16	17	18	19	20
Size	710	373	1131	73	723	266	227	191	109	250
RMSE 100	1.92	3.68	2.09	2.87	2.05	2.06	1.72	1.60	1.28	1.74
RMSE 95	1.79	3.53	2.02	2.72	2.00	2.00	1.67	1.55	1.21	1.68

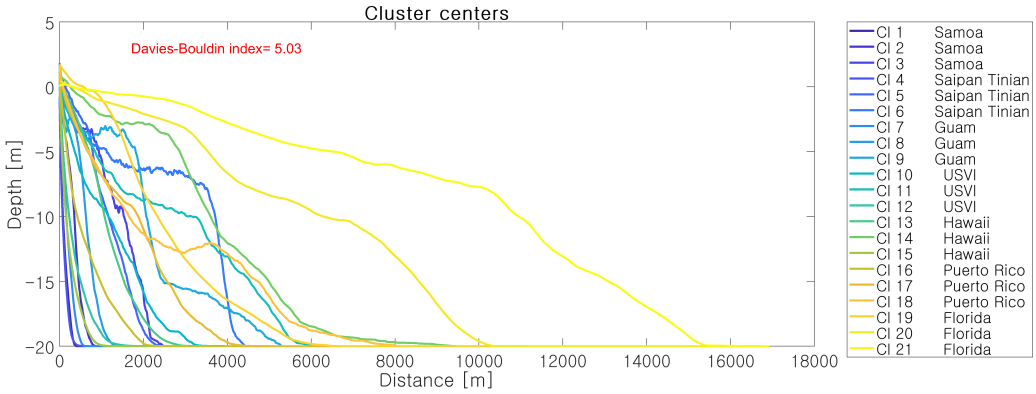

Figure B.4: Results of the cluster analysis with the GM model, with 21 cluster centers and regular depths as cluster variables, filtered per geographic region

Table B.4: Cluster center characteristics of the GM model with the regular depth as cluster variable, filtered per geographic region; the size of the represented profile dataset, the average of the RMSE of all profiles in a cluster center (RMSE 100) and the average of the 95 percentile lowest RMSE's (RMSE 95), thereby removing the influence of extreme outliers

Cluster nr	1	2	3	4	5	6	7	8	9	10	11
Size	920	239	39	808	176	51	844	401	50	401	220
RMSE 100	4.14	3.34	5.41	3.63	5.33	5.32	4.38	3.84	5.39	3.82	3.01
RMSE 95	3.93	3.08	5.26	3.40	5.15	5.18	4.14	3.60	5.16	3.65	2.85

Cluster nr	12	13	14	15	16	17	18	19	20	21
Size	1043	3305	526	9573	2881	1906	744	2425	2002	1612
RMSE 100	3.57	3.78	4.59	4.06	4.79	4.10	3.35	4.34	3.48	3.18
RMSE 95	3.37	3.53	4.31	3.80	4.50	3.93	3.18	4.13	3.38	3.08

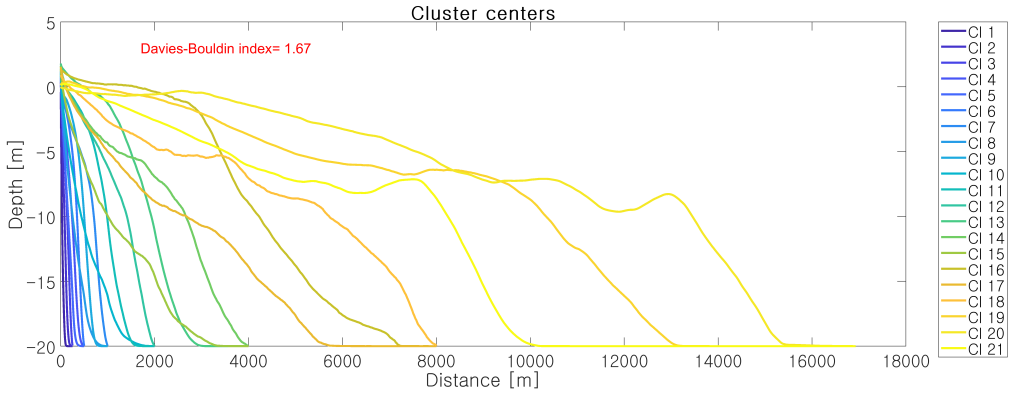

Figure B.5: Results of the cluster analysis with the GM model, with 21 cluster centers and regular depths as cluster variables, filtered per length bin

Table B.5: Cluster center characteristics of the GM model with the regular depth as cluster variable, filtered per length bin; the size of the represented profile dataset, the average of the RMSE of all profiles in a cluster center (RMSE 100) and the average of the 95 percentile lowest RMSE's (RMSE 95), thereby removing the influence of extreme outliers

Cluster nr	1	2	3	4	5	6	7	8	9	10	11
Size	2293	1833	1491	1610	1976	857	1299	1742	1568	1474	1689
RMSE 100	3.24	2.18	2.42	2.08	2.19	2.63	3.50	2.13	2.63	2.62	3.06
RMSE 95	3.07	2.04	2.22	1.95	2.03	2.44	3.29	2.00	2.50	2.48	2.92

Cluster nr	12	13	14	15	16	17	18	19	20	21
Size	1543	1952	1144	1487	1047	1707	618	1024	688	1116
RMSE 100	3.77	2.99	4.59	3.23	2.60	3.74	3.75	2.82	2.55	2.53
RMSE 95	3.53	2.85	4.38	3.07	2.47	3.58	3.57	2.73	2.50	2.41

In Figures B.6 and B.7, examples of cluster results are shown, pointing out the large number of profiles that are grouped in one short cluster and little number of long profiles in another cluster.

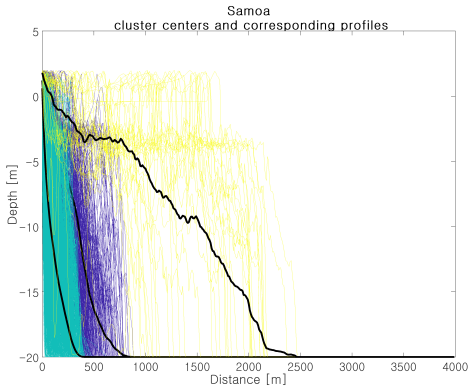

Figure B.6: Results of the cluster analysis with the GM model filtered per geographic region, displaying the three cluster centers of American Samoa

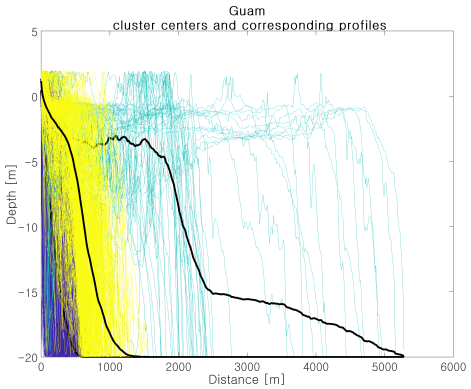

Figure B.7: Results of the cluster analysis with the GM model filtered per geographic region, displaying the three cluster centers of Guam

B.2. Analysis of cluster methods

Different cluster methods are explored with regular depths as cluster variables, filtered per length bin. Figures B.8 and B.9 and the corresponding tables support observations denoted in Section 5.4.2 of Chapter 5.

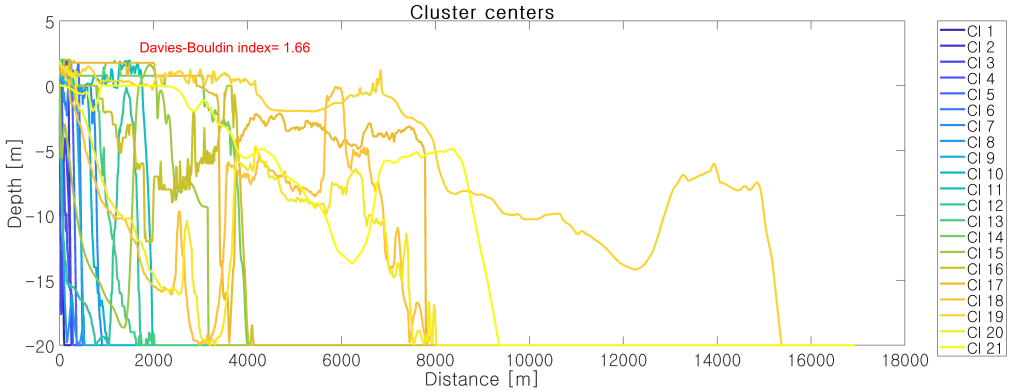

Figure B.8: Results of the cluster analysis with the Maximum Dissimilarity Algorithm, with 21 cluster centers and regular depths as cluster variables, filtered per length bin

Table B.6: Cluster center characteristics of the Maximum Dissimilarity Algorithm in combination with filtering of the profiles on their length

Cluster nr	1	2	3	4	5	6	7	8	9	10	11
Size	5067	270	280	3197	1120	126	989	935	2685	3976	624
RMSE 100	6.75	6.36	6.80	3.68	4.93	4.98	4.61	5.74	5.32	6.50	7.17
RMSE 95	6.38	6.23	6.70	3.51	4.82	4.83	4.44	5.61	5.18	6.28	7.04

Cluster nr	12	13	14	15	16	17	18	19	20	21
Size	106	3751	428	404	2971	284	117	898	13	1917
RMSE 100	7.94	7.20	7.38	8.66	6.33	5.96	5.71	4.34	5.33	4.37
RMSE 95	7.83	6.97	7.26	8.52	6.16	5.82	5.59	4.24	5.21	4.25

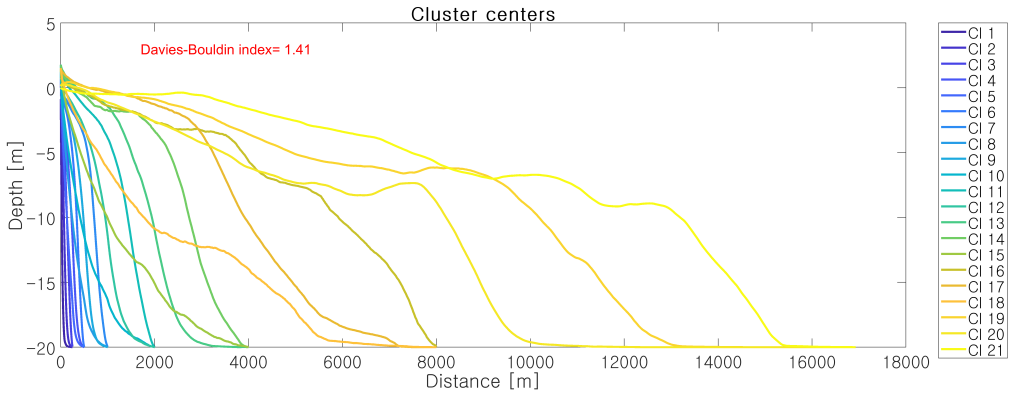

Figure B.9: Results of the cluster analysis with k-means, with 21 cluster centers and regular depths as cluster variables, filtered per length bin

Table B.7: Cluster center characteristics of the k-means algorithm in combination with filtering of the profiles on their length

Cluster nr	1	2	3	4	5	6	7	8	9	10	11
Size	1757	2159	1701	1921	1560	962	1124	1705	1780	1449	1332
RMSE 100	2.09	2.07	2.41	2.00	1.82	2.54	2.99	2.12	2.37	2.60	3.16
RMSE 95	1.99	1.98	2.23	1.90	1.68	2.38	2.84	1.98	2.26	2.44	2.98

Cluster nr	12	13	14	15	16	17	18	19	20	21
Size	1925	1952	842	1789	561	1423	1388	929	1131	768
RMSE 100	2.69	2.59	3.37	3.16	3.11	2.89	3.08	2.55	2.31	2.66
RMSE 95	2.58	2.48	3.13	3.01	2.94	2.77	2.94	2.48	2.20	2.60

B.3. Results cluster algorithm

Once the cluster variable and cluster method are established, the cluster algorithm is refined to increase the resolution of the results. For this, first, length bin borders are identified (See Figure B.10 for an illustration of how borders are defined). Then, representative profiles are extracted for each cluster center. In Figure B.11 an example is shown of how profiles belonging to a cluster center are further grouped to one of the five representative profiles. These figures support observations noted in Section 5.4.3 of Chapter 5.

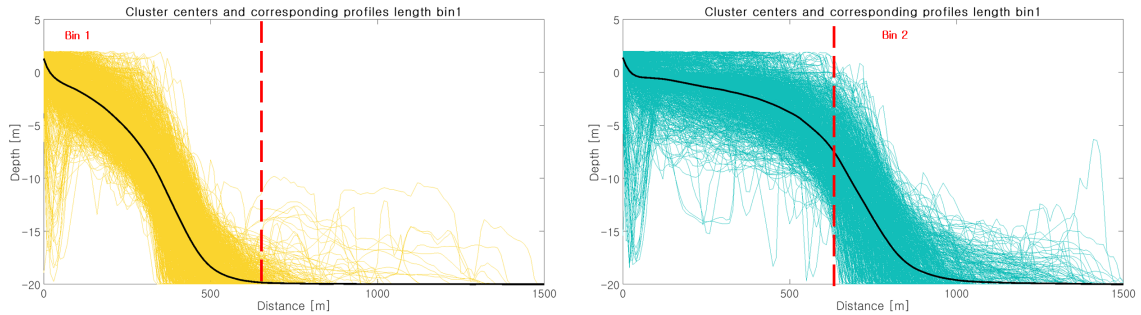

Figure B.10: Visual inspection of cluster center borders in order to find borders for the length bins

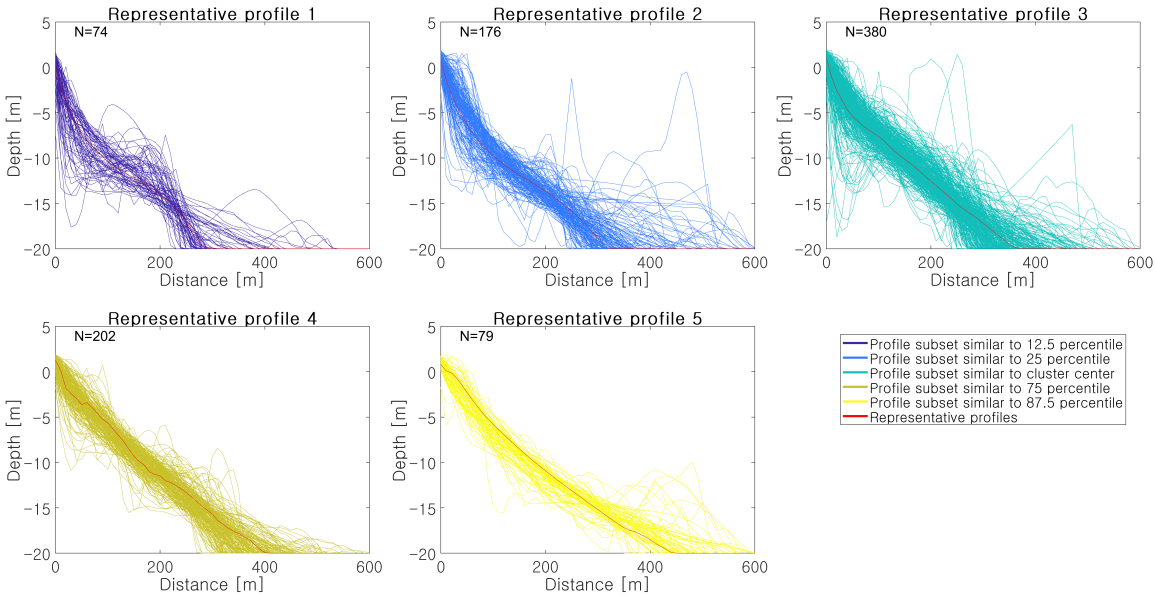

Figure B.11: Results of finding representative profiles for each cluster center that clearly show the topographic variation within cluster centers, depicting the results for Cluster Center 8 of Length bin 1

B.4. Final results

In this section the final results of the cluster analysis are depicted.

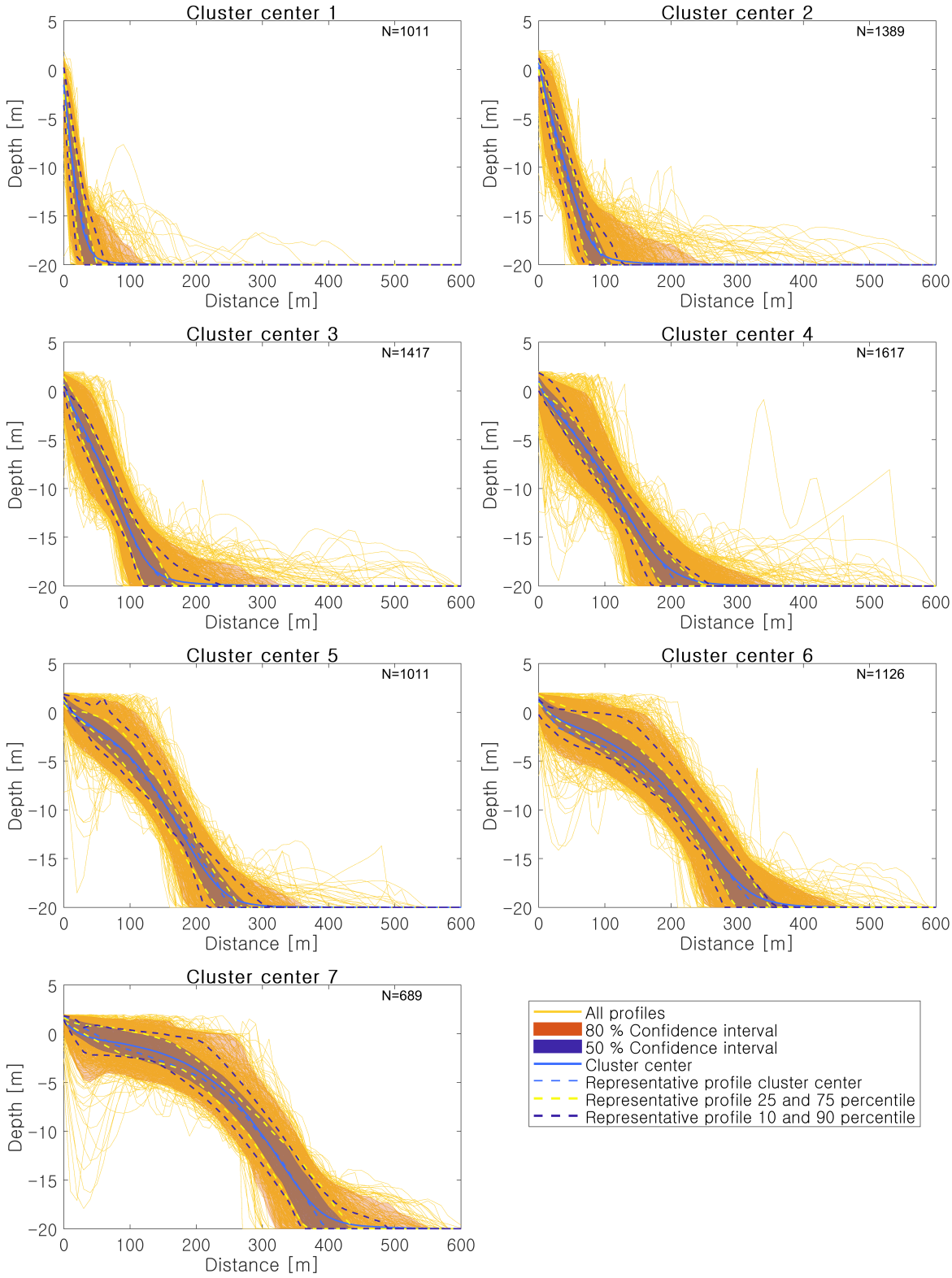

Figure B.12: Results of the cluster analysis for length bin 1 (0-600 m), clusters 1 to 7

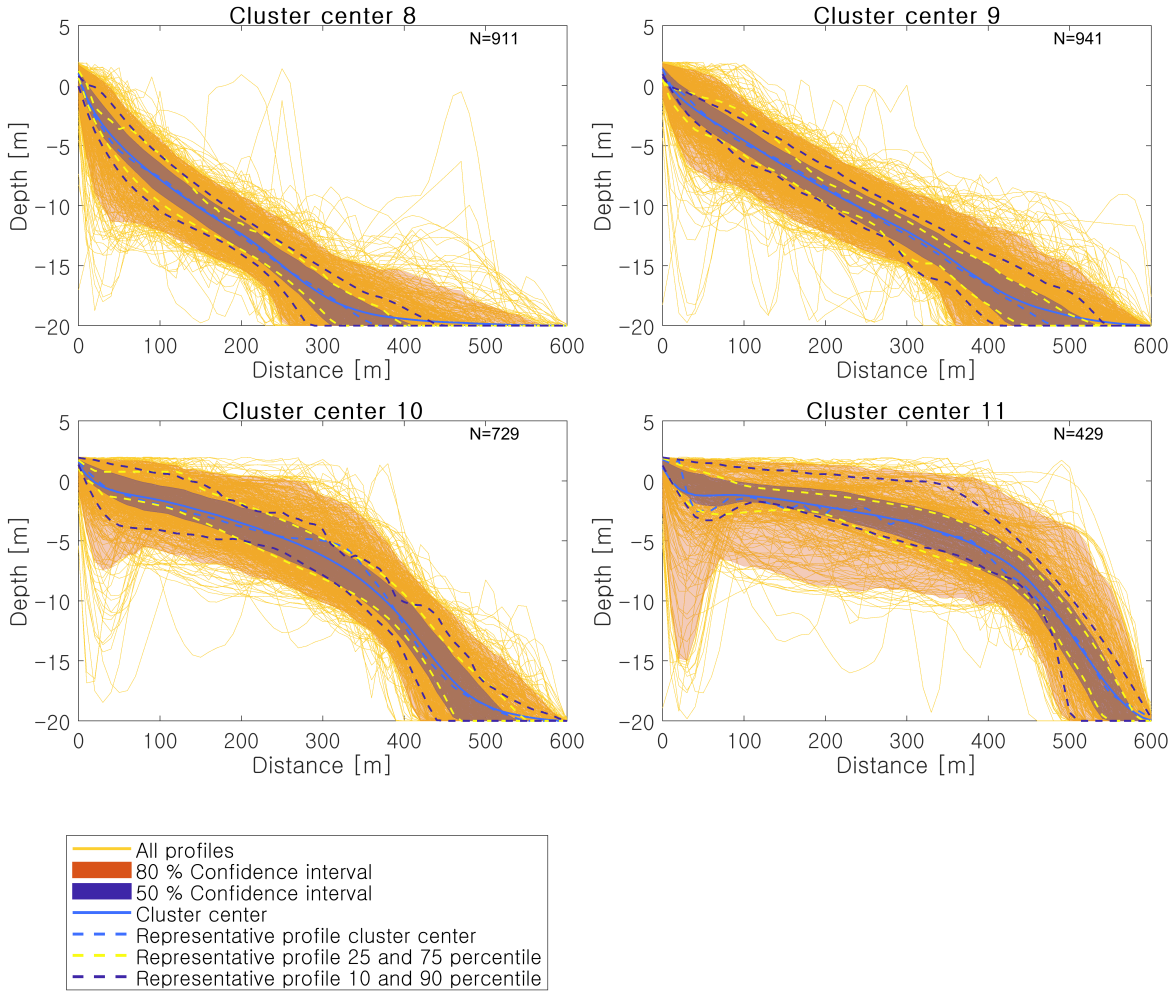

Figure B.13: Results of the cluster analysis for length bin 1 (0-600 m), clusters 8 to 11

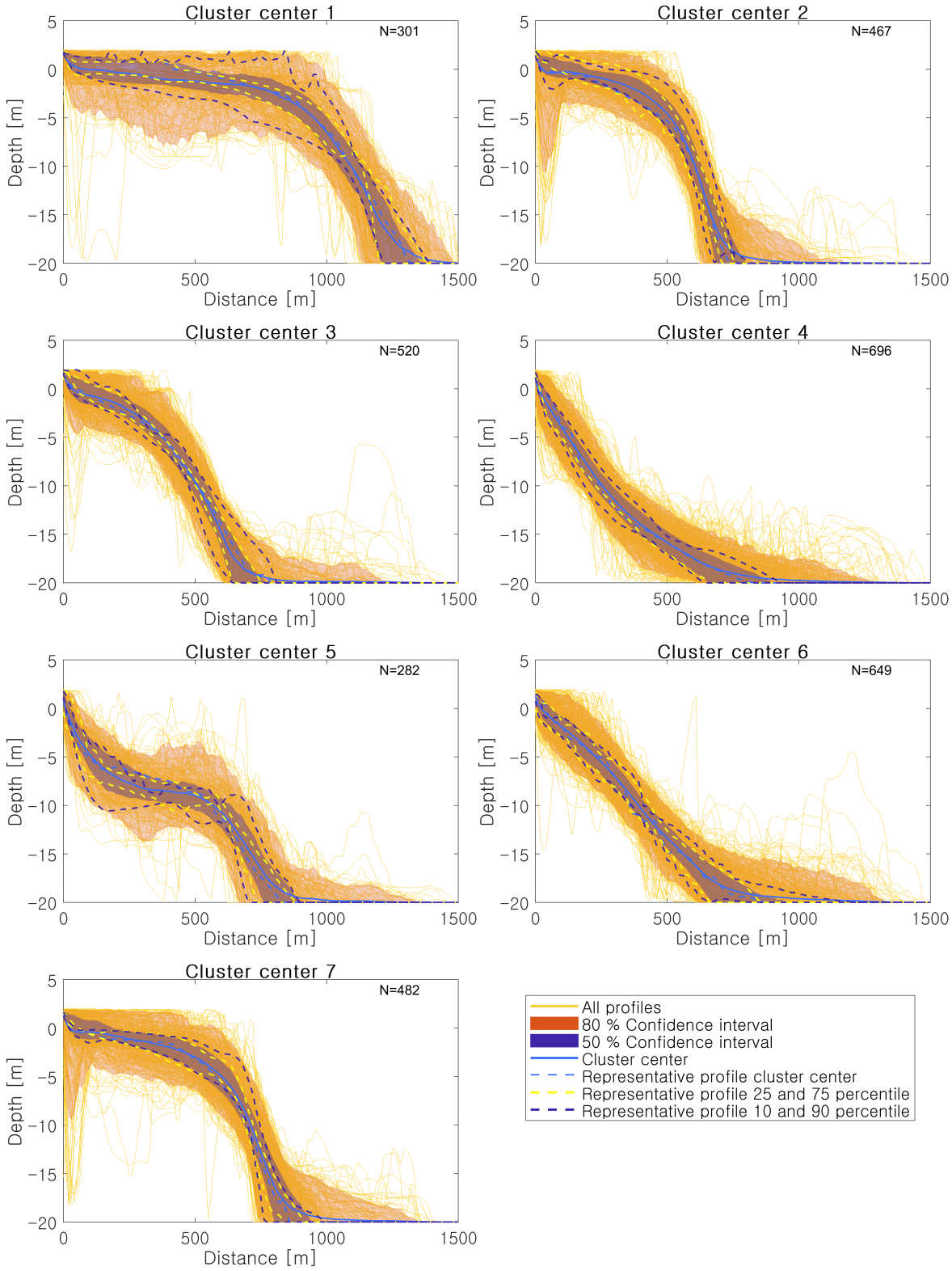

Figure B.14: Results of the cluster analysis for length bin 2 (600 - 1500 m), clusters 1 to 7

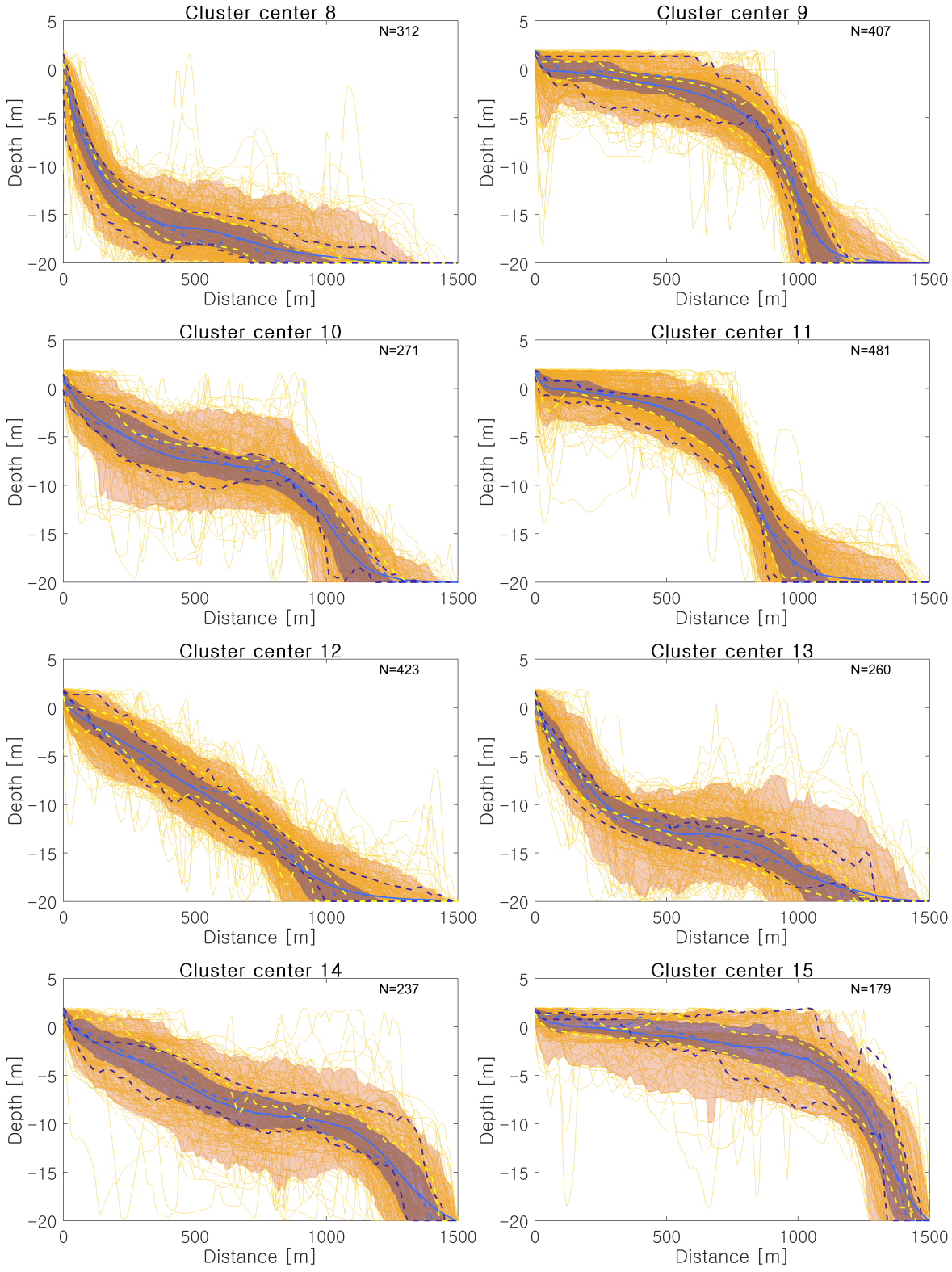

Figure B.15: Results of the cluster analysis for length bin 2 (600 - 1500 m), clusters 8 to 15

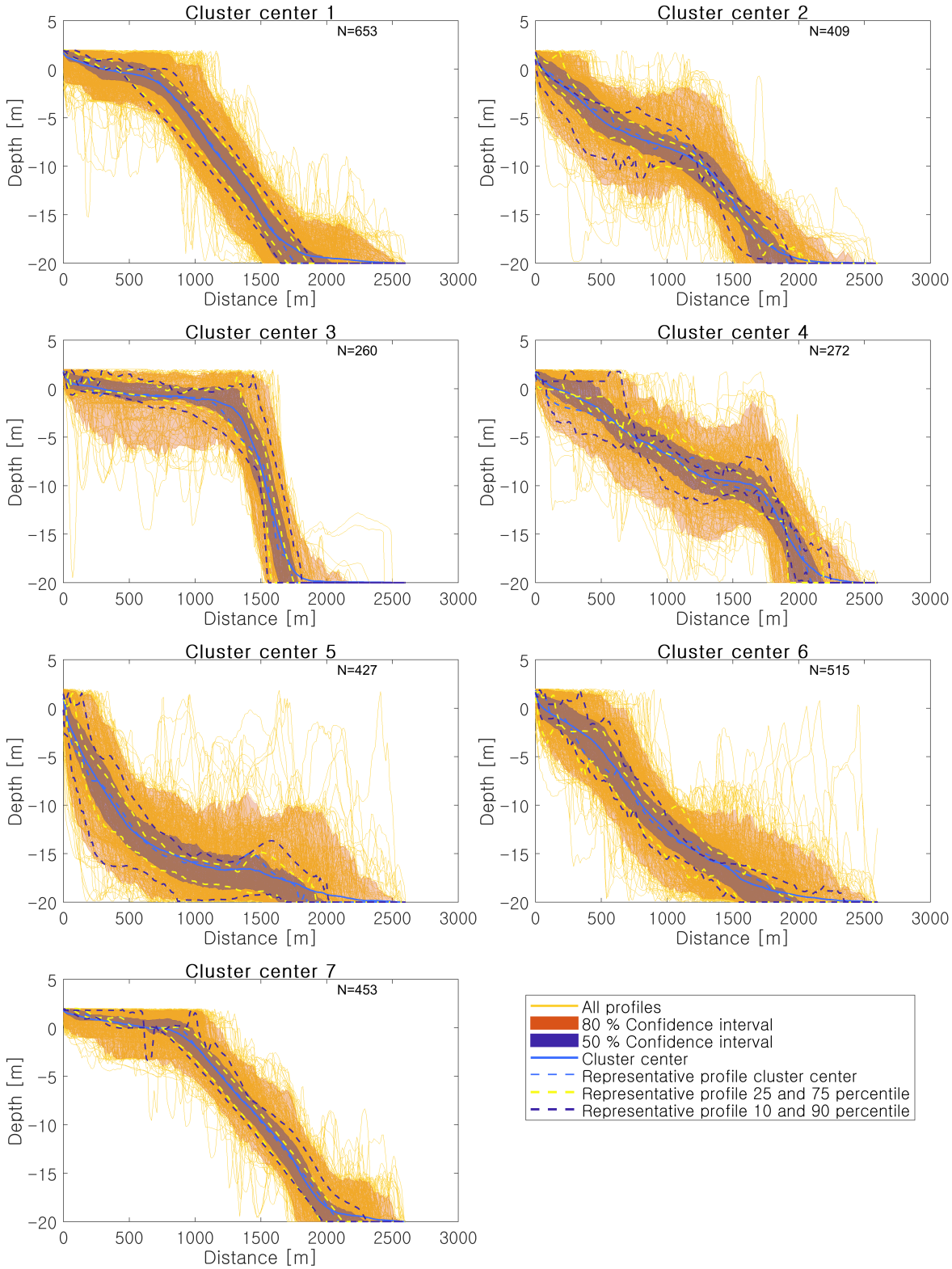

Figure B.16: Results of the cluster analysis for length bin 3 (1500 - 2600 m), clusters 1 to 7

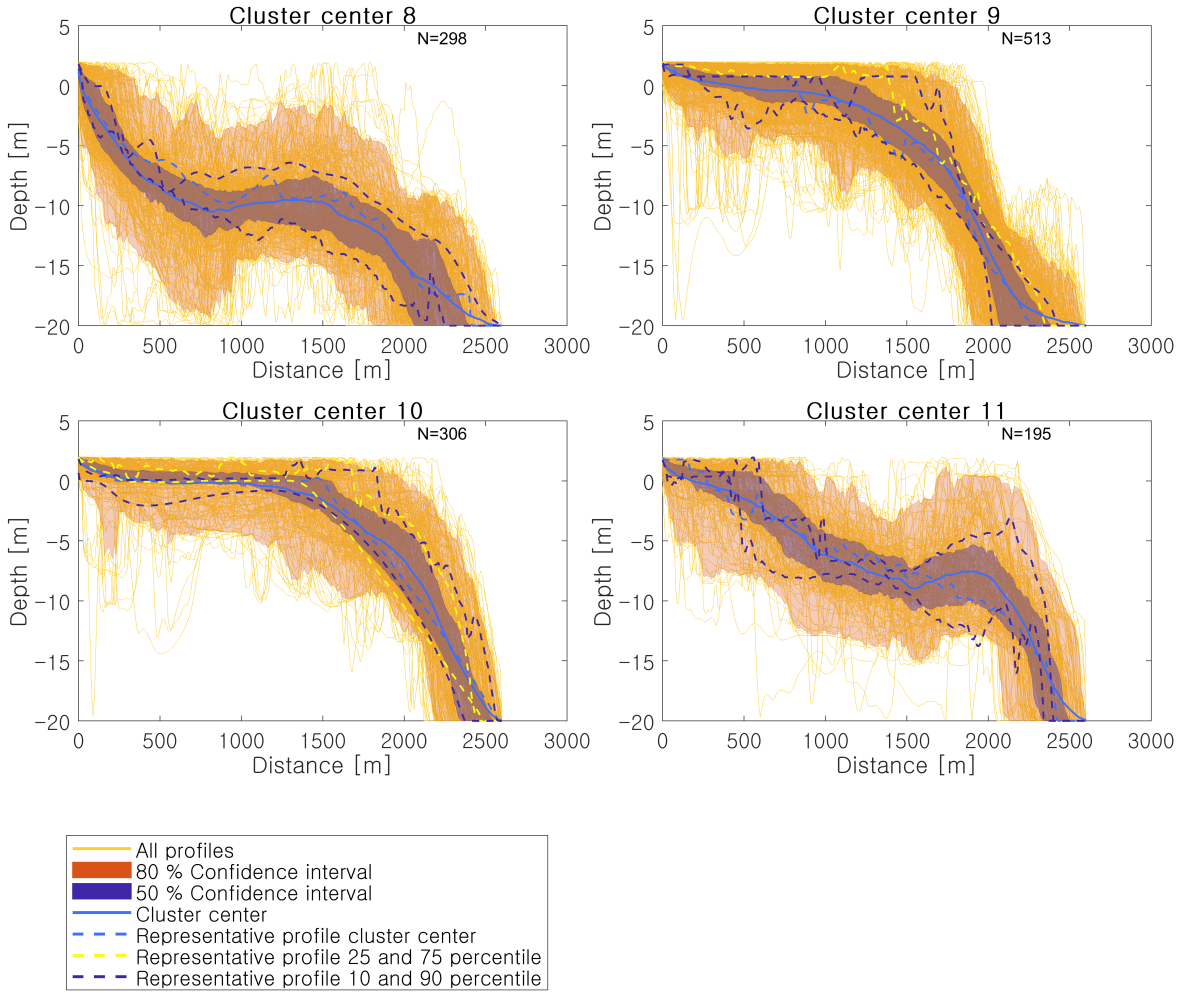

Figure B.17: Results of the cluster analysis for length bin 3 (1500 - 2600 m), clusters 8 to 11

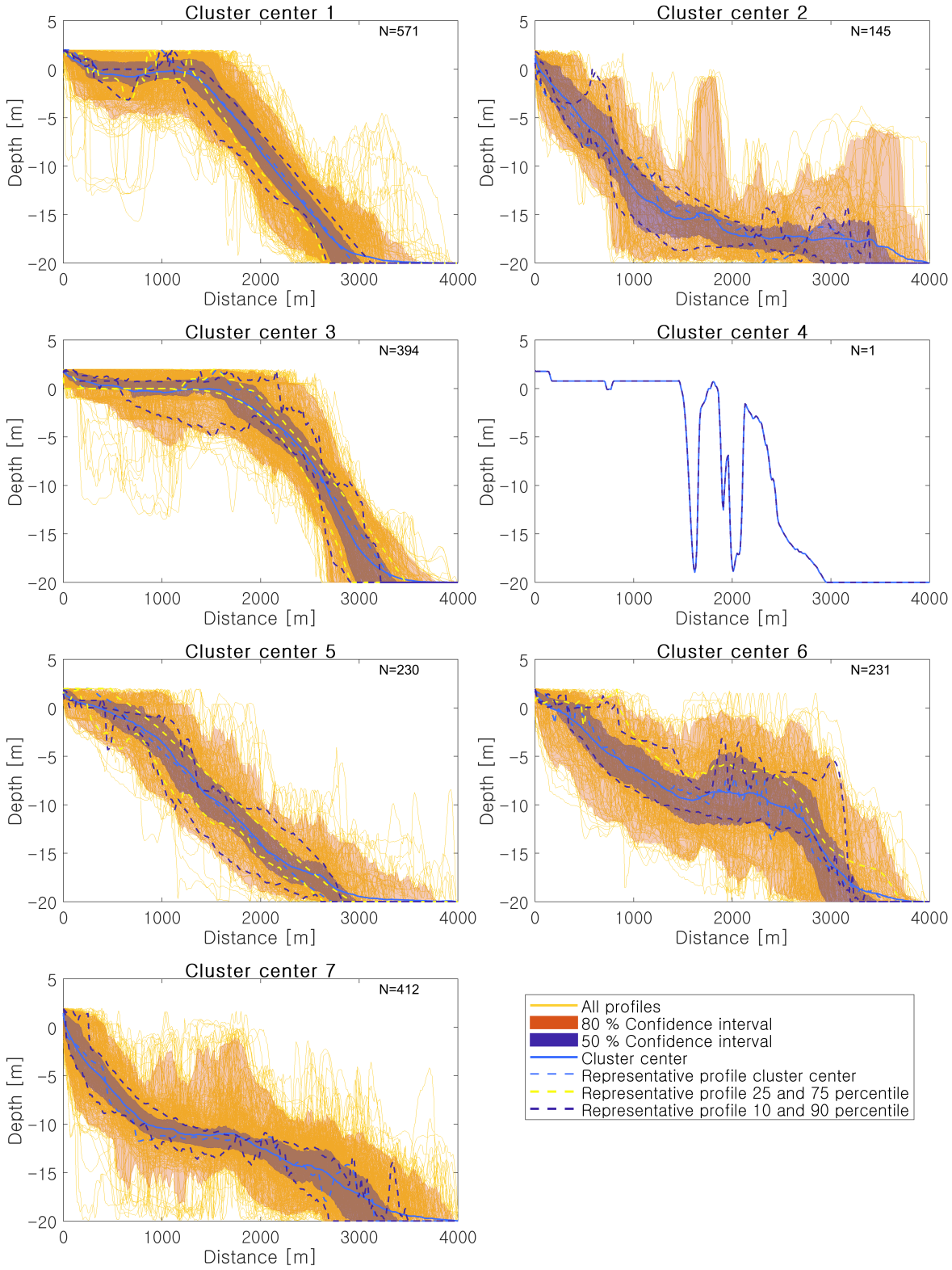

Figure B.18: Results of the cluster analysis for length bin 4 (2600 - 4000 m), clusters 1 to 7

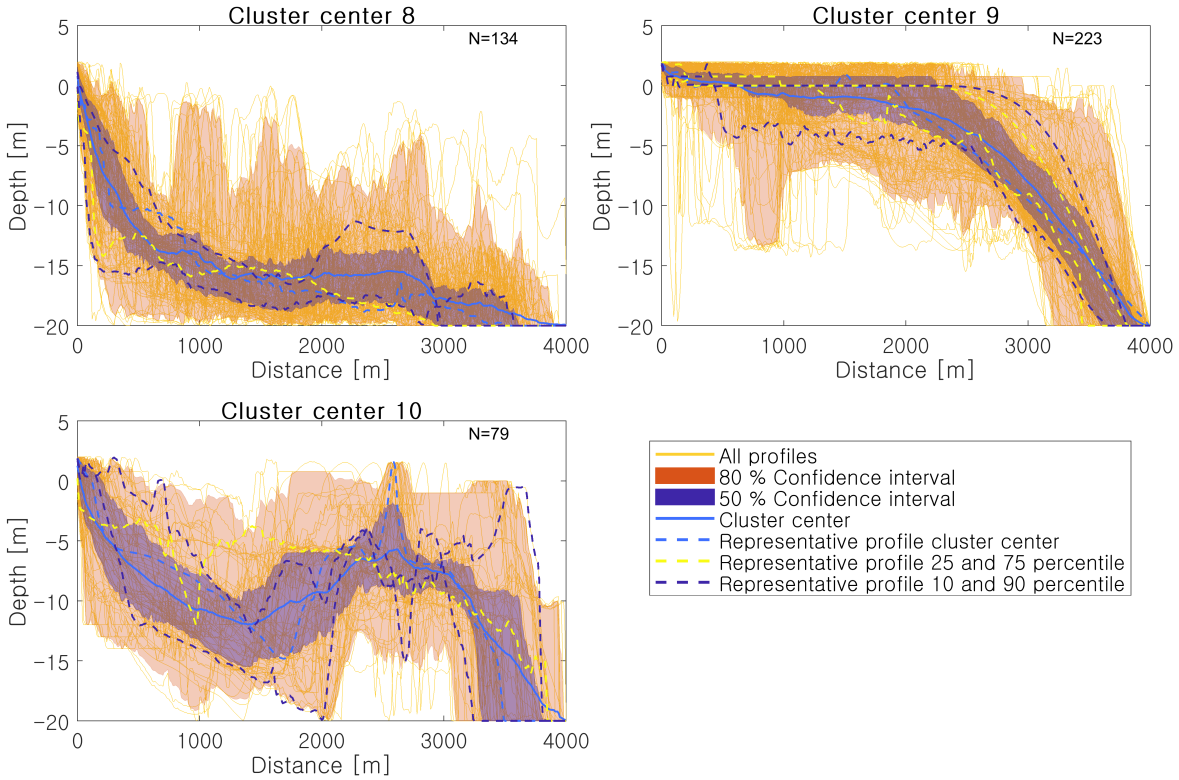

Figure B.19: Results of the cluster analysis for length bin 4 (2600 - 4000 m), clusters 8 to 10

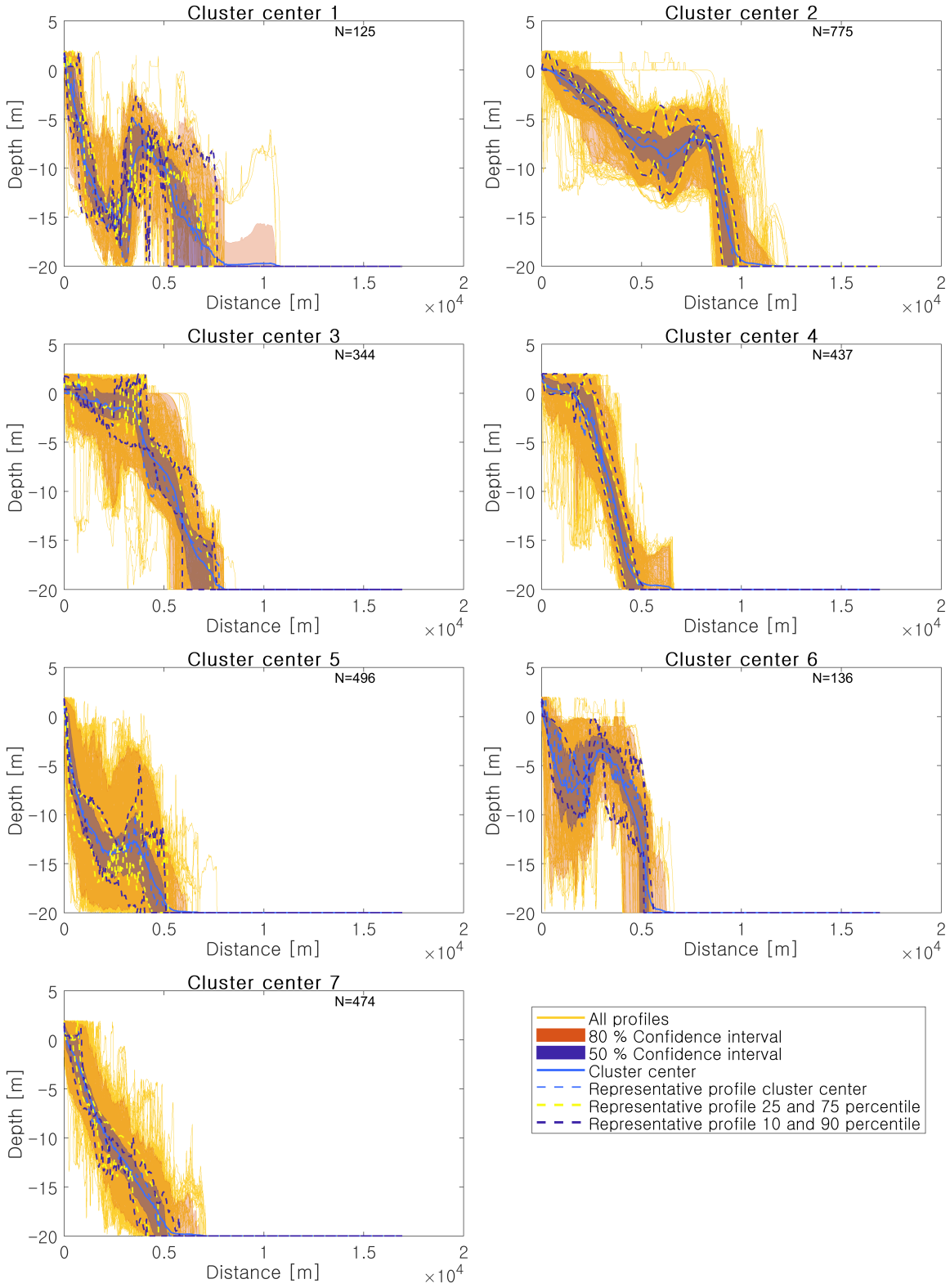

Figure B.20: Results of the cluster analysis for length bin 5 (4000 - 16930 m), clusters 1 to 7

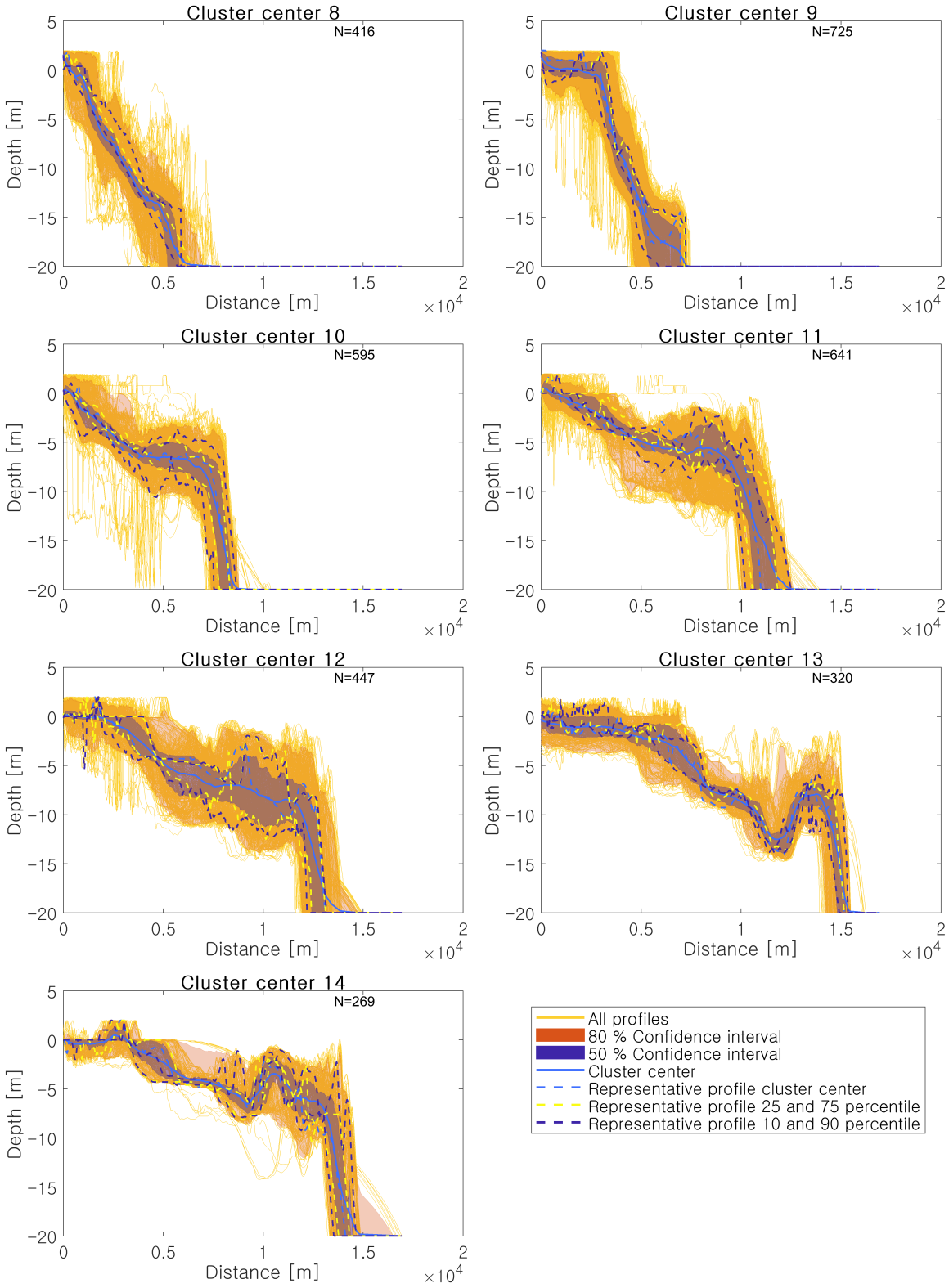

Figure B.21: Results of the cluster analysis for length bin 5 (4000 - 16930 m), clusters 8 to 14

C

XBeach model setup

C.1. Params file

In Figures C.1 to C.3, an example of an XBeach input ('params') file is depicted.

```
%%%%%%%%%%%%%%%%%%%%%%%%%%%%%%%%%%%%%%%%%%%%%%%%%%%%%%%%%%%%%%%%%%%%%%%%%%%%
%%%%%%%%%%%%%%%%%%%%
%%% XBeach parameter settings input file
%%%
%%%
%%%
%%% date:     30-May-2014 12:53:50
%%%
%%% function: xb_write_params
%%%
%%%%%%%%%%%%%%%%%%%%%%%%%%%%%%%%%%%%%%%%%%%%%%%%%%%%%%%%%%%%%%%%%%%%%%%%%%%%
%%%%%%%%%%%%%%%%%%%%

bedfriction = cf
bedfricfile = fric.txt
sedtrans    = 0
morphology  = 0
gammax      = 2.0
taper       = 3600.0
nonh        = 1
swave       = 0
front       = nonh_1d
back        = abs_1d
maxbrsteep  = 0.4
wavemodel   = nonh
CFL   = 0.9

%%% Flow boundary condition parameters
%%%%%%%%%%%%%%%%%%%%%%%%%%%%%%%%%%%%%%%%%%%%%%%%

epsi         = -1

%%% Grid parameters
%%%%%%%%%%%%%%%%%%%%%%%%%%%%%%%%%%%%%%%%%%%%%%%%%%%%%%%%%%%%%%%%%%%%%%%%%%%%

nx       = 204
ny       =  0
vardx    =  1
depfile  = profile.dep
xfile    = x.grd
posdwn   = -1
```

Figure C.1: XBeach input file - part 1

```
%%% Model time
%%%%%%%%%%%%%%%%%%%%%%%%%%%%%%%%%%%%%%%%%%%%%%%%%%%%%%%%%%%%%%%%%%%%%%%%%%%%
%%%

tstop        = 14400.0


%%% Tide boundary conditions
%%%%%%%%%%%%%%%%%%%%%%%%%%%%%%%%%%%%%%%%%%%%%%%%%%%%%%%%%%%%%%%%%%%%%%%%%%%%

zs0          = 2

%%% Wave boundary condition parameters
%%%%%%%%%%%%%%%%%%%%%%%%%%%%%%%%%%%%%%%%%%%%%%%%%%%%%%%%%%%%%%%%%%%%%%%%%%%%

instat       = reuse
bcfile       = nhbcflist.bcf

%%% Output variables
%%%%%%%%%%%%%%%%%%%%%%%%%%%%%%%%%%%%%%%%%%%%%%%%%%%%%%%%%%%%%%%%%%%%%%%%%%%%

outputformat = netcdf
tintg         = 1.0
tintm        = 1800.0
tstart       = 3600.0
tintp        = 1.0

npoints = 9
3.8738 1. offshore
54.3069 1. outerflat
104.7992 1. midflat
153.5961 1. innerflat
203.7403 1. beachtoe
177.1405 1. frontrestoration
181.221 1. midrestoration
185.7102 1. behindrestoration
453.2367 1. overtop
```

Figure C.2: XBeach input file - part 2

```
npointvar = 3
zs
uu
qx


nrugauge     =1
203.7403 1.
rugdepth     = 0.1

nglobalvar   = 3
zs
zb
uu


nmeanvar = 3
zs
uu
qx
```

Figure C.3: XBeach input file - part 3

D

Restoration

D.1. General overview of effect restoration

In this section, figures and tables are displayed that support the noted observations of Section 8.2.1 of Chapter 8. Figures D.1 to D.19 display the wave transformation of SS, IG and VLF waves and the setup across restorations at different locations and across varying reef shapes. Waves heights are split into incoming and outgoing wave heights, to capture the reflection at the restoration and at the steep interface of the reef. The results are summarized in a Tables D.1 to D.11, in which the wave transmission across the restoration, the beach toe wave heights and setup and the runup components are given. Below, all results are displayed per reef type. All summarizing tables that are displayed in Section 8.2.1 of Chapter 8 have been omitted here.

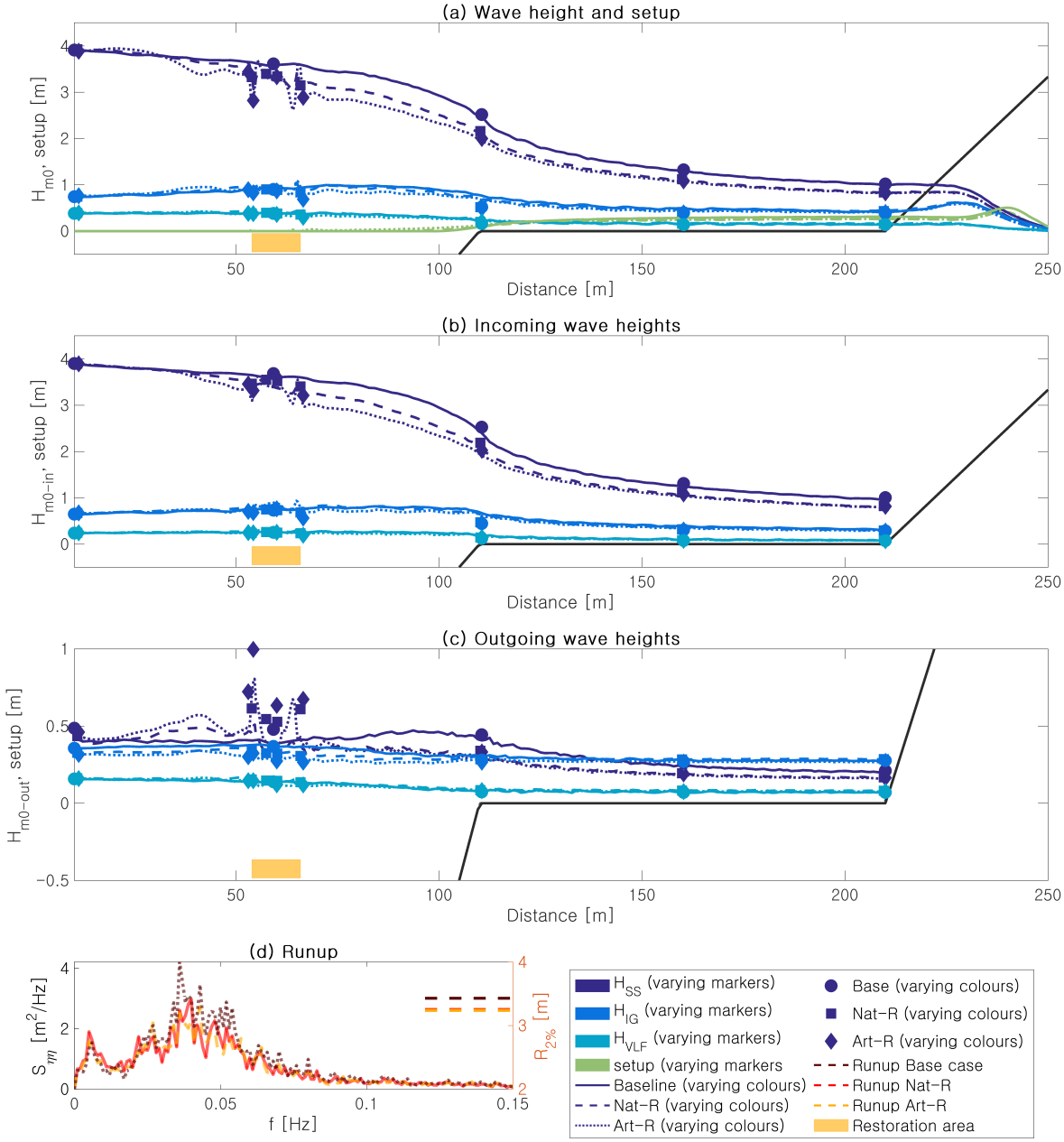

Figure D.1: Wave transformation and runup across a restoration at the **lower forereef of the typical profile**, displaying the total (subplot a), the incoming (subplot b) and the outgoing (subplot c) SS, IG and VLF waves, as well as the runup (subplot d)

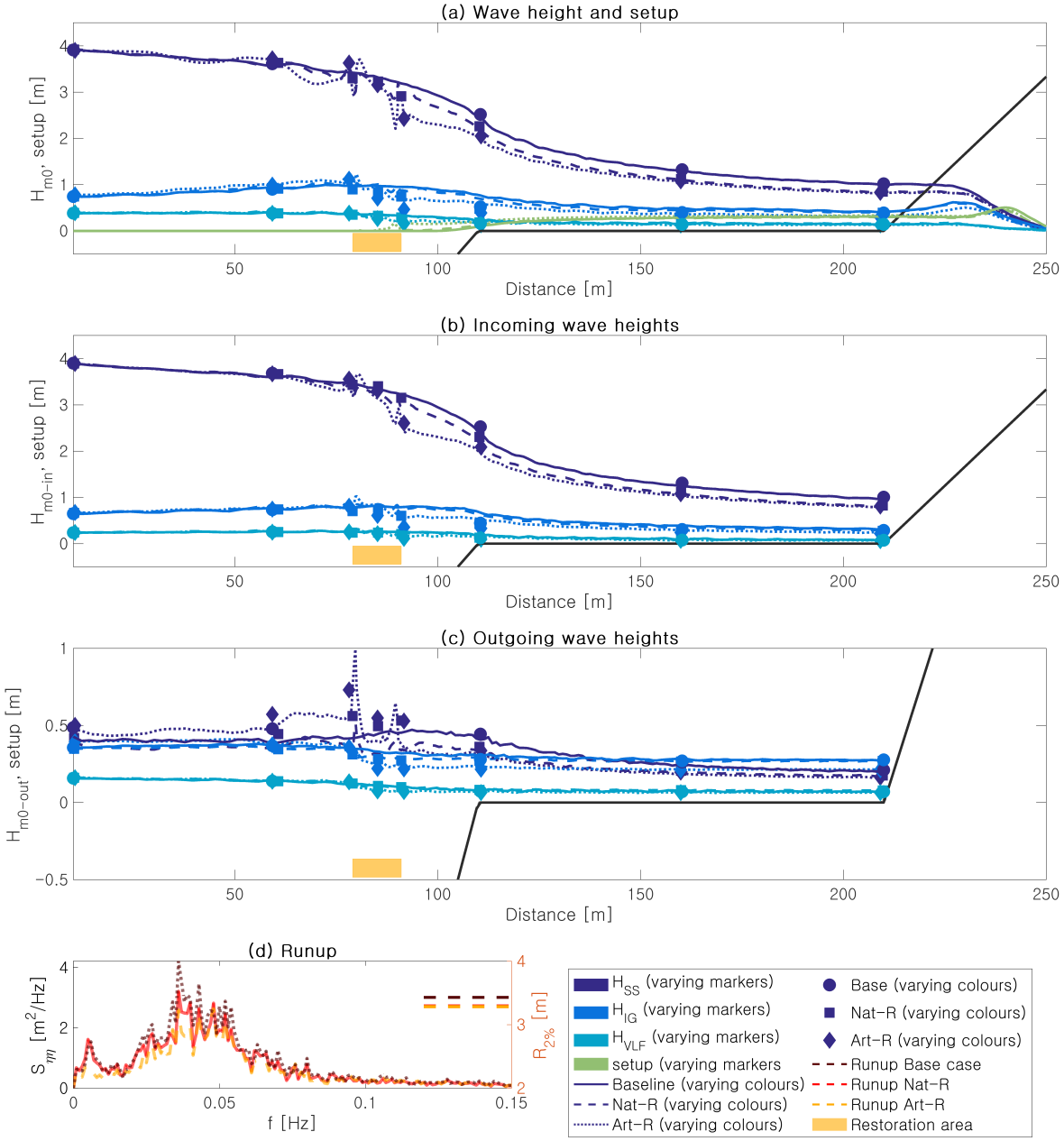

Figure D.2: Wave transformation and runup across a restoration at the **upper forereef of the typical profile**, displaying the total (subplot a), the incoming (subplot b) and the outgoing (subplot c) SS, IG and VLF waves, as well as the runup (subplot d)

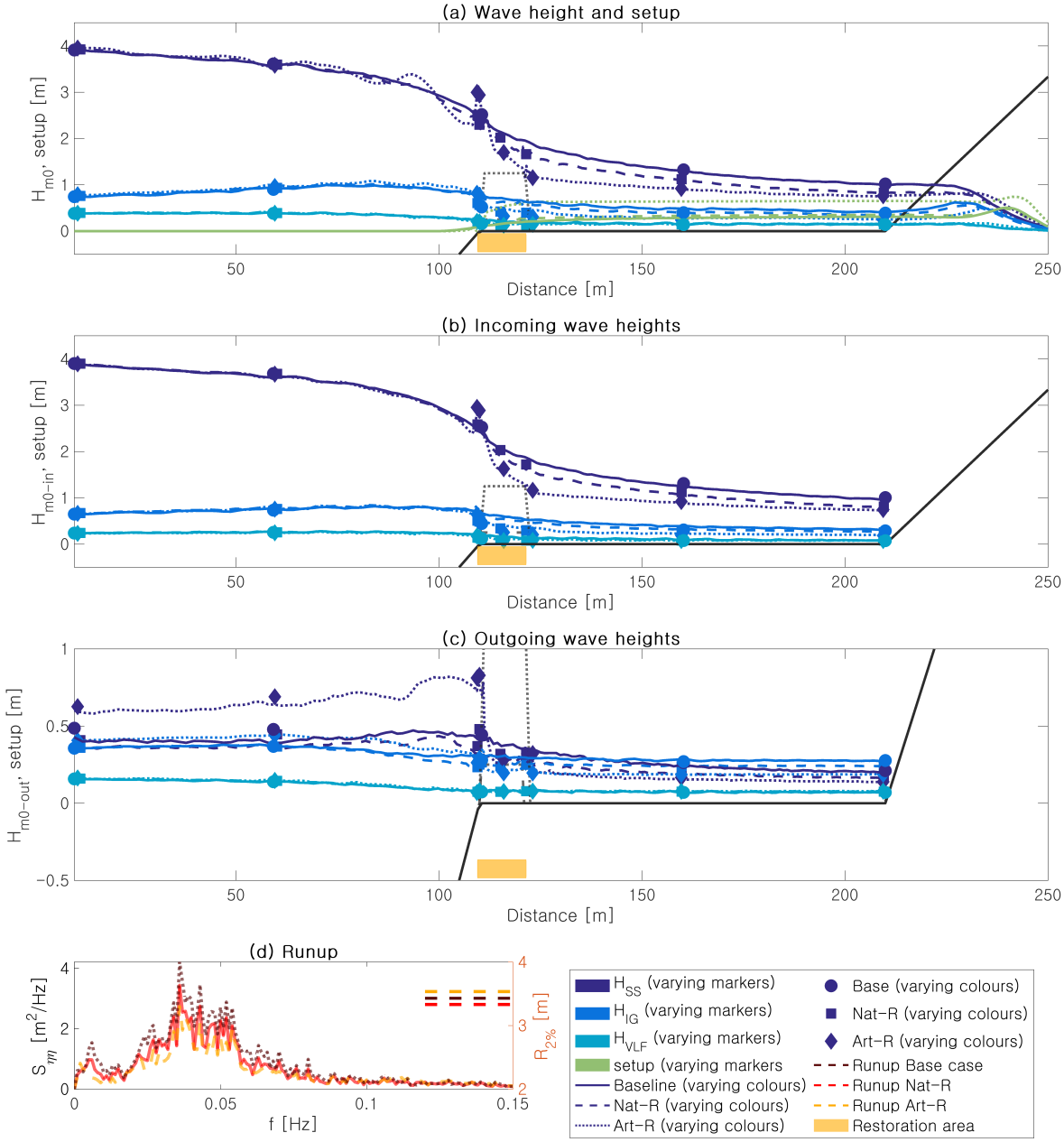

Figure D.3: Wave transformation and runup across a restoration at the **reef edge of the typical profile**, displaying the total (subplot a), the incoming (subplot b) and the outgoing (subplot c) SS, IG and VLF waves, as well as the runup (subplot d)

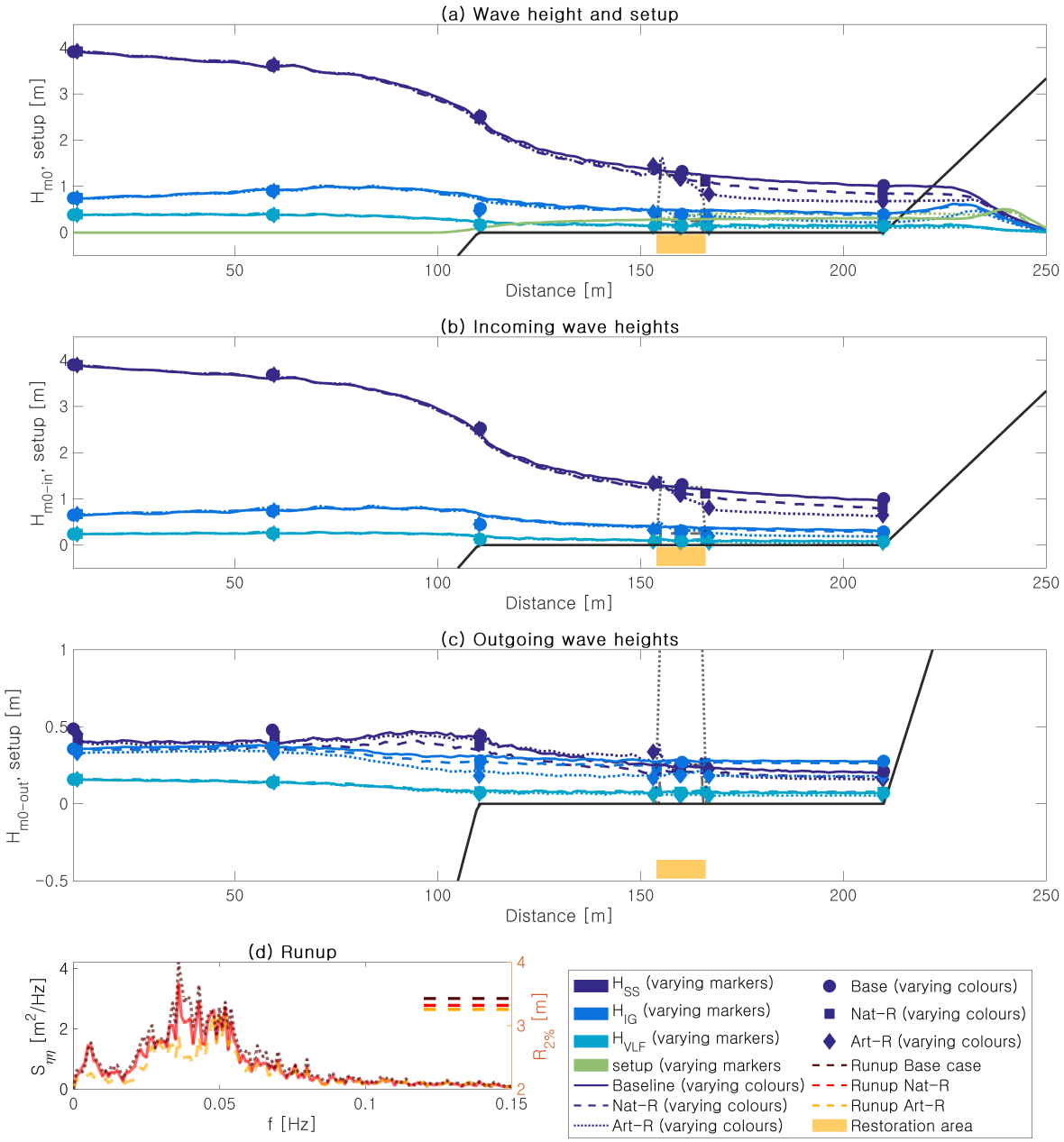

Figure D.4: Wave transformation and runup across a restoration at the **mid-flat of the typical profile**, displaying the total (subplot a), the incoming (subplot b) and the outgoing (subplot c) SS, IG and VLF waves, as well as the runup (subplot d)

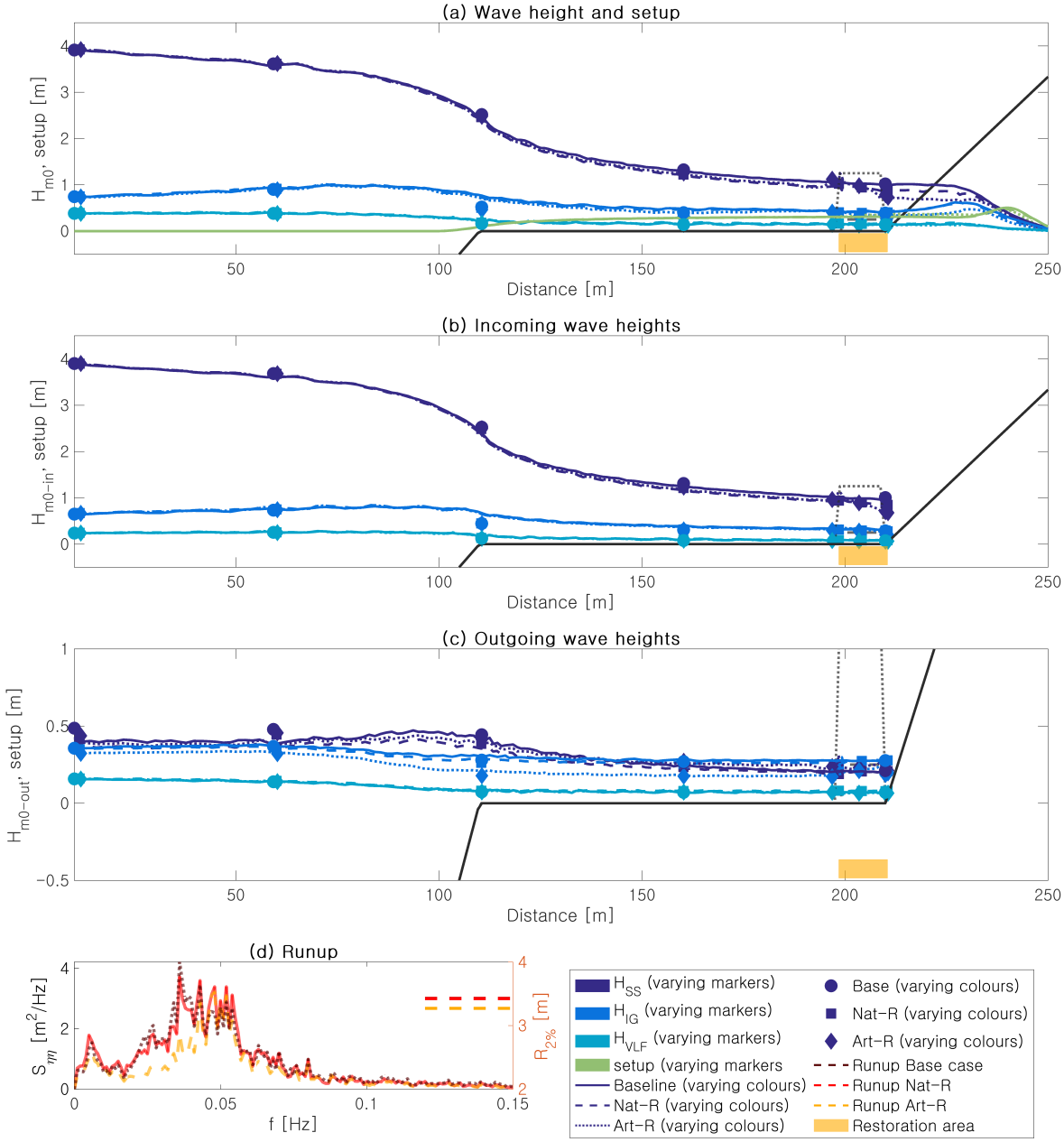

Figure D.5: Wave transformation and runup across a restoration at the **inner reef flat of the typical profile**, displaying the total (subplot a), the incoming (subplot b) and the outgoing (subplot c) SS, IG and VLF waves, as well as the runup (subplot d)

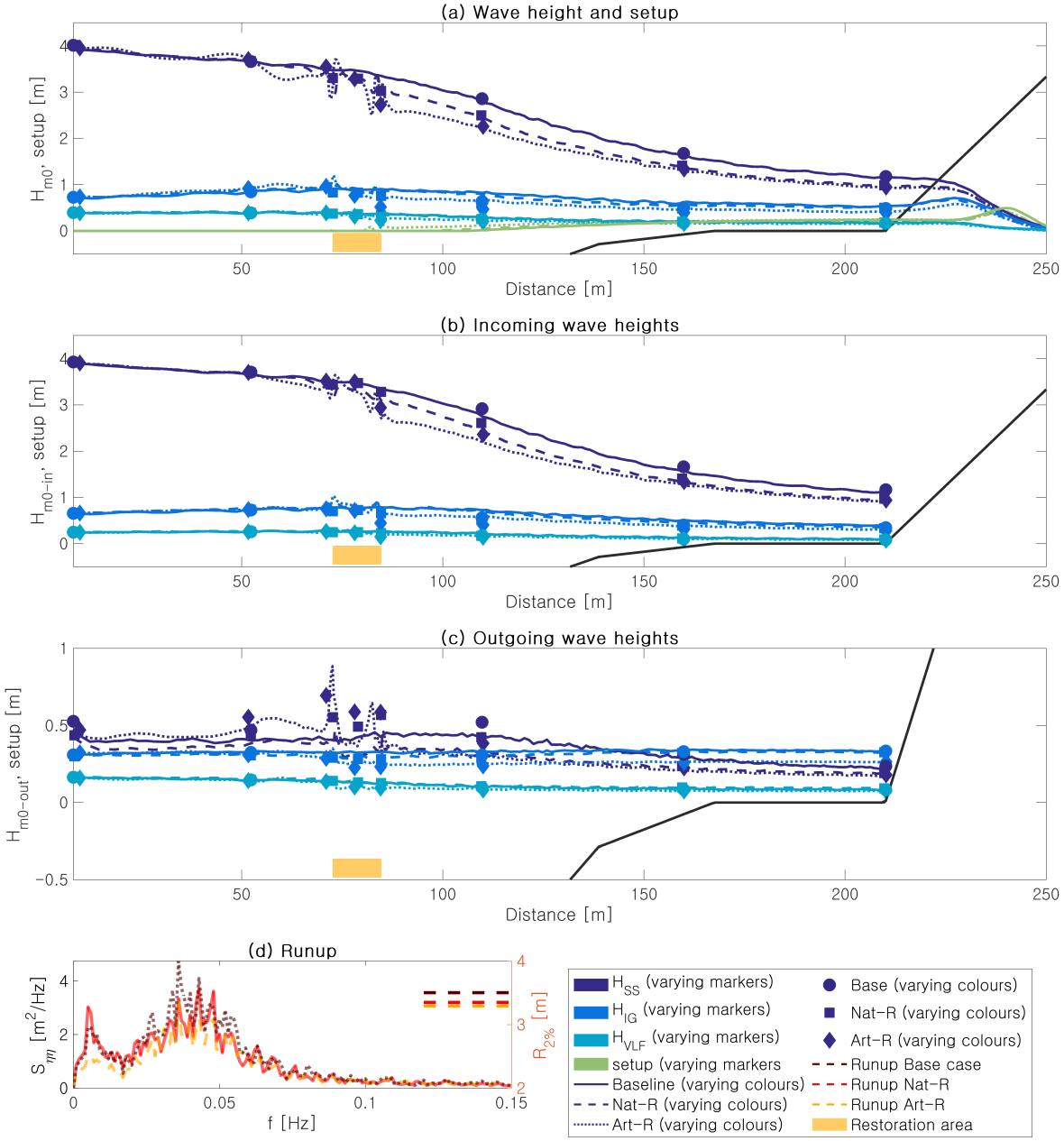

Figure D.6: Wave transformation and runup across a restoration at the **lower forereef of the convex profile**, displaying the total (subplot a), the incoming (subplot b) and the outgoing (subplot c) SS, IG and VLF waves, as well as the runup (subplot d)

Table D.1: Summary of wave transformation characteristics across the **lower forereef restoration of the convex reef profile** (restoration 1 in Figure 6.2), displaying the wave transmission across the restoration (ratio of wave heights shoreward versus seaward of the restoration), the setup across the restoration, the wave heights and total setup at the beach toe and the runup components. Other table characteristics are noted in the Intermezzo on page 78.

	Wave transmission restoration [-]			**Beach toe wave heights [m]**			**Runup [m]**		
	Baseline	*Natural*	*Artificial*	*Baseline*	*Natural*	*Artificial*	*Baseline*	*Natural*	*Artificial*
SS	0.96	0.93 *(-3 %)*	0.80 *(-16 %)*	1.13	0.95 *(-16 %)*	0.91 *(-19 %)*	0.51	0.52 *(+1 %)*	0.49 *(-5 %)*
IG	1.01	1.03 *(+2 %)*	0.76 *(-25 %)*	0.40	0.35 *(-13 %)*	0.30 *(-24 %)*	0.50	0.46 *(-8 %)*	0.38 *(-22 %)*
VLF	1.02	0.99 *(-2 %)*	0.67 *(-34 %)*	0.10	0.09 *(-8 %)*	0.08 *(-22 %)*	0.02	0.03 *(+36 %)*	0.01 *(-20 %)*
	Across restoration [m]			**Beach toe [m]**			**Runup [m]**		
	Baseline	*Natural*	*Artificial*	*Baseline*	*Natural*	*Artificial*	*Baseline*	*Natural*	*Artificial*
Setup	0.00	0.00	0.08	0.24	0.22 *(-9 %)*	0.25 *(+2 %)*	0.62	0.52 *(-16 %)*	0.53 *(-14 %)*
Total							1.64	1.52 *(-8 %)*	1.42 *(-14 %)*

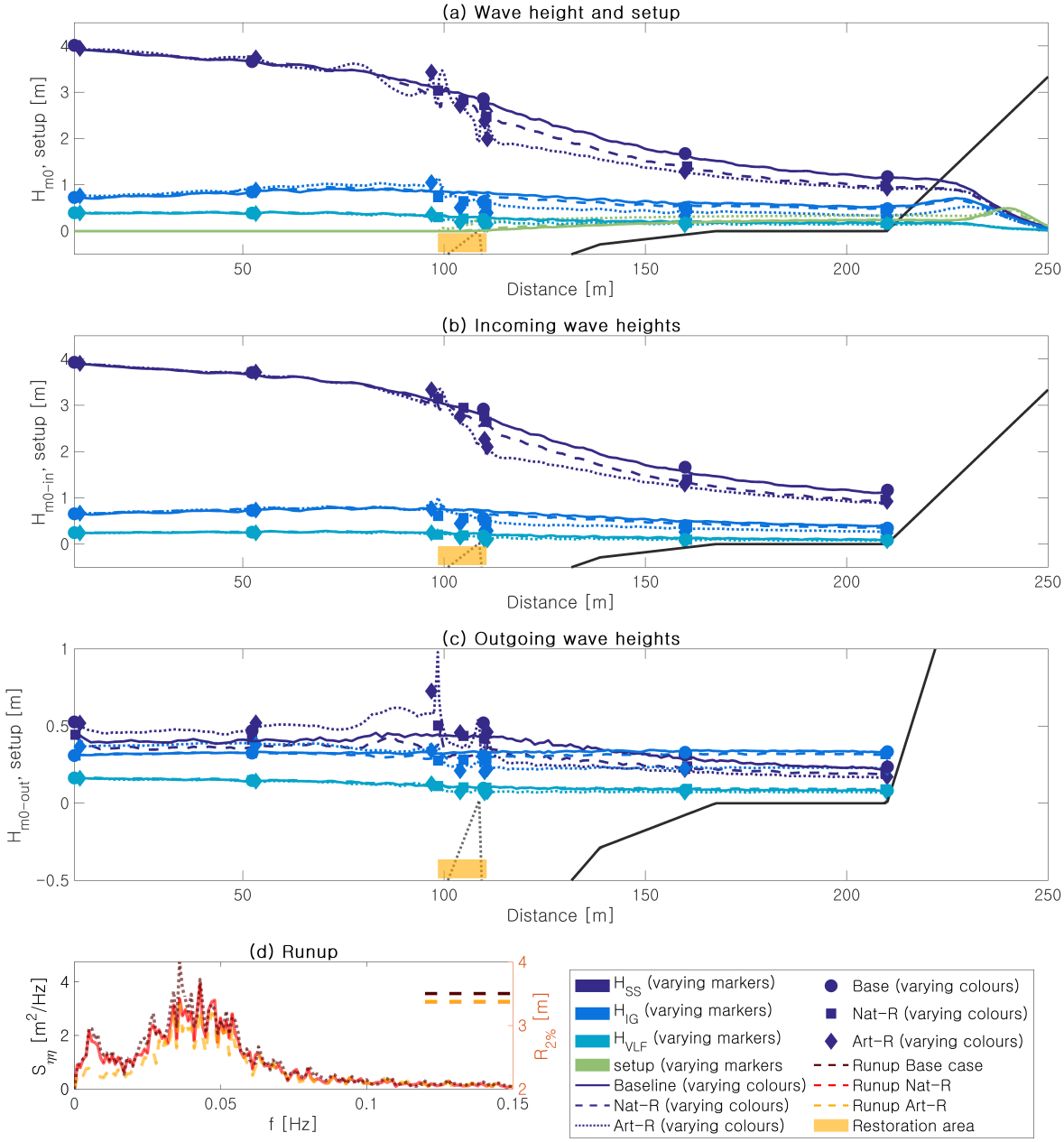

Figure D.7: Wave transformation and runup across a restoration at the **upper forereef of the convex profile**, displaying the total (subplot a), the incoming (subplot b) and the outgoing (subplot c) SS, IG and VLF waves, as well as the runup (subplot d)

Table D.2: Summary of wave transformation characteristics across the **upper forereef restoration of the convex reef profile** (restoration 2 in Figure 6.2), displaying the wave transmission across the restoration (ratio of wave heights shoreward versus seaward of the restoration), the setup across the restoration, the wave heights and total setup at the beach toe and the runup components. Other table characteristics are noted in the Intermezzo on page 78.

	Wave transmission restoration [-]			**Beach toe wave heights [m]**			**Runup [m]**		
	Baseline	*Natural*	*Artificial*	*Baseline*	*Natural*	*Artificial*	*Baseline*	*Natural*	*Artificial*
SS	0.89	0.83 *(-7 %)*	0.61 *(-31 %)*	1.11	0.93 *(-16 %)*	0.89 *(-20 %)*	0.51	0.51 *(-1 %)*	0.50 *(-2 %)*
IG	0.97	0.91 *(-6 %)*	0.53 *(-45 %)*	0.40	0.35 *(-11 %)*	0.27 *(-32 %)*	0.50	0.45 *(-10 %)*	0.36 *(-27 %)*
VLF	0.84	0.80 *(-5 %)*	0.50 *(-41 %)*	0.10	0.09 *(-4 %)*	0.09 *(-9 %)*	0.02	0.02 *(+1 %)*	0.02 *(-12 %)*
	Across restoration [m]			**Beach toe [m]**			**Runup [m]**		
	Baseline	*Natural*	*Artificial*	*Baseline*	*Natural*	*Artificial*	*Baseline*	*Natural*	*Artificial*
Setup	0.01	0.05	0.24	0.24	0.25 *(+3 %)*	0.34 *(+41 %)*	0.62	0.54 *(-13 %)*	0.62 *(+1 %)*
Total							1.64	1.51 *(-8 %)*	1.50 *(-8 %)*

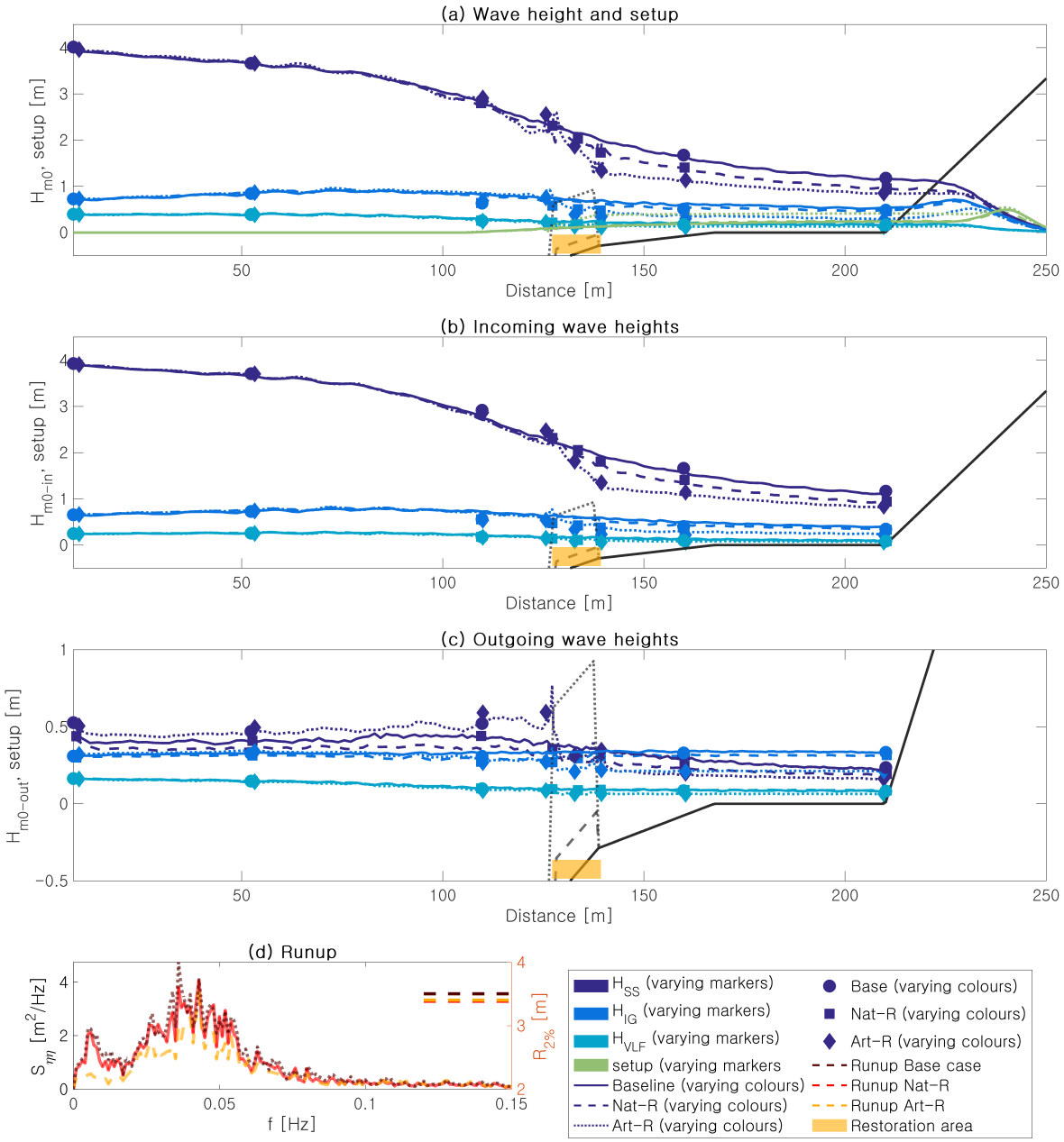

Figure D.8: Wave transformation and runup across a restoration at the **reef edge of the convex profile**, displaying the total (subplot a), the incoming (subplot b) and the outgoing (subplot c) SS, IG and VLF waves, as well as the runup (subplot d)

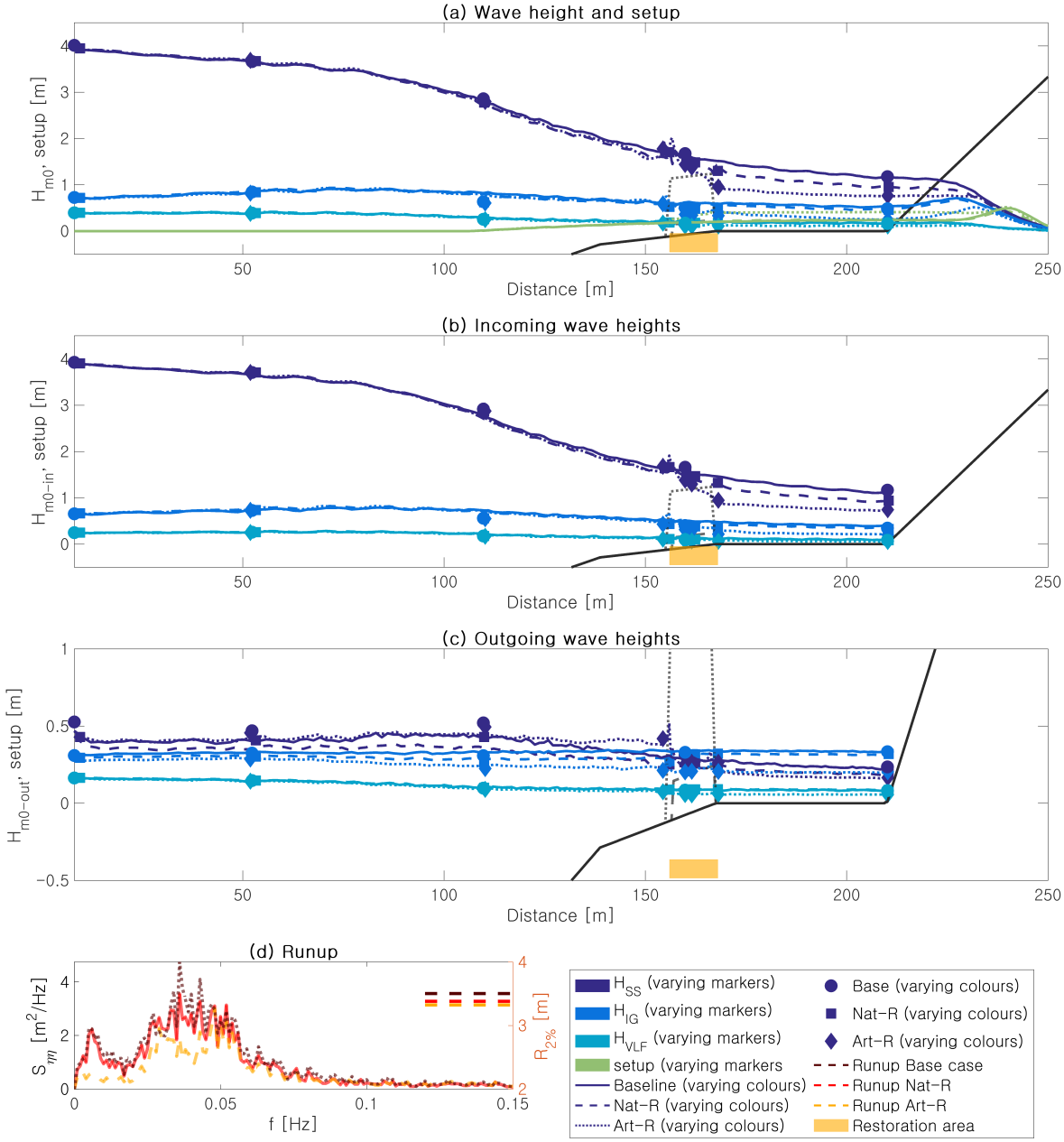

Figure D.9: Wave transformation and runup across a restoration at the **upper sloping part of the convex profile**, displaying the total (subplot a), the incoming (subplot b) and the outgoing (subplot c) SS, IG and VLF waves, as well as the runup (subplot d)

Table D.3: Summary of wave transformation characteristics across the **upper slope restoration of the convex reef profile** (restoration 4 in Figure 6.2), displaying the wave transmission across the restoration (ratio of wave heights shoreward versus seaward of the restoration), the setup across the restoration, the wave heights and total setup at the beach toe and the runup components. Other table characteristics are noted in the Intermezzo on page 78.

	Wave transmission restoration [-]			**Beach toe wave heights [m]**			**Runup [m]**		
	Baseline	*Natural*	*Artificial*	*Baseline*	*Natural*	*Artificial*	*Baseline*	*Natural*	*Artificial*
SS	0.90	0.79 *(-13 %)*	0.55 *(-39 %)*	1.13	0.92 *(-18 %)*	0.72 *(-36 %)*	0.51	0.51 *(-1 %)*	0.47 *(-7 %)*
IG	0.94	0.83 *(-11 %)*	0.57 *(-40 %)*	0.40	0.35 *(-13 %)*	0.21 *(-47 %)*	0.50	0.45 *(-9 %)*	0.33 *(-33 %)*
VLF	0.87	0.89 *(+3 %)*	0.67 *(-22 %)*	0.10	0.09 *(-7 %)*	0.06 *(-40 %)*	0.02	0.03 *(+36 %)*	0.02 *(-7 %)*
	Across restoration [m]			**Beach toe [m]**			**Runup [m]**		
	Baseline	*Natural*	*Artificial*	*Baseline*	*Natural*	*Artificial*	*Baseline*	*Natural*	*Artificial*
Setup	0.02	0.06	0.24	0.24	0.25 *(+4 %)*	0.41 *(+69 %)*	0.62	0.54 *(-13 %)*	0.63 *(+2 %)*
Total							1.64	1.52 *(-7 %)*	1.45 *(-12 %)*

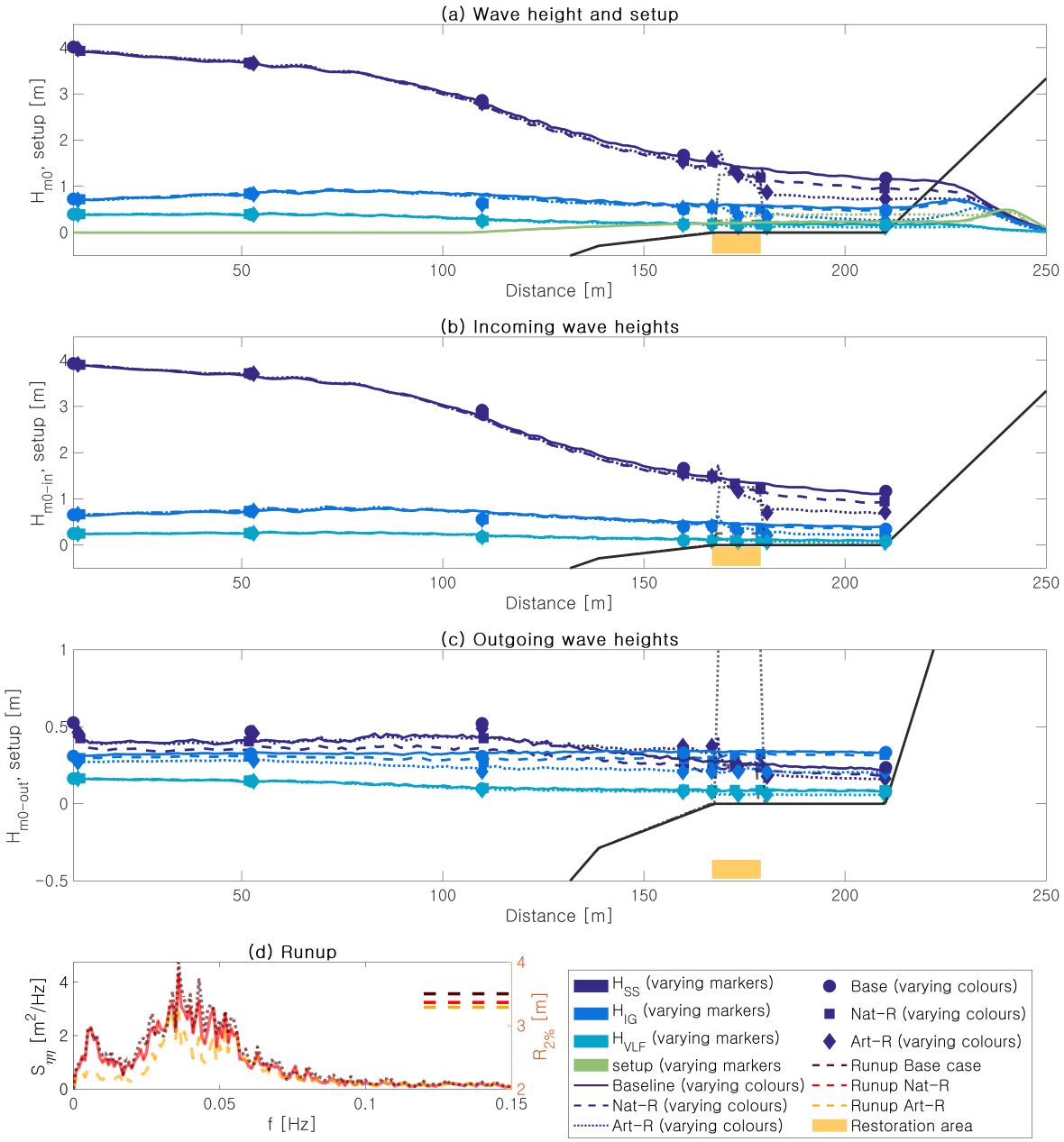

Figure D.10: Wave transformation and runup across a restoration at the **mid-flat of the convex profile**, displaying the total (subplot a), the incoming (subplot b) and the outgoing (subplot c) SS, IG and VLF waves, as well as the runup (subplot d)

Table D.4: Summary of wave transformation characteristics across the **mid-flat restoration of the convex reef profile** (restoration 5 in Figure 6.2), displaying the wave transmission across the restoration (ratio of wave heights shoreward versus seaward of the restoration), the setup across the restoration, the wave heights and total setup at the beach toe and the runup components. Other table characteristics are noted in the Intermezzo on page 78.

	Wave transmission restoration [-]			**Beach toe wave heights [m]**			**Runup [m]**		
	Baseline	*Natural*	*Artificial*	*Baseline*	*Natural*	*Artificial*	*Baseline*	*Natural*	*Artificial*
SS	0.91	0.81 *(-11%)*	0.55 *(-40%)*	1.13	0.93 *(-17%)*	0.69 *(-39%)*	0.51	0.49 *(-4%)*	0.45 *(-13%)*
IG	0.94	0.80 *(-14%)*	0.58 *(-38%)*	0.40	0.35 *(-12%)*	0.22 *(-45%)*	0.50	0.48 *(-4%)*	0.36 *(-27%)*
VLF	0.98	0.81 *(-17%)*	0.77 *(-22%)*	0.10	0.09 *(-10%)*	0.06 *(-43%)*	0.02	0.02 *(+14%)*	0.02 *(-10%)*
	Across restoration [m]			**Beach toe [m]**			**Runup [m]**		
	Baseline	*Natural*	*Artificial*	*Baseline*	*Natural*	*Artificial*	*Baseline*	*Natural*	*Artificial*
Setup	0.02	0.05	0.20	0.24	0.25 *(+4%)*	0.39 *(+62%)*	0.62	0.54 *(-13%)*	0.60 *(-2%)*
Total							1.64	1.52 *(-7%)*	1.43 *(-13%)*

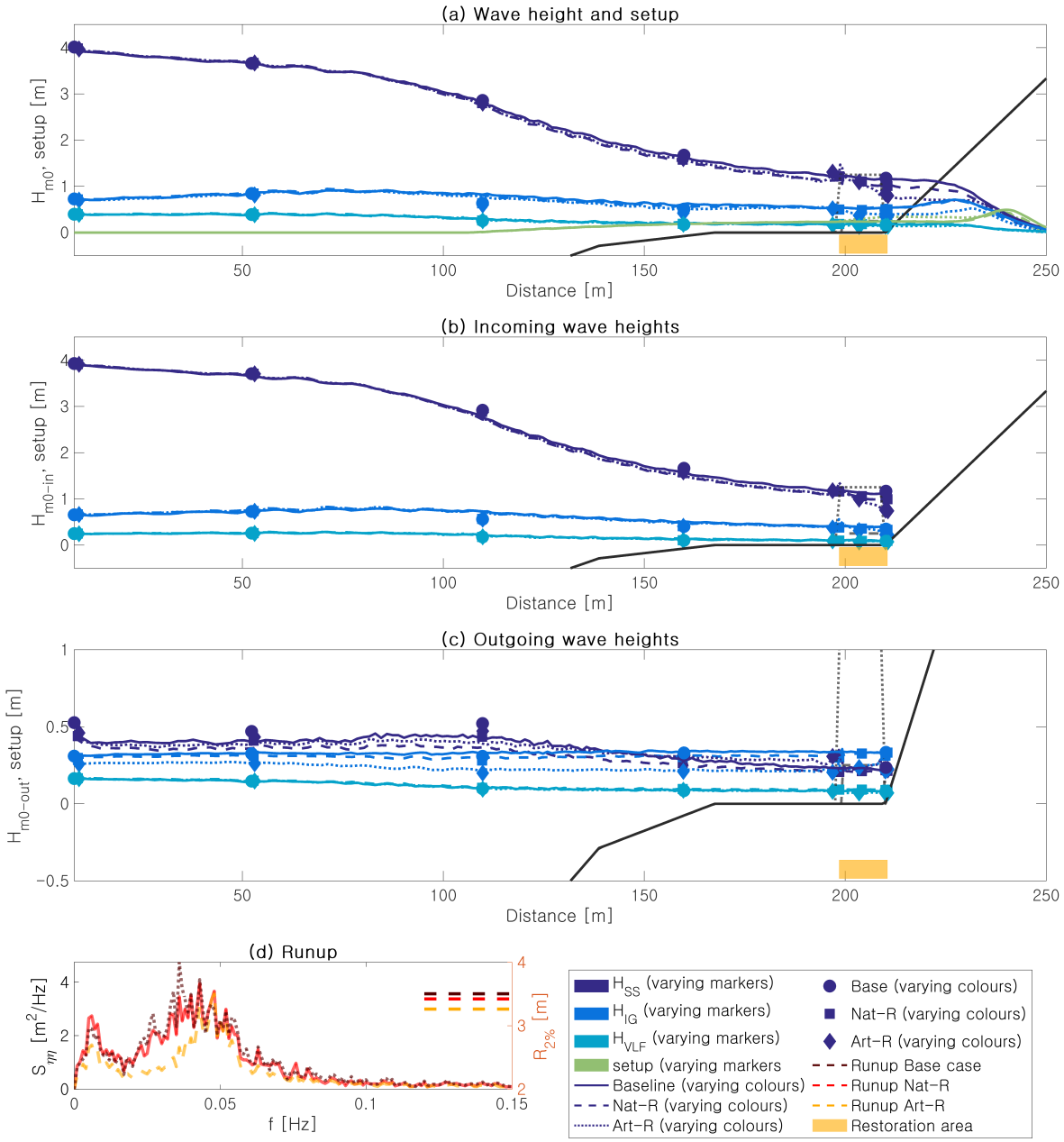

Figure D.11: Wave transformation and runup across a restoration at the **inner reef flat of the convex profile**, displaying the total (subplot a), the incoming (subplot b) and the outgoing (subplot c) SS, IG and VLF waves, as well as the runup (subplot d)

Table D.5: Summary of wave transformation characteristics across the **inner flat restoration of the convex reef profile** (restoration 6 in Figure 6.2), displaying the wave transmission across the restoration (ratio of wave heights shoreward versus seaward of the restoration), the setup across the restoration, the wave heights and total setup at the beach toe and the runup components. Other table characteristics are noted in the Intermezzo on page 78.

	Wave transmission restoration [-]			**Beach toe wave heights [m]**			**Runup [m]**		
	Baseline	*Natural*	*Artificial*	*Baseline*	*Natural*	*Artificial*	*Baseline*	*Natural*	*Artificial*
SS	0.96	0.86 *(-10 %)*	0.63 *(-35 %)*	1.13	1.01 *(-11 %)*	0.72 *(-36 %)*	0.51	0.52 *(+2 %)*	0.51 *(-1 %)*
IG	0.97	0.86 *(-12 %)*	0.65 *(-33 %)*	0.40	0.39 *(-4 %)*	0.29 *(-28 %)*	0.50	0.49 *(-1 %)*	0.31 *(-37 %)*
VLF	1.12	1.05 *(-7 %)*	0.91 *(-19 %)*	0.10	0.10 *(0 %)*	0.09 *(-16 %)*	0.02	0.03 *(+53 %)*	0.02 *(+27 %)*
	Across restoration [m]			**Beach toe [m]**			**Runup [m]**		
	Baseline	*Natural*	*Artificial*	*Baseline*	*Natural*	*Artificial*	*Baseline*	*Natural*	*Artificial*
Setup	0.01	0.02	0.11	0.24	0.23 *(-3 %)*	0.32 *(+33 %)*	0.62	0.54 *(-12 %)*	0.54 *(-13 %)*
Total							1.64	1.58 *(-4 %)*	1.38 *(-16 %)*

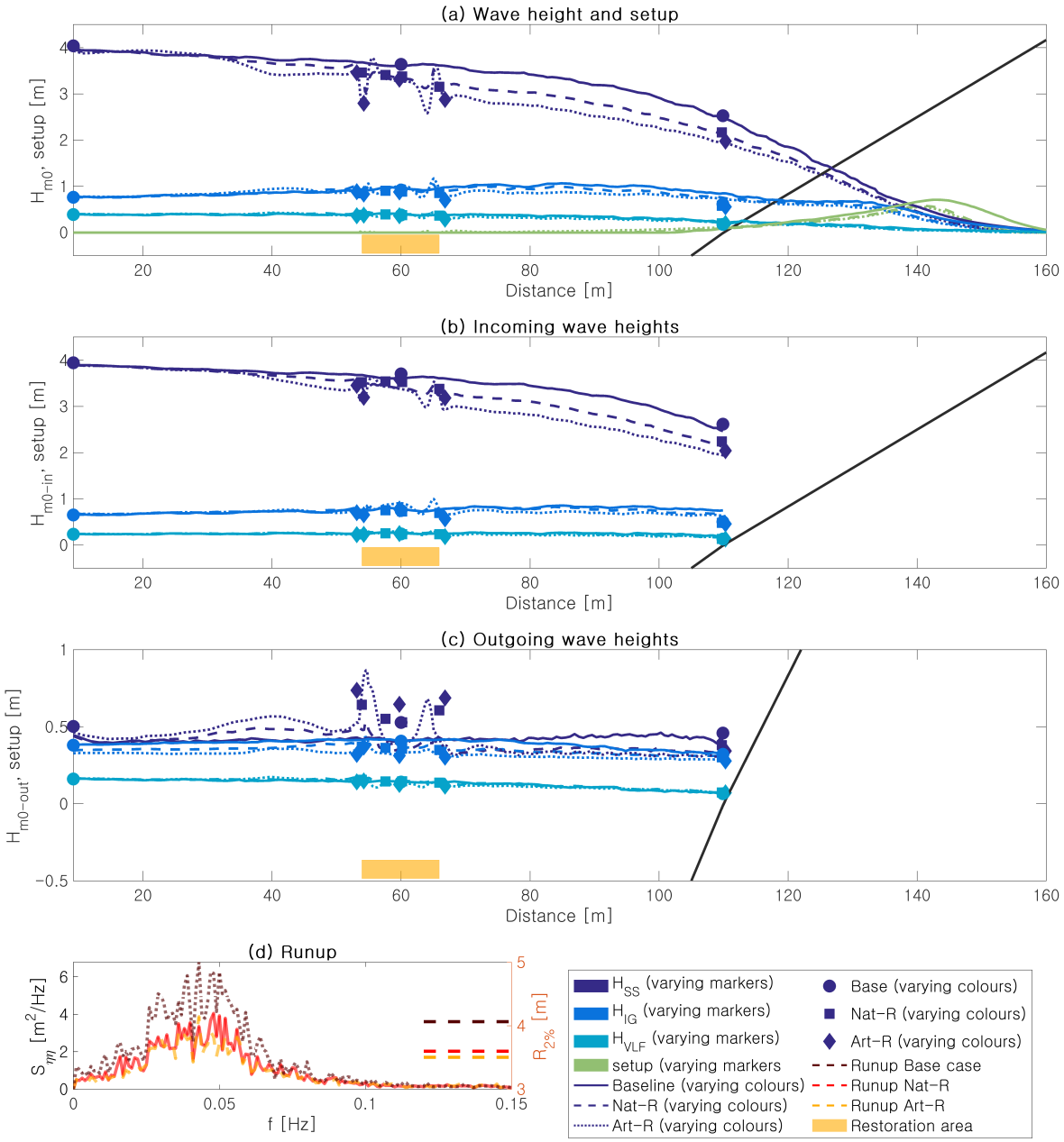

Figure D.12: Wave transformation and runup across a restoration at the **lower forereef of the straight profile**, displaying the total (subplot a), the incoming (subplot b) and the outgoing (subplot c) SS, IG and VLF waves, as well as the runup (subplot d)

Table D.6: Summary of wave transformation characteristics across the **lower forereef restoration of the straight reef profile** (restoration 1 in Figure 6.2), displaying the wave transmission across the restoration (ratio of wave heights shoreward versus seaward of the restoration), the setup across the restoration, the wave heights and total setup at the beach toe and the runup components. Other table characteristics are noted in the Intermezzo on page 78.

	Wave transmission restoration [-]			**Beach toe wave heights [m]**			**Runup [m]**		
	Baseline	*Natural*	*Artificial*	*Baseline*	*Natural*	*Artificial*	*Baseline*	*Natural*	*Artificial*
SS	0.98	0.94 *(-4 %)*	0.88 *(-11 %)*	2.46	2.13 *(-13 %)*	1.93 *(-22 %)*	0.60	0.56 *(-7 %)*	0.52 *(-13 %)*
IG	1.01	1.05 *(+4 %)*	0.93 *(-8 %)*	0.75	0.67 *(-11 %)*	0.62 *(-17 %)*	0.66	0.44 *(-34 %)*	0.43 *(-35 %)*
VLF	1.06	1.08 *(+1 %)*	0.95 *(-10 %)*	0.19	0.16 *(-15 %)*	0.15 *(-20 %)*	0.05	0.03 *(-37 %)*	0.02 *(-53 %)*
	Across restoration [m]			**Beach toe [m]**			**Runup [m]**		
	Baseline	*Natural*	*Artificial*	*Baseline*	*Natural*	*Artificial*	*Baseline*	*Natural*	*Artificial*
Setup	0.00	0.00	0.02	0.08	0.09 *(+5 %)*	0.12 *(+40 %)*	0.95	0.72 *(-24 %)*	0.69 *(-28 %)*
Total							2.26	1.75 *(-23 %)*	1.66 *(-27 %)*

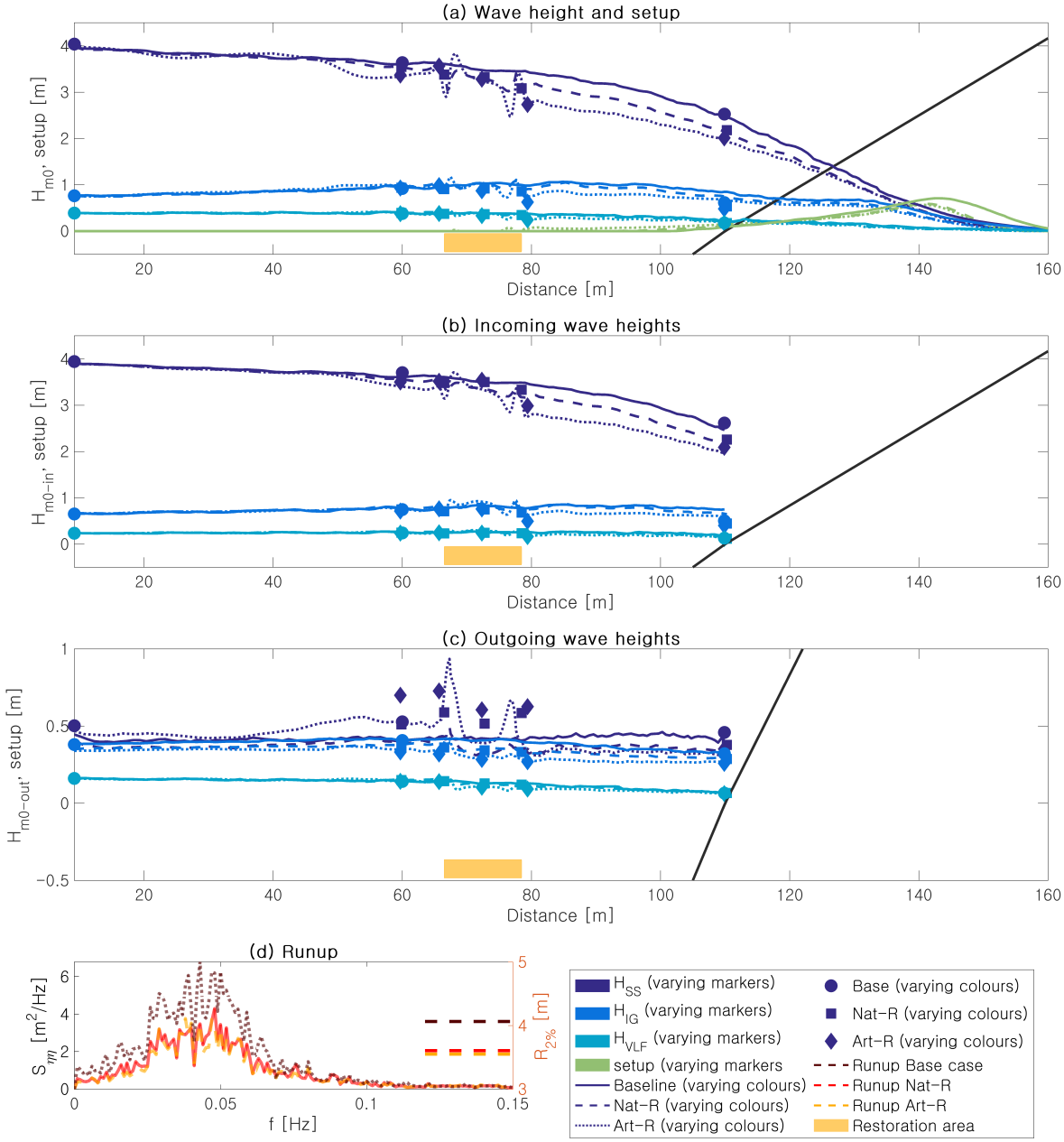

Figure D.13: Wave transformation and runup across a restoration at the **mid-forereef of the straight profile**, displaying the total (subplot a), the incoming (subplot b) and the outgoing (subplot c) SS, IG and VLF waves, as well as the runup (subplot d)

Table D.7: Summary of wave transformation characteristics across the **mid-forereef restoration of the straight reef profile** (restoration 2 in Figure 6.2), displaying the wave transmission across the restoration (ratio of wave heights shoreward versus seaward of the restoration), the setup across the restoration, the wave heights and total setup at the beach toe and the runup components. Other table characteristics are noted in the Intermezzo on page 78.

	Wave transmission restoration [-]			**Beach toe wave heights [m]**			**Runup [m]**		
	Baseline	*Natural*	*Artificial*	*Baseline*	*Natural*	*Artificial*	*Baseline*	*Natural*	*Artificial*
SS	0.97	0.93 *(-4 %)*	0.81 *(-16 %)*	2.45	2.13 *(-13 %)*	1.96 *(-20 %)*	0.60	0.56 *(-7 %)*	0.53 *(-12 %)*
IG	1.01	1.02 *(+1 %)*	0.79 *(-22 %)*	0.75	0.65 *(-13 %)*	0.60 *(-20 %)*	0.66	0.43 *(-34 %)*	0.43 *(-35 %)*
VLF	1.04	1.03 *(-1 %)*	0.79 *(-24 %)*	0.18	0.15 *(-19 %)*	0.15 *(-18 %)*	0.05	0.02 *(-45 %)*	0.02 *(-59 %)*
	Across restoration [m]			**Beach toe [m]**			**Runup [m]**		
	Baseline	*Natural*	*Artificial*	*Baseline*	*Natural*	*Artificial*	*Baseline*	*Natural*	*Artificial*
Setup	0.00	0.00	0.05	0.09	0.11 *(+21 %)*	0.14 *(+55 %)*	0.95	0.73 *(-23 %)*	0.71 *(-26 %)*
Total							2.26	1.75 *(-22 %)*	1.68 *(-25 %)*

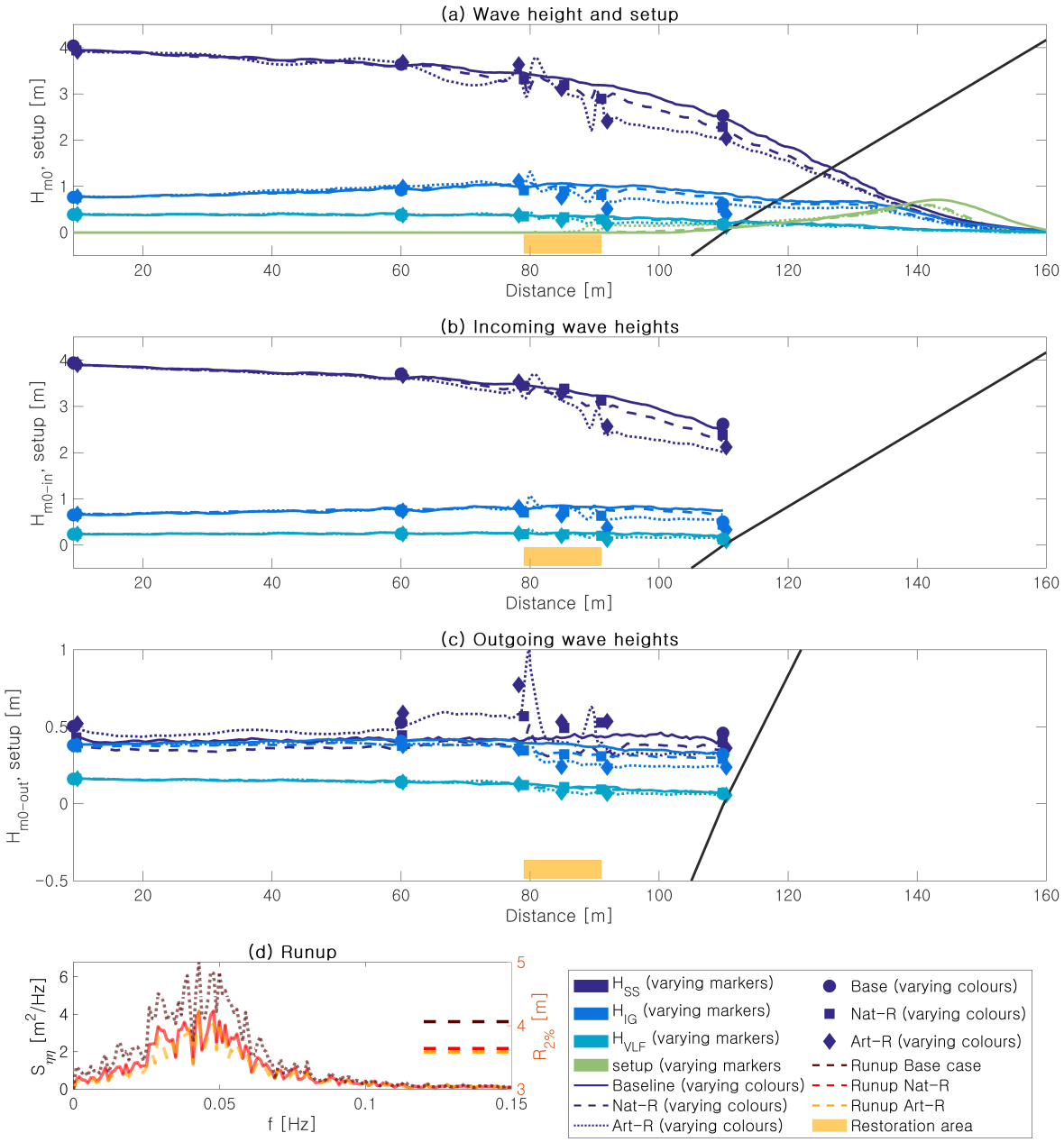

Figure D.14: Wave transformation and runup across a restoration at the **upper forereef of the straight profile**, displaying the total (subplot a), the incoming (subplot b) and the outgoing (subplot c) SS, IG and VLF waves, as well as the runup (subplot d)

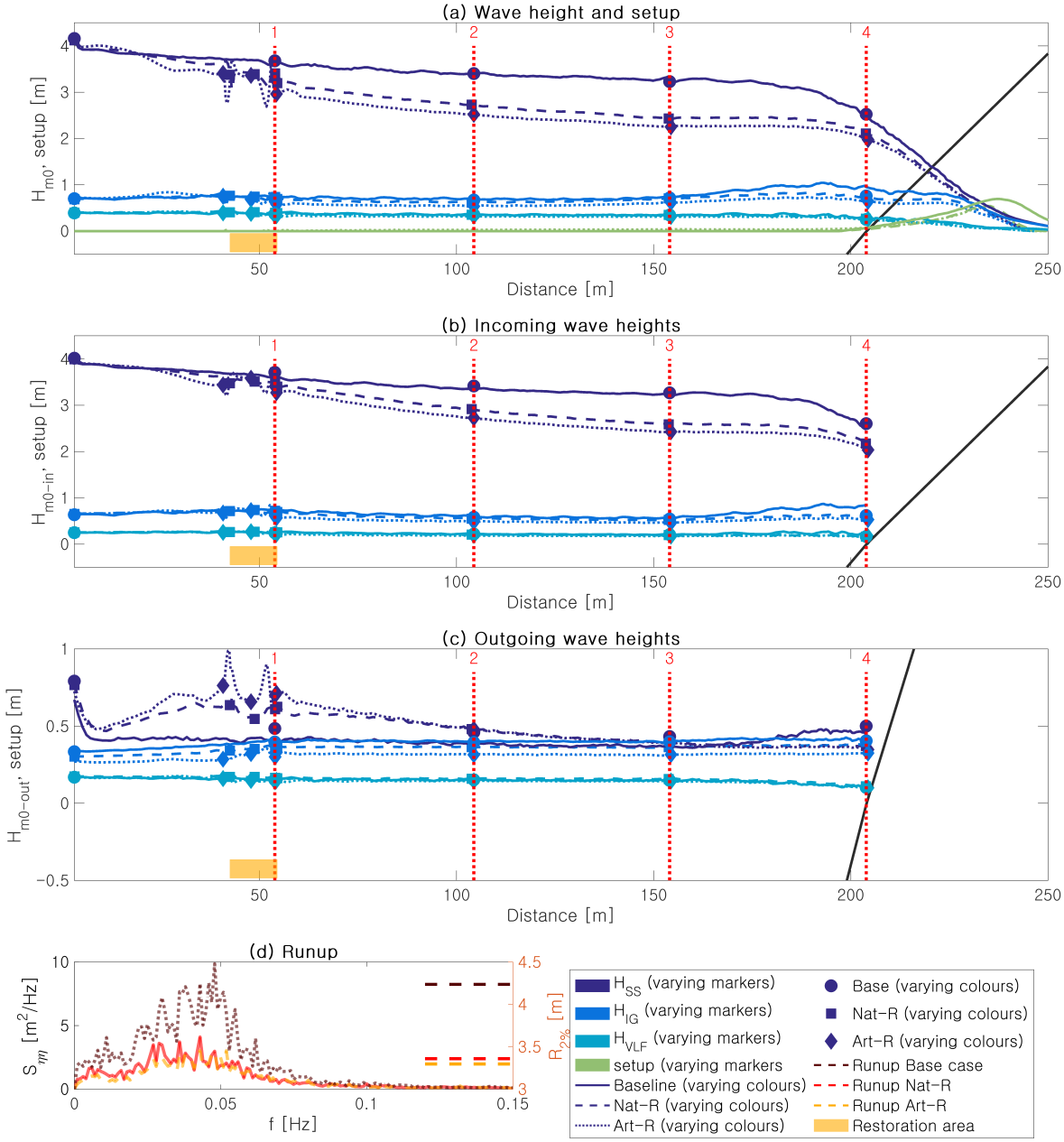

Figure D.15: Wave transformation and runup across a restoration at the **lower forereef of the three-slope profile**, displaying the total (subplot a), the incoming (subplot b) and the outgoing (subplot c) SS, IG and VLF waves, as well as the runup (subplot d). Locations 1 to 4 indicate the shelf edge, the mid-shelf, the inner shelf and the beach toe, respectively.

Table D.8: Summary of wave transformation characteristics across the **lower forereef restoration of the three-slope reef profile** (restoration 1 in Figure 6.2), displaying the wave transmission across the restoration (ratio of wave heights shoreward versus seaward of the restoration), the setup across the restoration, the wave heights and total setup at the beach toe and the runup components. Other table characteristics are noted in the Intermezzo on page 78.

	Wave transmission restoration [-]			**Beach toe wave heights [m]**			**Runup [m]**		
	Baseline	*Natural*	*Artificial*	*Baseline*	*Natural*	*Artificial*	*Baseline*	*Natural*	*Artificial*
SS	0.98	0.98 *(0 %)*	0.95 *(-3 %)*	2.47	2.17 *(-12 %)*	2.04 *(-18 %)*	0.60	0.38 *(-37 %)*	0.40 *(-33 %)*
IG	1.01	0.97 *(-3 %)*	0.85 *(-16 %)*	0.82	0.59 *(-28 %)*	0.53 *(-35 %)*	0.83	0.42 *(-49 %)*	0.38 *(-54 %)*
VLF	0.94	0.98 *(+5 %)*	0.85 *(-10 %)*	0.24	0.16 *(-31 %)*	0.16 *(-32 %)*	0.06	0.01 *(-79 %)*	0.01 *(-82 %)*
	Across restoration [m]			**Beach toe [m]**			**Runup [m]**		
	Baseline	*Natural*	*Artificial*	*Baseline*	*Natural*	*Artificial*	*Baseline*	*Natural*	*Artificial*
Setup	0.00	0.00	0.00	0.06	0.04 *(-37 %)*	0.07 *(+14 %)*	0.95	0.63 *(-34 %)*	0.61 *(-37 %)*
Total							2.45	1.44 *(-41 %)*	1.40 *(-43 %)*

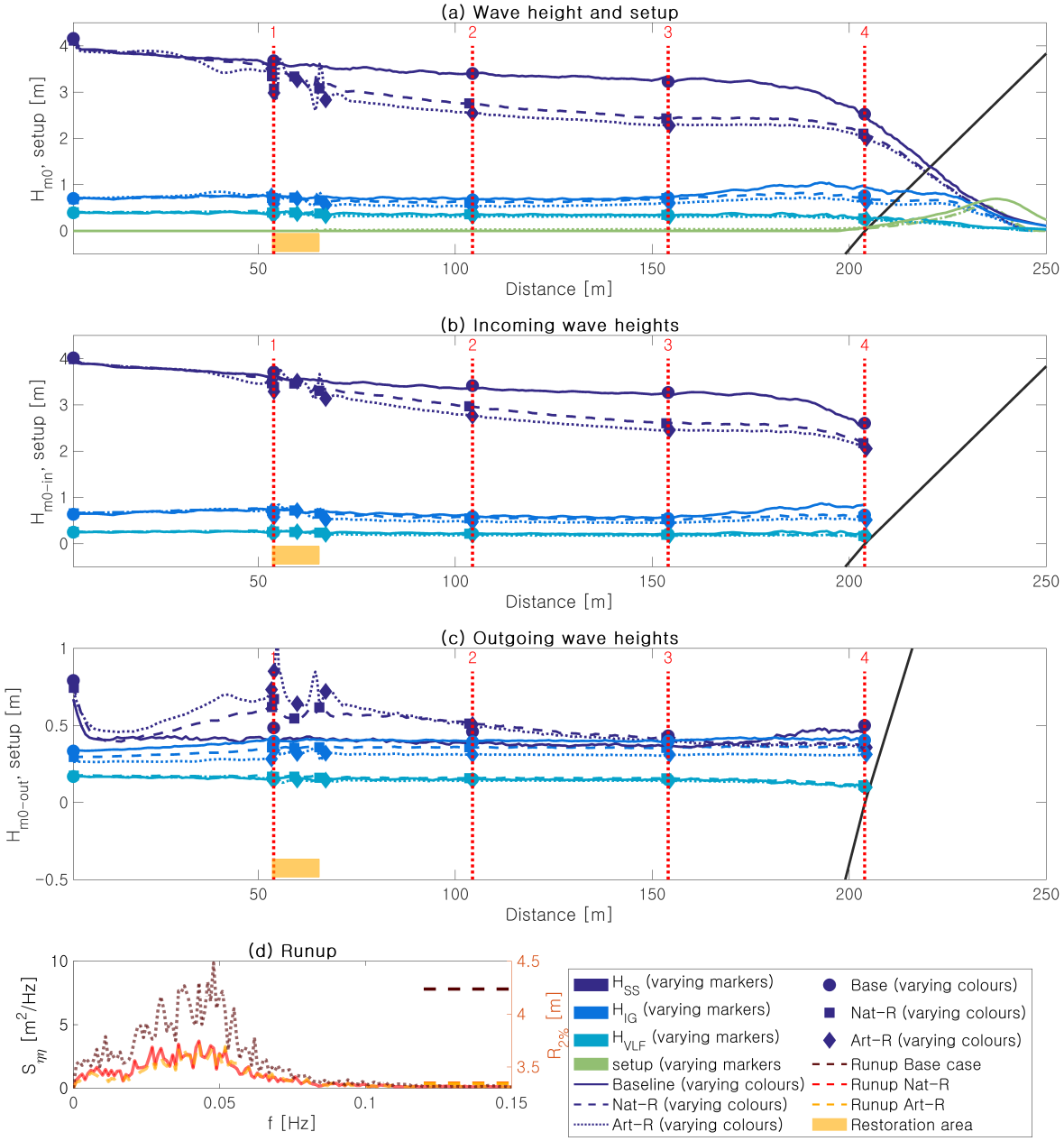

Figure D.16: Wave transformation and runup across a restoration at the **shelf edge of the three-slope profile**, displaying the total (subplot a), the incoming (subplot b) and the outgoing (subplot c) SS, IG and VLF waves, as well as the runup (subplot d). Locations 1 to 4 indicate the shelf edge, the mid-shelf, the inner shelf and the beach toe, respectively.

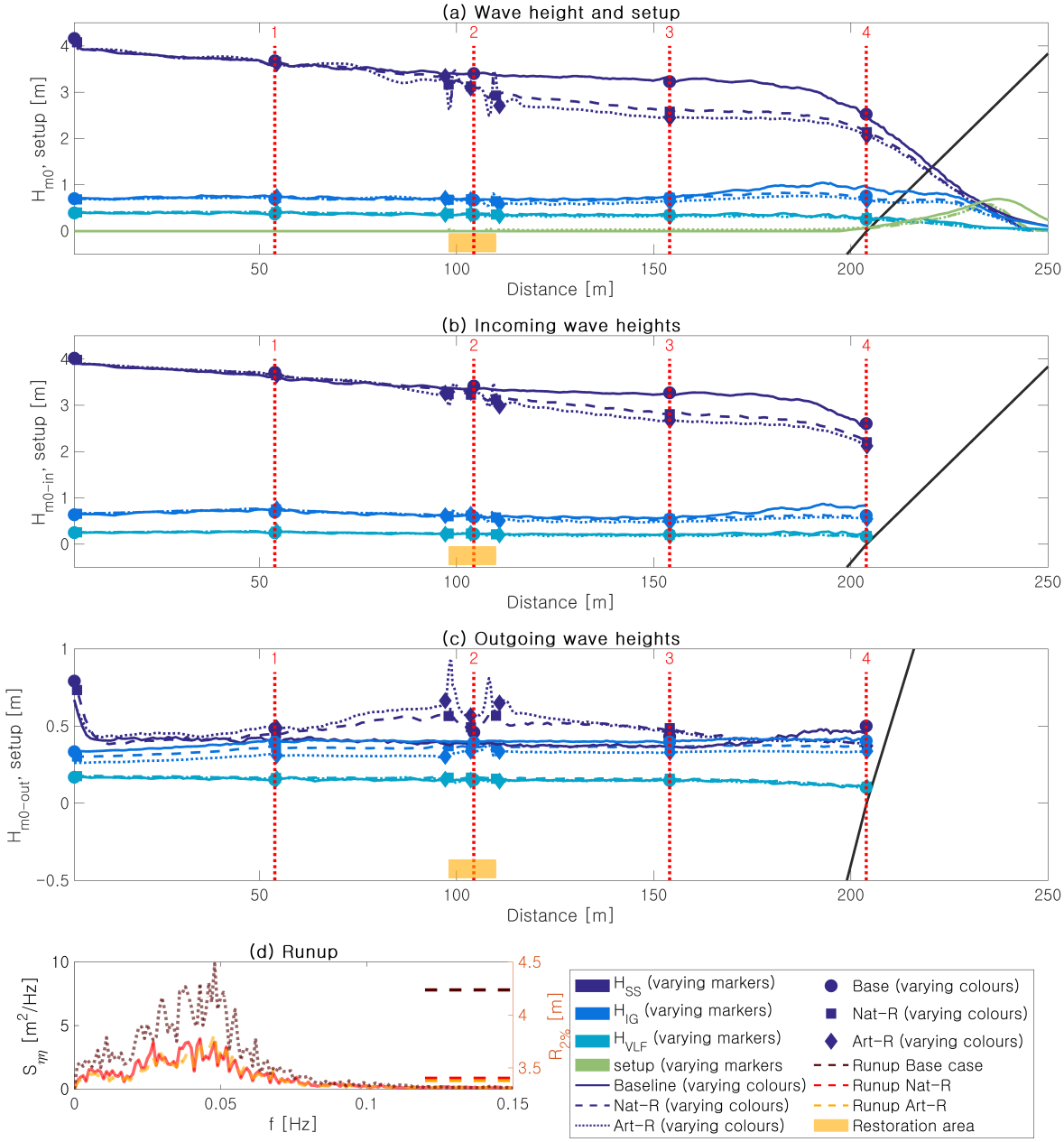

Figure D.17: Wave transformation and runup across a restoration at the **mid-shelf of the three-slope profile**, displaying the total (subplot a), the incoming (subplot b) and the outgoing (subplot c) SS, IG and VLF waves, as well as the runup (subplot d). Locations 1 to 4 indicate the shelf edge, the mid-shelf, the inner shelf and the beach toe, respectively.

Table D.9: Summary of wave transformation characteristics across the **mid-shelf restoration of the three-slope reef profile** (restoration 3 in Figure 6.2), displaying the wave transmission across the restoration (ratio of wave heights shoreward versus seaward of the restoration), the setup across the restoration, the wave heights and total setup at the beach toe and the runup components. Other table characteristics are noted in the Intermezzo on page 78.

	Wave transmission restoration [-]			**Beach toe wave heights [m]**			**Runup [m]**		
	Baseline	*Natural*	*Artificial*	*Baseline*	*Natural*	*Artificial*	*Baseline*	*Natural*	*Artificial*
SS	0.99	0.96 *(-2%)*	0.91 *(-7%)*	2.47	2.20 *(-11%)*	2.12 *(-14%)*	0.60	0.39 *(-36%)*	0.41 *(-32%)*
IG	0.96	0.96 *(-1%)*	0.82 *(-15%)*	0.82	0.58 *(-29%)*	0.55 *(-33%)*	0.83	0.44 *(-47%)*	0.40 *(-51%)*
VLF	1.01	0.94 *(-7%)*	0.92 *(-9%)*	0.24	0.17 *(-26%)*	0.17 *(-29%)*	0.06	0.02 *(-64%)*	0.02 *(-69%)*
	Across restoration [m]			**Beach toe [m]**			**Runup [m]**		
	Baseline	*Natural*	*Artificial*	*Baseline*	*Natural*	*Artificial*	*Baseline*	*Natural*	*Artificial*
Setup	0.00	0.00	0.03	0.06	0.06 *(-11%)*	0.08 *(+27%)*	0.95	0.66 *(-31%)*	0.64 *(-33%)*
Total							2.45	1.51 *(-38%)*	1.47 *(-40%)*

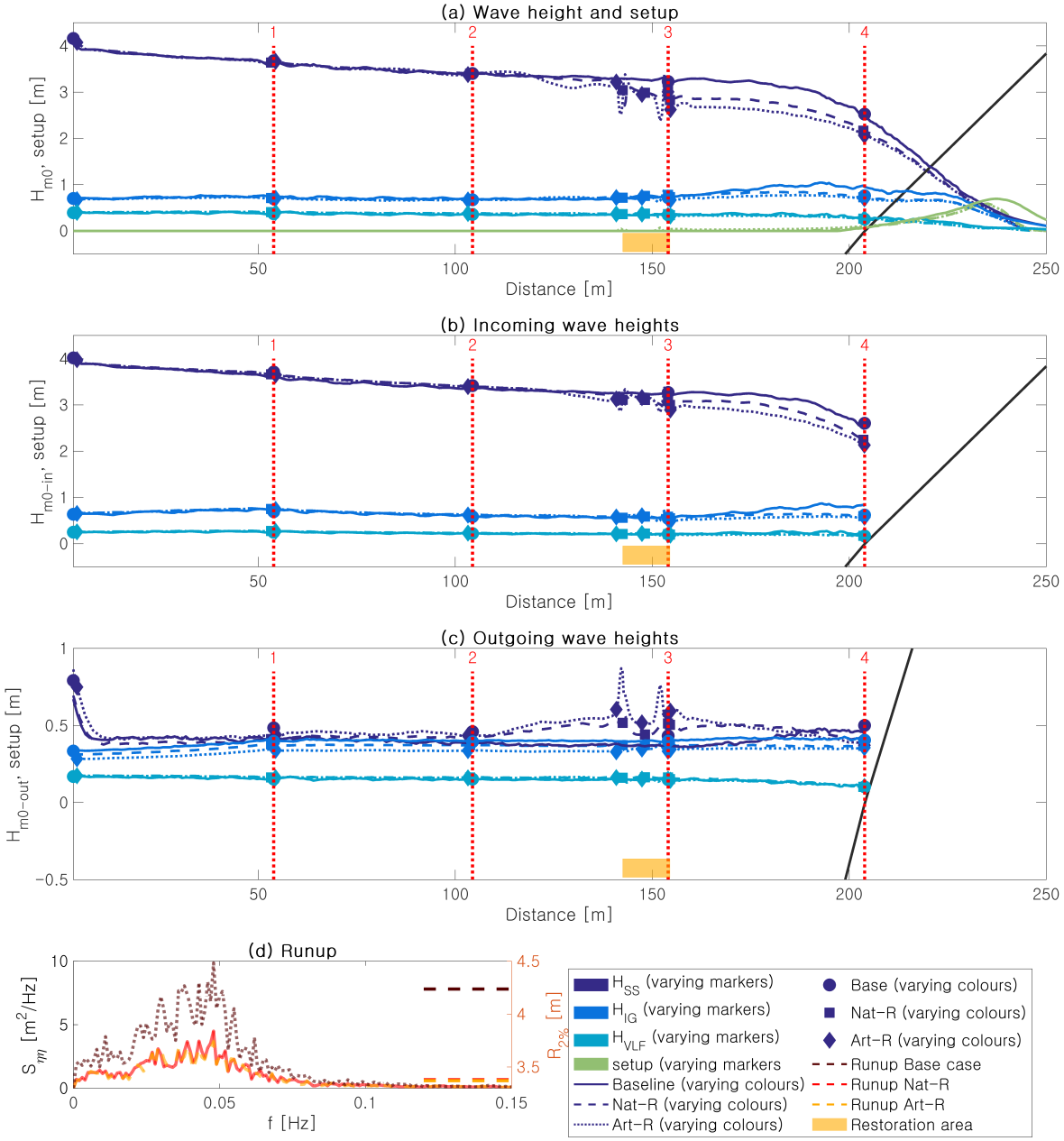

Figure D.18: Wave transformation and runup across a restoration at the **inner shelf of the three-slope profile**, displaying the total (subplot a), the incoming (subplot b) and the outgoing (subplot c) SS, IG and VLF waves, as well as the runup (subplot d). Locations 1 to 4 indicate the shelf edge, the mid-shelf, the inner shelf and the beach toe, respectively.

Table D.10: Summary of wave transformation characteristics across the **inner shelf restoration of the three-slope reef profile** (restoration 4 in Figure 6.2), displaying the wave transmission across the restoration (ratio of wave heights shoreward versus seaward of the restoration), the setup across the restoration, the wave heights and total setup at the beach toe and the runup components. Other table characteristics are noted in the Intermezzo on page 78.

	Wave transmission restoration [-]			**Beach toe wave heights [m]**			**Runup [m]**		
	Baseline	*Natural*	*Artificial*	*Baseline*	*Natural*	*Artificial*	*Baseline*	*Natural*	*Artificial*
SS	0.99	0.96 *(-2 %)*	0.92 *(-6 %)*	2.50	2.24 *(-10 %)*	2.13 *(-15 %)*	0.60	0.43 *(-29 %)*	0.40 *(-34 %)*
IG	0.96	0.98 *(+2 %)*	0.86 *(-11 %)*	0.84	0.59 *(-29 %)*	0.57 *(-32 %)*	0.83	0.37 *(-55 %)*	0.40 *(-51 %)*
VLF	1.00	0.94 *(-6 %)*	0.88 *(-12 %)*	0.23	0.17 *(-27 %)*	0.17 *(-25 %)*	0.06	0.01 *(-79 %)*	0.01 *(-84 %)*
	Across restoration [m]			**Beach toe [m]**			**Runup [m]**		
	Baseline	*Natural*	*Artificial*	*Baseline*	*Natural*	*Artificial*	*Baseline*	*Natural*	*Artificial*
Setup	0.00	0.00	0.03	0.06	0.08 *(+25 %)*	0.10 *(+60 %)*	0.95	0.66 *(-31 %)*	0.65 *(-32 %)*
Total							2.45	1.48 *(-39 %)*	1.46 *(-40 %)*

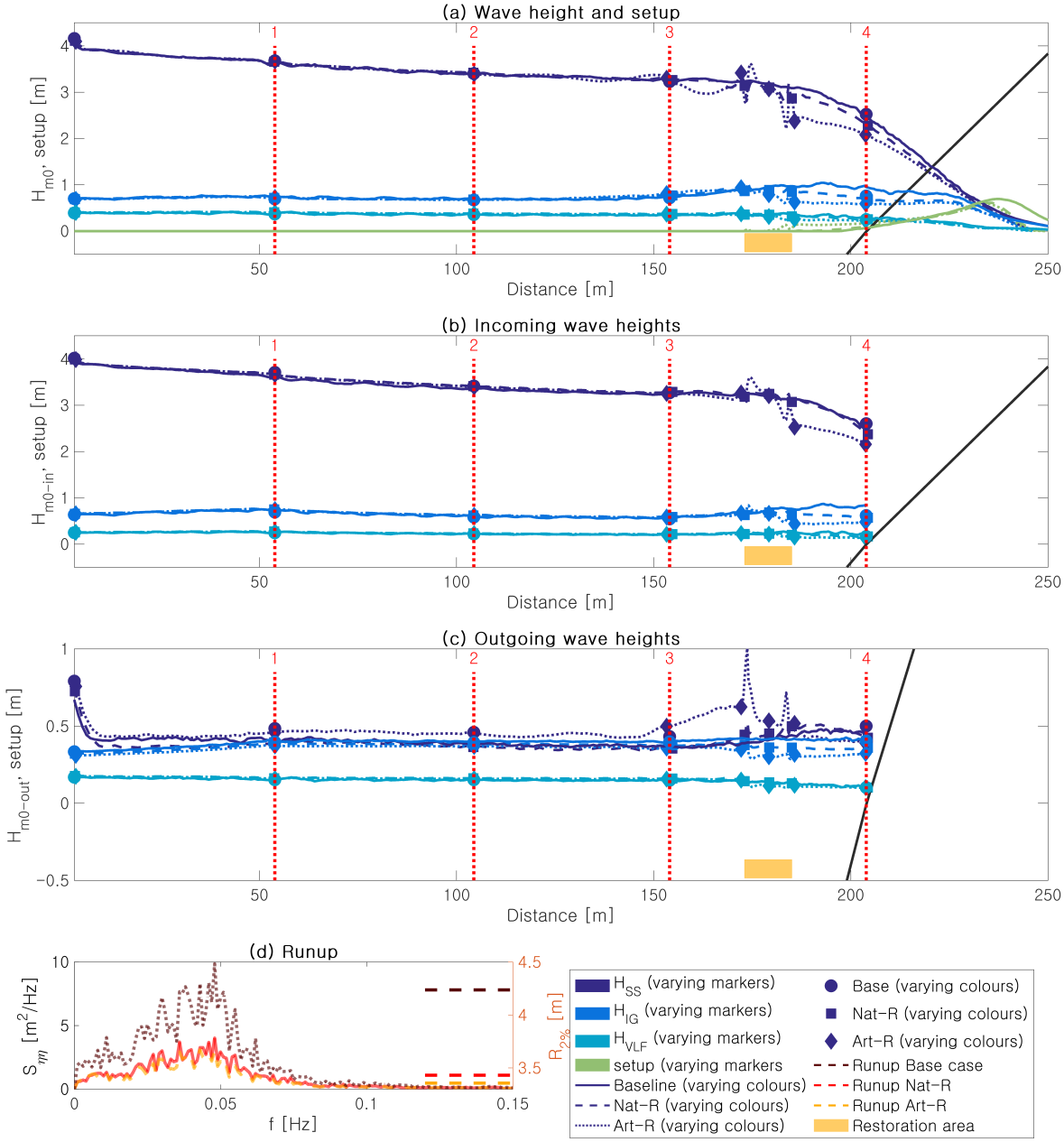

Figure D.19: Wave transformation and runup across a restoration at the **upper forereef of the three-slope profile**, displaying the total (subplot a), the incoming (subplot b) and the outgoing (subplot c) SS, IG and VLF waves, as well as the runup (subplot d). Locations 1 to 4 indicate the shelf edge, the mid-shelf, the inner shelf and the beach toe, respectively.

Table D.11: Summary of wave transformation characteristics across the **upper forereef restoration of the three-slope reef profile** (restoration 5 in Figure 6.2), displaying the wave transmission across the restoration (ratio of wave heights shoreward versus seaward of the restoration), the setup across the restoration, the wave heights and total setup at the beach toe and the runup components. Other table characteristics are noted in the Intermezzo on page 78.

	Wave transmission restoration [-]			**Beach toe wave heights [m]**			**Runup [m]**		
	Baseline	*Natural*	*Artificial*	*Baseline*	*Natural*	*Artificial*	*Baseline*	*Natural*	*Artificial*
SS	0.96	0.96 *(0%)*	0.77 *(-19%)*	2.44	2.37 *(-3%)*	2.16 *(-12%)*	0.60	0.41 *(-33%)*	0.36 *(-40%)*
IG	1.15	1.01 *(-12%)*	0.65 *(-43%)*	0.81	0.57 *(-29%)*	0.48 *(-41%)*	0.83	0.41 *(-50%)*	0.40 *(-52%)*
VLF	1.10	0.92 *(-17%)*	0.67 *(-39%)*	0.22	0.16 *(-26%)*	0.14 *(-38%)*	0.06	0.01 *(-81%)*	0.01 *(-89%)*
	Across restoration [m]			**Beach toe [m]**			**Runup [m]**		
	Baseline	*Natural*	*Artificial*	*Baseline*	*Natural*	*Artificial*	*Baseline*	*Natural*	*Artificial*
Setup	0.00	0.00	0.13	0.07	0.10 *(+40%)*	0.17 *(+133%)*	0.95	0.70 *(-27%)*	0.67 *(-29%)*
Total							2.45	1.53 *(-37%)*	1.44 *(-41%)*

D.2. The effect of varying boundary conditions

Below (Figures D.20 to D.26), the effect of varying boundary conditions on runup is depicted for each restoration separately. These plots support observations elaborated in Section 8.2.2 of Chapter 8.

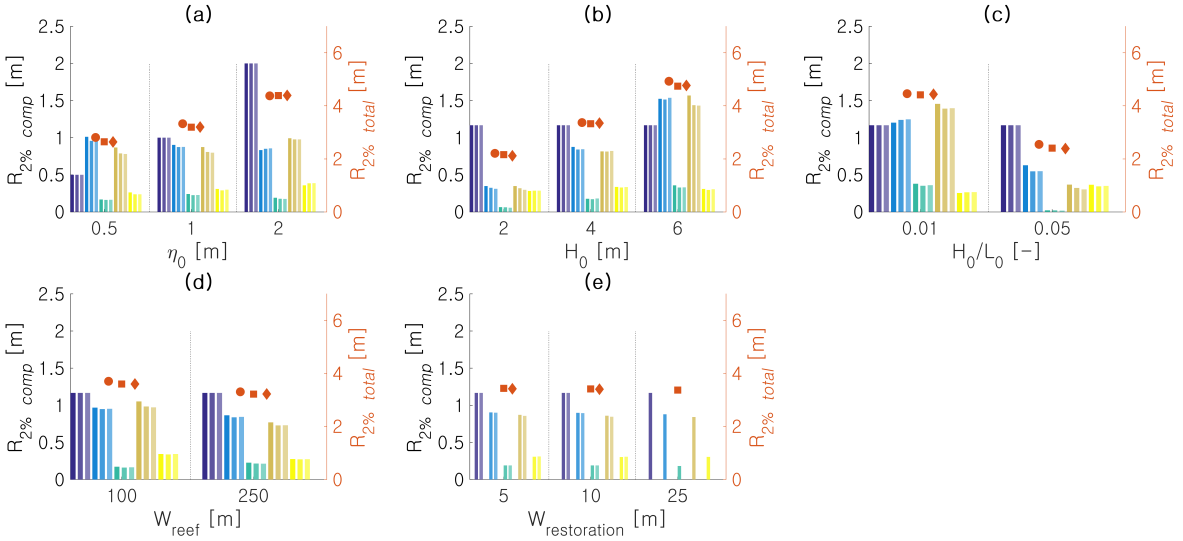

(a) Lower forereef restoration

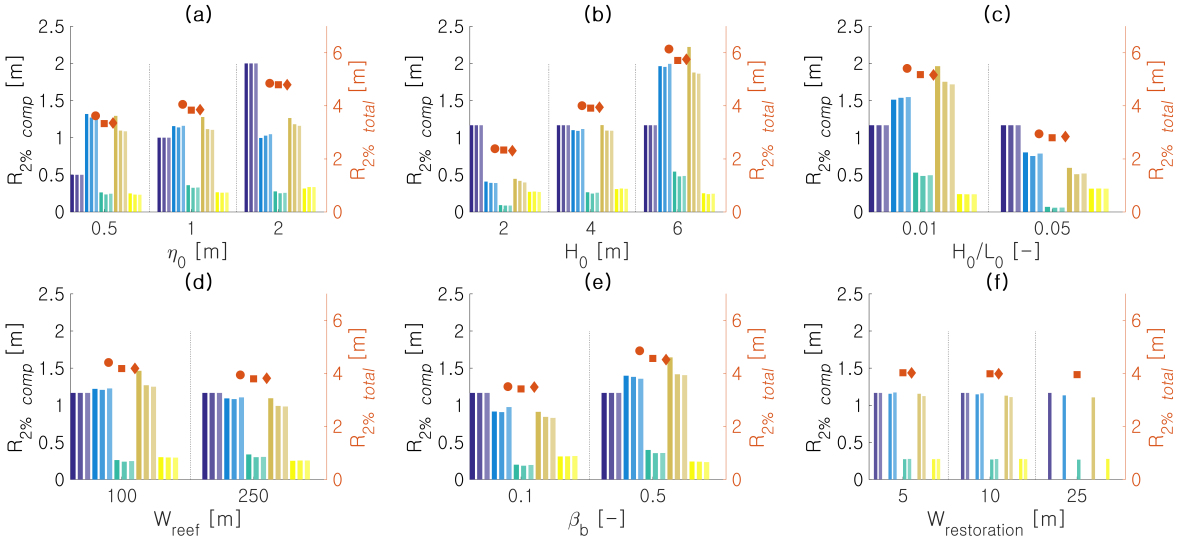

(b) Upper forereef restoration

Figure D.20: **Runup at the restored typical fringing reef: (a) lower forereef and (b) upper forereef restoration**. Plots of the different runup components (indicated by the different colours, from left to right the offshore water level, the setup, the VLF, the IG and the SS wave height component), for (from left to right) the baseline scenario, the natural restoration and the artificial restoration (indicated by differences in transparency). The total runup is indicated by orange round (baseline), square (natural restoration) and diamond (artificial restoration) markers, whose magnitude is given on the right y-axis

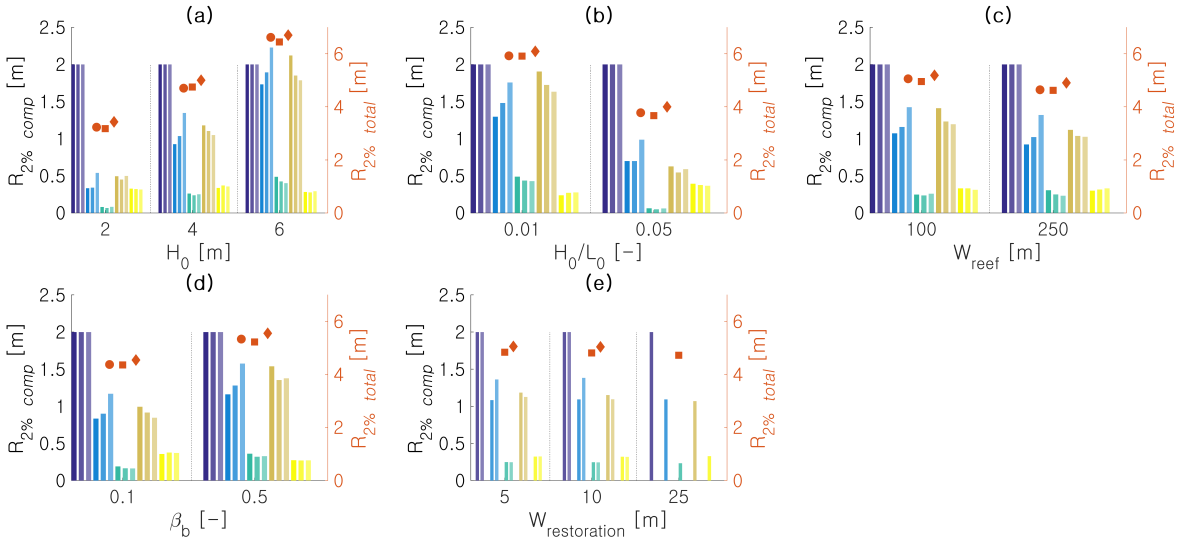

(a) Reef edge restoration

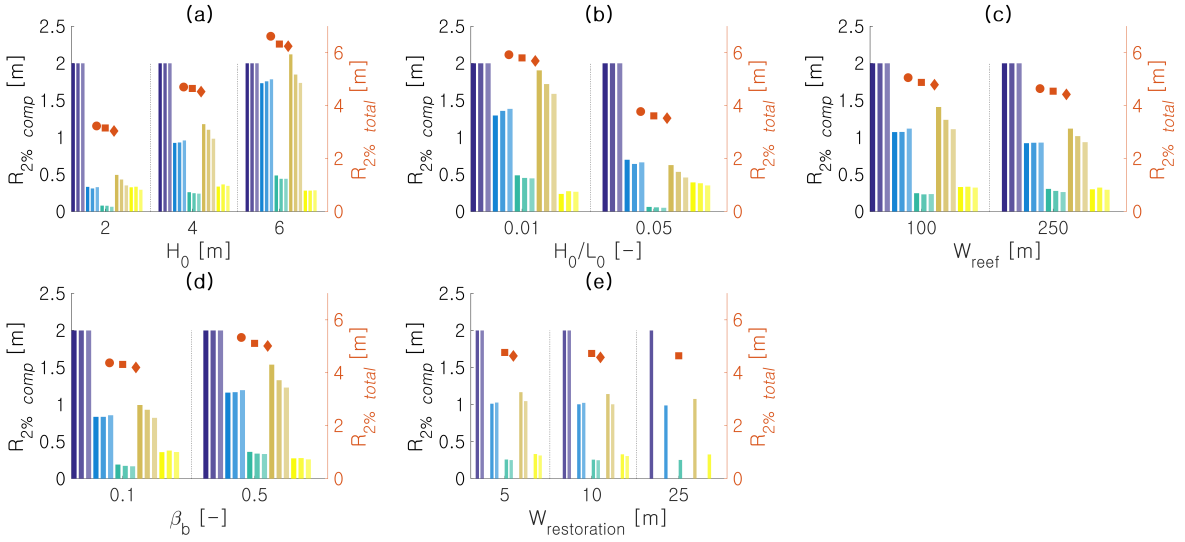

(b) Mid-flat restoration

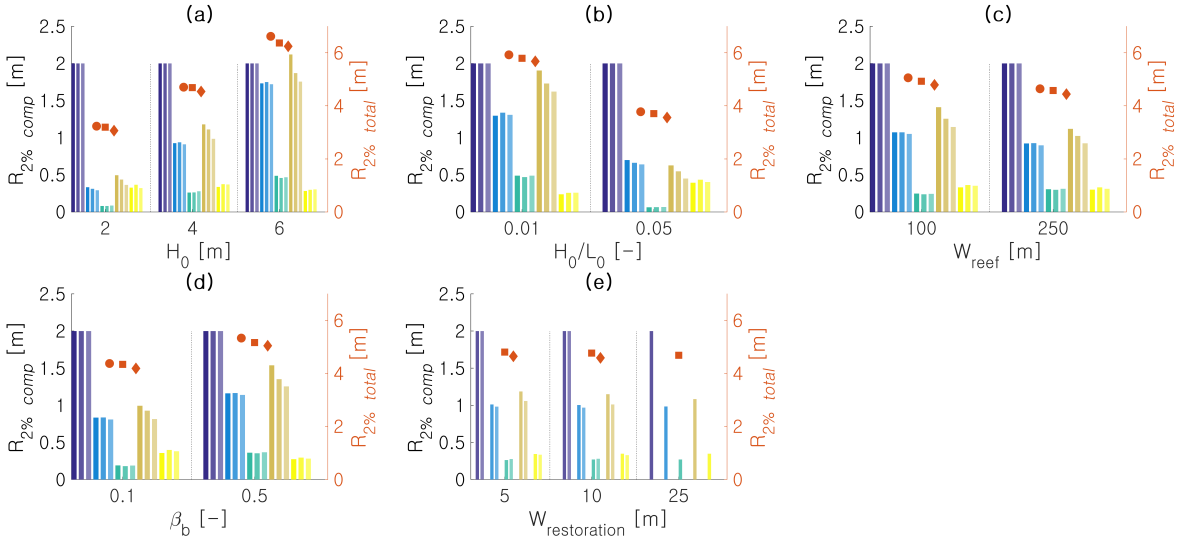

(c) Inner flat restoration

Figure D.21: **Runup at the restored typical fringing reef:(a) reef edge, (b) mid-flat and (c) inner flat restoration**. Plots of the different runup components (indicated by the different colours, from left to right the offshore water level, the setup, the VLF, the IG and the SS wave height component), for (from left to right) the baseline scenario, the natural restoration and the artificial restoration (indicated by differences in transparency). The total runup is indicated by orange round (baseline), square (natural restoration) and diamond (artificial restoration) markers, whose magnitude is given on the right y-axis

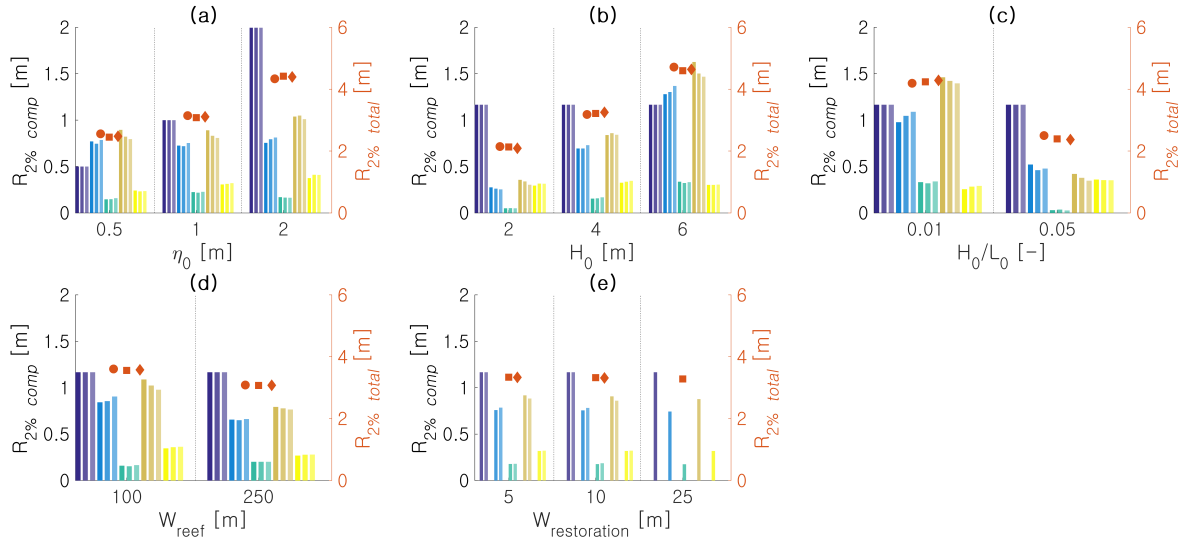

(a) Lower forereef restoration

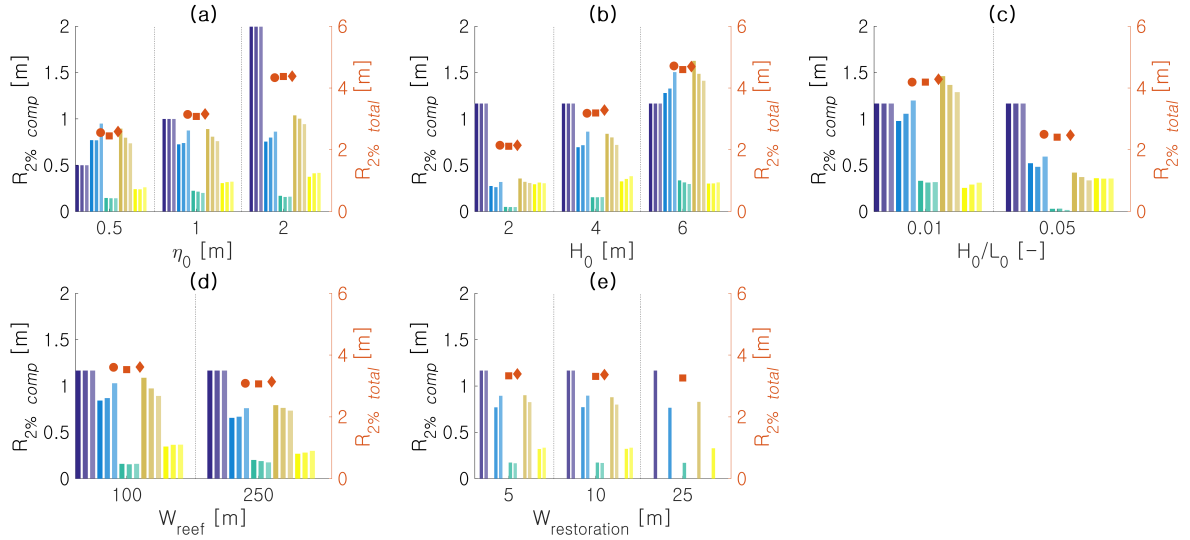

(b) Upper forereef restoration

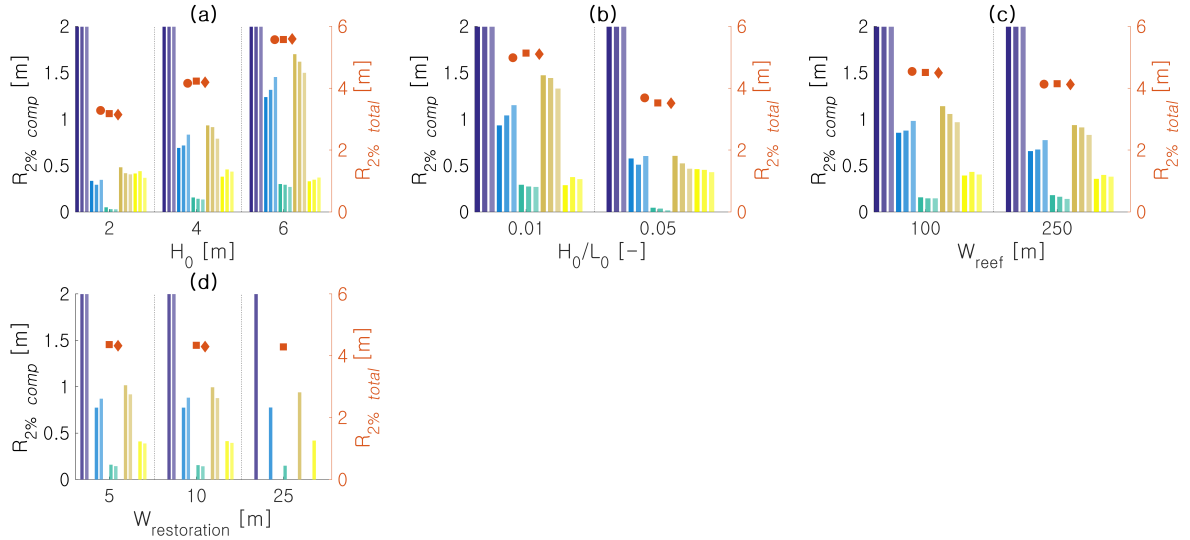

(c) Reef edge restoration

Figure D.22: **Runup at the restored convex reef: (a) lower forereef, (b) upper forereef and (c) reef edge restoration**. Plots of the different runup components (indicated by the different colours, from left to right the offshore water level, the setup, the VLF, the IG and the SS wave height component), for (from left to right) the baseline scenario, the natural restoration and the artificial restoration (indicated by differences in transparency). The total runup is indicated by orange round (baseline), square (natural restoration) and diamond (artificial restoration) markers, whose magnitude is given on the right y-axis

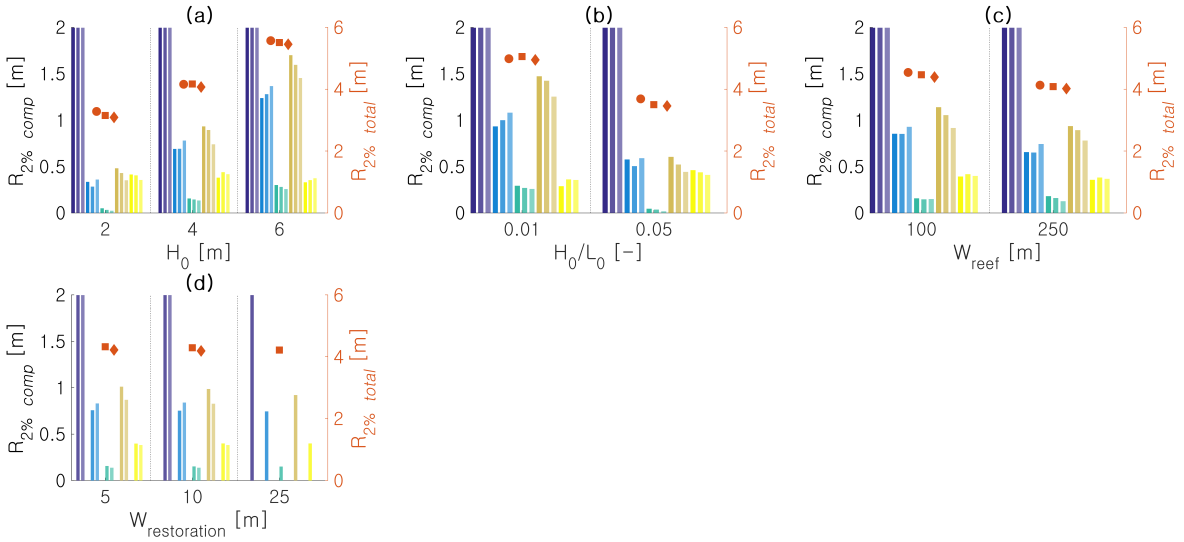

(a) Upper sloping region restoration

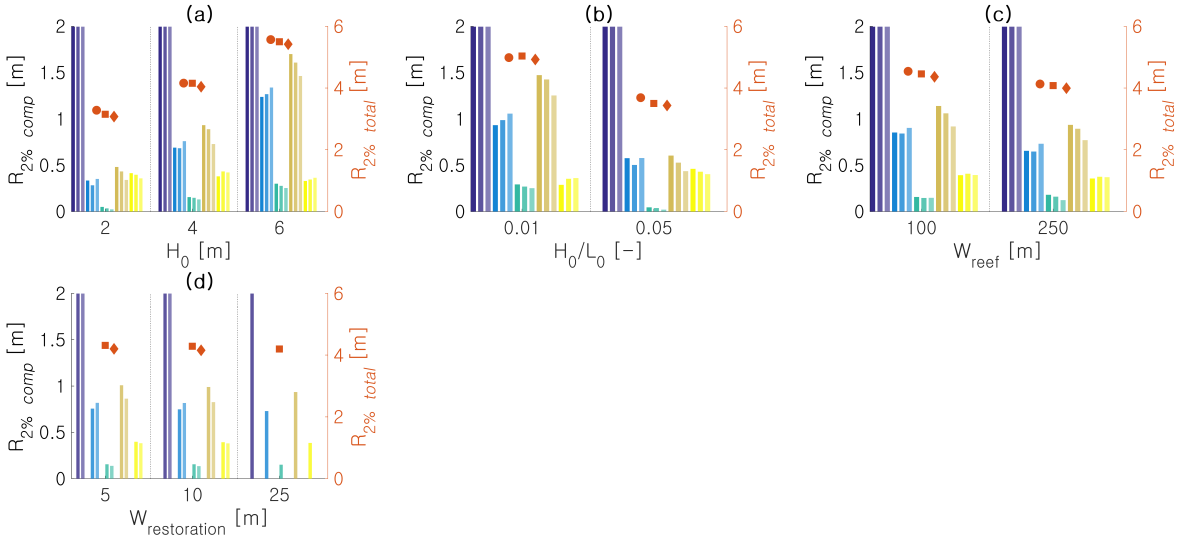

(b) Mid-flat restoration

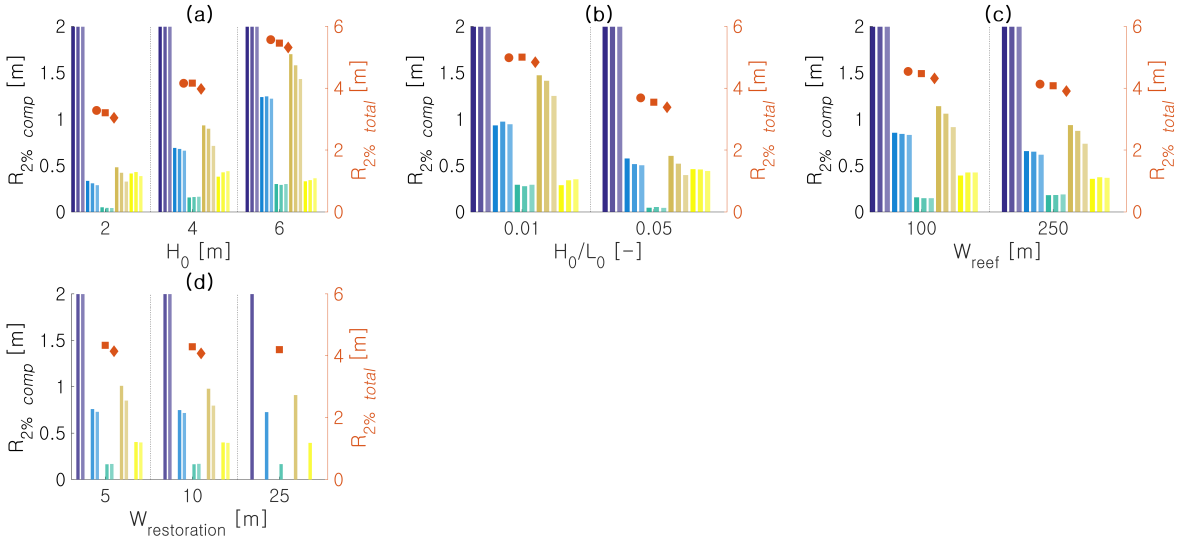

(c) Inner flat restoration

Figure D.23: **Runup at the restored convex reef: (a) upper sloping region, (b) mid-flat and (c) inner flat restoration**. Plots of the different runup components (indicated by the different colours, from left to right the offshore water level, the setup, the VLF, the IG and the SS wave height component), for (from left to right) the baseline scenario, the natural restoration and the artificial restoration (indicated by differences in transparency). The total runup is indicated by orange round (baseline), square (natural restoration) and diamond (artificial restoration) markers, whose magnitude is given on the right y-axis

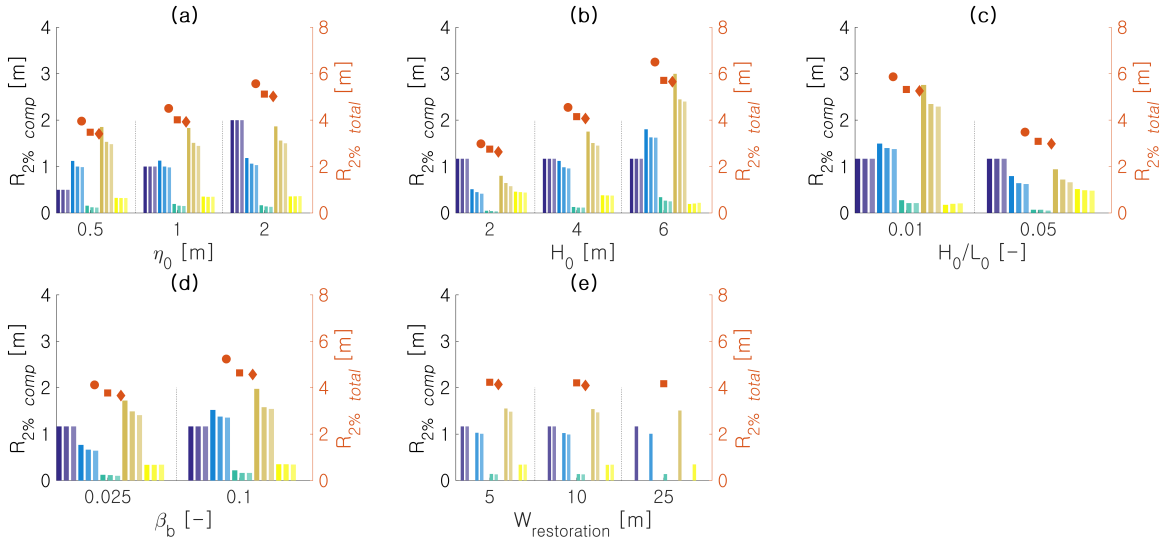

(a) Lower forereef restoration

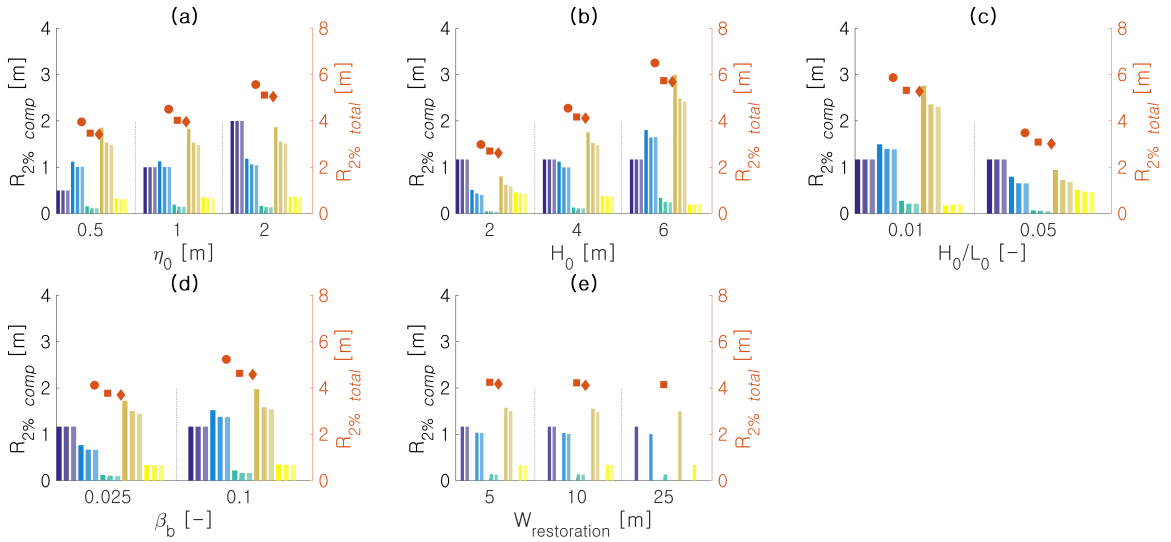

(b) Mid-forereef restoration

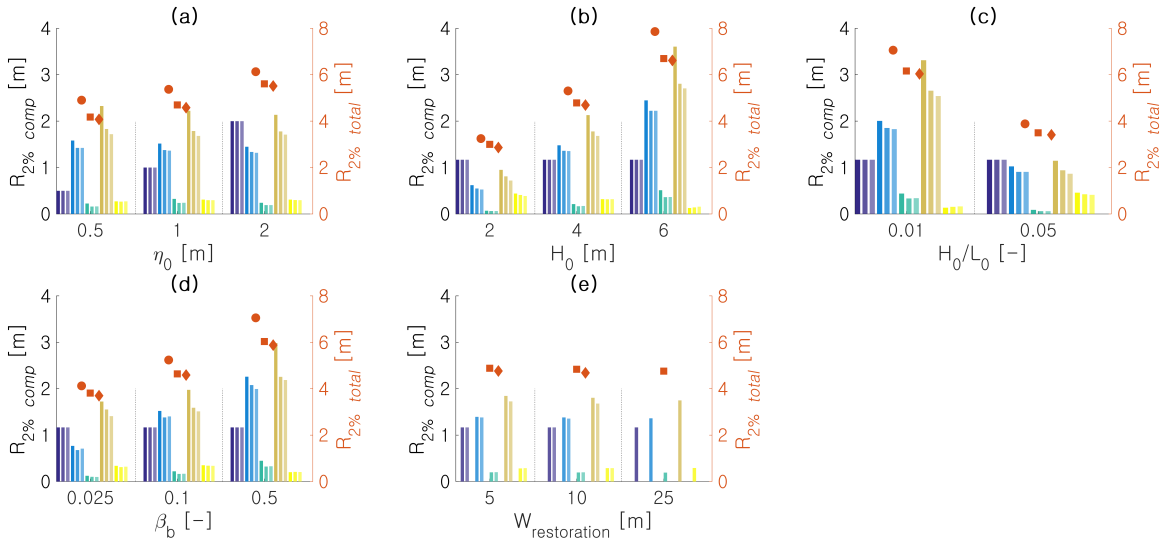

(c) Upper forereef restoration

Figure D.24: **Runup at the restored straight reef: (a) lower forereef, (b) mid-forereef and (c) upper forereef restoration**. Plots of the different runup components (indicated by the different colours, from left to right the offshore water level, the setup, the VLF, the IG and the SS wave height component), for (from left to right) the baseline scenario, the natural restoration and the artificial restoration (indicated by differences in transparency). The total runup is indicated by orange round (baseline), square (natural restoration) and diamond (artificial restoration) markers, whose magnitude is given on the right y-axis

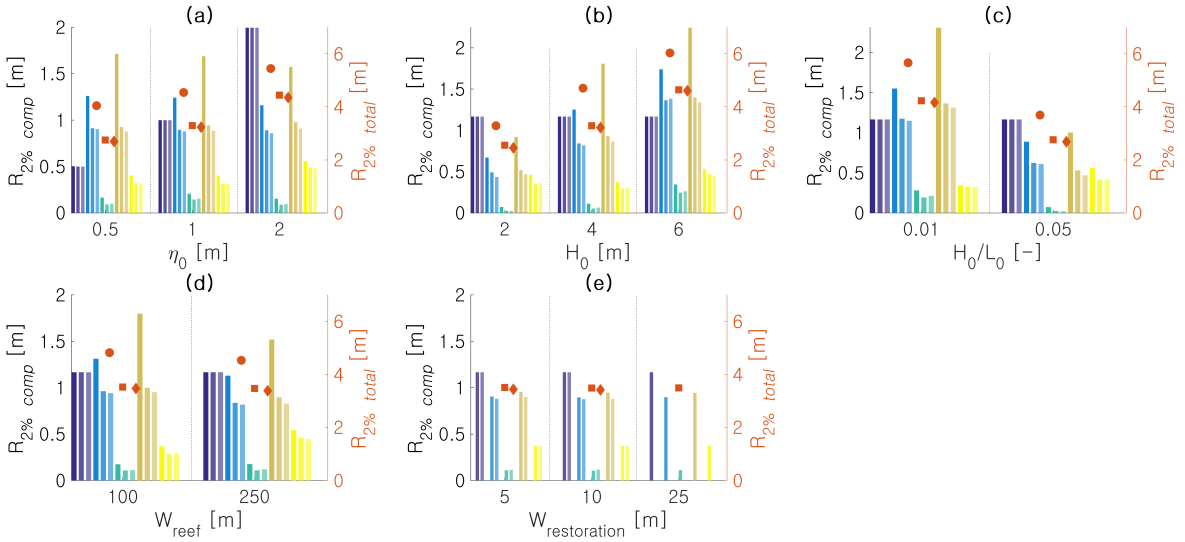

(a) Lower forereef restoration

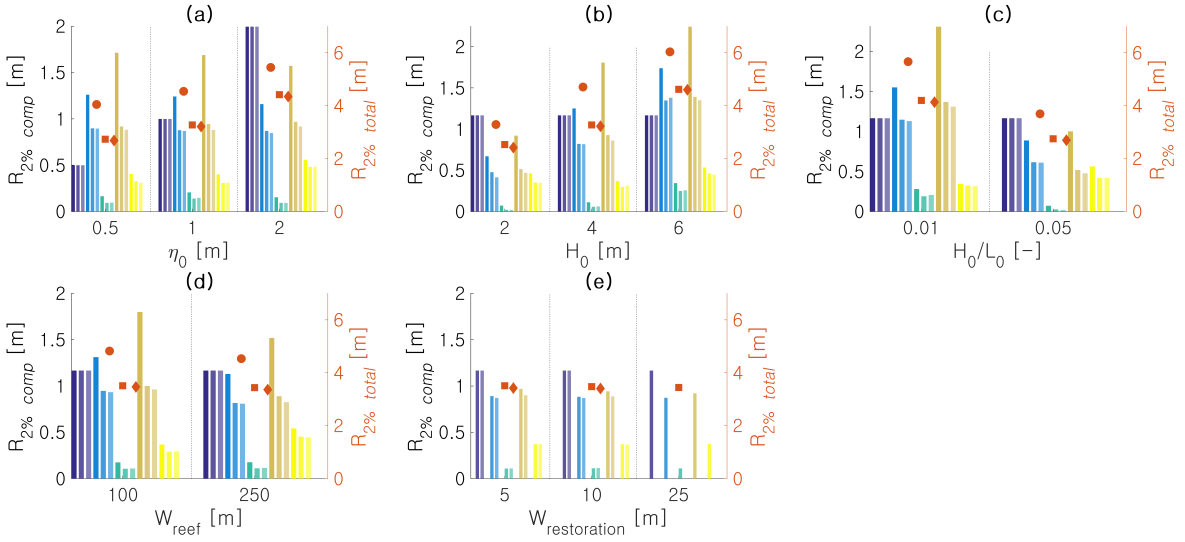

(b) Shelf edge restoration

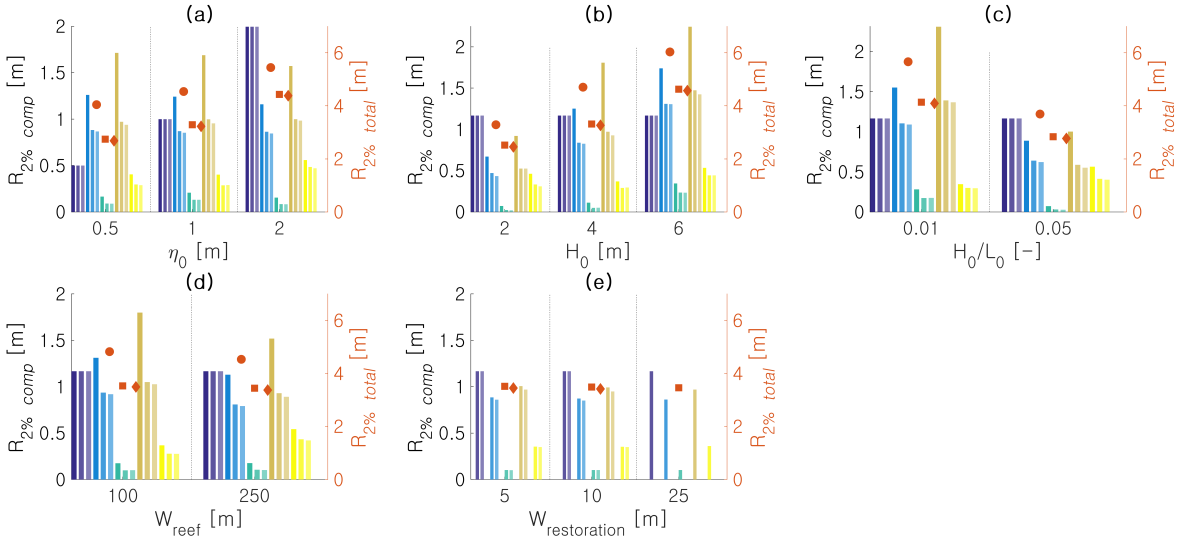

(c) Mid-shelf restoration

Figure D.25: **Runup at the restored three-slope reef: (a) lower forereef, (b) shelf edge and (c) mid-shelf restoration**. Plots of the different runup components (indicated by the different colours, from left to right the offshore water level, the setup, the VLF, the IG and the SS wave height component), for (from left to right) the baseline scenario, the natural restoration and the artificial restoration (indicated by differences in transparency). The total runup is indicated by orange round (baseline), square (natural restoration) and diamond (artificial restoration) markers, whose magnitude is given on the right y-axis

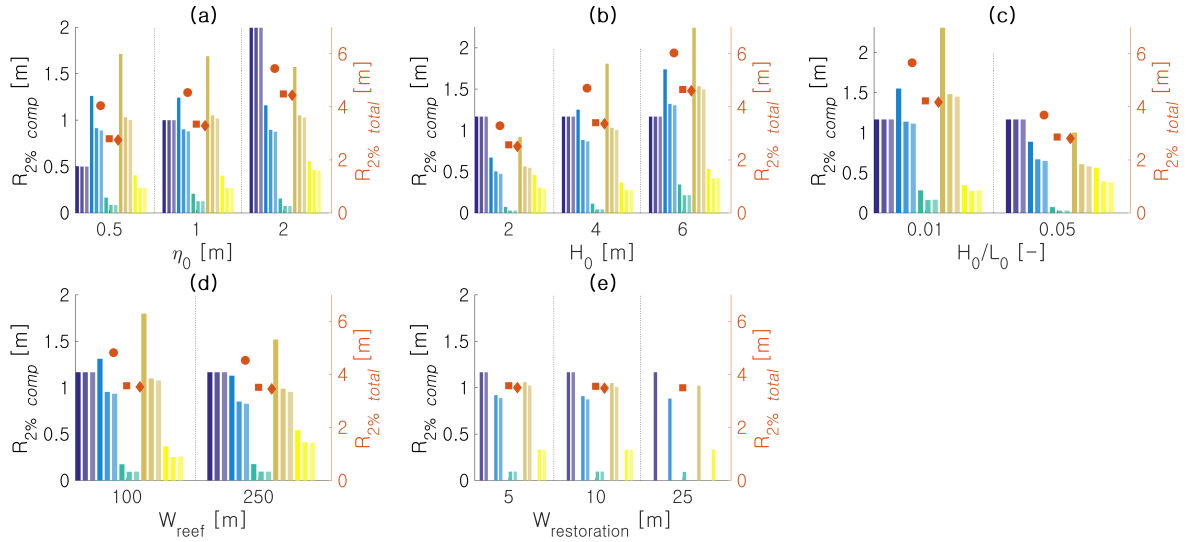

(a) Inner shelf restoration

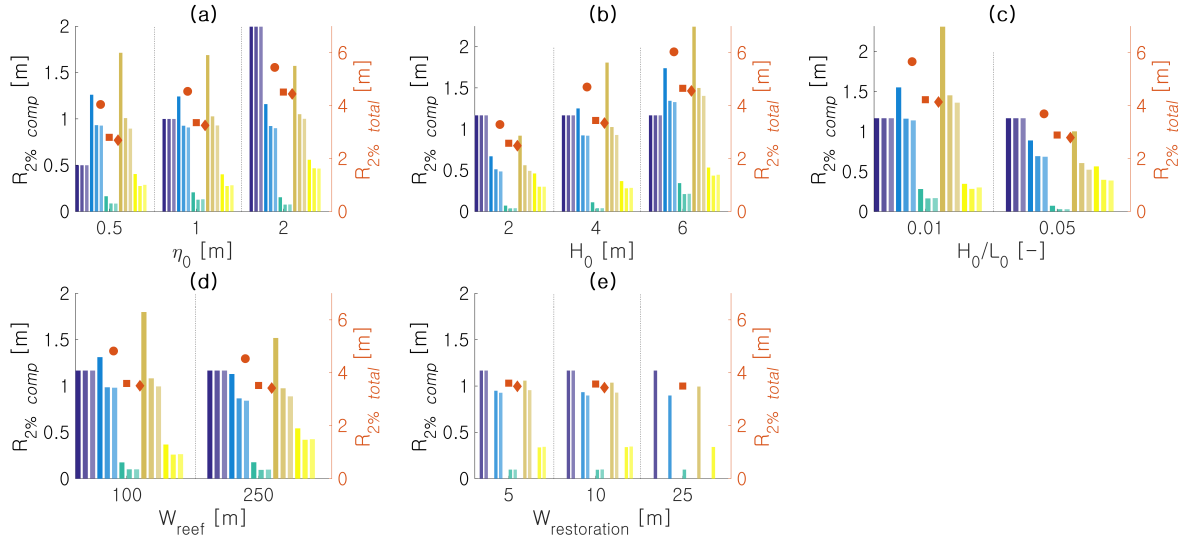

(b) Upper forereef restoration

Figure D.26: **Runup at the restored three-slope reef: (a) inner shelf and (b) upper forereef restoration**. Plots of the different runup components (indicated by the different colours, from left to right the offshore water level, the setup, the VLF, the IG and the SS wave height component), for (from left to right) the baseline scenario, the natural restoration and the artificial restoration (indicated by differences in transparency). The total runup is indicated by orange round (baseline), square (natural restoration) and diamond (artificial restoration) markers, whose magnitude is given on the right y-axis